ParisTech
INSTITUT DES SCIENCES ET TECHNOLOGIES
PARIS INSTITUTE OF TECHNOLOGY

AgroParisTech
INSTITUT DES SCIENCES ET INDUSTRIES DU VIVANT ET DE L'ENVIRONNEMENT
PARIS INSTITUTE OF TECHNOLOGY FOR LIFE, FOOD AND ENVIRONMENTAL SCIENCES

Ecole Doctorale ABIES
Agriculture Agriculture Alimentation Food Biologie Biology Environnement Environment Santé Health

Doctorat ParisTech

T H È S E

pour obtenir le grade de docteur délivré par

L'Institut des Sciences et Industries du Vivant et de l'Environnement

(AgroParisTech)

Spécialité: Génie des Procédés Alimentaires

présentée et soutenue publiquement par

Marcela Patricia ARELLANO SALAZAR

le 7 décembre 2012

Experimental characterization and modelling of multiphase systems during the freezing process at the pilot scale. Application to sorbet manufacturing in scraped surface heat exchangers.

Caractérisation expérimentale et modélisation de systèmes multiphasiques au cours du procédé de congélation à l'échelle pilote. Application à la fabrication de sorbets dans des échangeurs de chaleur à surface raclée.

Directeur de thèse: Graciela ALVAREZ
Co-Directeur de thèse: Denis FLICK
Travail réalisé à l'UR GPAN – IRSTEA en collaboration avec l'UMR GENIAL (N°1145) – AgroParisTech

Jury

Mme Laurence Fournaison, DR, UR GPAN, IRSTEA	Président
Mme Francine FAYOLLE, PR, Université de Nantes	Rapporteur
M. Jean-François MAINGONNAT, DR, INRA Avignon	Rapporteur
M. Denis FLICK, PR, UMR GENIAL, AgroParisTech	Examinateur
Mme Graciela ALVAREZ, DR, UR GPAN, IRSTEA	Examinateur
M. Richard HARTEL, PR, Université de Wisconsin-Madison	Examinateur
Mme Hayat BENKHELIFA, MC, UMR GENIAL, AgroParisTech	Examinateur

To my parents, Luis and Patty, and to my husband Vincent

For your endless love, patience and encouragement

REMERCIEMENTS

Je remercie vivement mes directeurs de thèse, *Mme Graciela Alvarez*, pour ses conseils scientifiques, la liberté de travail et la confiance qu'elle m'a accordée au cours de ces trois années, et *M. Denis Flick*, pour son encadrement, ses conseils scientifiques et ses lectures minutieuses des articles.

Je remercie sincèrement *Mme Hayat Benkhelifa*, encadrante de cette thèse, pour son suivi du travail expérimental, ses révisions des rapports d'avancement, et particulièrement pour son aide dans la révision finale de ce manuscrit de thèse.

Je remercie également *Mme Laurence Fournaison*, chef de l'unité de recherche Génie des Procédés Frigorifiques à l'IRSTEA, pour m'avoir accueillie au sein de son équipe pendant ces trois années et pour avoir accepté d'examiner ce travail.

Je tiens à remercier chaleureusement *Mme Francine Fayolle* et *M. Jean-François Maingonnat* pour avoir accepté d'être les rapporteurs de cette thèse, ainsi que *M. Richard Hartel* pour avoir accepté d'examiner ce travail de thèse.

Un grand merci aux personnes qui ont rendu possible, par leur aide technique, le bon déroulement des expériences dans le freezer pilote, *M. Denis Leducq*, ingénieur de recherche, ainsi que *MM Joseph Andreu*, *Ali Bouchaid, Jérôme Gahartian*, *Romuald Hunlede, Christophe Jouquin* et *Carlos Zambrana*. Un merci supplémentaire à *Christophe* et *Ali* pour m'avoir servi de chauffeurs lorsque j'avais une jambe dans le plâtre. Je remercie également tous les membres de l'unité pour leur accueil chaleureux et leur présence amicale au cours de ces trois années.

Je remercie particulièrement mes parents, *Luis* et *Patty*, pour leur soutien et leurs encouragements pendant l'ensemble de mes études supérieures.

Merci à mon époux, *Vincent*, pour sa patience et son aide, ainsi que son support technique en informatique et pour la réalisation de certains graphiques.

CONTENTS

List of Figures 13

List of Tables 21

Framework of this work 25

Chapter 1 - Introduction 27

1.1. General introduction 29

1.2. Methodology 31

1.3. Structure of the thesis 33

Cadre de ce travail 35

Chapitre 1 - Introduction 37

1.1. Introduction générale 39

1.2. Méthodologie 43

1.3. Structure de la thèse 45

Chapter 2 - Background 47

2.1. Sorbet manufacturing process 50

2.1.1. Ice crystallization mechanism in a SSHE 51

2.1.2. Influence of the operating conditions on ice crystallization in SSHEs 53

2.2. Flow behaviour in SSHEs 56

2.3. Temperature profile and heat transfer in SSHEs 57

2.4. Residence time distribution (RTD) 60

2.4.1. Residence time distribution in SSHEs 61

2.5. Residence time distribution modelling 63

2.5.1. Plug-flow with axial dispersion model (ADM) 63

2.5.2. Tanks-in-series model (TSM) 64

2.5.3. The gamma distribution model (GDM) 64

2.5.4. RTD models used for the flow behaviour description in SSHEs 64
2.6. Rheological properties of sorbet 66
2.6.1. Rheological models 68
2.7. Modelling of the freezing process 71
2.7.1. Population balance approach 71
2.7.2. Crystallization modelling approaches for SSHEs 72
2.8. Bibliographical review conclusions 74
2.9. Aim of this work 77
References of bibliographic review 79
Chapter 3 - Materials and methods 87
3.1. Working fluid - Lemon sorbet mix 89
3.2. Description of the experimental platform 90
3.2.1. Control of process conditions and data acquisition in Labview® 93
3.3. Online sensors 93
3.3.1. Draw temperature measurements and ice volume fraction calculations 93
3.3.2 Ice crystal chord length distribution (CLD) measurements by the FBRM probe 94
3.3.3. Temperature profile measurement 96
3.4. Apparent viscosity measurements 97
3.5. Residence time distribution measurements 99
Chapter 4 - Articulation of the scientific papers 101
4.1. Online ice crystal size measurements during sorbet freezing by means of the focused beam reflectance measurement (FBRM) technology. Influence of operating conditions 103
4.2. Experimental study and modelling of the residence time distribution in a scraped surface heat exchanger during sorbet freezing 106
4.3. Rheological characterization of sorbet using pipe rheometry during the freezing process 108

4.4. Influence of ice and air volume fractions on the rheological properties of sorbet 110
5.5. Coupling population balance and residence time distribution for the ice crystallization modelling in a scraped surface heat exchanger 112
Chapter 5 - Results and discussion 117
5.1. Online ice crystal size measurements during sorbet freezing by means of the focused beam reflectance measurement (FBRM) technology. Influence of operating conditions 119
Abstract 119
1. Introduction 120
2. Materials and methods 124
2.1. Sorbet freezing 124
2.2. Experimental design and statistical analysis 125
2.3. Draw temperature measurements and ice mass fraction calculations 127
2.4. Ice crystal CLD measurements by the FBRM probe 129
3. Results and discussion 133
3.1. Freezer operating conditions and global ANOVA analysis 133
3.2. Influence of refrigerant fluid temperature and mix flow rate on draw temperature 134
3.3. Influence of refrigerant fluid temperature and mix flow rate on mean chord length 136
3.4. Influence of dasher speed on draw temperature 138
3.5. Influence of dasher speed on mean chord length 140
4. Conclusions 141
5.2. Experimental study and modelling of the residence time distribution in a scraped surface heat exchanger during sorbet freezing 149
Abstract 149
1. Introduction 150
2. Materials and methods 153

2.1. Working fluid 153

2.2. Crystallization process equipment and operating conditions 154

2.3. Temperature profile measurement 156

2.4. Residence time distribution measurement 157

2.5. Residence time distribution data treatment 158

3. Residence time distribution models 160

3.1. Plug-flow with axial dispersion model 161

3.2. Tanks-in-series model 161

3.3. The gamma distribution model 161

3.4. RTD model fitting to experimental RTD data 162

4. Results and discussion 162

4.1. Influence of refrigerant fluid temperature on axial temperature profile and RTD 166

4.2. Influence of mix flow rate on axial temperature profile and RTD 169

4.3. Influence of rotational speed on axial temperature profile and RTD 172

5. Conclusions 175

5.3. Rheological characterization of sorbet using pipe rheometry during the freezing process 183

1. Introduction 184

2. Materials and methods 188

2.1. Sorbet freezing and operating conditions 188

2.2. Pipe rheometry measurements 189

2.3. Ice volume fraction calculations 192

3. Results and discussion 194

3.1. Wall slip and viscous dissipation effects on the apparent viscosity of sorbet 195

3.2. Effect of draw temperature and ice volume fraction on the apparent viscosity 196

3.3. Experimental uncertainty 199

4. Rheological model 201

4.1. Model description 201

5. Conclusions 204

5.4. Influence of ice and air volume fractions on the rheological properties of sorbet 213

Abstract 213

1. Introduction 214

2. Materials and methods 215

2.1. Sorbet freezing and operating conditions 215

2.2. Pipe rheometry measurements 217

2.3. Ice volume fraction calculations 218

3. Results and discussion 219

3.1. Influence of ice and air volume fraction on the flow behaviour index 219

3.2. Influence of ice and air volume fractions on the apparent viscosity 221

4. Conclusions 223

5.5. Coupling population balance and residence time distribution for the ice crystallization modelling in a scraped surface heat exchanger 227

Abstract 227

1. Introduction 228

2. Experimental 232

2.1. Ice crystallization process equipment and operating conditions 232

2.2 Residence time distribution measurement and modelling 233

3. PBE and plug flow modelling approach 235

3.1. Fluid flow 235

3.2. Energy balance 236

3.3. Population balance 238
4. Modelling approach coupling PBE and RTD 242
5. Numerical solution of the models 244
6. Results and discussion 245
6.1. PBE and plug flow modelling approach 245
6.2 Coupling of PBE and RTD modelling approach 248
7. Conclusions 254
Chapter 6 - Conclusions and perspectives 263
Chapitre 6 - Conclusions et perspectives 273
Publications and communications 283
Appendix 287
Abstract 295
Résumé 297

List of Figures

Chapter 2 - Background

Fig. 2.1. Schematic representation of the ice crystallization mechanism in a SSHE 51

Chapter 3 - Materials and methods

Fig. 3.1. Freezing point depression curve at equilibrium (Gonzalez, 2012) 90

Fig. 3.2. (a) Schematic representation of the experimental platform. 1. Refrigerated storage tank (200 litres capacity). 2. Volumetric piston pump. 3. Freezer. 4. Outlet pipe. 5. Pt100 probe inserted into the outlet pipe. 6. FBRM probe inserted into the outlet pipe. 7. Product exit. 8. Reception tank. (b) Real representation of the SSHE instrumented with the Pt100 and FBRM sensors 91

Fig. 3.3. Schematic representation of the SSHE WCB® Model MF 50. 1. Inlet connection for sorbet mix. 2. Inlet cover bowl. 3. Rotor. 4. Scraper blades rows. 5. Heat exchange cylinder jacket with vaporizing r22. 6. Heat exchange cylinder. 7. Outlet cover bowl. 8. Outlet pipe for sorbet 92

Fig. 3.4. Real representation of the integrating parts of the SSHE. (a) 1. Inlet connection for sorbet mix. 2. Inlet cover bowl. 3. Rotor. 4. Outlet cover bowl. (b) Rotor equipped with two rows of scraper blades. (c) Front view of rotor with the scraper blades rows 92

Fig. 3.5. (A) Cutaway view of the FBRM probe. (B) Measurement principle of a particle's chord length by the FBRM technique (Figure provided by Mettler-Toledo) 95

Fig. 3.6. Axial position of iButton® sensors in the SSHE 96

Fig. 3.7. Schematic representation of the experimental platform. 1. Refrigerated storage tank (200 l capacity). 2. Volumetric piston pump. 3. Freezer. 4. Contraction/enlargement pipe. 5. Pt100 probe inserted into the inlet of the rheometer. 6. Pipe rheometer. 7. Pressure manometers. 8. Pt100 probe inserted into the outlet of the rheometer. 9. Product exit ... 97

Fig. 3.8. Real representation of the experimental platform. 1. Refrigerated storage tank (200 l capacity). 2. Volumetric piston pump. 3. SSHE. 4. Contraction/enlargement pipe. 5. Pipe rheometer. 6. Pressure manometers. 7. Product exit 98

Fig. 3.9. Experimental setup for injection of tracer. 99

Fig. 3.10. Real representation of experimental setup for the injection of tracer. (Left) 1. Syringe and valve for tracer injection. 2. Inlet thermocouple. 3. SSHE. 4. Outlet pipe of SSHE with valve. 5. Derivation pipe with valve (not shown in the picture). (Right) 1. Sampling cup 100

Chapter 4 - Articulation of scientific papers

Fig. 4.1. Schematic representation of the study carried out in article 1 103

Fig. 4.2. Schematic representation of the study carried out article 2 106

Fig. 4.3. Schematic representation of the study carried out in article 3 108

Fig. 4.4. Schematic representation of the study carried out in article 4 110

Fig. 4.5. Schematic representation of the study carried out in article 5 113

Fig. 4.6. Articulation of the 5 articles 115

Chapter 5 - Results and discussion

Article 1

Fig. 5.1.1. Schematic diagram of pilot Freezer WCB MF 50. 1. Inlet connection for sorbet mix. 2. Inlet cover bowl. 3. Rotor. 4. Scraper blades. 5. Freezer jacket with vaporizing r22. 6. Heat exchange cylinder. 7. Outlet cover bowl. 8. Outlet pipe for sorbet 125

Fig. 5.1.2. Schematic representation of the experimental platform. 1. Refrigerated storage tank (200 litres capacity). 2. Volumetric piston pump. 3. Freezer. 4. Outlet pipe. 5. Pt100

probe inserted into the outlet pipe. 6. FBRM probe inserted into the outlet pipe. 7. Product exit. 8. Reception tank. 128

Fig. 5.1.3. (A) Cutaway view of the FBRM probe. (B) Measurement principle of a particle's chord length by the FBRM technique (Figure provided by Mettler-Toledo). 130

Fig. 5.1.4. Schematic diagram of the chord length measurement of an aggregate with the 'Fine' and 'Coarse' mode. 131

Fig. 5.1.5. Comparison of the calculated CLD from PSD data determined by video microscopy, and the CLD measured by the FBRM probe (PSP at 0.25% w/w suspended in ethanol, of mean size of 27.5 μm). 132

Fig. 5.1.6. Influence of evaporation temperature and mix flow rate at DRS = 78.54 rad.s^{-1} on the draw temperature and ice mass fraction of sorbet. 135

Fig. 5.1.7. Influence of evaporation temperature and mix flow rate at DRS = 78.54 rad.s^{-1} on the mean chord length of sorbet 136

Fig. 5.1.8. Measured ice crystal CLD at refrigerant fluid temperature of -10.6, -15.3 and -19.8 ºC at DRS = 78.5 rad.s^{-1} and MFR = 0.014 kg.s^{-1}. 137

Fig. 5.1.9. Influence of dasher speed and evaporation temperature at MFR = 0.014 kg.s^{-1} on the draw temperature and ice mass fraction of sorbet. 139

Fig. 5.1.10. Influence of dasher speed and evaporation temperature at MFR = 0.014 kg.s^{-1} on the mean chord length of sorbet. 140

Article 2

Fig. 5.2.1. Schematic representation of the SSHE WCB® Model MF 50. 1. Inlet connection for sorbet mix. 2. Inlet cover bowl. 3. Rotor. 4. Scraper blades rows. 5. Heat exchange cylinder jacket with vaporizing r22. 6. Heat exchange cylinder. 7. Outlet cover bowl. 8. Outlet pipe for sorbet. 154

Fig. 5.2.2. Axial position of iButton® sensors in the SSHE. 156

Fig. 5.2.3. Experimental setup for injection of tracer. 158

Fig. 5.2.4. RTD experimental curve fitting for the axial dispersion, tank in series and gamma distribution models at mix flow rate of 0.014kg.s^{-1}, rotational speed of 78.5 rad.s^{-1} and refrigerant temperature of -15.3ºC. 164

Fig. 5.2.5. Schematic representation of the laminar flow of different fluids passing through an annular space with and without rotating blades. 165

Fig. 5.2.6. Axial temperature profile of sorbet as a function of refrigerant fluid temperature at mix flow rate of 0.014 kg.s^{-1}and rotational speed of 78.5 rad.s^{-1}. FP = Freezing point temperature -2.6 °C. 167

Fig. 5.2.7. Residence time distribution as a function of refrigerant fluid temperature at mix flow rate of 0.014 kg.s^{-1} and rotational speed of 78.5 rad.s^{-1}. 168

Fig. 5.2.8. Schematic representation of the laminar flow of sorbet passing through an annular space with rotating blades at different refrigerant temperatures. 169

Fig. 5.2.9. Axial temperature profile of sorbet as a function of mix flow rate at rotational speed of 78.5 rad.s^{-1} and refrigerant fluid temperature of -15.3 °C. FP = Freezing point temperature -2.6 °C. 170

Fig. 5.2.10. Residence time distribution as a function of mix flow rate at rotational speed of 78.5 rad.s^{-1} and refrigerant fluid temperature of -15.3 ºC. 171

Fig. 5.2.11. Axial temperature profile of sorbet as a function of rotational speed at mix flow rate of 0.014kg.s^{-1} and refrigerant fluid temperature of -15.3°C. FP = Freezing point temperature -2.6 °C. 173

Fig. 5.2.12. Residence time distribution as a function of rotational speed at mix flow rate of 0.014 kg.s^{-1} and refrigerant fluid temperature of -15.3 ºC. 173

Article 3

Fig. 5.3.1. Schematic representation of the experimental platform. 1. Refrigerated storage tank (200 l capacity). 2. Volumetric piston pump. 3. Freezer. 4. Contraction/enlargement pipe. 5. Pt100 probe inserted into the inlet of the rheometer. 6. Pipe rheometer. 7. Pressure manometers. 8. Pt100 probe inserted into the outlet of the rheometer. 9. Product exit .. 188

Fig. 5.3.2. Flow behavior curves for sorbet at different temperatures and ice volume fractions. (A) Sorbet at -2.89 °C and $\phi_{v.ice}$ = 0.058. (B) Sorbet at -3.11 °C and $\phi_{v.ice}$ = 0.106. (C) Sorbet at -3.44 °C and $\phi_{v.ice}$ = 0.166. (D) Sorbet at -3.90 °C and $\phi_{v.ice}$ = 0.234. (E) Sorbet at -4.55 °C and $\phi_{v.ice}$ = 0.305. (F) Sorbet at -5.68 °C and $\phi_{v.ice}$ =0.390. Power law model along with the fitted indices correspond only to the rheological measurement of sorbet at a mix flow rate of 0.007 kg.s^{-1} and 78.5 rad.s^{-1}. 194

Fig. 5.3.3. Measured apparent viscosity of sorbet at different temperatures, mix flow rate of 0.007 kg.s^{-1} and dasher speed of 78.5 rad.s^{-1} as function of the shear rate. 198

Fig. 5.3.4. Experimental uncertainty of the apparent viscosity of sorbet flowing through pipes of different diameters as a function of the ice volume fraction. 200

Fig. 5.3.5. Comparison between experimental and predicted values of the flow behaviour index as a function of the ice volume fraction. 203

Fig. 5.3.6. Comparison between experimental and predicted values of the apparent viscosity of sorbet at different temperature and different ice volume fractions. 204

Article 4

Fig. 5.4.1. Schematic representation of the experimental platform. 1. Refrigerated storage tank (200 l capacity). 2. Volumetric piston pump. 3. Freezer. 4. Contraction/enlargement pipe. 5. Pt100 probe inserted into the inlet of the rheometer. 6. Pipe rheometer. 7. Pressure manometers. 8. Pt100 probe inserted into the outlet of the rheometer. 9. Product exit. 215

Fig. 5.4.2. (A) Flow behaviour of sorbet mix and frozen sorbet as a function of the ice volume fraction at mix flow rate of 0.007 kg.s^{-1} and rotational speed of 78.5 rad.s^{-1}. (B) Flow behaviour of sorbet at -3.9 °C ($\phi_{v.ice}$ = 0.23) as a function of the air volume fraction ($\phi_{v.a}$) at mix flow rate of 0.007 kg.s^{-1} and rotational speed of 78.5 rad.s^{-1}. 221

Fig. 5.4. 3. (A) Apparent viscosity of sorbet mix and frozen at 10s^{-1} as a function of ice volume fraction at mix flow rate of 0.007 kg.s^{-1} and rotational speed of 78.5 rad.s^{-1}. (B) Apparent viscosity of aerated frozen sorbet at 10s^{-1}, as a function of air volume fraction $\phi_{v.a}$, at $\phi_{v.ice}$ of 0.23, mix flow rate of 0.007 kg.s^{-1} and rotational speed of 78.5 rad.s^{-1} 222

Article 5

Fig. 5.5.1. Schematic diagram of pilot Freezer WCB MF 50. 1. Inlet connection for sorbet mix. 2. Inlet cover bowl. 3. Rotor. 4. Scraper blades. 5. Freezer jacket with vaporizing r22. 6. Heat exchange cylinder. 7. Outlet cover bowl. 8. Outlet pipe for sorbet..... 232

Fig. 5.5.2. Schematic representation of the considered plug flow behaviour of the SSHE ... 235

Fig. 5.5.3. Schematic representation of the considered residence time distribution behaviour of the SSHE. 243

Fig. 5.5.4. Plug flow model predicted mean values of temperature T, ice volume fraction φ, mean crystal chord length C_i, surface mean crystal chord length $C_{i3.2}$ and apparent viscosity η_{app} at $\dot{\gamma}$ = 10 s^{-1} during the freezing of sorbet in the SSHE at $\dot{V}$ = 0.014 kg.s^{-1}, N_R = 78.5 rad.s^{-1} and T_{rf} = -15.3 °C. Point D = end of heat exchange cylinder. Point E = outlet of the SSHE (measurement point). 246

Fig. 5.5.5. RTD curve during the freezing of sorbet in the SSHE at $\dot{V}$ = 0.014 kg.s^{-1}, N_R = 78.5 rad.s^{-1} and T_{rf} = -15.3 °C. 248

Fig. 5.5.6. RTD model predicted mean values of draw temperature T, ice volume fraction φ, mean crystal chord length C_i, surface mean crystal chord length $C_{i2,3}$ and apparent viscosity η_{app} at $\dot{\gamma} = 10$ s^{-1} during the freezing of sorbet in the SSHE at $\dot{V} = 0.014$ kg.s^{-1}, $N_R = 78.5$ rad.s^{-1} and $T_{rf} = -15.3$ °C. 249

Fig. 5.5.7. Ice crystals number density CSD at different residence times t_T, during ice crystallization of sorbet in the SSHE at $\dot{V} = 0.014$ kg.s^{-1}, $N_R = 78.5$ rad.s^{-1} and $T_{rf} = -15.3$ °C. 251

Fig. 5.5.8. Comparison between the CSDs predicted by the plug flow (PF) and the residence time distribution (RTD) models at mean residence times t_T during the ice crystallization of sorbet in a SSHE at 0.014 kg.s^{-1}, 78.5 rad.s^{-1} and -15.3 °C. 252

Fig. 5.5.9. Comparison of the predicted values of draw temperature (A) and mean chord length (B) by the PBE-PF and the PBE-RTD models with the experimental measurements during the ice crystallization of sorbet in a SSHE for the operating conditions tested. 254

List of Tables

Chapter 2 – Background

Table 2.1. Summary of RTD studies of Non-Newtonian shear thinning fluids in SSHEs under isothermal and cooling conditions. 62

Table 2.2. Rheological models to predict the viscosity of a Newtonian suspension as a function of the volume fraction of particles. 68

Chapter 4 - Articulation of scientific papers

Table 4.1. Central composite experimental design carried out in article 1 104

Table 4.2. Operating conditions tested during the experiments carried out in article 2..... 107

Table 4.3. Operating conditions tested during the experiments carried out in article 3..... 109

Table 4.4. Operating conditions tested during the measurements carried out in article 4..... 111

Table 4.5. Operating conditions tested during the modelling study carried out in article 5 113

Chapter 5 - Results and discussion

Article 1

Table 5.1.1. Real freezing conditions during measurements and obtained responses 133

Table 5.1.2. Analysis of variance for responses of mean chord length and draw temperature.... 134

Table 5.1.3. Regression coefficients of the experimental behavior model and significance levels at 95% (p-values) for responses of mean chord length and draw temperature 134

Article 2

Table 5.2.1. Summary of RTD studies of Non-Newtonian shear thinning fluids in SSHEs under isothermal and cooling conditions 152

Table 5.2.2. Physical properties of the working fluid at different temperatures..... 154

Table 5.2.3. Geometrical characteristics of the SSHE WCB® Model MF 50 155

Table 5.2.4. Operating conditions and calculated flow regimes during RTD experiments ... 160

Table 5.2.5. Flow regimes criteria according to Härröd (1986) 163

Table 5.2.6. RTD experimental and modelling data at different refrigerant fluid temperatures at 0.014kg.s^{-1}and 78.5 rad.s^{-1} 168

Table 5.2.7. RTD experimental and modelling data at different mix flow rates at -15.3 ºC and 78.5 rad.s^{-1} 171

Table 5.2.8. RTD experimental and modelling data at different dasher rotation speeds at 0.014kg.s^{-1} and -15.3 ºC 174

Article 3

Table 5.3.1. Rheological models to predict the viscosity of a Newtonian suspension as a function of the volume fraction of particles 186

Table 5.3.2. Operating conditions, used rheometer pipes (diameter d_i) and estimated values of Nahme number (*Na*) for sorbet produced at different draw temperatures and different product flow rates at dasher speed = 78.5 rad.s^{-1} 195

Table 5.3.3. Operating conditions and measured responses during the rheology experiments ... 196

Table 5.3.4. Measured responses during the rheology experiments 197

Article 4

Table 5.4.1. Operating conditions and experimental data obtained during the rheology measurements for non aerated sorbet and for aerated sorbet, produced at a flow rate of 0.007 kg.s^{-1} and dasher rotational speed of 78.5 rad.s^{-1} 220

Article 5

Table 5.5.1. Operating conditions and obtained responses during the ice crystallization modelling 245

Framework of this work

This research is part of the European Project CAFÉ "Computer Aided Food processes for control Engineering" (Project number 212754). This project aims to improve the operation modes of several food processes, including the lyophilization process of lactic acid bacteria (preservation process), microfiltration of beverages (separation process), wine fermentation (bioconversion process) and crystallization of sorbet (structuring process).

The main objectives of the CAFÉ project are firstly, to obtain a better control of the final quality of the product, and secondly, to reduce the operation costs and the environmental impact of these food processes. In this project, Irstea and AgroParisTech are the responsible for the understanding and the improvement of the freezing process of ice creams and sorbets.

Two PhD theses were carried out for the characterization of the freezing process within the framework of the CAFÉ project: the PhD work achieved by Gonzalez (2012) and the present PhD work.

The work reported by Gonzalez (2012) concerned the experimental characterization of the energy consumption of the process and a contribution to the improvement of the online automatic control of the operating conditions of the freezing process.

This work concerns the experimental characterization and modelling of the freezing process of sorbet, so as to provide a better understanding of the ice crystallization kinetics taking place during the process and to improve the product quality control.

This work is also the continuation of a first research on the flow and heat transfer during the freezing of water-sucrose solutions in a SSHE at the pilot and laboratory scale, carried out by Cerecero in 2003, and a second research that investigated the thermo-physical properties of water-sucrose solutions, ice cream and sorbet during the freezing process in a batch SSHE at the laboratory scale, carried out by Haddad in 2009.

Chapter 1 - Introduction

Chapter 1 - Introduction

1.1. General introduction

Sorbet is an aerated frozen dessert, made of a fruit concentrate, sweeteners and stabilizers (polysaccharides). Sorbet is as the same time a dispersion and a foam. The dispersion consists of ice crystals distributed randomly in a freeze-concentrated continuous liquid phase, which is composed of water, sugars, stabilizers and salts. The foam consists of air bubbles dispersed randomly in the liquid phase. As with all processed foods, the physical and sensory properties of sorbet are determined by its microstructure. In order to deliver a product with a smooth texture and good palatability, it is necessary to obtain a small mean ice crystal size (<50 μm) and a narrow ice crystal size distribution.

The most critical stage in the manufacturing of sorbet is the initial freezing process, which is carried out in a scraped surface heat exchanger (SSHE). This process represents the only step of creation of ice crystals. During the subsequent hardening step, the existing ice crystals will grow to adjust the ice content, following the equilibrium freezing point curve. Therefore, the main objective of the initial freezing process is to form the smallest possible ice crystals, so as to assure a smooth texture in the final product.

From an industrial point of view, the progress in the control and the design of the freezing process within the manufacturing of frozen desserts has been performed by using an empirical approach. The choice of the operating conditions of the freezing process is based on trial-and-error results. Manufacturers have limited understanding about the influence of the operating conditions of the freezing process on the ice crystallization kinetics and on the development of the texture of the product.

The ice crystallization mechanism in a SSHE is exceedingly complex and involves coupled interactions of fluid flow, heat transfer, phase change and shear. The optimization of

the initial freezing process requires thus a good control of the operating conditions and the understanding of the development of the ice crystals inside the SSHE. The ice crystallization mechanism is affected by the operating conditions of the freezing process, such as the evaporation temperature of the refrigerant fluid, the dasher rotational speed, the product flow rate and the amount of air incorporated into the product. The temperature of the refrigerant fluid vaporizing in the jacket of the SSHE determines the heat removal rate, and provides the driving force for ice crystal nucleation and growth. It also determines the apparent viscosity and the flow behaviour of the product. The product flow rate governs the residence time of the product and its flow behaviour and the time available to remove heat from the product, affecting consequently, the ice nucleation and growth phenomena. The rotation of the scraper blades affects the flow behaviour and determines the shear applied to the product. It also improves the heat transfer rate between the refrigerated SSHE wall and the product, but simultaneously increases the amount of frictional heat generated by the blades, which could dissipate into the product and affect the heat removal rate. Finally, the amount of air incorporated into the product affects in part the apparent viscosity of the product, the ice crystal size and the heat removal rate of the system, since air bubbles act as an insulating material.

From a scientific point of view, the stakes are to study the coupling of the different phenomena occurring during the ice crystallization process as a function of the freezing operating conditions, so as to improve the understanding of the development of the ice crystals in the SSHE and consequently aid to improve the product quality control. The experimental characterization and the modelling of the freezing process make it possible to have a better understanding of the coupled interactions between the different phenomena occurring in the SSHE.

1.2. Methodology

The methodology adopted in this work consisted first on a bibliographic review that responds to a certain number of scientific questions about the coupled interactions between ice crystallization kinetics, fluid flow, heat transfer and shear, occurring during the initial freezing process. This review made it possible to identify the knowledge gaps in the ice crystallization process that needed to be addressed. The research in this work was then focused on the development of new knowledge that can be useful for the optimization of the freezing process.

The experimental characterization of the freezing process of sorbet was carried out in a continuous SSHE at the laboratory pilot scale. The SSHE was instrumented with online sensors such as the focused beam reflectance measurement (FBRM) probe and a Pt100 probe, to follow in situ the evolution of the ice crystal size distribution and the temperature of the product, respectively, as a function of the operating conditions of the process. These measurements make it possible to understand the relationship between heat transfer and the ice crystallization kinetics taking place in the SSHE.

The apparent viscosity of the product was measured in situ as a function of the temperature of the product, by means of a pipe viscometer developed and built in our laboratory and connected at the exit of the SSHE. These measurements allow us to understand the coupling of the interactions between the product temperature and apparent viscosity on the effects on the fluid flow behaviour in the SSHE.

Furthermore, the experimental study and modelling of the residence time distribution (RTD) of the product as a function of the operating conditions of the freezing process was carried out. These measurements make it possible to understand the interactions between heat transfer and fluid flow behaviour in the SSHE.

Finally, two modelling approaches of the ice crystallization process are presented. The first modelling approach combines heat transfer and population balance (PB) equations for the

ice nucleation, growth and breakage of the ice crystals, assuming plug flow. The second approach is a coupled model of heat transfer and PB equations combined with an empirical RTD model, which makes it possible to take into account the fact that the fluid fractions flowing throughout the SSHE do not have the same time-temperature history.

This approach was first conducted for the freezing of sorbet without aeration. Feasibility tests performed for the characterization of the freezing process with aeration will also be presented. The influence of the amount of air incorporated into the sorbet was assessed on the apparent viscosity of the product.

1.3. Structure of the thesis

The manuscript is organized as follows:

Chapter 2 – Background, presents a bibliographic review of four main topics: the mechanism of ice crystallization in a SSHE, an overview about heat transfer, flow behaviour and residence time distribution in SSHEs, a review of the characterization of the rheological properties of sorbet and the bases for the ice crystallization modelling.

Chapter 3 – Materials and methods, presents a brief description of the experimental platform and its instrumentation.

Chapter 4 – Scientific papers articulation, presents a brief description of the scientific articles which constitute the presentation of the results and discussion of the thesis. Four scientific papers are consecrated to the study of the freezing process of sorbet without aeration, and a communication paper presents the feasibility tests for the study of the freezing process with aeration.

Chapter 5 – Results and discussion, presents the full text of the four scientific articles and the communication.

Chapter 6 – Conclusion and perspectives, presents a summary of the observed trends based on the results obtained. Further research recommendations are also given for subsequent work.

Finally, the supporting materials are collected in the appendix.

Cadre de ce travail

Ce travail de thèse s'inscrit dans le cadre des travaux de recherche du projet européen CAFÉ « Computer Aided Food processes for control Engineering » (Numéro de projet 212754). Ce projet vise à améliorer les modes opératoires de divers procédés alimentaires, dont le procédé de lyophilisation des bactéries lactiques (procédé de conservation), la microfiltration des boissons (procédé de séparation), la fermentation du vin (procédé de bio-conversion) et la cristallisation du sorbet (procédé de structuration). Les principaux objectifs du projet sont d'une part, d'obtenir une meilleure maîtrise de la qualité finale du produit et d'autre part, de réduire les coûts opérationnels et l'impact environnemental du procédé. Dans ce projet, Irstea et AgroParisTech travaillent en collaboration et sont responsables de la compréhension et de l'amélioration du procédé de congélation des crèmes glacées et des sorbets.

Deux thèses de doctorat ont été effectuées autour de la caractérisation expérimentale du procédé de congélation dans le cadre du projet CAFÉ: le travail de thèse de doctorat réalisé par Gonzalez (2012) et le travail de la présente thèse. Le travail effectué par Gonzalez (2012) concerne la caractérisation expérimentale de la consommation énergétique du procédé et une contribution à l'amélioration du contrôle automatique en ligne des conditions opératoires du procédé de congélation. Le travail de la présente thèse porte sur la caractérisation expérimentale et la modélisation du procédé de congélation du sorbet, afin d'apporter une meilleure compréhension des cinétiques de cristallisation qui ont lieu pendant le procédé et d'améliorer le contrôle de la qualité du produit.

Ce travail est également la suite d'une première étude, portant sur l'écoulement et le transfert de chaleur lors de la congélation de solutions eau-saccharose dans des ECSR aux échelles pilote et laboratoire, effectuée par Cerecero en 2003, et une deuxième étude portant sur les propriétés physiques des solutions eau-sucre, ainsi que de mix de sorbets et de crèmes glacées lors du procédé de congélation dans un ECSR batch à l'échelle laboratoire, effectuée par Haddad en 2009.

Chapitre 1 - Introduction

Chapitre 1 - Introduction

1.1. Introduction générale

Un sorbet est un dessert congelé et aéré, fabriqué à partir de jus de fruit concentré, de sucres et de stabilisants (polysaccharides). Le sorbet est à la fois une dispersion et une mousse. La dispersion consiste en une distribution aléatoire de cristaux de glace dans une phase liquide continue (concentrée par congélation). La mousse consiste en une distribution aléatoire des bulles de gaz dans la phase liquide. Comme tous les aliments transformés, les propriétés physiques et sensorielles du sorbet sont déterminées par la microstructure du produit. Afin de conférer une texture lisse au produit final et d'améliorer l'acceptation par le consommateur, il est nécessaire d'obtenir une petite taille de cristaux de glace (<50 μm) et une distribution étroite de taille de cristaux de glace.

L'étape la plus critique dans la fabrication des crèmes glacées et des sorbets est le procédé de congélation, qui est effectué dans un échangeur de chaleur à surface raclée (ECSR). Ce procédé est la seule étape de formation des cristaux de glace. Pendant l'étape suivante de durcissement, les cristaux de glace existants grossissent pour ajuster la teneur en glace dans le produit, en suivant la courbe du liquidus (à l'équilibre). Ainsi, le principal objectif du procédé de congélation consiste à former des cristaux de glace avec la plus petite taille possible, afin d'assurer une texture lisse dans le produit final.

Du point de vue industriel, des progrès dans le contrôle et la conception du procédé de congélation pour la fabrication des desserts congelés ont été réalisés par une approche empirique. En effet, le choix des conditions opératoires du procédé de congélation s'effectue en procédant par tâtonnement. Les fabricants ont une compréhension limitée de l'influence des conditions opératoires du procédé de congélation sur les cinétiques de cristallisation et le développement de la texture du produit.

Le mécanisme de cristallisation dans un ECSR est particulièrement complexe et il implique le couplage des phénomènes d'écoulement du produit, de transfert de chaleur, de changement de phase et de cisaillement. Ainsi, l'optimisation du procédé de congélation exige un bon contrôle des conditions opératoires et une bonne compréhension du développement des cristaux de glace dans l'ECSR. Le mécanisme de cristallisation de la glace est influencé principalement par les conditions opératoires du procédé de congélation, comme la température d'évaporation du fluide frigorigène, la vitesse de rotation des lames racleuses, le débit de mix introduit dans le système et la quantité d'air incorporé dans le produit. La température du fluide frigorigène en évaporation dans la double enveloppe de l'ECSR, détermine la quantité de chaleur évacuée du produit et est le moteur de la nucléation et la croissance des cristaux de glace. Elle détermine aussi la viscosité du produit et le comportement de l'écoulement du fluide. Le débit de mix introduit dans le système affecte le temps de séjour du produit dans l'ECSR, c'est-à-dire le temps disponible pour évacuer la chaleur du produit et, par conséquent, les phénomènes de nucléation et de croissance des cristaux de glace. La vitesse de rotation des lames racleuses détermine le niveau de cisaillement appliqué au produit. Une augmentation de cette vitesse de rotation améliore le transfert de chaleur entre la paroi du cylindre d'échange et le produit, mais dans le même temps elle augmente la chaleur de friction, générée par les lames, qui est dissipée dans le produit. Finalement, la quantité d'air incorporé dans le produit lors du procédé de congélation affecte la viscosité apparente du produit et la taille des cristaux de glace. L'incorporation d'air dans le produit influe également sur le taux d'élimination de la chaleur du produit, du fait des propriétés isolantes des bulles d'air.

Du point de vue scientifique, l'enjeu est d'étudier le couplage des différents phénomènes qui ont lieu pendant le procédé de cristallisation en fonction des conditions opératoires de congélation, afin d'améliorer la compréhension du développement des cristaux

de glace dans l'ECSR et, par conséquent, d'améliorer le contrôle de la qualité du produit. La caractérisation expérimentale et la modélisation du procédé de congélation permettent d'avoir une meilleure compréhension du couplage des différents phénomènes qui ont lieu dans l'ECSR.

1.2. Méthodologie

La méthodologie adoptée dans ce travail commence par une étape d'étude bibliographique qui répond à un certain nombre de questions scientifiques sur les couplages des phénomènes des cinétiques de cristallisation, de l'écoulement du produit, du transfert de chaleur et du cisaillement qui ont lieu dans le procédé de congélation. Cette étude bibliographique a permis d'identifier les lacunes présentes dans la compréhension du procédé de cristallisation de la glace. Ensuite, ce travail s'est focalisé sur le développement des nouvelles connaissances qui peuvent être utiles pour l'optimisation du procédé de congélation.

La caractérisation expérimentale du procédé de congélation a été effectué dans un ECSR continu à l'échelle pilote. L'ECSR a été instrumenté avec des capteurs en ligne, tels que la sonde FBRM (Focused Beam Reflectance Measurement) et une sonde Pt100, afin de suivre respectivement l'évolution de la distribution de taille des cristaux de glace et la température de sortie du produit in situ, en fonction des conditions opératoires du procédé. Ces mesures expérimentales ont permis de comprendre la relation entre le transfert de chaleur et les cinétiques de cristallisation de la glace qui ont lieu dans un ECSR.

La viscosité apparente du produit a été mesurée in situ en fonction de la température du produit, au moyen d'un viscosimètre tubulaire construit dans notre laboratoire et connecté directement à la sortie de l'ECSR. Ces mesures ont rendu possible la compréhension du couplage entre la température du produit, la viscosité apparente et les effets sur le comportement du fluide dans l'ECSR.

En outre, une étude expérimentale et une modélisation de la distribution de temps de séjour (DTS) du produit en fonction des conditions opératoires du procédé ont été effectuées. Ces mesures ont permis de comprendre les interactions entre le transfert de chaleur et le comportement de l'écoulement du fluide dans l'ECSR.

Finalement, deux approches de modélisation de la cristallisation de la glace sont présentées. La première approche combine des équations de transfert de chaleur et de bilan de population, en supposant un écoulement de type piston. La deuxième approche est un couplage des équations de transfert de chaleur et de bilan de population avec un modèle empirique DTS, qui permet de prendre en compte le fait que les différentes fractions de fluide s'écoulant à travers l'ECSR n'ont pas le même temps de séjour dans l'échangeur et engendrent des différences de traitement thermique.

Cette démarche a été suivie pour la congélation du sorbet sans aération. Des tests de faisabilité effectués pour la caractérisation du procédé de congélation avec aération seront également présentés. L'influence de la quantité d'air incorporé dans le sorbet sur la viscosité apparente du produit a notamment été évaluée.

1.3. Structure de la thèse

Le mémoire est organisé de la façon suivante:

Le Chapitre 2 – Étude bibliographique, présente une synthèse bibliographique sur quatre sujets principaux: le mécanisme de cristallisation de la glace dans un ECSR, un aperçu sur le comportement de l'écoulement, le transfert de chaleur et la distribution des temps de séjour dans un ECSR, une étude sur la caractérisation des propriétés rhéologiques des sorbets et les bases pour la modélisation de la cristallisation de la glace.

Le Chapitre 3 – Matériels et méthodes, présente une brève description de la plateforme expérimentale et son instrumentation.

Le Chapitre 4 – Articulation des publications scientifiques, présente une brève description des articles scientifiques qui constituent la présentation des résultats et discussion de la thèse. Quatre articles scientifiques sont consacrés à l'étude du procédé de congélation du sorbet sans aération, et une communication scientifique présente les essais de faisabilité pour l'étude du procédé de congélation avec aération.

Le Chapitre 5 – Résultats et discussion, compile les textes complets des quatre articles scientifiques et la communication.

Le Chapitre 6 – Conclusions et perspectives, présente une synthèse des tendances observées sur la base des résultats obtenus. Des recommandations pour des travaux ultérieurs sont également données.

Finalement, des documents d'appui sont donnés dans les annexes.

Chapter 2 - Background

Chapter 2 - Background

This bibliographic review provides the available information in the literature for the understanding of the influence of the freezing operating conditions on the ice crystallization process in SSHEs. This section is divided in four main topics, and each topic broaches different scientific questions.

- Ice crystallization mechanism in SSHEs
  - What are the mechanisms of ice crystallization in sorbet manufacturing?
  - What are the operating conditions of the freezing process that most directly affect the formation of the ice crystals in the SSHE, and how they affect product quality?
- Fluid flow behaviour and heat transfer in SSHEs
  - How the product temperature and fluid flow profiles are affected by the operating conditions of the freezing process?
  - What is the influence of the operating conditions of the freezing process on the residence time distribution and the product flow behaviour in the SSHE?
- Rheological properties of sorbet
  - What are the rheological behaviour and the apparent viscosity of sorbet?
  - What are the effects of the ice content and the amount of air incorporated within sorbet on the apparent viscosity of the product as it flows out from the SSHE?
- Modelling approaches for the ice crystallization mechanism
  - What are the available modelling approaches in the literature for the ice crystallization process in a SSHE?
  - How the coupled interactions between the ice crystallization kinetics, heat transfer, fluid flow behaviour and shear have been combined for the modelling of the freezing process?

2.1. Sorbet manufacturing process

The manufacturing process of sorbet requires several stages; firstly, the ingredients are blend together in order to constitute the mix, this mix is then pasteurized, homogenized, cooled and ripened at 5 °C for a duration between 12 to 24 h. Subsequently, during the initial freezing stage, the mix is pumped into a scraped surface heat exchanger (SSHE) or freezer, where roughly half of the total amount of water is frozen (Hartel, 1996). Depending on the formulation and the operating conditions of the process, the product exits the SSHE at a draw temperature between -4 to -6 °C, having an adequately low viscosity to be pumped for moulding and packaging. Afterwards, during the hardening stage, the sorbet is introduced into a blast freezer to attain a core temperature of -18 °C (Cook & Hartel, 2010), where roughly 80% of the amount of water is frozen (Marshall et al. 2003). The final product is then stored and distributed at temperatures between -18 °C to -30 °C (Ben-Yoseph and Hartel, 1998).

The most critical stage in the manufacturing of sorbet is the initial freezing process. This process represents the only stage where new ice crystals are produced. During the hardening step, the existing ice crystals will grow to adjust the ice content, following the equilibrium freezing point curve. Hence, the final ice crystal size of the product will be governed to a large extent by the evolution during the hardening step of the ice crystals that were formed during the initial freezing. Therefore, it is important to have a good control of the ice crystal nucleation and growth during the initial freezing in the SSHE, so as to produce ice crystals with the smallest possible ice crystal size and assure a smooth texture in the final product.

A continuous SSHE is composed of a stationary heat exchange cylinder (barrel) that is surrounded by a cooling jacket in which a refrigerant fluid is vaporizing; and an internal rotating cylinder (dasher) that is equipped with scraping blades. During freezing, ice nucleation occurs at the heat exchanger wall, where there is enough subcooling (roughly

between -15 to -30 °C) between the refrigerant fluid and the mix to form ice nuclei (Hartel, 1996). As the ice crystal slush layer forms at the wall, the blades of the dasher continually scrape off the ice crystals and disperse them into the bulk fluid of the mix at the core of the exchanger, as shown schematically in Fig. 2.1. Simultaneously, the scraping action of the blades will reduce the size of the air bubbles that are introduced into the SSHE, and incorporate them into the bulk fluid.

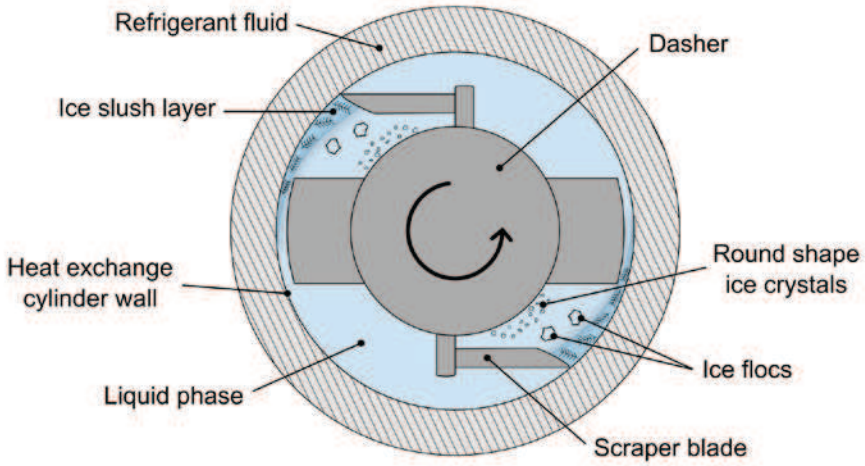


Fig. 2.1. Schematic representation of the ice crystallization mechanism in a SSHE.

The mean size of the ice crystals that exit from the SSHE is within the range between 15 to 27 µm (Drewett and Hartel, 2007; Marshall et al., 2003; Russell et al., 1999; Sofjan and Hartel, 2004). The mean size of the air bubbles at the outlet of the SSHE is within the range between 12 to 23 µm depending on the amount of air incorporated into the product (Sofjan and Hartel, 2004; Goff et al., 1995).

2.1.1. Ice crystallization mechanism in a SSHE

Schwartzberg and Liu (1990) proposed a model for the ice crystallization mechanism in SSHEs. Based on observations of dendritic growth during the quiescent freezing of sucrose

solutions on a chilled surface, these authors suggested that due to the high rate of subcooling at the heat exchange cylinder wall, dendrites are likely to grow there, then are cut off and dispersed into the bulk flow by the scraper blades of the dasher. The dendrites are then ripened and become round shape ice crystals in the bulk warm region of the SSHE. Schwartzberg (1990) reported that the space between dendrites was proportional to the freezing rate to the -1/2 power, which means that high subcooling rates lead to a faster growth of more dendrites, with closely spaced branches and a thinner structure.

Sodawala and Garside (1997) used video microscopy to examine the freezing of a 10% sucrose solution on a cold surface with a rotating scraper blade. These authors observed the formation of ice in flocs which grew parallel to the surface after each scrape, then merged and grew vertically. They also observed that at low scraping speeds the ice flow were removed from the freezing surface and transported into the bulk solution. They also reported that an increase in the scraping frequency of the blade led to more frictional heat and to smaller flocs being cut off from the surface.

Cebula and Russell (1998) distinguished two different zones in which the freezing of ice cream occurs in a SSHE: a wall zone and a bulk zone. The freezing at the wall zone was simulated by a cold plate upon which a thin layer of ice cream mix was spread, and frozen at temperatures close to the temperatures of the heat exchanger wall. Based on observations of a cross section by scanning electron micrographs, these authors reported in the region adjacent to the cold surface the formation of small globular ice crystals, the effect of which was attributed to heterogeneous nucleation due to the sufficient subcooling in this zone. Further away from the surface, they also observed the formation of columnar ice crystals which do not attached themselves to the wall, but that grow out from the small nuclei near the cold surface. Visualization experiments on the crystallization of sucrose solutions on a cooled surface with a rotating scraper blade, showed that immediately after the surface was scraped,

fragments of ice remained attached to the surface and served as points of growth for 'islands' of new ice that subsequently came together into a solid layer depending on the scraping frequency of the blades. For the simulation of the bulk zone, Cebula and Russell (1998) used a two stage freezer: in the first freezer the ice crystals were formed, and in the second freezer no cooling was employed so that there was no new ice crystals formed. Experiments at constant residence time and different dasher speeds to vary the mechanical energy dissipated into the system showed that the increase in the amount of mechanical heat reduced significantly the number of ice crystals and increase the ice crystal size. This effect was attributed to the melting of the smaller ice crystals with the increase in the energy input.

More recently, on the basis of thermal conductivity measurements of a sucrose solution in a flowcell equipped with a scraper blade and a chilled surface, Zheng (2006) concluded that the ice layer formed at the freezer wall was in fact a slush layer composed of both ice and concentrated sucrose solution. Zheng (2006) also observed that after each scrape of the blade, many ice nuclei grew rapidly from the ice debris remaining from previous scraping, and continued to grow along the chilled surface before merging and growing vertically. It was then concluded that the main effect of the scraper blades was to induce the secondary nucleation at the surface.

2.1.2. Influence of the operating conditions on ice crystallization in SSHEs

The temperature of the refrigerant fluid determines the heat removal rate of the system and provides the driving force for ice nucleation and growth. Lower refrigerant fluid temperatures result in a faster freezing and consequently lead to the formation of smaller ice crystals. Koxholt et al. (2000) as well as Drewett and Hartel (2007) reported ice creams with

smaller ice crystals by using low refrigerant fluid temperatures, the effect of which was attributed to the higher subcooling applied to the product which enhanced the nucleation rate.

The scraping action of the dasher improves the heat transfer rate between the freezer wall and the product (Ben Lakhdar et al., 2005). Higher dasher speeds would thus be expected to give lower draw temperatures and smaller ice crystals. However, an increase in dasher speed would also increase the amount of frictional heat generated by the blades and the viscous dissipation, producing warmer draw temperatures. This effect will cause the melting of the small ice nuclei, and consequently, the reduction in the effective ice nucleation rate (Cebula and Russell, 1998). Furthermore, an increase in dasher speed may also lead to the attrition of the larger ice crystals (Haddad, 2009; Windhab and Bolliger, 1995). The scraping action of the blades would also be expected to produce new smaller ice nuclei from the ice debris remaining of previous scrapings at the cooling surface by secondary nucleation (Sodawala and Garside, 1997; Zheng, 2006). It has been demonstrated that the dasher speed has an effect on the ice crystal size. However, not all the studies available in literature are in agreement as to its effects. An increase in dasher speed has been found to increase (Russell et al., 1999; Drewett and Hartel, 2007), to decrease (Inoue et al., 2008) and not to affect (Koxholt et al., 2000) the ice crystal size.

The mix flow rate determines the residence time of the product, affecting the time available to remove heat from the product, and consequently, the ice nucleation and growth mechanisms of ice crystals. A number of studies in the literature have observed that high mix flow rates (short residence times) for a given draw temperature (by adjusting the temperature of the refrigerant fluid) and dasher speed produced smaller ice crystals due to the reduction in recrystallization phenomena in the bulk region of the product (Drewett and Hartel, 2007; Koxholt et al., 2000; Russell et al., 1999). For a given refrigerant fluid temperature (varying exit temperature) and dasher speed, Russell et al. (1999) also found smaller ice crystals

produced at higher mix flow rates, the effect of which was attributed to the reduction in ice crystal coarsening. During the freezing of 30% sucrose/water solutions in an SSHE, Ben Lakhdar et al. (2005) reported that low product flow rates (long residence times) led to a reduction in the exit temperature of the product, and therefore to an increase of the ice mass fraction in the product.

The incorporation of air within sorbet mix leads to the increase in the volume of the aerated sorbet over the volume of mix used. The volume fraction of air $\phi_{v.a.}$ is the ratio between the volume occupied by the air V_{air} (at atmospheric pressure) and the total volume of the aerated product V_{Total}, given by the following expression:

$$\phi_{v.a.} = \frac{V_{air}}{V_{mix} + V_{air}} = \frac{V_{air}}{V_{Total}} \qquad (1)$$

However, the percentage of overrun is a notion more widely used in the food industry and it can be defined as the ratio between the increase in volume due to the incorporation of air V_{air} to the initial volume of mix V_{mix}, written as follows:

$$Overrun = \frac{V_{air}}{V_{mix}} \times 100 \qquad (2)$$

The incorporation of air bubbles within the sorbet has an effect on the development of the ice crystals in the SSHE. During freezing, the scraping action of the blades leads to a reduction in the size of the air bubbles and disperse them continuously along with the ice crystals into the continuous liquid phase. Depending on the operating conditions of the SSHE, the commercial values of overrun are set from 80 to 100% (Drewett and Hartel, 2007; Russell et al., 1997). An increase in overrun has been found to decrease the ice crystal size (Inoue et al., 2008; Sofjan and Hartel, 2004). An increase in the amount of air would also be expected to slow the heat transfer rate in the SSHE since air behaves as an insulating material.

2.2. Flow behaviour in SSHEs

The flow behaviour in SSHEs is the result of axial flow through an annular gap (Poiseuille flow) due to the imposed product flow rate, and rotational flow (Couette flow) due to the rotation of the internal dasher and the scraping blades (Wang et al., 1998). The velocity vectors of these two flows form a helical fluid flow pattern in the middle section of the exchanger (Fayolle et al., 2005; Härröd, 1986; Yataghene et al., 2011). The axial flow can be characterized by the axial Reynolds number, Re_{ax}, and the rotational flow by the rotational Reynolds number, Re_r, and the rotational Taylor number, Ta_r. When the rotational flow is progressively increased, near a critical Taylor number, Ta_{rc}, the purely laminar flow becomes unstable and toroidal Taylor vortices appear (vortex flow), encircle the rotor and are piled up in the axial direction (Härröd, 1986). The transition from laminar flow to vortex flow has been widely studied for annular gap without blades, and reported to occur at a critical Taylor number $Ta_{rc} \approx 45$ for $r_r/r_c = 0.6$ (Cognet, 1984; Härröd, 1986). More recently, on the basis of visual and electrochemical techniques Dumont et al. (2000) studied the transition of flow patterns for shear thinning fluids through an annular gap in the presence of blades. These authors demonstrated that the transition between the laminar and vortex flow regime in SSHEs occurs at a critical Taylor number $Ta_{rc} \approx 80$ for $r_r/r_c = 0.6$.

Furthermore, the efficiency of the thermal treatment of the product strongly depends on the radial and axial dispersion in the SSHE. An increase in radial dispersion will enhance the heat transfer rate and ensure a more uniform thermal treatment of the product (Härröd, 1986). Contrariwise, an increase in axial dispersion will decrease the driving force for heat transfer, by reducing the temperature gradient between the heat transfer medium and the product (Trommelen and Beek, 1971; Härröd, 1986; Benezech and Maingonnat, 1989).

2.3. Temperature profile and heat transfer in SSHEs

The temperature distribution inside the SSHE is highly heterogeneous. The heat transfer at the wall creates a radial temperature gradient, with the lowest temperature at the wall. Temperatures at the wall vary within a range between -15 to -30 °C, then the temperature of the product rises from the wall to the core of the heat exchange cylinder. The axial temperature profile in the SSHE also varies significantly. Russell et al. (1999) measured the axial temperature profile at the wall region by means of thermocouples mounted on a scraper blade. These authors found that during the first 15% of the axial fraction length of the SSHE, the temperature of ice cream decreases rapidly to a temperature range between -5 to -7 °C. Then the product temperature decreases more slowly to reach a temperature range between -6 to -10 °C within the axial fraction length from 15 to 65% of the SSHE. Finally the temperature of the product increases at the outlet pipe of the SSHE. It was also reported that the increase in dasher speed led to the increase in the axial temperature profile of the product, the effect of which was attributed to the increase in the rate of mechanical dissipation.

The mechanism of heat transfer in a SSHE can be explained by the penetration theory, which describes the heat transfer mechanism in two steps: firstly, heat penetrates by molecular conduction into an immobile thin product layer along the heat exchanger wall during the time interval between two scraping blades. Secondly, a heat transfer convection stage, in which the thin product layer is detached from the wall by the scraper blades and assumed to be perfectly mixed within the rest of the product, and simultaneously, new product enters into contact with the cold surface of the heat exchange cylinder (Maingonnat and Corrieu, 1983).

The internal heat transfer coefficient was calculated by Latinen (1958) and Harriott (1969) from the measured amount of heat transferred between the internal face of the heat

exchanger wall and the product. The empirical relation for a votator SSHE proposed by Latinen (1958) to calculate the Nusselt number, Nu, is:

$$Nu = 1.6\, Re_r^{0.5}\, Pr^{0.5} \tag{3}$$

where Re_r is the rotational Reynolds number and Pr is the Prandtl number.

Harriott (1969) analysed the adequacy of Eq. 3 for the heat transfer coefficients in SSHEs for low viscosity fluids (water), and higher viscosity fluids such as carrot puree and oil. Results showed that the heat transfer coefficient predicted by Eq. 3 for carrot puree and oil were underestimated by 50%. The effect of which was attributed to the uncompleted mixing of the scraped off thin product layer within the bulk of the fluid in the case of higher viscosity fluids.

Qin et al. (2003) studied the heat transfer in a subcooled scraped surface with phase change during the freeze concentration of milk. The authors distinguished three stages of heat transfer during freezing: chilling, nucleation and crystallization. Experimental results showed that the heat transfer coefficient was 1.5 times larger during the ice crystallization stage that during the chilling stage, suggesting that the liberation of latent heat ice crystallization on the cold surface actually increased heat transfer.

Zheng (2006) studied the heat transfer during the freezing of a sucrose solution in a chilled surface with a scraper blade. Results showed that ice crystallization at the surface greatly increased heat transfer, due to the fact that heat could be transferred directly from the crystal, through the wall and to the refrigerant fluid, without having to be transmitted through the liquid.

Ben Lakhdar et al. (2005) reported the heat transfer study during the freezing of sucrose-water solutions in a SSHE at the pilot scale. These authors proposed an empirical relation to predict the internal heat transfer coefficient in terms of the rotational Reynolds number, Re_r, and the initial sucrose mass fraction concentration, w_o, written as:

$$Nu = 0.63\, Re_r^{0.61}\, w_o^{0.34} \tag{4}$$

The physical properties used in the dimensionless numbers were those of the diphasic product at the outlet of the SSHE. In particular, the Prandtl number takes into account the phase change because the latent heat of fusion appears in the apparent heat capacity.

2.4. Residence time distribution (RTD)

The ice crystallization mechanism that occurs during the initial freezing process is closely related to the residence time distribution (RTD) of the product. During ice crystallization, the phase change involved leads to an increase in the ice volume fraction, and to an increase in the apparent viscosity of the product. This effect modifies the fluid flow behaviour, the RTD of the product and the temperature profile inside the equipment. Furthermore, due to the different lengths of time that each fraction of fluid spends in the SSHE, each fluid fraction will have a different degree of thermal treatment and of shear rate, thus affecting the final ice crystal size distribution of the product.

The residence time distribution is useful to describe the flow behaviour of the fluid in the SSHE. Information on the RTD is also essential for the scale-up of the process. The RTD measurement technique consists of a pulse injection of a small amount of concentrated tracer at the inlet and the continuous measurement of the concentration-time tracer response at the product exit stream of the exchanger. The residence time of an element of fluid is defined as the time elapsed from its entry into the system until it reaches the exit. The RTD of a process can be characterized by the age distribution function $E(t)$, where $E(t)dt$ represents the fraction of fluid that has passed through the exchanger for a length of time between t and $t + dt$ (Danckwerts, 1953). For a pulse injection, the $E(t)$ function is given as:

$$E(t) = \frac{C(t)}{\int_0^\infty C(t)dt} \tag{5}$$

where $C(t)$ is the exit concentration of tracer at a certain time t (% w/w).

The normalization condition for the probability density $E(t)$ function implies that:

$$\int_0^\infty E(t)dt = 1 \tag{6}$$

The experimental mean residence time t_s is the first moment of the distribution defined as:

$$\mu_1 = t_s = \int_0^\infty t \cdot E(t)dt \tag{7}$$

For a fluid flow without dead volume, t_s is equal to the theoretical mean residence time τ given by Eq. (8):

$$\tau = \frac{V}{\dot{V}} \tag{8}$$

where V is the volume available to the fluid in the exchanger and $\dot{V}$ the volumetric flow rate. Normalized concentration $E(\theta)$ and time θ can be calculated by the following expressions:

$$\theta = \frac{t}{t_s} \tag{9}$$

$$E(\theta) = t_s \cdot E(t) \tag{10}$$

2.4.1. Residence time distribution in SSHEs

Sorbet behaves as a non-Newtonian shear-thinning fluid. Thus, this section will only review the available RTD studies for shear-thinning fluids. A number of studies in the literature have determined the RTD of non-Newtonian shear-thinning fluids flowing through SSHEs under isothermal conditions (Benezech and Maingonnat, 1989; Alcairo and Zuritz, 1990; Lee and Singh, 1991; Russell et al., 1997). However, there is a paucity of information available on the RTD of food products when crystallization occurs under cooling conditions (Russell et al., 1997; Belhamri, et al., 2009). At isothermal conditions, it has been demonstrated that the operating conditions, such as the product flow rate, the rotational speed and the apparent viscosity of the product, have an effect on the RTD of non-Newtonian fluids. Not all authors agree as to their effects, however. An increase in product flow rate has been found to narrow (Alcairo and Zuritz, 1990; Lee and Singh, 1991), or not to affect the RTD (Benezech and Maingonnat, 1989). An increase in rotational speed has been found to broaden

(Benezech and Maingonnat, 1989; Russell et al., 1997), to narrow (Alcairo and Zuritz, 1990) or not to affect the RTD (Lee and Singh, 1991). An increase in the apparent viscosity of the product has been found to broaden (Lee and Singh 1991) or not to affect the RTD (Benezech and Maingonnat, 1989; Alcairo and Zuritz, 1990). At cooling conditions, during the crystallization of water in ice cream, Belhamri et al. (2009) found that an increase in product flow rate and in rotational speed led to a narrowing of the RTD. Furthermore, in the case of ice cream freezing, Russell, et al. (1997) found that ice cream exhibited a broader RTD, as compared to a less shear-thinning fluid, Carbopol. Table 2.1 shows a summary of the observed effects by various authors on RTD studies of non-Newtonian shear-thinning fluids in SSHEs under isothermal and cooling conditions.

Table 2.1. Summary of RTD studies of Non-Newtonian shear thinning fluids in SSHEs under isothermal and cooling conditions.

RTD studies of Non-Newtonian shear thinning fluids in SSHEs under isothermal conditions

Reference	Non - Newtonian shear thinning fluid	Rotation speed effect	Product flow rate effect	Apparent viscosity effect
Benezech and Maingonnat, 1989	Aqueous Solutions of Guar gum, CMC, and Na Alginate	$\uparrow N_R$ broadened RTD	$\uparrow \dot{V}$ no effect on RTD	$\uparrow \eta_{app}$ no effect on RTD
Alcairo and Zuritz, 1990	A single sphere suspended in aqueous solutions of CMC	$\uparrow N_R$ narrowed RTD	$\uparrow \dot{V}$ narrowed RTD	$\uparrow \eta_{app}$ no effect on RTD
Lee and Singh, 1991	Potato cubes with aqueous solutions of CMC	$\uparrow N_R$ no effect on RTD	$\uparrow \dot{V}$ narrowed RTD	$\uparrow \eta_{app}$ broadened RTD
Russell et al., 1997	Carbopol	$\uparrow N_R$ broadened RTD	-	-

RTD studies of Non-Newtonian shear thinning fluids in SSHEs under cooling conditions

Reference	Non - Newtonian shear thinning fluid	Rotation speed effect	Product flow rate effect	Apparent viscosity effect
Russell et al., 1997	Carbopol and Ice cream	-	-	$\uparrow \eta_{app}$ broadened RTD
Belhamri et al., 2009	Ice cream	$\uparrow N_R$ narrowed RTD	$\uparrow \dot{V}$ narrowed RTD	-

2.5. Residence time distribution modelling

The experimental RTD data can be represented by hydrodynamic models that can be used to describe the flow pattern in the SSHE. Ideal models such as plug flow or completely mixed tank rarely represent accurately the flow behaviour in real reactors. In order to account for the deviations from ideal flow behaviour, non-ideal models such as the plug-flow with axial dispersion model (ADM) and the tank-in-series model (TSM) can be useful to represent the experimental RTD profile of real systems. Mathematical models such as the Gamma distribution model (GDM) approximate the exit age distribution of the reactor to the gamma distribution. Although, the GDM is not a hydrodynamic model, the influence of the model parameters on the flow behaviour can be interpreted (Wen and Fan, 1975). The main assumptions and equations for the last three models are given below before recalling the RTD modelling in the case of SSHEs.

2.5.1. Plug-flow with axial dispersion model (ADM)

The plug-flow with axial dispersion model assumes a tracer pulse dispersion process superimposed on a plug flow (Levenspiel, 1999). The model parameter is the Peclet number, which is defined as $Pe = uL/D_{ax}$, where u is the mean velocity in the exchanger, L is its length, and D_{ax} *is* the axial dispersion coefficient. The analytical solution of the axial dispersion model with open system boundary conditions is given by:

$$E(\theta) = \frac{1}{2}\left(\frac{Pe}{\pi \cdot \theta}\right)^{1/2} \exp\left(-\frac{Pe(1-\theta)^2}{4\theta}\right) \tag{11}$$

The lower the Peclet number is, the higher the axial dispersion is (Villermaux, 1993).

2.5.2. Tanks-in-series model (TSM)

The tanks-in-series model by assimilating the reactor to a number N of completely stirred tanks in series of the same volume. For this model the $E(\theta)$ function is calculated by:

$$E(\theta) = \frac{N \cdot (N \cdot \theta)^{N-1}}{(N-1)!} \exp(-N \cdot \theta) \tag{12}$$

For $N = 1$, the exchanger corresponds to a single completely stirred tank. When $N \to \infty$, the system approaches to a plug flow (Villermaux, 1993; Levenspiel, 1999).

2.5.3. The gamma distribution model (GDM)

The normalized age distribution $E(\theta)$ is approximated by the Γ-distribution, defined as:

$$E(\theta) = \frac{p^p}{(1-\theta_0)^p \Gamma(p)} (\theta - \theta_0)^{p-1} \exp\left[-p\left(\frac{\theta - \theta_0}{1-\theta_0} \right) \right] \tag{13}$$

where p and θ_0 are the model parameters and Γ denotes the gamma function defined as $\Gamma(p) = \int_0^\infty x^{p-1} e^{-x} dx$.

The parameter θ_0 is considered as a delay dimensionless time of the systems, defined as $\theta_0 = D/t_s$, where D represents the delay time, and t_s the mean residence time. The parameter p is related to the extent of fluid mixing in the axial flow direction. A decrease in both parameters θ_0 and p will increases the axial dispersion in the flow system (Wen and Fan, 1975).

2.5.4. RTD models used for the flow behaviour description in SSHEs

Benezech and Maingonnat (1989) reported the use of both the ADM and the TSM to describe the RTD of 3.8% (w/w) CMC/water solutions flowing through a SSHE at isothermal conditions. These authors found that both models represented the experimental RTD with the

same accuracy. For the ADM the Peclet numbers varied between 20 to 23 and for the TSM model the number of tanks-in-series reported was 11.

Russell et al. (1997) used as well the ADM and TSM model to represent the RTD of 0.4% (w/w) carbopol/water solutions flowing through a SSHE at isothermal conditions. These authors reported that the TSM was the most adequate model to represent the experimental RTD, followed by the ADM. The values obtained for the Peclet number and the tanks-in-series number were 35 and 18, respectively.

Alcairo and Zuritz (1990) use the TSM to describe the RTD of polystyrene spheres suspended in CMC/waters solutions in a SSHE at isothermal conditions. This author reported the number of tank-in-series to vary between 54 to 288 depending on the operating conditions.

Lee and Singh (1991) reported the use of the TSM and the analysis of variance to describe the effect of the process parameters during the flow of a suspension of potato cubes on CMC/water solutions. The characteristic tank-in-series number varied between 29 to 49 depending on the process conditions.

Belhamri et al. (2009) reported a more elaborated model to describe the RTD of ice cream during the freezing process. The RTD model represented the flow behaviour in the SSHE by two plug flow compartments with axial dispersion positioned in parallel and exchanging fluid by radial mixing. The first compartment was located adjacent to the cooling wall and the second was next to the rotor. After the adjustment of the model parameters, a good agreement between experimental and modelling RTD data was obtained.

The use of the GDM has not been reported for the description of experimental RTD data in SSHEs. The GDM has been used for the modelling of the RTD of low-density polyethylene flowing through a corotating twin-screw extruder (Puaux et al., 2000), and for the modelling of the RTD of water in catchments areas (Hrachowitz et al., 2010).

2.6. Rheological properties of sorbet

The understanding of the effect of the freezing operating conditions on the rheological properties of sorbet is necessary for the improvement of the control of the process and the quality of the product. The knowledge of the apparent viscosity of the product is essential for the selection of process equipment, and for the optimal design of piping systems. During freezing, the formation of ice crystals leads to the freeze concentration of the non-frozen sorbet mix and increases the viscosity of this continuous liquid phase. Simultaneously, the dispersion of the ice crystals and the air bubbles in the liquid sorbet mix by the rotation of the scraping blades modifies the fluid flow field and increases further the viscosity of the product (Burns and Russell, 1999; Goff et al., 1995). Therefore, it is important to understand the effect of the evolution of the viscosity of the liquid phase and the effect of the volume fractions of ice crystals and air bubbles on the apparent viscosity of sorbet.

Goff et al. (1995) performed an experiment to assess the evolution of the apparent viscosity of the unfrozen liquid phase by simulating the process of freeze-concentration. Water was removed from the original ice cream mix formulation including stabilizers, at different percents varying from 15 to 50%, corresponding to the freeze-concentration of the ice cream mix from its initial freezing point temperature to -5.5 °C (by relating the amount of water removed to the temperature, with the equilibrium freezing curve). Ice cream mix exhibited a non-Newtonian shear-thinning fluid. For a shear rate of $50s^{-1}$ and at 4 °C, the viscosity of the original ice cream mix was roughly 0.8 Pa.s and the viscosity of the ice cream mix with the removal of 50% of water was roughly 3 Pa.s. The apparent viscosity of the unfrozen liquid phase at -5.5 °C represents thus roughly 4 times the viscosity of the original ice cream mix. This significant increase in the viscosity of the liquid phase with the freeze concentration of solids shows the importance in considering the evolution of the apparent viscosity of the unfrozen continuous phase on the final apparent viscosity of the product.

The measurement of the viscosity of frozen sorbet and ice cream is highly complex, because the product is temperature sensitive and it behaves as a non-Newtonian shear-thinning fluid (Burns and Russell, 1999; Haddad, 2009). A number of studies in the literature, based on oscillatory rheometry for the analysis of the viscosity of ice cream, have also reported a viscoelastic behaviour (Goff et al. 1995; Wildmoser et al., 2004). Based on oscillatory thermal rheometry measurements, Wildmoser (2004) reported for a shear rate of 10 s^{-1} the increase in the viscosity of ice cream at 100% overrun (8% milk fat and 0.5% emulsifier/stabilizer blend) with the decrease in the product temperature, from 23 Pa.s (-5 °C) to 243 Pa.s (-10 °C) and 2540 Pa.s (-15 °C).

Other studies in literature have reported in situ apparent viscosity measurements carried out by means of a pipe rheometer connected at the outlet of the SSHE during the freezing process (Russell et al., 1997; Cerecero, 2003; Martin et al., 2008; Elhweg et al., 2009). Russell et al., (1997) reported for ice cream (8% milk fat) at 100% overrun and -5 °C, a flow behaviour index n of 0.4 and a consistency index k of 100 $Pa.s^n$, corresponding to an apparent viscosity of 25 Pa.s at $10s^{-1}$. Cerecero (2003) reported for a shear rate of 10 s^{-1} the increase in the apparent viscosity of 30% sucrose/water solutions with the decrease in the product temperature and the increase in the ice content, from 0.06 Pa.s (6% ice content) to 0.29 Pa.s (18% ice content). Martin et al. (2008) reported for ice cream (8% milk fat and 0.16% stabilizers) at 100% overrun and -9.5 °C, a flow behaviour index of 0.442 and a consistency index of 2320 $Pa.s^n$, corresponding to an apparent viscosity of 642 Pa.s at $10s^{-1}$. Elhweg et al. (2009) measured a flow behaviour index of 0.43 and a consistency index of 200 $Pa.s^n$ for ice cream (8% milk fat, 0.16% stabilizers, 0.3% emulsifiers) at -5 °C, corresponding to an apparent viscosity of 54 Pa.s at $10s^{-1}$. These studies have demonstrated the strong dependency of the apparent viscosity of sorbet and ice cream on the temperature of the product and the ice content. Yet, information is still needed to understand the influence of

the amount of air incorporated into the product on the apparent viscosity of sorbet and ice cream.

2.6.1. Rheological models

Sorbet produced without aeration is a suspension of ice crystals distributed randomly in a freeze concentrated liquid phase. The flow of this suspension will be affected by the viscosity of the continuous liquid phase, the volume fraction (ϕ) of ice crystals, crystal-crystal interactions and the ice crystal size. A number of theoretical and empirical equations have been developed to predict the viscosity of concentrated suspensions (Einstein, 1906; Mooney, 1951; Thomas, 1965; Krieger and Dougherty, 1959; Batchelor, 1977). Table 2.2. shows a summary of the available models in the literature.

Table 2.2. Rheological models to predict the viscosity of a Newtonian suspension as a function of the volume fraction of particles.

Reference	Viscosity Expression	Particle concentration
Einstein. 1906	$\eta = \eta_l(1 + 2.5\phi)$	$\phi < 0.02$
Mooney. 1951	$\eta = \eta_l \exp\left(\frac{2.5\phi}{1 - k\phi}\right)$	For $k = 1.43$ $\phi < 0.35$ For $k = 0.75$ $\phi < 0.58$
Thomas. 1965	$\eta = \eta_l\left(1 + 2.5\phi + 10.05\phi^2 + 0.00273\exp(16.6\phi)\right)$	$\phi < 0.625$
Krieger and Dougherty. 1959	$\eta = \eta_l \exp\left(1 - \frac{\phi}{\phi_{\max}}\right)^{-2.5\phi_{\max}}$	For high shear rates $\phi_{\max} = 0.71$ For low shear rates $\phi_{\max} = 0.63$
Batchelor. 1977	$\eta = \eta_l\left(1 + 2.5\phi + 6.2\phi^2\right)$	$\phi < 0.2$

Most of these models are extended versions of the expression developed by Einstein (1906) to predict the evolution of the viscosity of a Newtonian suspension of rigid spheres

(ϕ < 0.02), as a function of the volume fraction ϕ of the suspended spheres and of the viscosity of the continuous phase η_l, written as:

$$\eta = \eta_l(1 + 2.5\phi) \tag{14}$$

This model takes only into account the Brownian movement of the spheres, neglects particle-particle interactions, and is only valid in the case of dilute solutions.

For higher particle concentrations (ϕ < 0.625) and a range of particle size between 0.099 to 435 μm, Thomas (1965) proposed a semi-empirical expression which predicts the viscosity of Newtonian suspensions as a function of the viscosity of the continuous phase η_l and the volume fraction ϕ of the suspended rigid spheres, expressed as:

$$\eta = \eta_l\left(1 + 2.5\phi + 10.05\phi^2 + 0.00273\exp(16.6\phi)\right) \tag{15}$$

In this model, the first three terms inside the parentheses account for the effect of the hydrodynamic interactions of spheres and particle-particle interactions, whereas the exponential term considers the rearrangement of particles as the suspension is sheared (Thomas, 1965). This model has been widely used to predict the viscosity of ice slurries (Ayel et al., 2003; Hansel, 2000), but has been reported to overestimate the viscosity of crystals slurries when the ice concentration exceeds ϕ > 0.15 (Hansel, 2000). Haddad (2009) compared experimental viscosity data obtained in a scraped rheometer, during the batch freezing of a 30% sucrose solution with the predicted values by Thomas equation. Results showed that the model of Thomas underestimates the viscosity of non-Newtonian shear-thinning suspensions of ice crystals.

Cerecero (2003) proposed a rheological empirical model to predict the apparent viscosity of sucrose/water solutions as a function of the initial sucrose concentration w_0, the ice volume fraction $\phi_{v.ice}$ and the shear rate $\dot{\gamma}$, expressed as follows:

$$\eta = (1.8w_0 - 0.3) \cdot \dot{\gamma}^{(0.646-1)} \, exp\{(24w_0 - 2.87)\phi_{v.ice}\} \quad (16)$$

This model is valid for initial sucrose concentrations w_0 within the range between 0.30 to 0.40, and for shear rates between $50s^{-1}$ to $4000s^{-1}$. However, this model does not take into account the influence of the evolution of the viscosity of the continuous liquid phase.

It has been shown in this section that the reported rheological models in the literature do not describe adequately the evolution of the apparent viscosity of non-Newtonians shear thinning fluids such as ice cream and sorbet. Furthermore, the existing rheological models that could be applied for the prediction of the viscosity of sorbets and ice creams, do not consider the evolution of the apparent viscosity of the liquid continuous phase during the freezing process.

2.7. Modelling of the freezing process

In the manufacturing of sorbet, the quality is mainly governed by the microstructure of the product: shape, mean size and ice crystal size distribution (CSD). Furthermore, the CSD should be reproducible in order to assure a constant product quality. It is therefore important to understand the influence of the operating conditions of the freezing process on the kinetics of ice crystallization, so as to improve the control of the process and the quality of the final product. The modelling of the ice crystallization process can help to gain deeper understanding of the freezing process in a SSHE, and also for the identification of new ways to improve the performance of the process. Furthermore, it can reduce the time of scale-up of the process from laboratory scale equipment to industrial scale production.

2.7.1. Population balance approach

The evolution of the CSD in the time and size domain can be modelled by a hyperbolic partial differential equation referred to as the population balance equation (PBE), and introduced by Hulburt and Katz (1964) and further developed by Randolph and Larson (1988). The population balance is written as follows:

$$\frac{\partial \psi(L,t)}{\partial t} = -\frac{\partial G.\psi(L,t)}{\partial L} + B(L) - D(L) \qquad (17)$$

where the first term in the equation is the number density function $\psi(L,t)dL$, which represents the number of crystals of size between L and $L+dL$ per unit volume at a time t. The second term represents the crystal growth rate. The third term represents the birth of crystals by nucleation and/or breakage phenomena. Finally, the fourth term represents the disappearance of crystals for a given crystal size class.

The PBE is usually coupled with heat transfer and fluid flow equations to describe the non-ideal mixing in crystallizers such as the SSHE. In order to solve the PBE, for these more

complex cases, it is necessary to adapt existing numerical methods, such as the method of moments and the method of classes. The method of moments transforms the PBE into a set of ordinary differential equations, in terms of the moments of the CSD. This method considers only the first four moments of the distribution and provides information about the number density, mean size and volume fraction of crystals. This method however, does not make it possible to fully reconstruct the CSD from its moments since it would be numerically unstable (Rigopoulus and Jones, 2003). The method of classes introduced by Marchal et al. (1988), transforms the PBE into a set of ordinary differential equations, by discretizing the size domain. This method makes it possible to obtain the full CSD.

2.7.2. Crystallization modelling approaches for SSHEs

Lian et al. (2006) reported a combined computational fluid dynamics (CFD) and PBE to simulate the ice crystallization of 25% sucrose solution in a SSHE. In order to simplify the fluid flow conditions, the flow field was solved at steady state for a 2D geometry, in which a constant viscosity and negligible ice crystal dispersion were assumed. The PBE was solved by the method of classes by discretizing the size domain in 14 granulometric classes. The comparison between experimental and modelling data showed that the predicted ice CSD overestimated the number of small ice crystal and underestimated the number of large ice crystals. The discrepancies between the model predictions and the experimental data were attributed in part to the lack of accuracy of the measurement technique of the ice crystal size, and to the assumptions made to simplify the fluid flow.

Dorneanu et al. (2010) proposed a reduced model for the freezing process of ice cream in a SSHE. The model considers two layers of fluid: a thin frozen ice layer adjacent to the wall of the SSHE, and a bulk layer located between the rotor and the frozen ice layer. It was considered that within the frozen ice layer the ice crystals form and grow into an ice layer of

variable thickness, which is periodically removed into the bulk of the fluid by the rotation of the scraper blades. Within the bulk region the ice crystals are dispersed into the bulk fluid and only ice melting was considered. The fluid flow within the SSHE was simplified by considering a plug flow at steady state and the product to be well mixed within a cross-sectional area, perpendicular to the axial direction. Heat transfer and population balance equations were solved for 12 size classes. Simulation results predicted well the expected trends; nevertheless parameter estimation using experimental data was still required to assure more accurate results.

More recently Freireich et al. (2011) reported the incorporation of particle flow information from discrete element simulation in the PB modelling of mixed-coaters. This modelling approach made it possible to account for flow heterogeneity in the mixer-coater. In this approach a discrete element model simulates the trajectory of the particles within each region of the reactor; then it determines the residence time of the particle and generates sub-compartments in order to reproduce the measured residence time of the particle in each region. Subsequently, a system of PBE is written based on the sub-compartments and simulate the population density of particles. Simulation results predicted well the experimental trends and provided accurate results for the behavior of the system.

The mathematical models available in the literature for the simulation of the ice crystallization process in SSHEs use simplified fluid flow conditions and do not consider the influence of the RTD on the final ice crystal size. Furthermore, the effect of the apparent viscosity on the viscous dissipation and its repercussion on heat transfer and consequently ice crystal size and product temperature are rarely taken into account for the modelling of ice crystallization in SSHEs.

2.8. Bibliographical review conclusions

The aim of the initial freezing process is to deliver a product with the smallest possible ice crystal size, so as to produce a high quality sorbet. The optimization of the freezing process requires a good control of the operating conditions and the understanding of the development of the ice crystals inside the scraped surface heat exchanger (SSHE).

The literature available has made it possible to elucidate some basics of the ice crystallization mechanism in SSHEs; however, more research is still needed to confirm the existing theories. In particular, experimental studies to examine the influence of the operating conditions on ice crystal size and product temperature are still pertinent, since they not only make it possible to confirm the proposed ice crystallization mechanism models, but also these studies can orient sorbet manufacturers in the possible ways in which the initial freezing process can be improved.

The temperature and flow profiles in SSHEs are highly heterogeneous. The bibliographic review showed that there is little information about the effect of the operating conditions on the axial temperature profile. This information would be highly valuable from an industrial point of view, since it makes it possible to identify the operating conditions that will induce a faster freezing and therefore a small ice crystal size in the final product.

Residence time distribution studies when ice crystallization occurs under cooling conditions are very rare. Information is still needed to have a better understanding of the effect of the freezing operating conditions on the fluid flow behaviour of sorbet within the SSHE. The experimental characterization and modelling of the RTD can provide valuable information to improve the understanding of the fluid flow behaviour that make it possible to assess the degree of thermal treatment applied to the product. This information may aid to identify the operating conditions that improve product quality.

The bibliographic review also exposed the importance of understanding the influence of the evolution of the viscosity of the liquid continuous phase and the effect of the volume fractions of ice crystals and air bubbles on the apparent viscosity of sorbet. Apparent viscosity data can be very useful on industrial sites for the online monitoring of the quality of the product. The measurement of the rheological properties of the product can also provide a better understanding of the fluid flow behaviour as affected by the freezing operating conditions. The construction of a rheological model is also pertinent not only for the online control of the process, but also it can help to account for viscous dissipation effects on the ice crystallization modelling in SSHEs.

Finally, it was shown that the fluid flow profile in a SSHE is not uniform, yet there is little information about ice crystallization modelling approaches that take into account the fluid flow heterogeneities. The coupling of heat transfer and PBE with an empirical RTD model is thus relevant, so as to examine the improvement that can be done for the ice crystallization modelling in SSHEs. This modelling approach can also give insight into the values of product temperature and ice crystal size for each fraction of fluid that flows through the SSHE.

2.9. Aim of this work

This work focuses on the initial freezing process of sorbet within a continuous SSHE at the pilot scale. The previous bibliographic review exposed the need of experimental and modelling studies to assess the influence of the freezing operating conditions on the heat transfer and ice crystallization mechanism in SSHEs, so as to improve the product quality control. Residence time distribution (RTD) studies during the ice crystallization process are very rare and yet necessary for the evaluation of the thermal treatment applied to the product, which may help for the improvement of the control of the crystallization process. It was also demonstrated that rheological data of sorbet when it flows out from the SSHE are still rare and thus necessary for the improvement of the control of the freezing operating conditions in order to deliver the desired product texture. Therefore, the main objectives of this work are:

Firstly, to study the effects of the freezing operating conditions on the evolution of the thermo-physical properties of sorbet, such as the size distribution of the ice crystals, the temperature and the apparent viscosity of the product, in order to provide a better understanding of the coupled interactions of heat transfer and ice crystallization kinetics on the development of the ice crystals in the SSHE. This will consequently help to improve the product quality control.

Secondly, to investigate the changes in the RTD and axial temperature profile of the product as a function of the freezing operating conditions, so as to describe the flow behaviour of the product, and to identify the possible ways to enhance heat transfer and to induce a faster freezing that leads to smaller ice crystals and to a better quality product.

Finally, to propose a mathematical model for the simulation of the ice crystallization process which considers heat transfer, product residence time distribution and ice crystallization kinetics, so as to predict the evolution of the temperature and the ice crystal size of the product inside the SSHE. This will add new knowledge about the formation of ice crystals during the freezing process.

References of bibliographic review

Abbas, A., Nobbs, D., Romagnoli, J. A. (2002). Investigation of on-line optical particle characterization in reaction, and cooling crystallization systems. Current state of the art. *Measurement Science & Technology,* 13 (3), 349-356.

Alcairo, E. R., and Zuritz, C. A. (1990). Residence Time Distributions of Spherical-Particles Suspended in Non-Newtonian Flow in a Scraped-Surface Heat-Exchanger. *Transactions of the ASAE*, 33, (5), 1621-1628.

Ayel, V., Lottin, O., Peerhossaini, H. (2003). Rheology, flow behaviour and heat transfer of ice slurries: a review of the state of the art. *International Journal of Refrigeration*. 26: 95–107.

Batchelor, G. K. (1977). The effect of Brownian motion on the bulk stress in a suspension of spherical particles. *Journal of Fluid Mechanics*. 83: 97-117.

Belhamri, R., Fayolle, F., Flick, D. (2009). Simplified flow pattern model in SSHE during crystallisation process. *8th World Congress of Chemical Engineering Montréal*, Quebec, Canada.

Ben Lakhdar, M., Cerecero, R., Alvarez, G., Guilpart, J., Flick, D., Lallemand, A. (2005). Heat transfer with freezing in a scraped surface heat exchanger. *Applied Thermal Engineering,* 25 (1), 45-60.

Ben-Yoseph, E. and Hartel, R. W. (1998). Computer simulation of ice recrystallization in ice cream during storage. *Journal of Food Engineering*. 38(3), 309-329.

Benezech, T. and Maingonnat, J. F. (1989). Etude de la distribution des temps de séjour dans des échangeurs à surface raclée traitant des fluides non-Newtoniens. *Entropie*, 151, 37-46.

Burns, I. and Russell A. (1999). Process rheology of ice-cream. In ZDS Inter-Ice, Solingen.

Cebula, D. J. and Russell, A. B. (1998). Ice crystallization control in ice cream. In *Ice cream. Proceedings of the International Dairy Federation Symposium, Athens, Greece, 18-19 September 1997.* (pp. 131-139).

Cerecero, R. (2003). *Etude des écoulements et de transferts thermiques lors de la fabrication d'un sorbet à l'échelle du pilote et du laboratoire.* PhD Thesis. INA-PG, Paris, France.

Cognet, G. (1984). Les étapes vers la turbulence dans l'écoulement de Couette-Taylor entre cylindres coaxiaux. *Journal de mécanique théorique et appliquée, Numéro spécial*, 7-44.

Cook, K. L. K. and Hartel, R. W. (2010). Mechanisms of Ice Crystallization in Ice Cream Production. *Comprehensive Reviews in Food Science and Food Safety,* 9 (2), 213-222.

Danckwerts, P. V. (1953). Continuous flow systems. Distribution of residence times. *Chemical Engineering Science*, 2, 1-13.

Dorneanu, B., Bildea, C., Grievink, J., Bongers, P. M. (2010). A reduced model for the freezing step in ice cream manufacture. *20th European Symposium on Computer Aided Process Engineering - ESCAPE.*

Drewett, E. M., and Hartel, R. W. (2007). Ice crystallization in a scraped surface freezer. *Journal of Food Engineering,* 78 (3), 1060-1066.

Dumont, E., Fayolle, F., Legrand, J. (2000). Flow regimes and wall shear rates determination within a scraped surface heat exchanger. *Journal of Food Engineering*, 45, (4), 195-207.

Einstein, A. (1906). Investigations on the theory of Brownian motion. *Annalen der Physik*. 19: 289-306.

Elhweg, B., Burns, I., Chew, Y., Martin, P., Russell, A., Wilson, D. (2009). Viscous dissipation and apparent wall slip in capillary rheometry of ice cream. *Food and Bioproducts Processing.* 87: 266-272.

Fayolle, F., Mabit, J., Legrand, J. (2005). Determination of heterogeneities in a scraped surface heat exchanger using electrochemical sensors. *Journal of Applied Electrochemistry*, 35, (5), 487-498.

Freireich, B., Li, J., Litster, J., Wassgrena, C. (2011). Incorporating particle flow information from discrete element simulations in population balance models of mixer-coaters. *Chemical Engineering Science.* 66, 3592-3604.

Goff, H. D., Freslon, B., Sahagian, M. E., Hauber, T. D., Stone, A. P., & Stanley, D. W. (1995). Structural development in ice cream - Dynamic rheological measurements. *Journal of Texture Studies,* 26 (5), 517-536.

Gonzalez, E. (2012). *Contribution au contrôle par la modélisation d'un procédé de cristallisation en continu.* PhD Thesis. AgroParisTech, Paris, France.

Haddad, A. (2009). *Couplage entre écoulements, transferts thermiques et transformation lors du changement de phase d'un produit alimentaire liquide complexe - Application à la maîtrise de la texture.* PhD Thesis. AgroParisTech, Paris, France.

Hansen, T.M., Kauffeld, M., Grosser, K., Zimmermann, R. (2000). Viscosity of ice-slurry. 2nd Workshop on ice-slurries, *International Institute of Refrigeration.* Paris, France.

Harriott, P. (1969). Heat transfer in scraped surface heat exchangers. *Chemical engineering progress symposium series*. 55(29), 137-139.

Härröd, M. (1986). Scraped surface heat exchangers - A literature survey of flow patterns, mixing effects, residence time distribution, heat transfer and power requirements. *Journal of Food Process Engineering*, 9, 1-62.

Hartel, R. W. (1996). Ice crystallization during the manufacture of ice cream. *Trends in Food Science & Technology,* 7 (10), 315-321.

Hrachowitz, M., Soulsby, D., Tetzlaff, Malcolm, I. A., Schoups, G. (2010) Gamma distribution models for transit time estimation in catchments: Physical interpretation of parameters and implications for time variant transit time assessment. *Water resources research.* 46 (W10536) 15 p.

Hulburt, H., and Katz, S. (1964). Some problems in particle technology: A statistical mechanical formulation. *Chemical Engineering Science,* 19, 555–574.

Inoue, K., Ochi, H., Taketsuka, M., Saito, K., Sakurai, K., Ichihashi, N., Iwatsuki, K., Kokubo, S., (2008). Modelling of the effect of freezer conditions on the principal constituent parameters of ice cream by using response surface methodology. *Journal of Dairy Science.* 91(5),1722-1732.

Krieger, I. M. and Dougherty, T. J. (1959). A mechanism for non-Newtonian flow in suspension of rigid spheres. *Transactions of the Society of Rheology*. 3: 137-152.

Koxholt, M., Eisenmann, B., Hinrichs, J. (2000). Effect of process parameters on the structure of ice-cream: possible methods of optimizing traditional freezer technology. *European Dairy Magazine,* 12 (1), 27-29.

Latinen, G. A. (1958). Discussion of the paper Correlation of scraped film heat transfer in the votator. *Chemical Engineering Science*. 9, 263-266.

Lee, J. H. and Singh, R. K. (1991). Particle residence time distribution in a model horizontal scraped surface heat exchanger. *Journal of Food Process Engineering*, 14, 125-146.

Levenspiel, O. (1999). Chemical Reaction Engineering, John Wiley & Sons Inc.

Lian, G., Moore, S., Heeney, L. (2006). Population balance and computational fluid dynamics modelling of ice crystallisation in a scraped surface freezer. *Chemical Engineering Science,* 61(23), 7819-7826.

Maingonnat, J. F., and Corrieu, G. (1983). Etude des performances thermiques d'un échangeur de chaleur à surface raclée 1ère partie. Revue des principaux modèles décrivant le transfert de chaleur et la consommation de puissance. *Entropie.* 111, 29-36.

Marchal, P., David, R., Klein, J. P., Villermaux, J. (1988). Crystallization and precipitation engineering—I. An efficient method for solving population balance in crystallization with agglomeration. *Chemical Engineering Science*, 43, 59–67.

Marshall, R. T., Goff, H. D., Hartel R. W. (2003). Ice cream. 6th Ed. New York: Klumer Academic/Plenum Publishers. 371 p.

Martin, P., Odic, K., Russell, A., Burns, I., Wilson, D. (2008). Rheology of commercial and model ice creams. *Applied Rheology*. 18: 11p.

Mooney M. (1951). The viscosity of a concentrated suspension of spherical particles. *Journal of Colloid Science*. 6: 162-170.

Puaux, J. P., Bozga, G., Ainser, A. (2000). Residence time distribution in a corotating twin-screw extruder. *Chemical Engineering Science.* 55, 1641-1651.

Qin, F. G. F., Chen, X. D., Russell, A. B. (2003). Heat transfer at the subcooled scraped surface with/without phase change. *American Institute of Chemical Engineers Journal.* 49, 1947-1955.

Randolph, A. and Larson, M. (1988). Theory of particulate processes: analysis and techniques of continuous crystallization. New York, NY: Academic Press.

Rigopoulos, S. and Jones A. G. (2001). Dynamic modelling of a bubble column for particle formation via a gas–liquid reaction. *Chemical Engineering Science*, 56, 6177–6184.

Russell, A. B., Burmester, S. S. H., Winch, P. J. (1997). Characterization of shear thinning flow within a scraped surface heat exchanger. *Food and Bioproducts Processing*, 75, (C3), 191-197.

Russell, A. B., Cheney, P. E., Wantling, S. D. (1999). Influence of freezing conditions on ice crystallisation in ice cream. *Journal of Food Engineering,* 39 (2), 179-191.

Schwartzberg, H. and Liu, Y. (1990). Ice crystal growth on chilled scraped surfaces. In *American Institution of Chemical Engineers. Summer National Meeting.* San Diego, CA, USA.

Schwartzberg, H. (1990). Food freeze concentration. In: H. G. Schwartzberg & M. A. Rao editors. *Biotechnology and food process engineering. IFT basic symposium series.* New York: Marcel Dekker. (pp. 127-201).

Sofjan, R. P. and Hartel, R. W. (2004) Effects of overrun on structural and physical characteristics of ice cream. *International Dairy Journal.* 14 (3). 255–262.

Sodawala, S. and Garside, J. (1997). Ice nucleation on cold surfaces: application to scraped surface heat exchangers. In *American Institution of Chemical Engineers Annual Meeting.* Los Angeles, California, USA.

Thomas, D. G. (1965). Transport characteristics of suspension: VIII. A note on the viscosity of newtonian suspensions of uniform spherical particles. *Journal of Colloid Science*. 20: 267-277.

Trommelen, A. M. and Beek, W. J. (1971). Flow phenomena in a scraped-surface heat exchanger (Votator-type). *Chemical Engineering Science*, 26, (11), 1933-1942.

Villermaux, J. (1993). Génie de la réaction chimique, conception et fonctionnement des réacteurs. Technique et documentation. Paris.

Wang, W., Walton, J. H., McCarthy, K. L. (1998). Flow profiles of power law fluids in scraped surface heat exchanger geometry using MRI. *Journal of Food Process Engineering*, 22, 11-27.

Wen, C. Y. and Fan, L. T. (1975). Models for flow systems and chemical reactors. New York, Marcel Decker. Wildmoser, H., Scheiwiller, J. and Windhab, E.J., 2004, Impact of disperse microstructure on rheology and quality aspects of ice cream. *Lebensmittel-Wissenschaft & Technologie*, 37(8): 881–891.

Wildmoser, H. (2004). *Impact of Low Temperature Extrusion Processing on Disperse Microstructure in Ice Cream Systems.* PhD Thesis. Swiss Federal Institute of Technology (ETH), Zurich, Switzerland.

Wildmoser, H., Scheiwiller, J. and Windhab, E.J. (2004). Impact of disperse microstructure on rheology and quality aspects of ice cream. *Lebensmittel-Wissenschaft & Technologie*, 37(8): 881–891.

Windhab, E. and Bolliger, S. (1995). Combined aerator/freezer for ice cream manufacture. *European Dairy Magazine,* 1, 28-34.

Yataghene, M., Fayolle, F., Legrand, J. (2011). Flow patterns analysis using experimental PIV technique inside scraped surface heat exchanger in continuous flow condition. *Applied Thermal Engineering*, 31, (14-15), 2855-2868.

Zheng, L. (2006). *Heat transfer during freezing on a scraped surface.* PhD Thesis. University of Auckland. Auckland, New Zealand.

Chapter 3 - Materials and methods

Chapter 3 - Materials and methods

This chapter presents a brief description of the experimental platform and its instrumentation. A more detailed explanation is given in each of the scientific articles that constitute Chapter 5 - Results and discussion.

3.1. Working fluid - Lemon sorbet mix

The sorbet mix used in the experiments was an ultra high temperature pasteurized lemon sorbet mix. Table 3.1. shows the composition of the sorbet mix.

Table 3.1. Composition of lemon sorbet mix.

Ingredient	Weight percent (%w/w)
Water	73.81
Lemon juice concentrate 60 Brix	3
Sucrose	14.6
Fructose	8
Dextrose	0.09
Blend stabilizer: locust bean gum / guar gum / hypromellose	0.5

The density of lemon sorbet mix density is 1110 kg/m^3. The initial mass fraction of sweeteners (solute) is 0.252, and the initial freezing point is -2.63 °C.

The freezing point depression curve of the sorbet mix was previously determined in our laboratory by using differential scanning calorimetric (DSC) measurements, as reported by Gonzalez, 2012. The freezing point depression curve at equilibrium is shown in Fig. 3.1., this curve represents the relationship between the freezing point temperature at equilibrium (T_{eq}) and the sweeteners content concentration (w). This curve and the temperature of sorbet were used for the calculation of the ice volume fraction present in sorbet, as shown in Section 3.3.1 of this chapter.

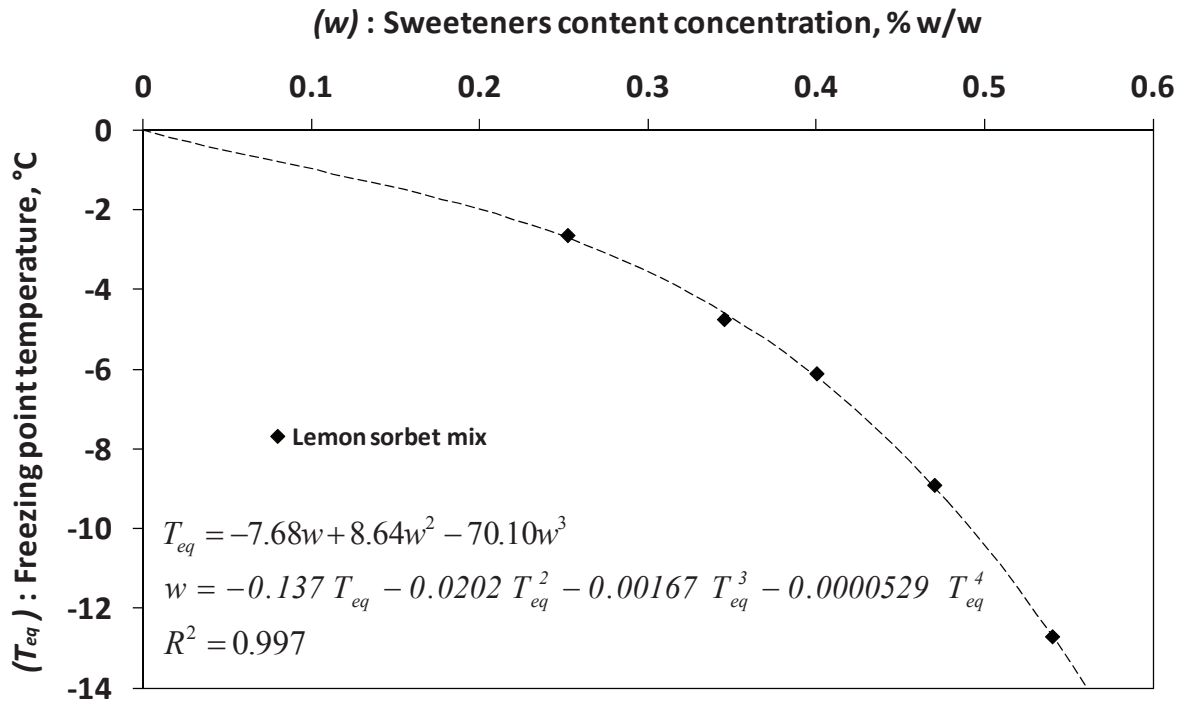


Fig. 3.1. Freezing point depression curve at equilibrium (Gonzalez, 2012).

3.2. Description of the experimental platform

The schematic representation of the experimental platform is presented in Fig. 2. Prior to use, the sorbet mix was stored in a refrigerated storage tank at 5 °C (cf. Fig. 3.2., element 1). During the freezing process, the sorbet mix was supplied into the SSHE by means of a volumetric piston pump (cf. Fig. 3.2., element 2). Once the sorbet was frozen in the SSHE (cf. Fig. 3.2., element 3), it flowed down through the outlet pipe of the SSHE (cf. Fig. 3.2., element 4). Two online sensors were introduced into the outlet pipe so as to measure the product as it flowed out from the SSHE: a Pt100 probe for the measurement of the temperature of the product (cf. Fig. 3.2., element 5), and the FBRM probe for the monitoring of the size distribution of the ice crystals (cf. Fig. 3.2., element 6).

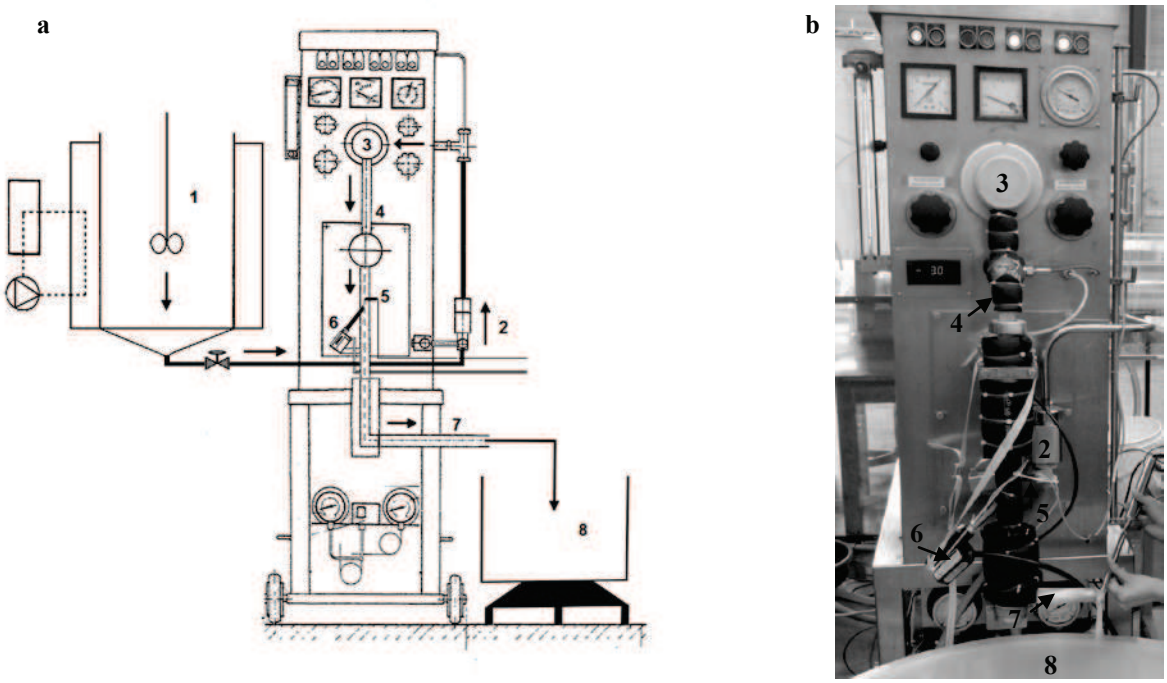


Fig. 3.2. (a) Schematic representation of the experimental platform. 1. Refrigerated storage tank (200 litres capacity). 2. Volumetric piston pump. 3. Freezer. 4. Outlet pipe. 5. Pt100 probe inserted into the outlet pipe. 6. FBRM probe inserted into the outlet pipe. 7. Product exit. 8. Reception tank. (b) Real representation of the SSHE instrumented with the Pt100 and FBRM sensors.

The sorbet mix was aerated and frozen in a continuous SSHE (WCB® Model MF 50), a schematic representation of which is shown in Fig. 3.3. The real representation of the integrating parts of the SSHE is presented in Fig. 3.4. The inner diameter of the heat exchange cylinder was 0.05 m and the length was 0.40 m. The rotor of the freezer was equipped with two rows of scraper blades and occupied roughly 46% of the volume of the heat exchange cylinder. The total volume of the SSHE available to the working fluid was 6.66×10^{-4} m^3, which includes the volume available within the heat exchange cylinder, the inlet and outlet bowls, as well as the outlet pipe. The outlet pipe of the SSHE represents 20% of the total available volume to the fluid.

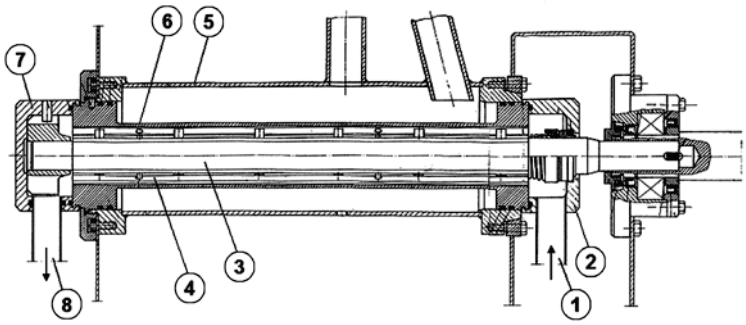


Fig. 3.3. Schematic representation of the SSHE WCB® Model MF 50. 1. Inlet connection for sorbet mix. 2. Inlet cover bowl. 3. Rotor. 4. Scraper blades rows. 5. Heat exchange cylinder jacket with vaporizing r22. 6. Heat exchange cylinder. 7. Outlet cover bowl. 8. Outlet pipe for sorbet.

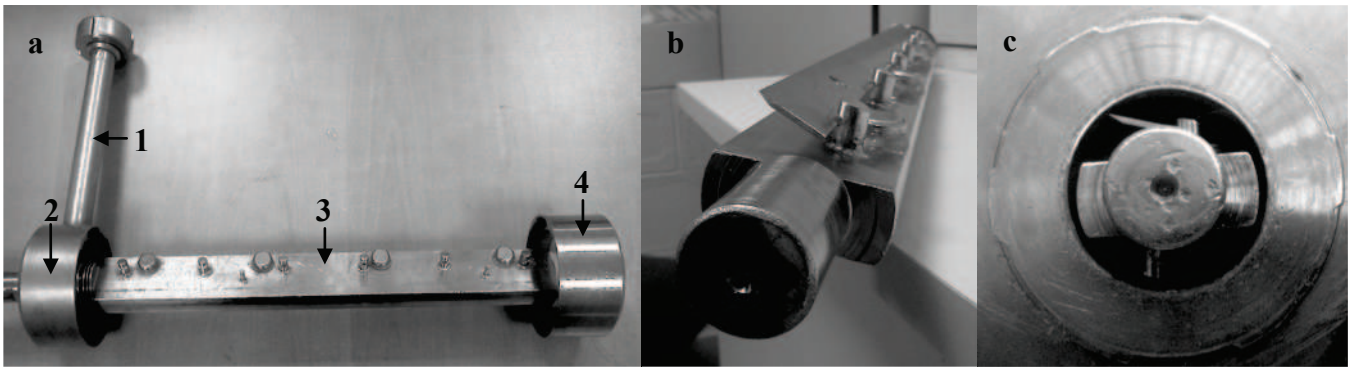


Fig. 3.4. Real representation of the integrating parts of the SSHE. (a) 1. Inlet connection for sorbet mix. 2. Inlet cover bowl. 3. Rotor. 4. Outlet cover bowl. (b) Rotor equipped with two rows of scraper blades. (c) Front view of rotor with the scraper blades rows.

The SSHE has a variable capacity of 0.007 to 0.021 $kg.s^{-1}$. The mix flow rate was determined by weighing the product exit stream during a given period of time. The accuracy of this measurement was determined to be $\pm 9.2 \times 10^{-5}$ $kg.s^{-1}$. The rotational speed of the dasher was varied from 57 to 105 $rad.s^{-1}$ (545 to 1000 rpm), according to experimental conditions. The dasher rotational speed was measured by means of a photoelectric tachometer (Ahlborn®, type FUA9192) with an accuracy of 1 rpm. The heat exchange cylinder was cooled by the evaporating refrigerant fluid r22 (Chlorodifluoromethane). The temperature of the refrigerant fluid was adjusted within the range of -10 to -20 °C according to experimental conditions. A calibrated type T (copper - constantan) thermocouple with an accuracy of ±0.2°C was fixed with conductive aluminium tape on the external surface wall of the cooling jacket, so as to measure the evaporation temperature of the refrigerant fluid. The exterior of the cooling jacket

was isolated with foam of 2 cm thickness in order to reduce heat loss. Air was added at the inlet of the SSHE at different flow rates so as to obtain the desired overruns, and the rotation of the scraping blades made it possible to incorporate the air into the sorbet mix.

3.2.1. Control of process conditions and data acquisition in Labview®

Two AC Drives (Series 650 Parker®) were connected to the SSHE and controlled by a program written in LabVIEW®. This setting makes it possible to control automatically the rotation speed of the dasher and the mix flow rate. The evaporation pressure (temperature) of the refrigerant fluid was controlled manually by means of a pressure valve integrated into the SSHE. The air flow rate was adjusted manually by means of a flowmeter and a regulating valve. The program written on Labview® collects the experimental data by means of two data acquisition units Agilent HP (Model 34970 A) and two Switch Units Agilent HP (Model 34901 A). The acquisition of data is performed every 5 s. The temperature of the refrigerant fluid and the product temperature were monitored online by the Labview® program.

3.3. Online sensors

In this section, we describe the online sensors that were used for the in situ measurements of draw temperature, temperature profile inside the SSHE, ice crystal size and apparent viscosity.

3.3.1. Draw temperature measurements and ice volume fraction calculations

The draw temperature of the product was measured online by means of a calibrated Pt100 probe (Baumer®, accuracy of ±0.1 °C). The Pt100 probe was inserted into the outlet pipe of the SSHE before the exit of the product as shown in Fig. 3.2.

Assuming the thermodynamic equilibrium between ice and the solution of solute (sweeteners content), the ice mass fraction in sorbet $\phi_{m.ice.}$ (kg of ice / kg of sorbet) can be determined from the freezing point curve of sorbet mix (cf. Fig 3.1.), which is a function of the mass fraction of solute w_{ms} in the residual liquid phase. According to a mass balance of solute (sweetener content), the solute is present in sorbet mix at a certain initial mass fraction ($w_{ms.i}$). Then the solute is concentrated as the freezing of sorbet occurs, until it reaches a final mass fraction ($w_{ms.f}$) in the liquid phase. The final liquid phase represents only a fraction $(1-\phi_{m.ice.})$ of sorbet, hence the ice mass fraction can be calculated by the following equation:

$$w_{ms.i} = (1-\phi_{m.ice.}) \cdot w_{ms.f}(T) \Leftrightarrow \phi_{m.ice.} = 1 - \frac{w_{ms.i}}{w_{ms.f}(T)}, \quad (1)$$

The ice volume fraction (m^3 of ice / m^3 of sorbet) is then determined as follows:

$$\phi_{v.ice} = \frac{\rho_s}{\rho_i}\phi_{m.ice}, \quad (2)$$

where ρ_s is the density of sorbet and ρ_i the density of ice.

3.3.2 Ice crystal chord length distribution (CLD) measurements by the FBRM probe

The ice crystal CLD was measured online using a Mettler-Toledo Lasentec® FBRM probe (Model S400A-8). This device is composed of a stainless steel body 8 mm in diameter. At the probe tip there is a sapphire window through which a 780nm laser beam is transmitted to the sample. A set of rotating optics, inside the probe, focuses the laser beam into a small spot, creating a scanning circular path at the interface between the window of the probe and the particles in suspension (cf. Fig. 3.5.A). When a particle is intersected by the laser beam, it reflects the laser light throughout the time it is being scanned (cf. Fig. 3.5.B). Simultaneously, the time period of reflection is detected by the FBRM probe and then multiplied by the

tangential speed of the laser beam, yielding a distance across the particle, which is a chord length (Greaves et al., 2008; Wynn, 2003). The tangential speed of 2 m/sec of the laser beam is typically much faster than that of the particles, which makes it possible to consider that the particles are fixed with respect to the laser scanning path. The effect of particle motion is therefore considered negligible for the measurements (Abbas et al., 2002).

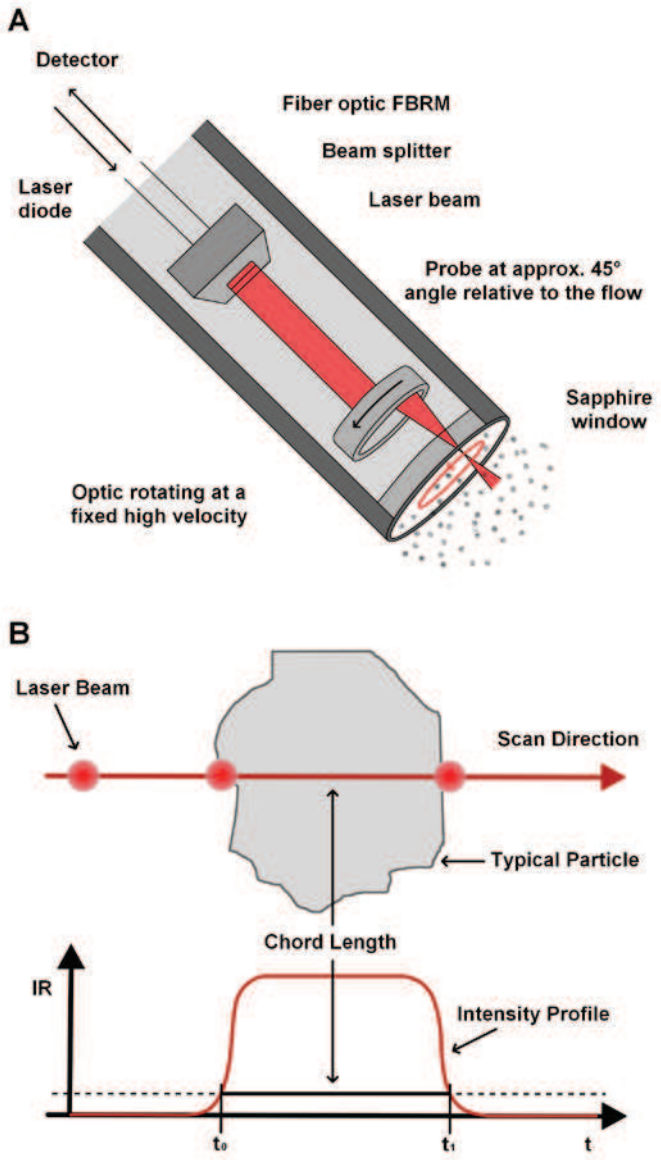


Fig. 3.5. (A) Cutaway view of the FBRM probe. (B) Measurement principle of a particle's chord length by the FBRM technique (Figure provided by Mettler-Toledo).

The FBRM probe measures thousands of chords per second, providing a CLD i.e. the number of counts per second sorted by chord length into 100 logarithmic size classes. Starting

with this information, the mean chord length of the ice crystals is obtained by the following equation:

$$MCL = \sum_{i=1}^{100} n_i c_i \,/\, \sum_{i=1}^{100} n_i \,, \tag{3}$$

where n_i is the number of particles for each of the size classes i of chord length c_i.

3.3.3. Temperature profile measurement

Wireless temperature sensors data loggers were used to measure the average axial temperature profile inside the SSHE. The thermochron iButton® DS1922L (Maxim®) device is a computer chip enclosed in a stainless steel case (diameter=16.3mm, thickness=6.4mm). The iButton® device includes an internal 3V Lithium battery source, a read/write memory (NV RAM), a real-time clock, and a semiconductor temperature sensor (temperature sensitive p-n silicon diode). The iButton® sensors were calibrated individually to an accuracy of ±0.2 °C within a range of -20 to +20 °C for a sampling rate of 5 seconds. The iButton® sensors were positioned through the axial length of the rotor as shown in Fig. 3.6. Data measurements were then transferred to a personal computer by means of a USB port adapter and the read/write software OneWireViewer.

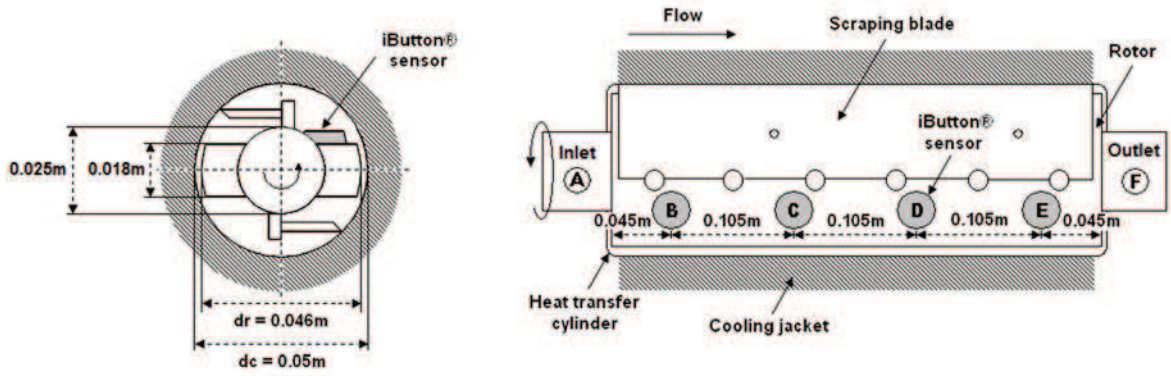


Fig. 3.6. Axial position of iButton® sensors in the SSHE.

3.4. Apparent viscosity measurements

Frozen sorbet was pumped from the SSHE, first, into a contraction/enlargement pipe, and then into an instrumented pipe rheometer as shown in Fig. 3.7. The real representation of the integrating parts of the experimental platform is presented in Fig. 3.8.

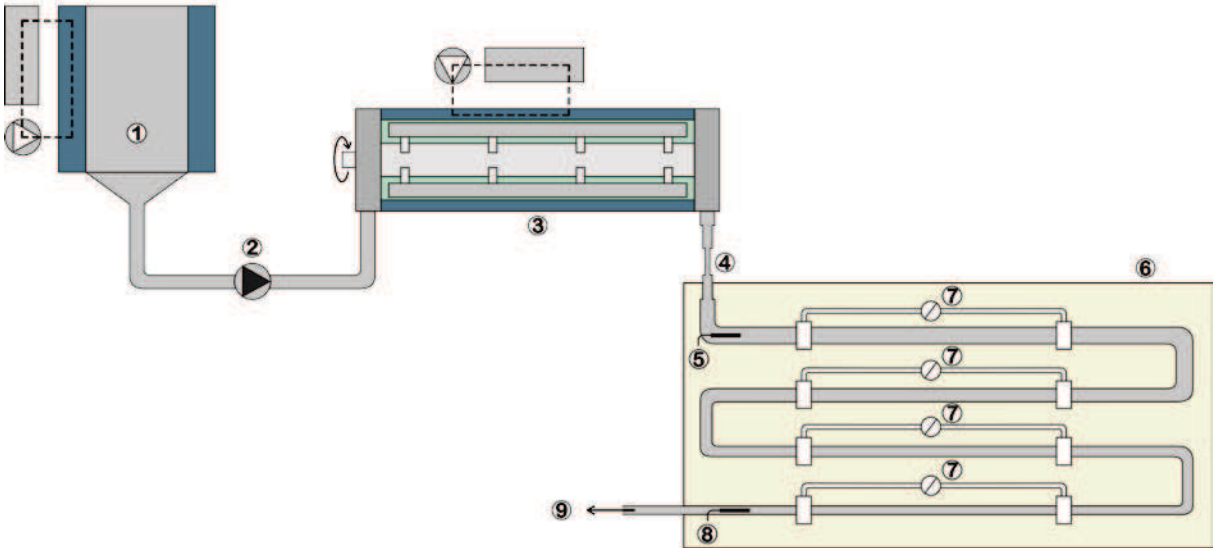


Fig. 3.7. Schematic representation of the experimental platform.
1. Refrigerated storage tank (200 l capacity). 2. Volumetric piston pump. 3. Freezer.
4. Contraction/enlargement pipe. 5. Pt100 probe inserted into the inlet of the rheometer. 6. Pipe rheometer.
7. Pressure manometers. 8. Pt100 probe inserted into the outlet of the rheometer. 9. Product exit.

The contraction/enlargement pipe was composed of 5 pipes in copper plumbing of 0.10 m length each and of different internal diameters ($d_{1c/e}$=0.025m; $d_{2c/e}$=0.0157m; $d_{3c/e}$=0.0094m; $d_{4c/e}$=0.0157m; $d_{5c/e}$=0.025m). This contraction/enlargement pipe was used to pre-shear the sorbet before it entered into the pipe rheometer, so as to prevent any thixotropic behaviour and to obtain repeatable measurements. The rheometer was composed of sets of 4 pipes in clear polyvinyl chloride (PVC) of different internal diameters (d_1=0.0272m, d_2=0.0212m, d_3=0.0167m, d_4=0.013m, d_5=0.01m, d_6=0.0058m[1]) connected in series, making it possible to apply an apparent shear rate range of $4 < \dot{\gamma}_w < 430$ s^{-1}. All pipes were insulated with polystyrene foam of 2 cm thickness in order to reduce heat loss. Two piezometric rings,

[1] 4 of these 6 pipe diameters were used depending on the ice volume fraction.

located at the measuring points of each pipe, made it possible to measure a pressure drop within each pipe for a length of 0.5 m. Pressure drop measurements were performed by liquid column manometers with an accuracy of ± 2% of the measured value. Pressure drop and flow rate were used to calculate the shear stress and the shear rate, as shown in Article 3 Section 2.2. The draw temperature of sorbet was measured as it flowed through the pipes of the rheometer by means of calibrated Pt100 probes (accuracy of ±0.1°C) located in the centre of the inlet and outlet pipes of the rheometer (cf. Fig. 3.7.). Thermal steady state in the pipe rheometer was achieved by pumping sorbet into it, until the measured temperatures at the inlet and outlet of the rheometer were brought to the desired experimental draw temperature. Measurements were performed under laminar conditions.

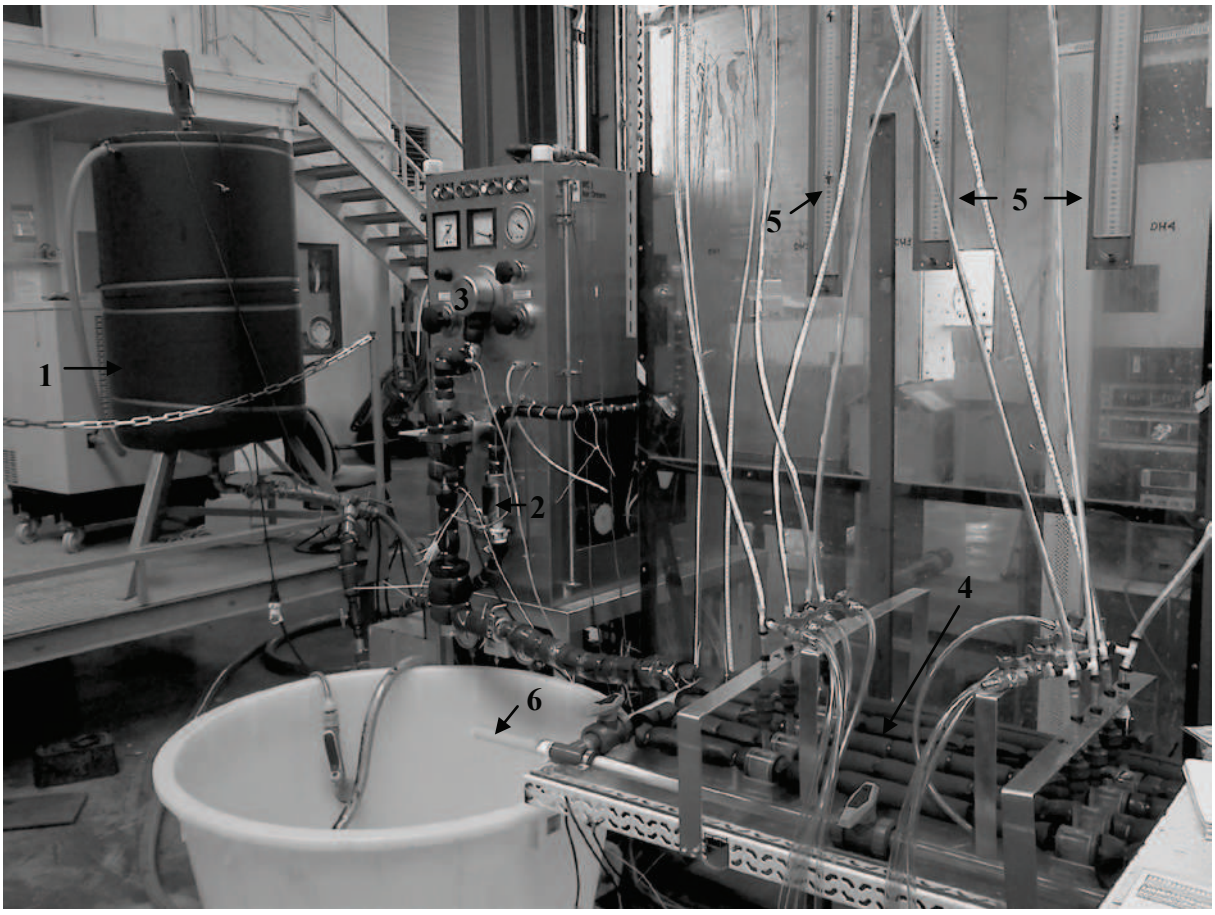


Fig. 3.8. Real representation of the experimental platform. 1. Refrigerated storage tank (200 l capacity). 2. Volumetric piston pump. 3. SSHE. 4. Contraction/enlargement pipe. 5. Pipe rheometer. 6. Pressure manometers. 7. Product exit.

3.5. Residence time distribution measurements

RTD experiments during sorbet freezing were carried out by means of a colorimetric method. A 13 ml pulse of unfrozen sorbet mix coloured with methylene blue (MB) dye at 0.008% (w/w) was used as tracer. The experimental setup for the injection of the tracer is schematically represented in Fig. 3.9. The real representation of the integrating parts of the experimental setup is presented in Fig. 3.10. The dyed sorbet mix was stored in a syringe connected to a valve and to a stainless steel tube (internal volume of 4 ml). This tube was inserted into the T pipe at the inlet connexion for sorbet mix, making it possible to inject the tracer immediately at the entrance of the SSHE. Before the pulse injection was performed, the volume of the stainless steel tube was filled with tracer, so that the tracer volume of 13 ml was completely injected for each experimental run. The tracer injection was achieved in roughly 0.7 seconds. This represents between 1 to 2% of the theoretical residence time of all the experimental conditions studied, and thus the pulse injection assumption is acceptable for all RTD experiments.

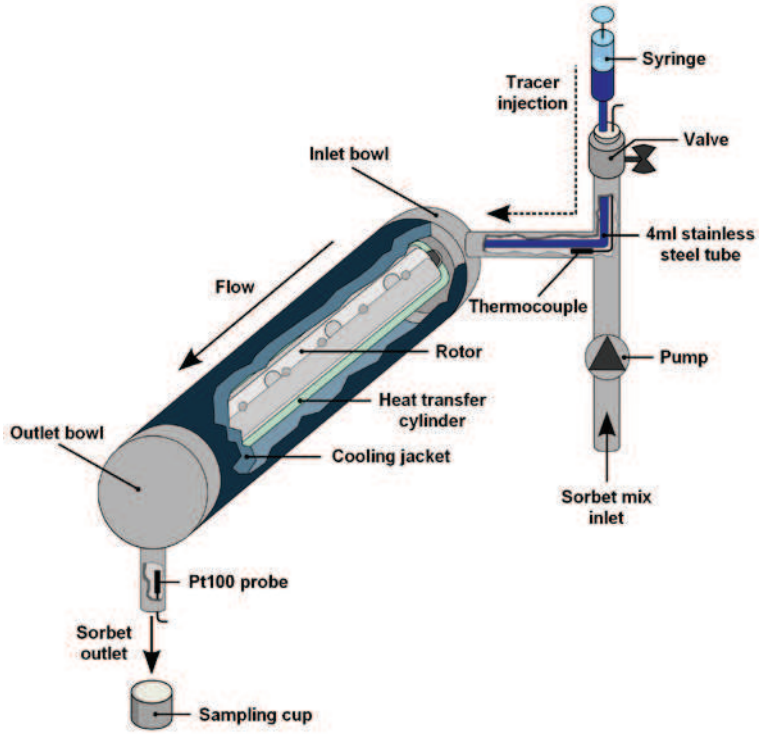


Fig. 3.9. Experimental setup for injection of tracer.

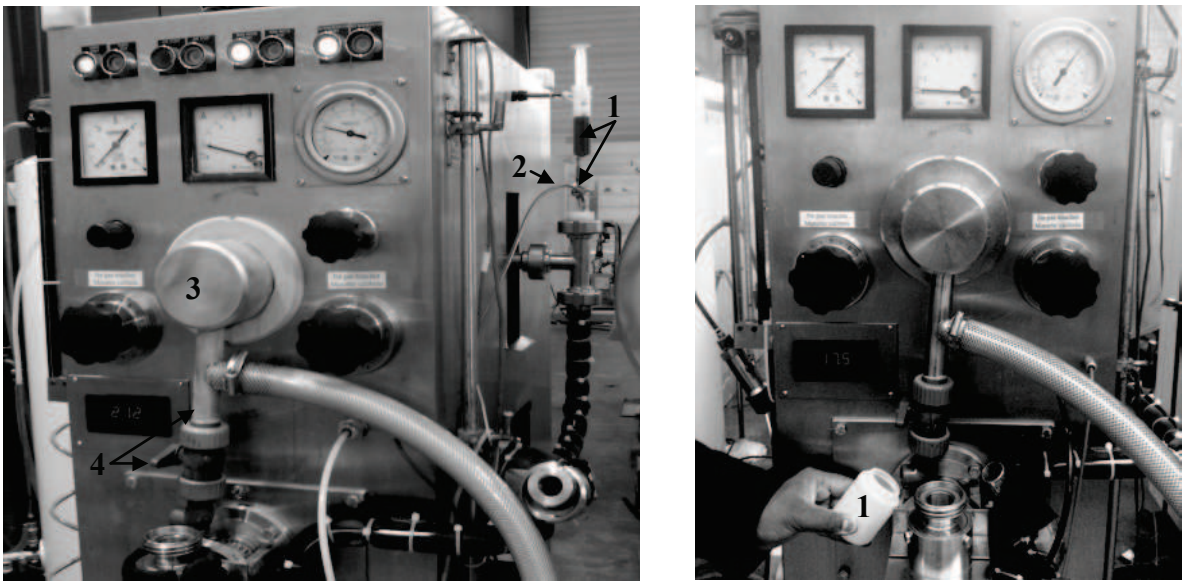


Fig. 3.10. Real representation of experimental setup for the injection of tracer.
(Left) 1. Syringe and valve for tracer injection. 2. Inlet thermocouple. 3. SSHE 4. Outlet pipe of SSHE with valve. 5. Derivation pipe with valve (not shown in the picture). (Right) 1. Sampling cup

Chapter 4 - Articulation of the scientific papers

Chapter 4 - Articulation of the scientific papers

This section presents a brief description of the scientific papers that constitute Chapter 5 - Results and discussion. These articles aim at providing new knowledge in order to respond to the scientific questions that were presented previously.

4.1. Online ice crystal size measurements during sorbet freezing by means of the focused beam reflectance measurement (FBRM) technology. Influence of operating conditions.

The first article intends to provide new knowledge about the effect of the freezing operating conditions on the ice crystallization mechanisms occurring in SSHEs in order to improve the product quality. In this article, temperature and ice crystal size measurements were performed at the outlet of the SSHE, so as to identify the freezing operating conditions that most directly affect the ice crystal size and the draw (exit) temperature of sorbet. The evolution of ice crystal size was tracked with the focused beam reflectance measurement (FBRM) technique, which uses an in situ sensor that makes it possible to monitor online the chord length distribution (CLD) of ice crystals in sorbets containing up to 40% of ice. In parallel, the temperature of the product was measured with a Pt100 probe. A schematic representation of the study of the freezing process, with the operating conditions used and the obtained responses is shown in Fig. 4.1.

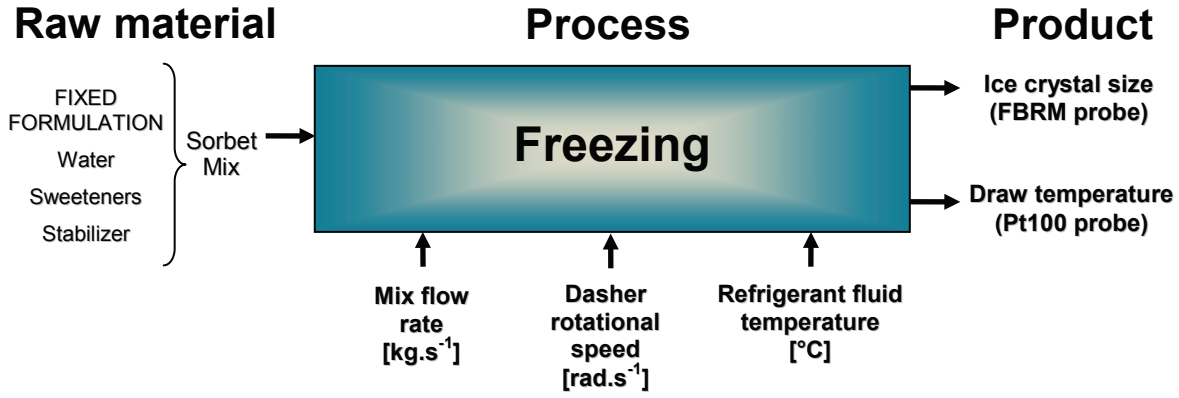


Fig. 4.1. Schematic representation of the study carried out in article 1.

A central composite experimental design was used to study the effect of 3 operating conditions: mix flow rate (MFR), dasher rotational speed (DRS) and evaporation temperature of r22 (TR22). The operating conditions tested in this article are shown in Table 4.1. The experimental design was performed twice and 5 replicates were performed for run 10.

Table 4.1. Central composite experimental design carried out in article 1.

Run	Freezing conditions			Sorbet characterization
	MFR [a] kg.s^{-1}	TR22 [a] °C	DRS [a] rad.s^{-1}	
1	0.018	-18	94.3	**Ice crystal chord length distribution** - FBRM (Focused beam reflectance method) **Draw temperature** - Pt100 probe **Ice mass fraction** -Pt100 and freezing point depression curve
2	0.018	-18	62.8	
3	0.018	-12.6	94.3	
4	0.018	-12.5	62.8	
5	0.010	-18.1	94.3	
6	0.010	-18.1	62.8	
7	0.010	-12.5	94.3	
8	0.010	-12.5	62.8	
9	0.007	-15.3	78.5	
10	0.014	-15.3	78.5	
11	0.021	-15.4	78.5	
12	0.014	-15.2	57.1	
13	0.014	-19.8	78.5	
14	0.014	-10.6	78.5	
15	0.014	-15.4	104.7	

[a] MFR = mix flow rate; TR22 = evaporation temperature of r22; DRS = dasher rotational speed.

The main results obtained in this study are: the refrigerant fluid temperature had the most significant influence on the mean ice crystal chord length, followed by the dasher speed, whereas the mix flow rate had no significant influence. The ice crystal mean chord length was significantly reduced by using lower refrigerant fluid temperatures. This effect can be explained by the growth of more small ice crystals left behind on the scraped wall from previous scrapings. Concerning the effect of the process parameters on sorbet draw temperatures, this study showed that for a given refrigerant fluid temperature and dasher speed, low mix flow rates resulted in lower draw temperatures, due to the fact that the product remains in contact with the cooling wall longer.

High dasher speeds warmed the product slightly, due to the increase in the dissipation of frictional energy in the product, the effect of which was in part moderated by the improvement in the heat transfer coefficient between the product and the freezer wall.

The experimental data obtained in this article made it possible to identify the parameters of the ice crystallization models presented in article 5.

4.2. Experimental study and modelling of the residence time distribution in a scraped surface heat exchanger during sorbet freezing.

During the freezing of sorbet, the increase in the ice volume fraction leads to an increase in the apparent viscosity of the product. This effect modifies the fluid flow behaviour, the residence time distribution (RTD) and the temperature profile inside the equipment. Due to the little information available on the RTD in SSHEs when crystallization occurs under cooling conditions, the second article focuses on the experimental study of the axial temperature profile and the residence time distribution (RTD) of the product, so as to characterize the heterogeneities of product temperature profile and fluid flow that exist in SSHEs, and to identify the operating conditions that can enhance the heat transfer and that may improve product quality. An empirical RTD model is also presented, so as to adequately represent the flow behaviour of the product in the SSHE, and to contribute to the improvement of the ice crystallization modelling. A schematic representation of the study of the RTD, with the studied control variables and the obtained responses is shown in Fig. 4.2.

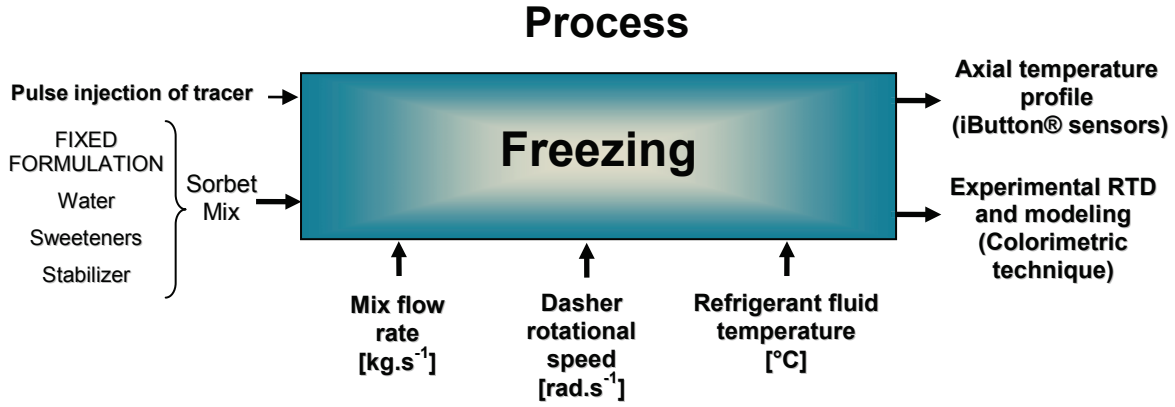


Fig. 4.2. Schematic representation of the study carried out article 2.

The effect of the freezing operating conditions on the axial product temperature profile was measured by means of wireless temperature sensors (iButtons®) positioned through the axial length of the rotor as shown in Chapter 3. The RTD experiments were carried out in the SSHE by means of a colorimetric technique. Three different hydrodynamic RTD models were

fitted to the experimental RTD data: gamma distribution model (GDM), tank-in-series model (TSM) and plug flow with axial dispersion model (ADM). Table 4.2. presents the operating conditions tested in article 2. Two replicates were performed for each of the operating conditions shown in Table 4.2.

Table 4.2. Operating conditions tested during the experiments carried out in article 2.

	Operating conditions			**Fluid flow characterisation**
Run	**MFR[a] kg.s^{-1}**	**TR22[a] °C**	**DRS[a] rad.s^{-1}**	**Axial product temperature profile** - iButton® sensors **Experimental Residence Time Distribution (RTD)** - Colorimetric technique **Modelling of RTD** - Gamma distribution model (GDM) - Tank-in-series model (TSM) - Axial dispersion model (ADM)
1	0.007	-15.4	78.5	
2	0.014	-15.3	78.5	
3	0.021	-15.4	78.5	
4	0.014	-10.6	78.5	
5	0.014	-20.1	78.5	
6	0.014	-15.4	57.1	
7	0.014	-15.3	104.7	

[a] MFR = mix flow rate; TR22 = evaporation temperature of r22; DRS = dasher rotational speed.

Experimental RTD data showed that high product flow rates led to a narrowing of the RTD and thus to less axial dispersion. This effect can be explained by the enhancement of the radial mixing with the decrease in the apparent viscosity of the product. Spreading of the RTD was obtained for lower refrigerant fluid temperatures. Indeed, in this case, there is a higher radial temperature gradient between the wall and the core of the exchanger, leading to a higher gradient of the apparent viscosity. This effect increased the difference in axial flow velocities and thus an increase in axial dispersion. An increase in the rotation speed led to a broadening of the RTD curve and increased the axial dispersion in the SSHE.

The GDM model was the most appropriate to describe the experimental RTD data, followed by the TSM model and the ADM model.

The experimental and modelling data in this article made it possible to take into account the RTD for the modelling of the ice crystallization process as presented in article 5.

4.3. Rheological characterization of sorbet using pipe rheometry during the freezing process.

The third article presents the rheological measurements of sorbet without aeration. The aim of this article was to investigate the influence of the temperature of the product and therefore the ice content on the apparent viscosity of non-aerated sorbet when the product flows out from the SSHE. In this article we also propose an empirical rheological model that predicts the apparent viscosity of sorbet as a function of the evolution of the apparent viscosity of the continuous liquid phase, the product temperature and the ice volume fraction. This information will make it possible to have a better understanding of the development of the texture of the product, and can contribute to the improvement in the design of piping systems and the modelling of the freezing process of sorbet. A schematic representation of the study of the apparent viscosity carried out in this article is shown in Fig. 4.3.

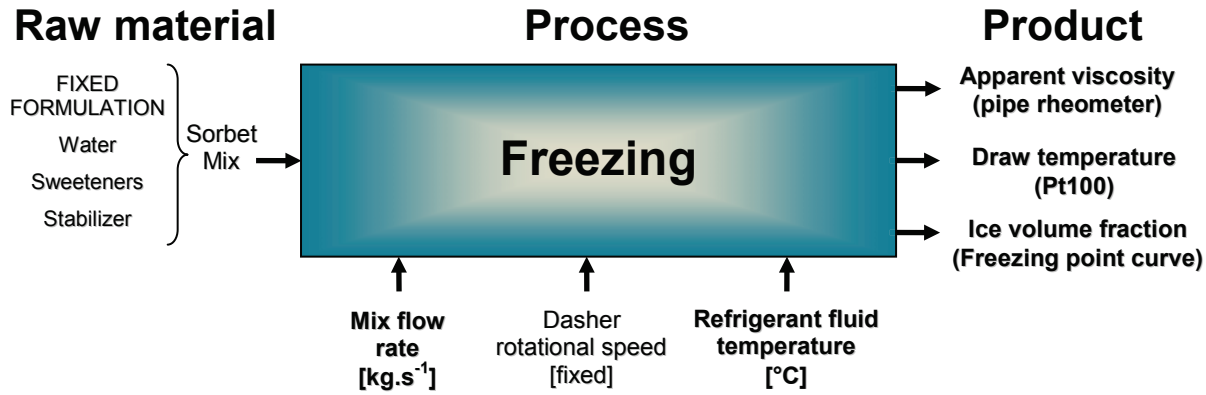


Fig. 4.3. Schematic representation of the study carried out in article 3.

The rheological properties of sorbet were measured in situ by means of a pipe rheometer connected at the outlet pipe of the SSHE. The pipe rheometer was composed of a series of pipes in PVC of different diameters, making it possible to apply a range of apparent shear rate from 4 to 430 s^{-1}. Table 4.3. presents the operating conditions under which the viscosity measurements were carried out. Three replicates were performed for the rheology experiments carried out at a mix flow rate of 0.007 $kg.s^{-1}$, and two replicates for the measurements performed at 0.010 and 0.014 $kg.s^{-1}$.

Table 4.3. Operating conditions tested during the experiments carried out in article 3.

Run	Operating conditions			Product characterisation
	MFR[a] ($kg.s^{-1}$)	DRS[a] ($rad.s^{-1}$)	TR22[a] (°C)	
1	0.007	78.5	-7.20	**Apparent viscosity**
2	0.007	78.5	-8.26	- Pipe rheometer
3	0.007	78.5	-9.40	**Draw temperature**
4	0.007	78.5	-11.37	- Pt100 probe
5	0.007	78.5	-12.91	**Ice volume fraction**
6	0.007	78.5	-16.34	- Pt100 and freezing point depression curve

[a] MFR = mix flow rate; DRS = dasher rotational speed; TR22 = evaporation temperature of r22.

The additional experiments performed with product flow rates of 0.010 and 0.014 $kg.s^{-1}$ made it possible to demonstrate that no wall slip occurred during the measurements. Results showed a decrease of the flow behaviour index with the decrease in the temperature of the product, the effect of which indicates that the product becomes more shear-thinning as the freezing of sorbet occurs. The consistency coefficient and therefore the magnitude of the apparent viscosity of sorbet increase with the decrease in product temperature and with the increase of the ice volume fraction. This effect can be explained by two simultaneous effects occurring during freezing: firstly, the freeze concentration of polysaccharides and sweeteners increases the colloidal forces between particles and leads to the increase in the apparent viscosity of the liquid phase. Secondly, the increase in the ice volume fraction leads to the increase in the hydrodynamic alterations in the flow field and thus to the increase in the apparent viscosity of the product.

A rheological model that predicts the apparent viscosity of the product was presented. The comparison between experimental and predicted data showed that the model presents a relative close fit to the experimental data within a 20% error.

The rheological model proposed in this article was used in the modelling of the ice crystallization process and made it possible to account for viscous dissipation occurring during the freezing process in the SSHE as presented in article 5.

4.4. Influence of ice and air volume fractions on the rheological properties of sorbet.

The rheology of sorbet is strongly related to microstructure features, such as the dispersion of the air bubbles and ice crystals in the continuous liquid phase. However, there is little information available in the literature on the separated effects of the ice volume fraction and the air volume fraction on the apparent viscosity of the product as it flows out from the SSHE. The fourth article presents the rheological measurements of sorbet with aeration. In this article we study separately the influence of the ice volume fraction ($\phi_{v.ice}$.) on the increase in the apparent viscosity (η_{app}) of a non aerated frozen sorbet, and the influence of the air volume fraction ($\phi_{v.a.}$) on the increase in the viscosity of an aerated frozen sorbet. This article may help to improve the control of the incorporation of air and the formation of the ice crystals during the freezing process of sorbet, so as to obtain a better control of the product quality. A schematic representation of the study of the apparent viscosity carried out in this article, with the control variables and the obtained responses is shown in Fig. 4.4.

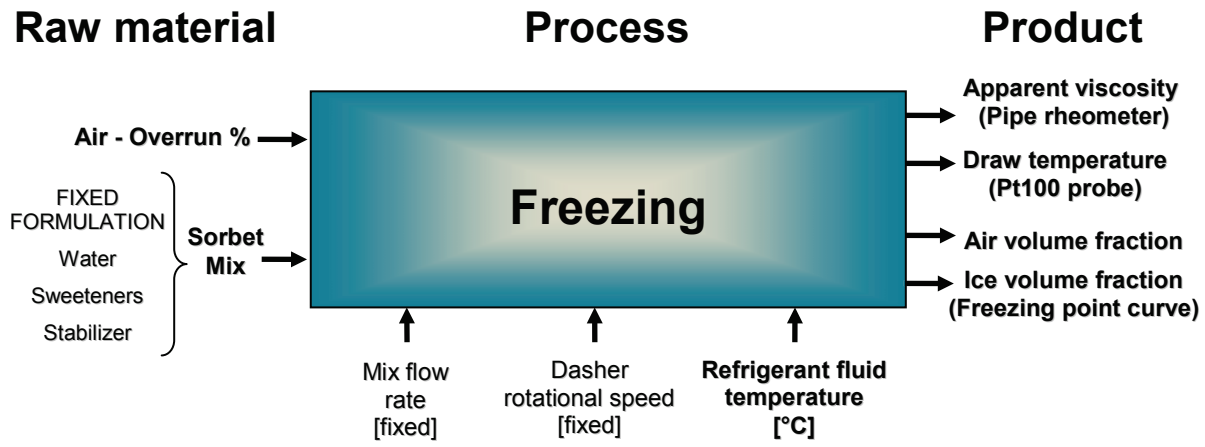


Fig. 4.4. Schematic representation of the study carried out in article 4.

In this work, the rheological properties of sorbet have been studied in situ by means of a pipe rheometer connected at the exit of the SSHE. Table 4.4. presents the operating conditions tested in article 4. Two replicates were performed for the rheology measurements

of non-frozen sorbet mix and frozen aerated sorbet. Three replicates were performed for the apparent viscosity measurements of non-aerated frozen sorbet.

Table 4.4. Operating conditions tested during the measurements carried out in article 4

Rheological measurement for sorbet mix and frozen sorbet without aeration					
	Operating conditions [a]				**Product characterization**
Run	**TR22**[b] **(°C)**	**Overrun %**	$\phi_{v.a}$ [b]	$\phi_{v.ice}$ [b]	
1	-	-	-	-	**Apparent viscosity** - Pipe rheometer **Draw temperature** - Pt100 probe **Ice volume fraction** - Pt100 and freezing point depression curve
2	-7.20	-	-	0.058	
3	-8.26	-	-	0.11	
4	-9.40	-	-	0.17	
5	-10.79	-	-	0.23	
6	-11.09	25	0.2	0.23	
7	-11.31	50	0.34	0.23	
8	-11.53	100	0.5	0.23	

[a]Operating conditions performed at 0.007 kg.s^{-1} and dasher rotational speed of 78.5 rad.s^{-1}.
[b]TR22 = evaporation temperature of r22; $\phi_{v.a}$ = air volume fraction; $\phi_{v.ice}$ = Ice volume fraction.

Results showed that in the non aerated frozen sorbet, an increase in $\phi_{v.ice}$ of 23% led to an increase in η_{app} that represents 20 times the viscosity of the non frozen sorbet mix at $\dot{\gamma} = 10\text{s}^{-1}$. For this given $\phi_{v.ice}$, an increase in $\phi_{v.a.}$ of 50% led to an increase in η_{app} of the aerated frozen sorbet that represents 3 times the viscosity of the non aerated frozen sorbet. This indicates that the influence of $\phi_{v.ice}$ on the increase in η_{app} of the product is predominant, with respect to the effect of $\phi_{v.a.}$.

The results obtained in this work can be useful to improve the control of the incorporation of air and the amount of ice crystals formed during the freezing process of sorbet, so as to obtain a better control of the quality of frozen desserts.

5.5. Coupling population balance and residence time distribution for the ice crystallization modelling in a scraped surface heat exchanger.

The modelling of the ice crystallization process makes it possible to gain deeper understanding of the evolution of ice crystal size distribution during the freezing process in a SSHE. It has been shown in literature the importance of considering the effect of the ice crystallization on the flow behaviour of the product, which can be taken into account by considering the evolution of the apparent viscosity and the RTD of the product. However, little attention has been paid to the coupling of empirical models of RTD with heat transfer and population balance equations (PBE). This article presents the mathematical modelling of the ice crystallization process occurring during the freezing of sorbet (without air) in the SSHE.

Two different modelling approaches have been used, both of which include the nucleation, growth and breakage phenomena of the ice crystals. For both models, the rate of ice crystal nucleation and growth were determined by the subcooling degree. The first model combines heat transfer and population balance equations (PBE), assuming plug flow (PF). The evolution of the values of product temperature, mean chord length, ice volume fraction and apparent viscosity were determined as a function of the residence time. The second model is a coupled model of heat transfer and PBE combined with an empirical model of residence time distribution (RTD), which makes it possible to take into account the fact that the fluid fractions flowing throughout the SSHE do not have the same time-temperature history. The values of the variables (product temperature and mean chord length) were determined for each fraction of fluid exiting the SSHE, and the bulk values were then calculated using the RTD.

A schematic representation of the study carried out in this paper with the operating conditions and the crystallization model responses is shown in Fig. 4.5.

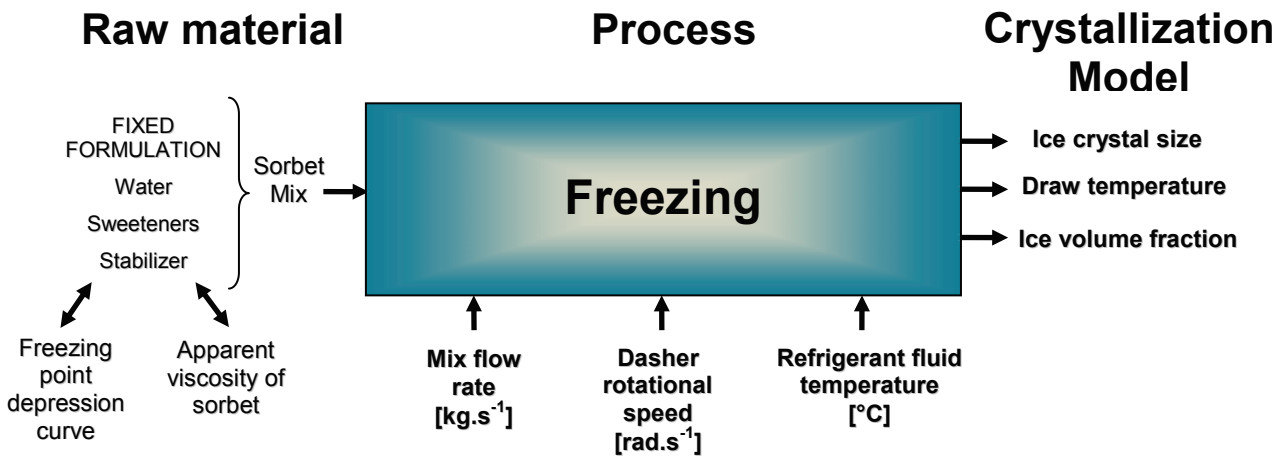


Fig. 4.5. Schematic representation of the study carried out in article 5.

Simulation results were compared to the set of experimental data obtained in article 1. Table 4.5., shows the operating conditions under which the experimental and modelling data were obtained.

Table 4.5. Operating conditions tested during the modelling study carried out in article 5.

Run	Operating conditions			Modelling results
	MFR [a] ($kg.s^{-1}$)	TR22 [a] (°C)	DRS [a] ($rad.s^{-1}$)	
1	0.007	-15.3	78.5	**Simulated ice crystal mean chord length (MCL)** - Comparison with experimental MCL data of article 1
2	0.014	-15.3	78.5	
3	0.021	-15.4	78.5	**Simulated ice crystal chord length distribution at different residence times.**
4	0.014	-10.6	78.5	
5	0.014	-19.8	78.5	
6	0.014	-15.2	57.1	**Simulated draw temperature** - Comparison with experimental MCL data of article 1
7	0.014	-15.3	104.7	

[a] MFR = mix flow rate; TR22 = evaporation temperature of r22; DRS = dasher rotational speed.

With a first estimated set of model parameters, it was shown that the experimental tendencies are represented very satisfactorily by the two models within a 10% error limit.

A comparison between the ice CSD at the outlet of the SSHE obtained by the PF model and by the RTD model showed that the ice CSD of both modelling approaches were very similar. This effect is explained by the blending of the fractions of fluid that constitute the ice CSD, some of which exit earlier from the SSHE and have a larger ice crystal size

(due to the survival of the larger ice crystals and to the melting of the small ice crystals), and others that exit later from the SSHE and have a smaller crystal size (due to the survival of a larger quantity of small ice crystals and to the breakage of the larger ones), resulting thus in a compensation effect between the ice crystal sizes of all the fractions of fluid.

These modelling approaches can then be considered as a promising tool for the better understanding of the formation of ice crystals in SSHEs, which may help to identify new ways to improve the performance of the process. Furthermore, this model can reduce the time of scale-up of the freezing process from laboratory scale equipment to industrial scale production.

Fig. 4.6. shows a schematic summary of the articulation of the 5 articles that constitute Chapter 5 - Results and discussion.

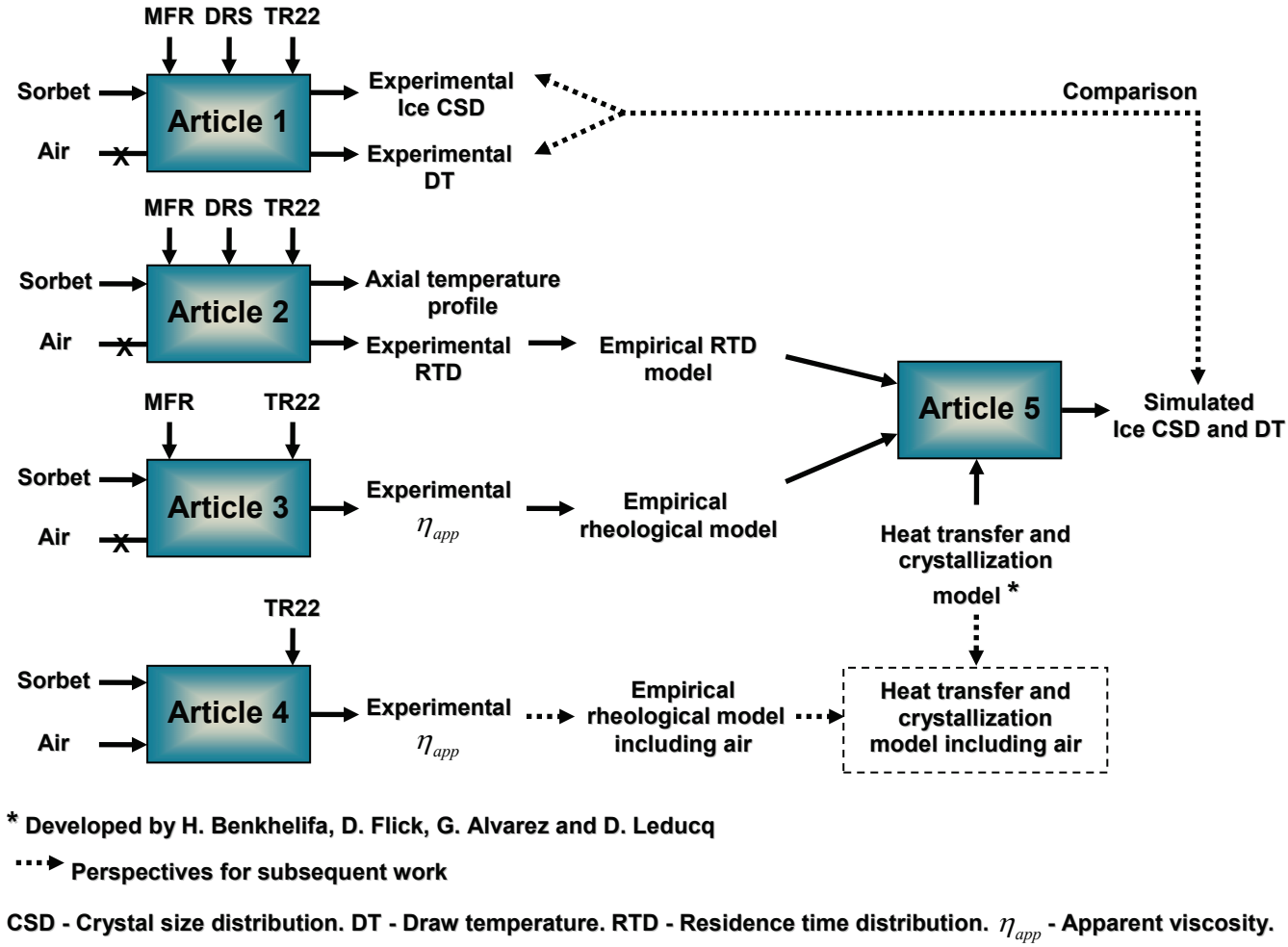


Fig. 4.6. Articulation of the 5 articles.

Chapter 5 - Results and discussion

5.1. Online ice crystal size measurements during sorbet freezing by means of the focused beam reflectance measurement (FBRM) technology. Influence of operating conditions.

Marcela Arellano[a,c,d], Hayat Benkhelifa[b,c,d], Denis Flick[b,c,d], Graciela Alvarez[a,2].

[a]*Irstea. UR Génie des Procédés Frigorifiques. 1 rue Pierre-Gilles de Gennes CS 10030, 92761 Antony Cedex, France*

[b]*AgroParisTech. UMR 1145 Ingénierie Procédés Aliments. 16 rue Claude Bernard, 75231 Paris Cedex 05, France*

[c]*INRA.UMR 1145 Ingénierie Procédés Aliments. 1 avenue des Olympiades, 91744 Massy Cedex, France*

[d]*CNAM. UMR 1145 Ingénierie Procédés Aliments. 292 rue Saint-Martin, 75141 Paris Cedex 03, France*

Abstract

In ice cream and sorbet manufacturing small ice crystals are desired to deliver a product with a smooth texture and good palatability. This research studied the influence of the operating conditions on the ice crystal size and the draw temperature of the sorbet during the freezing process. The evolution of ice crystal size was tracked with the focused beam reflectance measurement (FBRM) technique, which uses an in situ sensor that makes it possible to monitor online the chord length distribution (CLD) of ice crystals in sorbets containing up to 40% of ice. The refrigerant fluid temperature had the most significant influence on the mean ice crystal chord length, followed by the dasher speed, whereas the mix flow rate had no significant influence. A decrease in the refrigerant fluid temperature led to a reduction in ice crystal size, due to the growth of more small ice crystals left behind on the scraped wall from previous scrapings. Increasing the dasher speed slightly reduced the mean ice crystal chord length, due to the production of new small ice nuclei by secondary nucleation. For a given refrigerant fluid temperature and dasher speed, low mix flow rates resulted in lower draw temperatures, due to the fact that the product remains in contact with the freezer wall longer. High dasher speeds warmed the product slightly, due to the dissipation of frictional energy in the product, the effect of which was in part moderated by the improvement in the heat transfer coefficient between the product and the freezer wall.

Key words: Ice crystal size; Chord length; Draw temperature; Focused beam reflectance measurement; Freezing; Scraped surface heat exchanger.

2 Corresponding author. Tel.: +33 140 96 60 17; Fax: +33 140 96 60 75.
E-mail address: graciela.alvarez@irstea.fr

1. Introduction

In the manufacturing process of frozen desserts such as sorbet and ice cream, three main steps can be distinguished: preparation of the mix, initial freezing, and hardening of the product. The first step includes the blending of all the ingredients, its pasteurization and homogenization, as well as the cooling and ripening of the mix at 5 °C. During the initial freezing step, the mix is pumped through a scraped surface heat exchanger (SSHE) or freezer. The evaporation of the refrigerant fluid in the jacket of the freezer cools down the temperature of the mix below its freezing point, and causes formation of an ice layer at the wall of the freezer barrel (Cook and Hartel, 2010). Subsequently, the scraper blades of the rotating dasher remove the ice layer from the freezer wall. The small ice crystals contained in the ice layer are dispersed into the centre of the freezer barrel, where they grow and become disc-shaped ice crystals that exit the freezer with a mean size of 15 to 27 μm (Drewett and Hartel, 2007; Marshall et al., 2003; Russell et al., 1999; Sofjan and Hartel, 2004). At this stage, roughly half of the total amount of water is frozen (Hartel, 1996). Depending on the operating conditions of the process, the draw (exit) temperature of the product varies from -4 to -6 °C, having an adequately low viscosity to be pumped for moulding and packaging. Further on, in the hardening step, the product is introduced into a blast freezer to attain a core temperature of -18°C (Cook and Hartel, 2010), where roughly 80% of the amount of water is frozen (Marshall et al. 2003). Since the subcooling rate during hardening is not high enough to form new nuclei, the increase in the amount of ice formed with the decrease in temperature follows the equilibrium freezing point curve and leads to the increase in size of the existing ice crystals (Marshall et al. 2003). Hence, the final ice crystal size of the product will be dictated to a large extent by the evolution during the hardening step of the ice crystals that were formed during the initial freezing. Consequently, the initial freezing process is the most critical step in ice cream and sorbet manufacturing.

The mechanism of ice crystallization within a freezer is affected mainly by the operating conditions of the freezing process, such as the evaporation temperature of the refrigerant fluid, the dasher rotational speed and the mix flow rate. The temperature of the refrigerant fluid provides the driving force that triggers ice nucleation and it determines the heat removal rate of the system. During freezing, ice nucleation occurs at the freezer wall, where there is enough subcooling (roughly -30 °C) between the refrigerant fluid and the mix to form ice nuclei (Hartel, 1996). On the basis of dendritic growth observations in quiescently-frozen sucrose solutions on a chilled surface, Schwartzberg and Liu (1990) suggested that due to the high rate of subcooling at the heat exchange cylinder wall, dendrites are likely to grow there, then are cut off and dispersed into the bulk flow by the scraper blades of the dasher. Subsequently, ice nuclei ripen and become disc-shaped ice crystals in the bulk warm region of the freezer (Cook and Hartel, 2010). Schwartzberg (1990) reported that the space between dendrites was proportional to the freezing rate to the -1/2 power, which means that high subcooling rates lead to a faster growth of more dendrites, with closely spaced branches and a thinner structure. More recently, on the basis of thermal conductivity measurements of a sucrose solution in a flowcell equipped with a scraper blade and a chilled surface, Zheng (2006) concluded that the ice layer formed at the freezer wall was in fact a slush layer composed of both ice and concentrated sucrose solution. Zheng (2006) also found that after each scrape of the blade, many ice nuclei grew rapidly from the ice debris remaining from previous scrapings, and continued to grow along the chilled surface before merging and growing vertically. Hence, a decrease in temperature of the refrigerant fluid would be expected to enhance the cooling rate, causing the faster formation of more ice crystals from the ice debris left behind from previous scrapings, which will grow with a thinner structure and lead to smaller ice crystal sizes.

The scraping action of the dasher improves the heat transfer rate between the freezer wall and the product (Ben Lakhdar et al., 2005). Higher dasher speeds would thus be expected to give lower draw temperatures and smaller ice crystals. However, an increase in dasher speed would also increase the amount of frictional heat generated by the blades, which could dissipate into the product, producing warmer draw temperatures, the melting of the small ice nuclei, and consequently, a reduction in the effective ice nucleation rate. Also, by increasing dasher speed, we increase the movement of the fluid within the freezer, which leads to the enhancement of ice recrystallization phenomena (Cebula and Russell, 1998). Furthermore, an increase in dasher speed may also lead to the attrition of the larger ice crystals (Haddad, 2009; Windhab and Bolliger, 1995), the remaining ice debris of which can lead to the formation of new ice nuclei through secondary nucleation. Sodawala and Garside (1997) used video microscopy to examine the freezing of a 10% sucrose solution on a cold surface with a rotating scraper blade. They observed the formation of ice flocs which grew parallel to the surface after each scrape, then merged and grew vertically. They also observed that an increase in the scraping frequency of the blade led to more frictional heat and to smaller flocs being cut off from the surface. Hence, increasing dasher speed would also be expected to produce new smaller ice nuclei formed from the remaining smaller ice flocs at the surface of the freezer wall.

The mix flow rate dictates the residence time of the product within the freezer, affecting the time available to remove heat from the product, and consequently, the ice nucleation and growth mechanisms of ice crystals. A number of studies in the literature have observed that high mix flow rates (short residence times) for a given draw temperature (by adjusting the temperature of the refrigerant fluid) and dasher speed produced smaller ice crystals due to the reduction in recrystallization phenomena in the bulk region of the product (Drewett and Hartel, 2007; Koxholt et al., 2000; Russell et al., 1999). For a given refrigerant

fluid temperature (varying exit temperature) and dasher speed, Russell et al. (1999) also found smaller ice crystals produced at higher mix flow rates, the effect of which was attributed to the reduction in ice crystal coarsening. During the freezing of 30% sucrose/water solutions in an SSHE, Ben Lakhdar et al. (2005) reported that low product flow rates (long residence times) led to a reduction in the exit temperature of the product, and therefore to an increase of the ice mass fraction in the product.

Several studies have highlighted the importance of producing a narrow ice crystal size distribution (CSD) with a small mean size (< 50μm) so as to confer a smooth texture to the final product and enhance consumer acceptance (Cook and Hartel, 2010; Drewett and Hartel, 2007; Hartel, 1996; Russell et al., 1999). It is therefore important to identify the operating conditions of the freezing process that most directly affect ice crystal size so as to improve the quality of the final product.

In order to characterize the ice CSD, many methods have been used. However, some of these methods partially destroy the ice crystal structure during sample preparation, and none of them have been able to directly measure the ice crystal size in the exit stream of the product during the freezing process. Recently, online techniques such as the focused beam reflectance method (FBRM) have been developed for in situ monitoring of CSD in the crystallisation processes of chemical and pharmaceutical products (Barrett and Glennon, 2002; Negro et al., 2006). In the case of ice crystallization, Haddad et al. (2010) have successfully used the FBRM technique to follow the evolution of ice crystal size during batch freezing of sucrose/water solutions. The FBRM technique is based on the principle of a laser beam that is focused at the window of the tip of the measurement probe. The rotating optics inside the probe allows the laser beam to scan a circular path in the region near the window of the probe. When the laser beam intersects a particle, it traces a chord length across the particle. A chord length is defined as a straight line between any two points on the edge of a

particle, regardless of how the particle is presented to the probe. The sensor detects the light reflected by the particle, registers the time period of reflection and deduces the length of the chord. FBRM measures thousands of chord lengths per second, sorted into 100 logarithmic size classes and represented as a chord length distribution (CLD). One of the main advantages of this technique is its suitability for in situ measurements of particles at high solid concentrations. However, the FBRM technique gives no information about the morphology of the particles and it measures a CLD rather than a CSD. Still, this measurement can be useful for following the evolution of the ice crystal size.

The present work aimed at studying the influence of operating conditions on the ice crystal chord length monitored online by the FBRM probe, as well as on the draw temperature measured online by a Pt100 probe. The work was carried out during the freezing of lemon sorbet.

2. Materials and methods

2.1. Sorbet freezing

The mix used in these experiments was an ultra high temperature pasteurized lemon sorbet mix (14.6% w/w sucrose, 8% w/w fructose, 0.09% w/w dextrose, 3% w/w lemon juice concentrate 60 Brix, 0.5% w/w locust bean gum / guar gum / hydroxypropyl methylcellulose stabiliser blend). The mix was stored at 5 °C for 24 h prior to use. Freezing of the mix was carried out in a laboratory scale continuous pilot freezer (WCB® Model MF 50), a schematic representation of which is shown in Fig. 5.1.1. The inner diameter of the heat exchange cylinder was 0.05 m and the length was 0.40 m. The rotor of the freezer was equipped with two rows of scraper blades and occupied roughly 46% of the freezer barrel volume.

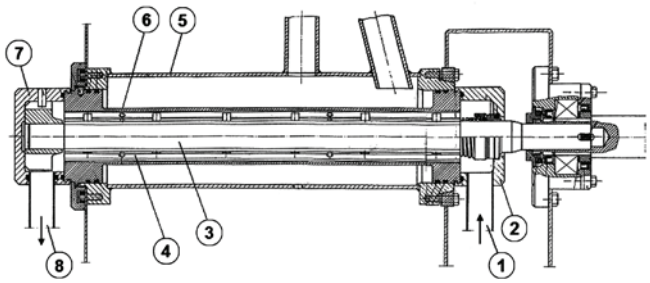


Fig. 5.1.1. Schematic diagram of pilot Freezer WCB MF 50. 1. Inlet connection for sorbet mix. 2. Inlet cover bowl. 3. Rotor. 4. Scraper blades. 5. Freezer jacket with vaporizing r22. 6. Heat exchange cylinder. 7. Outlet cover bowl. 8. Outlet pipe for sorbet.

The freezer had a variable capacity of 0.007 to 0.021 $kg.s^{-1}$. The mix flow rate was determined by weighing the product exit stream during a given period of time. The accuracy of this measurement was determined to be $\pm 9.2x10^{-5}$ $kg.s^{-1}$. The dasher speed of the freezer varied from 57 to 105 $rad.s^{-1}$ (545 to 1000 rpm) according to experimental conditions. The dasher speed was measured by means of a photoelectric tachometer (Ahlborn®, type FUA9192) with an accuracy of ± 0.105 $rad.s^{-1}$ (1 rpm). The evaporation temperature of the refrigerant fluid r22 (Chlorodifluoromethane) inside the jacket of the freezer was adjusted within the range of -10 to -20 °C as established by the experimental design described in the following section. A calibrated type T (copper - constantan) thermocouple with an accuracy of ±0.2 °C was fixed with conductive aluminium tape on the external surface wall of the freezer jacket, so as to measure the evaporation temperature of the refrigerant fluid. The exterior of the freezer jacket was isolated with foam of 2 cm thickness in order to reduce heat loss. No aeration was employed for any of the experiments.

2.2. Experimental design and statistical analysis

A central composite experimental design was used to assess the influence of 3 operating conditions – mix flow rate (MFR), dasher rotational speed (DRS) and evaporation temperature of R22 (TR22) – on the response variables: mean ice crystal chord length (MCL)

and draw temperature (DT) of the sorbet. The central composite experimental design was composed of three sets of experimental runs, a 2^3 set with experimental points at ±1, a 2x3 set with points at the extremes of the experimental region (±α, with α = 1.68) and a central point at zero (Sablani et al., 2007). The experimental design was performed twice and 5 replicates of the central point were performed in order to provide enough information to estimate experimental error. Table 5.1.1 shows the coded values of the experimental design and the real freezing operating conditions. Experimental data were analysed using the response surface methodology. The second-order polynomial model used to predict the experimental behaviour was the following:

$$\hat{Y} = \beta_0 + \sum_{i=1}^{3} \beta_i X_i + \sum_{i=1}^{3} \beta_{ii} X_i^2 + \sum \sum_{i<j=1}^{3} \beta_{ij} X_i X_j \qquad (1)$$

where $\hat{Y}$ is the predicted value of the response; β_0, β_i, β_{ii} and β_{ij} are the regression coefficients for interception, linear, quadratic and interaction effects, respectively, and X_i, X_j are the coded levels of the experimental conditions.

The adequacy of each model was assessed by a lack-of-fit test, which assumes *c* experimental points with d_i replicates. Subsequently, it decomposes the residual error sum of squares (*SS*) into one component due to the variation of the replication around their mean value (pure error sum of squares) and into another component due to the variation of the mean values around the model prediction (Lack-of-fit error sum of squares), as shown in the following equation:

$$\sum_{i=1}^{c} \sum_{j=1}^{d_i} \left(Y_{ij} - \hat{Y}_i\right)^2 = \sum_{i=1}^{c} \sum_{j=1}^{d_i} \left(Y_{ij} - \overline{Y}_i\right)^2 + \sum_{i=1}^{c} d_i \left(\overline{Y}_i - \hat{Y}_i\right)^2$$

Residual error SS = Pure error SS + Lack-of-fit Error SS (2)

and their associated degrees of freedom: (d – 2) = (d – c) + (c – 2)

where Y_{ij} is the experimental response, $\hat{Y}_i$ the predicted value of the response and $\overline{Y}_i$ the mean response value for d_i replicated experimental points (SAS Institute Inc., 2008).

The null hypothesis for the lack-of-fit test is that the proposed model predicts the response correctly. The statistical significance is assessed by the F ratio, given by the following equation:

$$F = \frac{\sum_{i=1}^{c} d_i \left(\overline{Y}_i - \hat{Y}_i\right)^2}{c-2} \Bigg/ \frac{\sum_{i=1}^{c}\sum_{j=1}^{d_i} \left(Y_{ij} - \overline{Y}_i\right)^2}{d-c} \qquad (3)$$

This F ratio is compared to the F-distribution for the associated degrees of freedom and provides a p-value. If the p-value for the F-test of lack-of-fit is non significant ($p > 0.05$), we do not reject the null hypothesis, i.e. the model is assumed to be correct.

2.3. Draw temperature measurements and ice mass fraction calculations

The draw (exit) temperature determines the ice mass fraction in sorbet $X_{m.i.}$ (kg of ice / kg of sorbet). A decrease in the draw temperature will result in an increase of the ice mass fraction, as well as an increase of the apparent viscosity of the product (Cerecero, 2003; Goff et al., 1995). The relationship between the draw temperature of sorbet and its ice mass fraction is established by the equilibrium freezing point curve of sorbet. This curve had been previously determined in our laboratory using differential scanning calorimetric (DSC) measurements. Furthermore, the calculation of the ice mass fraction $X_{m.i.}$, is based on a mass balance of solute (sweetener content), considering a thermodynamic equilibrium between the two phases (ice and concentrated solute solution) and taking into account the fact that ice crystals are constituted exclusively of water (Cerecero, 2003).

Initially, the solute is present in sorbet mix at a certain initial mass fraction ($X_{ms.i}$). Then, the solute is concentrated as freezing of the sorbet occurs, until it reaches a final mass

fraction ($X_{ms.f}$) in the liquid phase that is related to the temperature by the equilibrium freezing point curve. Since the final liquid phase represents only a fraction $(1 - X_{m.i.})$ of the sorbet, the ice mass fraction can be calculated by the following equation:

$$X_{ms.i} = (1 - X_{m.i.}) \cdot X_{ms.f}(T) \Leftrightarrow X_{m.i.} = 1 - \frac{X_{ms.i}}{X_{ms.f}(T)}, \qquad (4)$$

Once the experimental conditions of the freezer were set and the steady state of the system was attained, the draw temperature of the product was measured online by means of a calibrated Pt100 probe (Baumer®, accuracy of ±0.1 °C). The Pt100 probe was inserted into the outlet pipe of the freezer before the exit of the product as shown in Fig. 5.1.2. Draw temperature and ice mass fraction data were recorded and calculated every 5 seconds for a period of 10 minutes by using a program written in LabVIEW®.

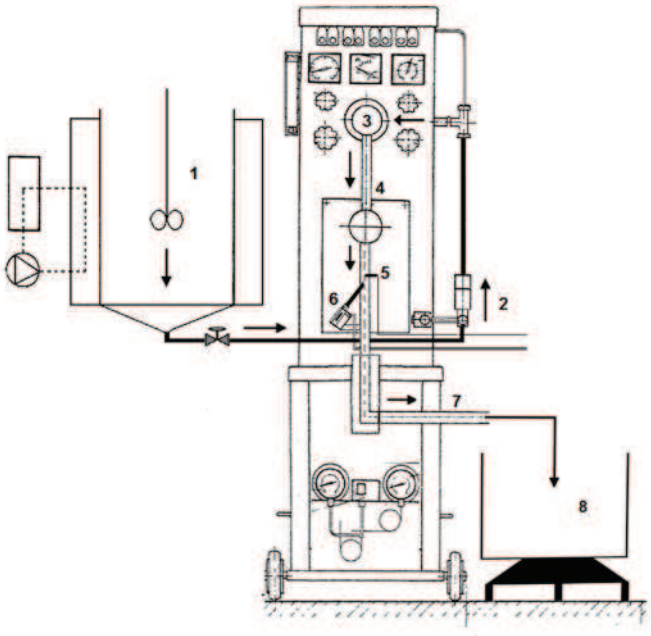


Fig. 5.1.2. Schematic representation of the experimental platform. 1. Refrigerated storage tank (200 litres capacity). 2. Volumetric piston pump. 3. Freezer. 4. Outlet pipe. 5. Pt100 probe inserted into the outlet pipe. 6. FBRM probe inserted into the outlet pipe. 7. Product exit. 8. Reception tank.

2.4. Ice crystal CLD measurements by the FBRM probe

The ice crystal CLD was measured online using a Mettler-Toledo Lasentec® FBRM probe (Model S400A-8). This device is composed of a stainless steel body 8 mm in diameter. At the tip of the probe tip there is a sapphire window through which a 780nm laser beam is transmitted to the sample. A set of rotating optics, inside the probe, focuses the laser beam into a small spot, creating a scanning circular path at the interface between the window of the probe and the particles in suspension (cf. Fig. 5.1.3A). When a particle is intersected by the laser beam, it reflects the laser light throughout the time it is being scanned (cf. Fig. 5.1.3B). Simultaneously, the time period of reflection is detected by the FBRM probe and then multiplied by the tangential speed of the laser beam, yielding a distance across the particle, which is a chord length (Greaves et al., 2008; Wynn, 2003). The tangential speed of 2 m/sec of the laser beam is typically much faster than that of the particles, which makes it possible to consider that the particles are fixed with respect to the laser scanning path. The effect of particle motion is therefore considered negligible for the measurements (Abbas et al., 2002).

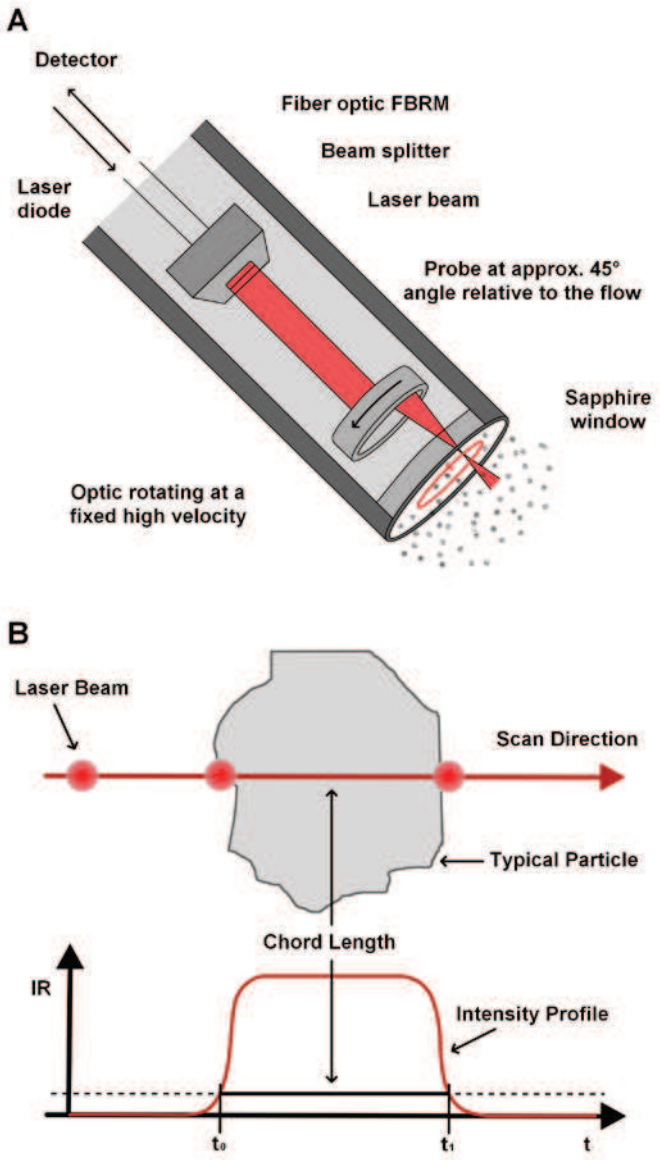


Fig. 5.1.3. (A) Cutaway view of the FBRM probe. (B) Measurement principle of a particle's chord length by the FBRM technique (Figure provided by Mettler-Toledo).

The signals produced by the FBRM probe can be processed in two different modes: the 'fine' mode and the 'coarse' mode. When the 'fine' mode is used, the particles measured are counted individually. The 'coarse' mode considers the individual particles that constitute an aggregate as a whole (cf. Fig 5.1.4.). Therefore, throughout our experiments the 'fine' mode was used in order to enhance the FBRM probe sensitivity to measure each ice crystal in the product individually.

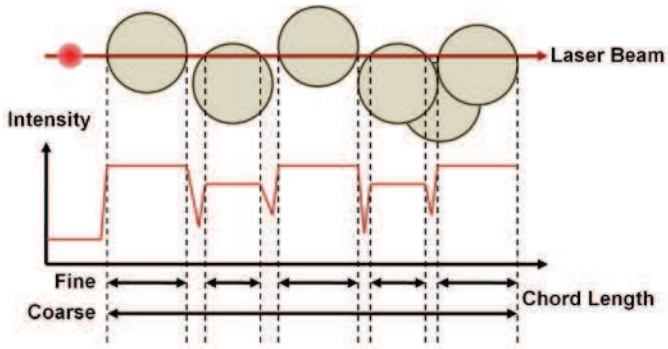


Fig. 5.1.4. Schematic diagram of the chord length measurement of an aggregate with the 'Fine' and 'Coarse' mode.

The FBRM probe measures thousands of chords per second, providing a CLD i.e. the number of counts per second sorted by chord length into 100 logarithmic size classes. Starting with this information, the mean chord length of the ice crystals is obtained by Eq. 2:

$$MCL = \sum_{i=1}^{100} n_i c_i \,/\, \sum_{i=1}^{100} n_i \,, \qquad (2)$$

where n_i is the number of particles for each of the size classes i of chord length c_i.

2.4.1. Relationship between CLD and PSD

Wynn (2003) established the relationship between the moments of CLD and PSD, and determined that the mean chord length of a sphere is $\pi/4 \cong 0.785$ times smaller than its diameter. Hence, the mean ice crystal chord length can be considered to be roughly 22% smaller than the mean particle size of the ice crystals, if we assume that they are spherical in shape. However, sometimes the mean chord length can be smaller than the mean particle size by a factor of less than 0.785 (Wynn, 2003). In order to illustrate this relationship, a simultaneous measurement of a known particle size suspension was performed using the FBRM probe and a video microscopy sensor probe, the EZ Probe D12® (developed by the ESCPE in Lyon, France), the measurement principle of which is explained elsewhere (Presles et al., 2009). The suspension was composed of polyamid seeding particles (PSP) with a mean size of 27.5 µm suspended at a concentration of 0.25% w/w in ethanol. The images generated

by the EZ Probe D12® sensor were processed by image analysis, so as to determine the PSD of the suspension (based on a sample of 3000 particles). Starting with this PSD data, the CLD was calculated by a conversion algorithm that follows the same mathematical approach as the one reported by Haddad (2009). Fig. 5.1.5. shows the comparison of the CLD calculated from the EZ Probe D12® PSD data and the CLD directly measured by the FBRM probe.

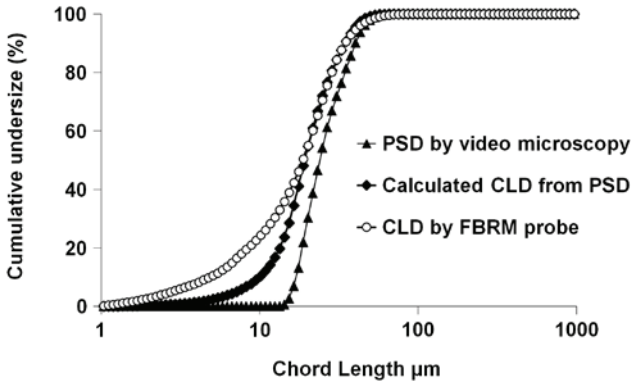


Fig. 5.1.5. Comparison of the calculated CLD from PSD data determined by video microscopy, and the CLD measured by the FBRM probe (PSP at 0.25% w/w suspended in ethanol, of mean size of 27.5 µm).

It can be observed from Fig. 5.1.5. that there is good agreement overall between the FBRM measurements and the calculated CLD, although the FBRM probe tends to overestimate the number of small particles. For these results, the calculated CLD has a mean chord length of 21.6 µm, while the CLD measured directly by the FBRM probe has a mean chord length of 20.5 µm. This means that there is roughly a 5% difference between the calculated CLD and the CLD measured by the FBRM probe.

2.4.2. CLD Measurements at the freezer outlet

When performing the freezing experiments, the FBRM probe was inserted into the outlet pipe of the freezer at a 45° angle relative to the flow (cf. Fig. 5.1.2.), making it possible to continuously renew the sorbet flow that was being measured. In this way, it was possible to measure the CLD of the ice crystals contained in the exit stream of the product directly, without any sample preparation, thus preserving the ice crystal structure. In order to avoid

condensation at the inside surface of the FBRM probe window, a purge was carried out with nitrogen at 1 bar with a flow rate of 5 l/min. Once the steady state of the freezer was established, the chord length acquisition data were synchronized with draw temperature measurements and recorded every 5 seconds for a period of 10 minutes.

3. Results and discussion

3.1. Freezer operating conditions and global ANOVA analysis

Table 5.1.1. presents the operating conditions under which measurements were taken and the mean values of the responses obtained. The results show that using the FBRM sensor makes it possible to directly monitor the evolution of the CLD of the ice crystals contained in the exit stream of the product during the freezing of sorbets containing up to 40% of ice online (without sample preparation), which was one of the objectives of this research.

Table 5.1.1. Real freezing conditions during measurements and obtained responses.

Run	*Coded values*			*Real values*			*Responses*		
	MFR	TR22	DRS	MFR $kg.s^{-1}$	TR22 °C	DRS $rad.s^{-1}$	MCL* µm	DT* ºC	$X_{m.i.}$ %
1	1	1	1	0.018	-18 ± 0.1	94.3	6 ± 0.1	-5.2 ± 0.2	31
2	1	1	-1	0.018	-18 ± 0.1	62.8	6.3 ± 0.1	-5.3 ± 0.1	31
3	1	-1	1	0.018	-12.6 ± 0.1	94.3	7.3 ± 0.1	-3.7 ± 0.1	18
4	1	-1	-1	0.018	-12.5 ± 0.1	62.8	7.3 ± 0.2	-3.7 ± 0.1	18
5	-1	1	1	0.010	-18.1 ± 0.1	94.3	5.9 ± 0.1	-6.2 ± 0.1	37
6	-1	1	-1	0.010	-18.1 ± 0.1	62.8	6.1 ± 0.2	-6.7 ± 0.1	38
7	-1	-1	1	0.010	-12.5 ± 0.1	94.3	7.1 ± 0.1	-4.6 ± 0.1	27
8	-1	-1	-1	0.010	-12.5 ± 0.1	62.8	7.5 ± 0.3	-4.7 ± 0.1	28
9	-α	0	0	0.007	-15.3 ± 0.1	78.5	6.3 ± 0.2	-6 ± 0.1	35
10	0	0	0	0.014	-15.3 ± 0.1	78.5	6.5 ± 0.2	-4.8 ± 0.1	28
11	+α	0	0	0.021	-15.4 ± 0.1	78.5	6.5 ± 0.1	-4 ± 0.1	21
12	0	0	-α	0.014	-15.2 ± 0.1	57.1	6.4 ± 0.1	-4.8 ± 0.1	28
13	0	+α	0	0.014	-19.8 ± 0.1	78.5	6 ± 0.2	-6.3 ± 0.1	37
14	0	-α	0	0.014	-10.6 ± 0.1	78.5	8.1 ± 0.1	-3.4 ± 0.1	14
15	0	0	+α	0.014	-15.4 ± 0.1	104.7	6.3 ± 0.2	-4.8 ± 0.1	28

[a] MFR = mix flow rate; TR22 = evaporation temperature of r22; DRS = dasher rotational speed; MCL = Mean Chord Length; DT = Draw temperature; $X_{m.i.}$ = ice mass fraction.
*Values are means of two replicates and 5 replicates for run 10.

The global ANOVA analysis in Table 5.1.2. shows that the mean chord length (MCL) response model is significant ($p < 0.0001$, $R^2 = 0.94$), with a non significant lack-of-fit ($p = 0.6$). Hence, we can consider that the second order polynomial model is adequate to predict the experimental behaviour of MCL. The model for the draw temperature of sorbet (DT) is also significant ($p < 0.0001$, $R^2 = 0.99$) and does not show lack-of-fit ($p = 0.8$). Therefore, the DT response can be adequately represented by the model. It is important to remind the reader that the use of these models should be limited to the range of experimental conditions used in this work.

Table 5.1.2. Analysis of variance for responses of mean chord length and draw temperature.

Response	R^2	F Value (Model)	p-value (Model)	p-value (Lack-of-Fit test)
MCL	0.94	55	<0.0001	0.6
DT	0.99	265	<0.0001	0.8

[a] MCL = Mean Chord Length; DT = Draw temperature; R^2 = coefficient of determination.

3.2. Influence of refrigerant fluid temperature and mix flow rate on draw temperature

According to the ANOVA analysis of the response variables in Table 5.1.3., the mix flow rate and the evaporation temperature of the refrigerant fluid had the most significant effect on the draw temperature (DT) at a 95% confidence interval.

Table 5.1.3. Regression coefficients of the experimental behavior model and significance levels at 95% (p-values) for responses of mean chord length and draw temperature.

	Interception		*Linear*		*Interaction*			*Quadratic*		
Response	β_0	β_1	β_2	β_3	β_{12}	β_{13}	β_{23}	β_{11}	β_{22}	β_{33}
MCL	17.896	-95.944	1.133	-9.05E-3	-2.714	0.731	-4.89E-5	334.98	0.028	-3.73E-5
p-value	<0.0001*	0.1636	<0.0001*	0.034*	0.4307	0.2329	0.9571	0.8658	<0.0001*	0.8157
DT	-4.771	285.87	0.262	0.031	-5.473	-0.902	-1.22E-3	-5896.98	-6.91E-3	-2.06E-4
p -value	<0.0001*	<0.0001*	<0.0001*	0.0014*	0.0284*	0.0391*	0.0626	0.0002*	0.0336*	0.0726

[a] MCL = Mean Chord Length; DT = Draw temperature.
Coefficients (β) subindex: 1 = Mix flow rate; 2 = Evaporation temperature r22; 3 = Dasher rotational speed.
* = significant influence at 95% confidence interval.

This effect concerned both their linear and quadratic terms ($p < 0.0001$ for β_1, $p < 0.0001$ for β_2, $p = 0.0002$ for β_{11} and $p = 0.0336$ for β_{22}), as well as their interaction effect ($p = 0.0284$ for β_{12}). Fig. 5.1.6. shows the surface plot of the draw temperature behaviour as a function of the evaporation temperature and mix flow rate at DRS = 78.5 rad.s^{-1}. The results show that a decrease in refrigerant fluid temperature leads to a reduction in the sorbet draw temperature as well as to an increase in the ice mass fraction (cf. Table 5.1.1., runs 10, 13 and 14) since more heat is removed from the product.

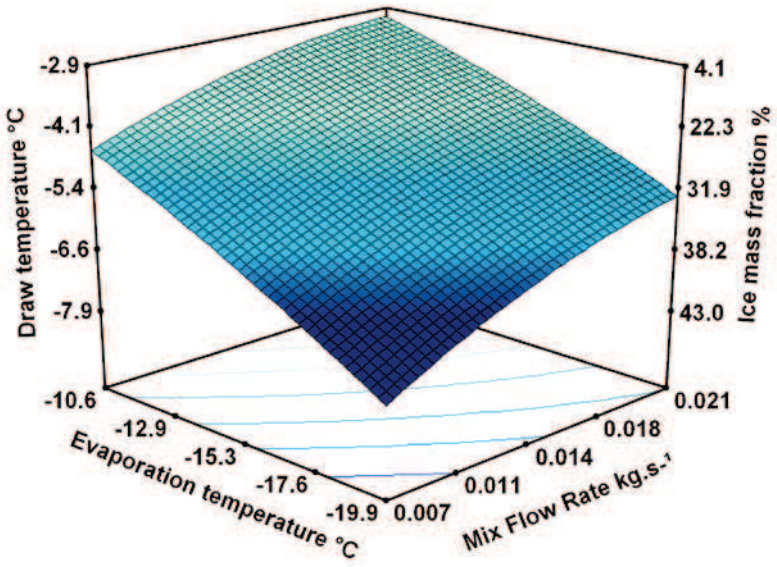


Fig. 5.1.6. Influence of evaporation temperature and mix flow rate at DRS = 78.54 rad.s^{-1} on the draw temperature and ice mass fraction of sorbet.

In Fig. 5.1.6. we can also observe that when the freezer operates at lower mix flow rates, the draw temperature of sorbet decreases, and inversely the ice mass fraction increases (cf. Table 5.1.1., runs 9, 10 and 11). This effect is explained by the increase in the residence time of the product with the decrease in the mix flow rate, since the product remains in contact with the freezer wall longer, so that more heat is removed from the product. Likewise, Ben Lakhdar et al. (2005) obtained higher ice mass fractions (lower product exit temperature) by reducing the product flow rate during the freezing of 30% sucrose/water solutions. For a given refrigerant fluid temperature (varying exit temperature) and dasher speed, Russell et al.

(1999) also found lower draw temperatures produced at lower mix flow rates due to the longer residence time available for heat removal.

3.3. Influence of refrigerant fluid temperature and mix flow rate on mean chord length

The ANOVA analysis in Table 5.1.3. shows that the mean chord length response was significantly affected at a 95% confidence interval by the evaporation temperature, for its linear and quadratic terms ($p < 0.0001$ for β_2 and $p < 0.0001$ for β_{22}). The mix flow rate did not show a significant effect ($p = 0.1636$ for β_1). Fig. 5.1.7. shows the surface response of the mean ice crystal chord length as a function of the evaporation temperature and mix flow rate at DRS = 78.5 $rad.s^{-1}$.

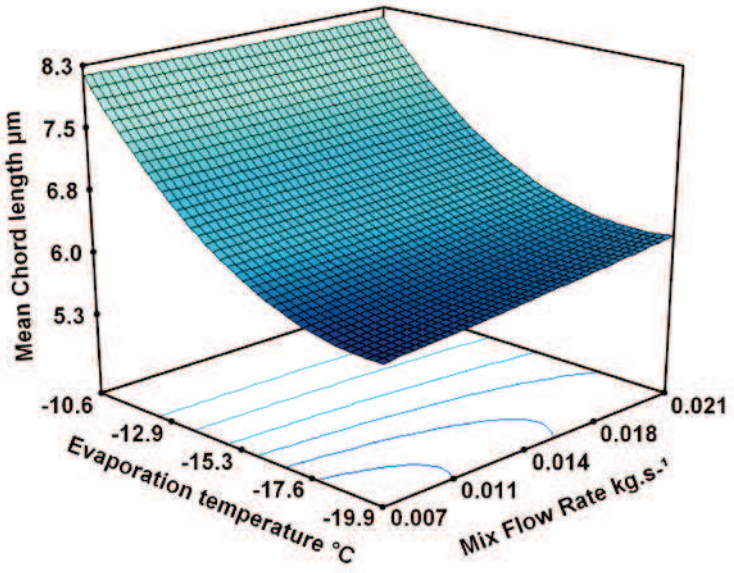


Fig. 5.1.7. Influence of evaporation temperature and mix flow rate at DRS = 78.54 $rad.s^{-1}$ on the mean chord length of sorbet

These results demonstrate that a decrease in the evaporation temperature of the refrigerant fluid leads to a reduction in the MCL. The influence of the refrigerant fluid temperature can be seen more clearly in Fig. 5.1.8., where the measured ice crystal CLD are shown at three different evaporation temperatures (cf. Table 5.1.1., runs 10, 13 and 14).

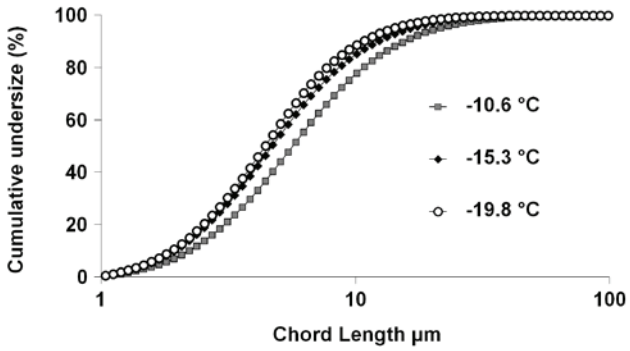


Fig. 5.1.8. Measured ice crystal CLD at refrigerant fluid temperature of -10.6, -15.3 and -19.8 ºC at DRS = 78.5 rad.s^{-1} and MFR = 0.014 kg.s^{-1}.

These results show that there is an increase in the population of small ice crystals with the decrease in the refrigerant fluid temperature. At -10.6 °C, 78% of the ice crystals are in the range of 1 to 10µm, and at -19.8 °C the population of the ice crystals in the same range increases to 88%. This effect can be explained by the enhancement of the cooling rate that leads to the formation of more ice crystals that grow with a thinner structure from the ice debris of previous scrapings, and therefore lead to the presence of a higher number of small ice crystals in the product. Similarly, Koxholt et al. (2000) as well as Drewett and Hartel (2007) obtained ice creams with smaller ice crystals by using low refrigerant fluid temperatures, the effect of which was attributed to the higher subcooling applied to the product which enhanced the nucleation rate.

It is generally accepted that the mean ice crystal size in ice creams and sorbets at the outlet of the freezer is 15 to 27 µm (Drewett and Hartel, 2007; Marshall et al., 2003; Russell et al., 1999; Sofjan and Hartel, 2004). However, Fig. 5.1.7. and 5.1.8. show that in the area of the experimental design of this work the MCL ranged from 5 to 9 µm. This difference between the ice crystal MCL and the ice crystal size can be explained by taking into account the fact that the MCL is often considered to be 0.785 times smaller than the particle size, and also, as previously discussed, the FBRM technique tends to overestimate the number of small particles.

Since the work of Russell et al. (1999), it has been commonly assumed that for a given refrigerant fluid temperature (varying exit temperature) and dasher speed, smaller ice CSD can be obtained by increasing the product flow rate, due to a reduction of crystal coarsening in the freezer. However, as we have just seen in our results (cf. Fig. 5.1.7. and Table 5.1.1., runs 9, 10 and 11), the mix flow rate did not have a significant effect on the mean ice crystal chord length (cf. Table 5.1.3., linear effect for β_1 on MCL). On the basis of these results it appears that there is a compensatory effect between two phenomena occurring in the freezer: on the one hand, as previously discussed, when using low mix flow rates, the residence time of the product is longer, leading to a decrease in the temperature of the product, as well as promoting further growth of the ice crystals. On the other hand, this reduction in the draw temperature of sorbet also corresponds to an increase in the ice mass fraction and therefore to an increase in viscosity. This tends to increase shear stress in the product at the freezer barrel, which increases the friction between ice crystals and results in the attrition of the larger ice crystals, the ice debris of which can generate new small ice nuclei by secondary nucleation.

3.4. Influence of dasher speed on draw temperature

According to the ANOVA analysis shown in Table 5.1.3., dasher speed had a significant influence on the draw temperature for its linear term ($p = 0.0014$ for β_3) and for its interaction with the mix flow rate ($p = 0.0391$ for β_{13}). The behaviour of the draw temperature response as a function of the evaporation temperature and the dasher speed at MFR = 0.014 $kg.s^{-1}$ is shown in Fig. 5.1.9.

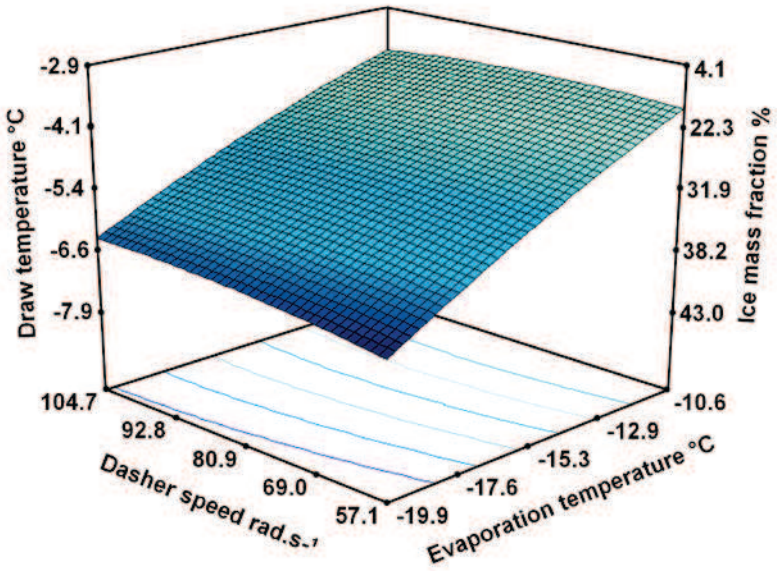


Fig. 5.1.9. Influence of dasher speed and evaporation temperature at MFR = 0.014 $kg.s^{-1}$ on the draw temperature and ice mass fraction of sorbet.

It can be seen that, although significant, the influence of dasher speed on the draw temperature is very small (cf. Table 5.1.1., runs 10, 12 and 15). However, its influence is slightly accentuated when low mix flow rates are used (cf. Table 5.1.3. interaction effect β_{13} on DT). Hence, we can consider that an increase in dasher speed at low mix flow rates leads to a very slight increase in the exit temperature of the product. In view of these results it is our opinion that this slight warming effect is due to an increase in the amount of frictional energy dissipated into the product, which is partially compensated by the improvement of the heat transfer rate produced by the faster removal of the ice layer at the freezer wall. Russell et al. (1999) also observed an increase in product temperature for a given refrigerant fluid temperature (varying exit temperature) and mix flow rate led by the increase in dasher speed, an effect which was attributed to the increased dissipation of frictional energy. Conversely, experiments performed by Ben Lakhdar et al. (2005) showed that an increase in dasher speed led to an increase in the heat transfer coefficient between the inner wall of the freezer and the product, producing lower draw temperatures.

3.5. Influence of dasher speed on mean chord length

The ANOVA analysis in Table 5.1.3. shows that the mean ice crystal chord length was significantly affected by the dasher speed at a 95% confidence interval in its linear term ($p = 0.034$ for β_3). The influence of the dasher speed and the evaporation temperature at MFR = 0.014 $kg.s^{-1}$ is shown in Fig. 5.1.10.

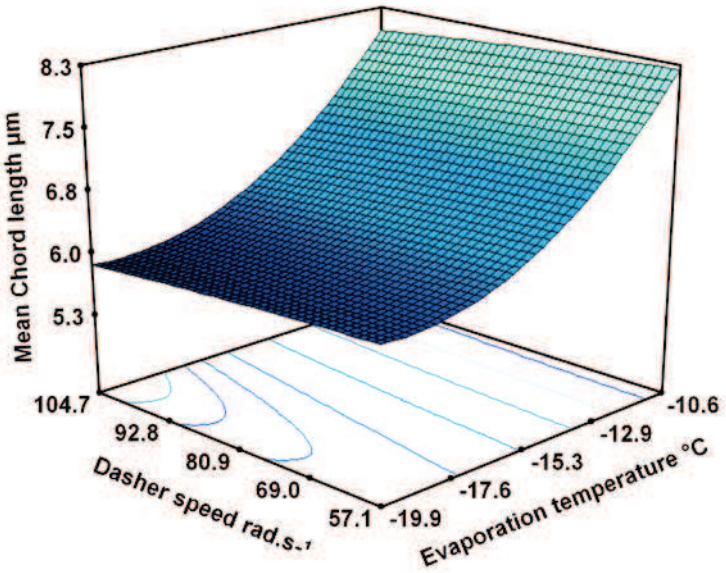


Fig. 5.1.10. Influence of dasher speed and evaporation temperature at MFR = 0.014 $kg.s^{-1}$ on the mean chord length of sorbet.

It can be seen that increasing the scraping action of the dasher slightly reduces the mean ice crystal chord length within sorbet (cf. Table 5.1.1., runs 10, 12 and 15). This result suggests that an increase of the dasher speed leads to the generation of new small ice nuclei by secondary nucleation, which are induced from the ice debris that result from either the attrition of the larger ice crystals (result of an increase in the shear rate within the product) or the smaller size of the ice flocs that are detached from the wall (result of an increase in the scraping frequency of the blades). Russell et al. (1999) found ice creams with larger ice crystals, produced by higher dasher speeds, for a given refrigerant fluid temperature (varying exit temperature) and mix flow rate. This effect was attributed to the increase of mechanical

dissipation which increased the temperature of the product and led to the melting of the small ice crystals and the increase of ice recrystallization.

4. Conclusions

This study has shown that the FBRM technique is a convenient tool that makes it possible to follow directly online the evolution of the ice crystal CLD in sorbets containing up to 40% of ice. Our results demonstrate that the temperature of the refrigerant fluid has the strongest effect on draw temperature as well as on the mean chord length of sorbet. Low evaporation temperatures led to lower draw temperatures (higher ice mass fractions) because more heat was removed from the product. The ice crystal mean chord length was significantly reduced by using lower refrigerant fluid temperatures due to the enhanced cooling rate that led to the growth of more ice crystals with a thinner structure from the ice debris of previous scrapings.

The mix flow rate significantly affected the draw temperature of sorbet. For a given evaporation temperature and dasher speed, lower mix flow rates (longer residence times) result in lower draw temperatures due to the fact that the product remains in the freezer longer, allowing more time for heat removal. No significant influence of the mix flow rate was observed on the mean ice crystal chord length, due to a compensatory effect between two phenomena: at lower mix flow rates, there is more time available for crystal coarsening. However, at lower mix flow rates there is also more time to decrease the draw temperature, which increases the ice mass fraction and therefore the viscosity of the product. The latter effect increases shear stress in the product, leading to the attrition of the larger ice crystals, the ice debris of which can induce the formation of new small ice nuclei by secondary nucleation.

The dasher speed showed a very slight effect on the draw temperature and the ice crystal mean chord length. Higher dasher speeds result in very slightly warmer draw temperatures due to frictional energy that is generated by the scraping action of the dasher.

However, this warming effect was moderated by improving the heat transfer between the product and the wall. An increase in dasher speed slightly reduced the ice crystal mean chord length, an effect which can be explained by the generation of new ice nuclei by secondary nucleation induced either by the smaller ice clumps detached from the scraped surface or by the remaining ice debris produced during the attrition of the larger ice crystals.

Acknowledgments

The authors gratefully acknowledge the financial support granted by the European Community Seventh Framework through the CAFÉ project (Computer Aided Food processes for control Engineering) Project number 212754.

Abbreviations

ANOVA – Analysis of Variance

CLD – Chord Length Distribution

CSD – Crystal Size Distribution

CV – Coefficient of Variation

DSC – Differential Scanning Calorimetry

DRS – Dasher Rotational Speed

DT – Draw Temperature

FBRM – Focused Beam Reflectance Measurement

MCL – Mean Chord Length

MFR – Mix Flow Rate

PSD – Particle Size Distribution

PSP – Polyamid Seeding Particles

SS – Sum of squares

SSHE – Scraped Surface Heat Exchanger

TR22 – Evaporation Temperature of r22

Nomenclature

$\hat{Y}_i$ Predicted value of the response

Y_{ij} Experimental response

$\overline{Y}_i$ Mean response value

β_0 Regression coefficient for interception effect

β_i Regression coefficient for linear effect

β_{ii} Regression coefficient for quadratic effect

β_{ij} Regression coefficient for interaction effect

X_i Coded values of the experimental factors

c Experimental points

d_j Replicated experimental points

n_i Number of particles for each of the size classes i

c_i Chord length

$X_{m.i.}$ Ice mass fraction

$X_{ms.i}$ Initial mass fraction of solute (sweetener content)

$X_{ms.f}$ Final mass fraction of solute (sweetener content)

References

Abbas, A., Nobbs, D., & Romagnoli, J. A. (2002). Investigation of on-line optical particle characterization in reaction, and cooling crystallization systems. Current state of the art. *Measurement Science & Technology,* 13 (3), 349-356.

Barrett, P. and Glennon, B. (2002). Characterizing the metastable zone width and solubility curve using lasentec FBRM and PVM. *Chemical Engineering Research & Design,* 80 (A7), 799-805.

Ben Lakhdar, M., Cerecero, R., Alvarez, G., Guilpart, J., Flick, D., & Lallemand, A. (2005). Heat transfer with freezing in a scraped surface heat exchanger. *Applied Thermal Engineering,* 25 (1), 45-60.

Cebula, D. J. and Russell, A. B. (1998). Ice crystallization control in ice cream. In *Ice cream. Proceedings of the International Dairy Federation Symposium, Athens, Greece, 18-19 September 1997.* (pp. 131-139).

Cerecero, R. (2003). *Etude des écoulements et de transferts thermiques lors de la fabrication d'un sorbet à l'échelle du pilote et du laboratoire.* PhD Thesis. INA-PG, Paris, France.

Cook, K. L. K. and Hartel, R. W. (2010). Mechanisms of Ice Crystallization in Ice Cream Production. *Comprehensive Reviews in Food Science and Food Safety,* 9 (2), 213-222.

Drewett, E. M. and Hartel, R. W. (2007). Ice crystallization in a scraped surface freezer. *Journal of Food Engineering,* 78 (3), 1060-1066.

Goff, H. D., Freslon, B., Sahagian, M. E., Hauber, T. D., Stone, A. P., Stanley, D. W. (1995). Structural development in ice cream - Dynamic rheological measurements. *Journal of Texture Studies,* 26 (5), 517-536.

Greaves, D., Boxall, J., Mulligan, J., Montesi, A., Creek, J., Sloan, E. D., Koh, C. A. (2008). Measuring the particle size of a known distribution using the focused beam reflectance measurement technique. *Chemical Engineering Science,* 63 (22), 5410-5419.

Haddad, A. (2009). *Couplage entre écoulements, transferts thermiques et transformation lors du changement de phase d'un produit alimentaire liquide complexe – Application à la maîtrise de la texture.* PhD Thesis. AgroParisTech, Paris, France.

Haddad, A., Benkhelifa, H., Alvarez, G., Flick, D. (2010). Study of crystal size evolution by focused-beam reflectance measurement during the freezing of sucrose/water solutions in a scraped-surface heat exchanger. *Process Biochemistry,* 45 (11), 1821-1825.

Hartel, R. W. (1996). Ice crystallization during the manufacture of ice cream. *Trends in Food Science & Technology,* 7 (10), 315-321.

Koxholt, M., Eisenmann, B., Hinrichs, J. (2000). Effect of process parameters on the structure of ice-cream: possible methods of optimizing traditional freezer technology. *European Dairy Magazine,* 12 (1), 27-29.

Marshall, R. T., Goff, H. D., Hartel R. W. (2003). Ice cream. 6th Ed. New York: Klumer Academic/Plenum Publishers. 371 p.

Negro, C., Sanchez, L. M., Fuente, E., Blanco, A., Tijero, J. (2006). Polyacrylamide induced flocculation of a cement suspension. *Chemical Engineering Science,* 61 (8), 2522-2532.

Presles, B., Debayle, J., Rivoire, A., Pinoli, J.-C., Fevotte, G. (2009). In situ particle size measurements during crystallization processes using image analysis. In Récents Progrès en Génie des Procédés. *Actes du XIIème Congrès de la Société Française de Génie des Procédés.* (Paper number 98). Marseille, France.

Russell, A. B., Cheney, P. E., Wantling, S. D. (1999). Influence of freezing conditions on ice crystallisation in ice cream. *Journal of Food Engineering,* 39 (2), 179-191.

Sablani, S. S., Rahman, M. S., Datta, A. K., Mujumdar, A. S. (2007). *Handbook of Food and Bioprocess Modelling.* Florida: CRC Press.

SAS Institute Inc. (2008). SAS/STAT® 9.2 User's Guide. In SAS Institute Inc. Cary, USA

Schwartzberg, H. and Liu, Y. (1990). Ice crystal growth on chilled scraped surfaces. In *American Institution of Chemical Engineers. Summer National Meeting.* San Diego, CA, USA. .

Schwartzberg, H. (1990). Food freeze concentration. In: H. G. Schwartzberg & M. A. Rao editors. *Biotechnology and food process engineering. IFT basic symposium series.* New York: Marcel Dekker. (pp. 127-201).

Sofjan, R. P., and Hartel, R. W. (2004) Effects of overrun on structural and physical characteristics of ice cream. *International Dairy Journal.* 14 (3). 255–262.

Sodawala, S. & Garside, J. (1997). Ice nucleation on cold surfaces: application to scraped surface heat exchangers. In *American Institution of Chemical Engineers Annual Meeting.* . Los Angeles, California, USA.

Windhab, E. and Bolliger, S. (1995). Combined aerator/freezer for ice cream manufacture. *European Dairy Magazine,* 1, 28-34.

Wynn, E. J. W. (2003). Relationship between particle-size and chord-length distributions in focused beam reflectance measurement: stability of direct inversion and weighting. *Powder Technology, 133* (1-3), 125-133.

Zheng, L. (2006). *Heat transfer during freezing on a scraped surface.* PhD Thesis. University of Auckland. Auckland, New Zealand.

5.2. Experimental study and modelling of the residence time distribution in a scraped surface heat exchanger during sorbet freezing.

Marcela Arellano[a,b,c,d], Hayat Benkhelifa[b,c,d,3], Graciela Alvarez[a], Denis Flick[b,c,d].

[a]*Irstea. UR Génie des Procédés Frigorifiques. 1 rue Pierre-Gilles de Gennes CS 10030, 92761 Antony Cedex, France*

[b]*AgroParisTech. UMR 1145 Ingénierie Procédés Aliments. 16 rue Claude Bernard, 75231 Paris Cedex 05, France*

[c]*INRA.UMR 1145 Ingénierie Procédés Aliments. 1 avenue des Olympiades, 91744 Massy Cedex, France*

[d]*CNAM. UMR 1145 Ingénierie Procédés Aliments. 292 rue Saint-Martin, 75141 Paris Cedex 03, France*

Abstract

Scraped surface heat exchangers (SSHE) are widely used for crystallization applications in several food processes (i.e. crystallization of margarine, tempering of chocolate, freezing of ice cream and sorbet). The final quality of these food products is highly related to crystal size distribution and apparent viscosity, both of which are determined by the operating conditions of the process. During the freezing of sorbet, the increase in the ice volume fraction leads to an increase in the apparent viscosity of the product. This effect modifies the fluid flow behaviour, the residence time distribution (RTD) and the temperature profile inside the equipment. This work aimed at studying the influence of the operating conditions on the RTD and the average axial temperature profile of the product in a SSHE, so as to characterize the product flow behaviour. RTD experiments were carried out in a continuous laboratory scale SSHE by means of a colorimetric method. Experiments showed that high product flow rates led to a narrowing of the RTD and thus to less axial dispersion, due to the enhancement of the radial mixing with the decrease in the apparent viscosity of the product. Spreading of the RTD was obtained for lower refrigerant fluid temperatures, due to a higher radial temperature gradient between the wall and the centre of the exchanger, leading to a higher gradient of the apparent viscosity. This effect increased the difference in axial flow velocities and thus the axial dispersion. These results can be useful for the optimization and modelling of crystallization processes in SSHEs.

Key words: Ice crystallization; Draw temperature; Residence time distribution; Freezing; Scraped surface heat exchanger.

3 Corresponding author. Tel.: +33 144 08 86 11; Fax: +33 144 08 16 66.
E-mail address: hayat.benkhelifa@agroparistech.fr

1. Introduction

Scraped surface heat exchangers (SSHE) are widely used in the food industry for crystallization applications in several food processes, such as the crystallization of margarine (Shahidi, 2005), the tempering of chocolate (Dhonsi and Stapley, 2006), the freeze concentration of milk (Sanchez et al., 2011) and the freezing of sorbet or ice cream (Cook and Hartel, 2010). The final quality of these food products is mainly governed by sensory properties related to crystal size distribution and apparent viscosity, both of which are highly dependent on the operating conditions (i.e. product flow rate, rotational speed, refrigerant fluid temperature), and therefore on the degree of thermal and mechanical treatment applied to the product. Furthermore, the crystallization phenomenon in these food processes is closely related to the residence time distribution (RTD) of the product. During the crystallization process, the phase transition involved leads to an increase in the crystal volume fraction, and to an increase in the apparent viscosity of the product, the effect of which modifies the fluid flow behaviour, the RTD of the product and the temperature profile inside the equipment. Also, due to the different lengths of time that each element of fluid spends in the SSHE, each fluid fraction will have a different degree of thermal treatment and of shear rate, thus affecting the final crystal size distribution of the product.

An analysis of the experimental RTD data provides valuable information about the fluid flow behaviour, the degree of radial and axial dispersion, and possible flow problems in the exchanger, such as stagnation or short-circuiting. It is therefore important to perform a RTD study, complemented with temperature profile measurements, in order to assess the influence of the operating conditions on the fluid flow behaviour and on the efficiency of the thermal treatment applied to the product, so as to optimize the crystallization process.

SSHEs are composed of two concentric cylinders: an external stationary cylinder which is in contact with the refrigerant fluid and therefore represents the heat transfer surface;

and an internal rotating cylinder (dasher) that is equipped with scraping blades (Härröd, 1986). The main advantage of SSHEs is the scraping action of the blades, which continually remove the crystal build-up at the heat transfer cylinder wall, improving the heat transfer rate from the wall to the core of the exchanger. The fluid flow behaviour in SSHEs is the result of axial flow through an annular gap (Poiseuille flow) due to the imposed product flow rate, and rotational flow (Couette flow) due to the rotation of the internal cylinder and the scraping blades (Wang et al., 1998). The velocity vectors of these two flows form a helical fluid flow pattern in the middle section of the exchanger (Härröd, 1986; Fayolle et al., 2005; Yataghene et al., 2011). Furthermore, the efficiency of the thermal treatment of the product strongly depends on the radial and axial dispersion in the SSHE. An increase in radial dispersion will enhance the heat transfer rate and ensure a more uniform thermal treatment of the product (Härröd, 1986). Contrariwise, an increase in axial dispersion will decrease the driving force for heat transfer, by reducing the temperature gradient between the heat transfer medium and the product (Trommelen and Beek, 1971; Härröd, 1986; Benezech and Maingonnat, 1989).

A number of studies in the literature have determined the RTD of non-Newtonian shear-thinning fluids flowing through SSHEs under isothermal conditions (Benezech and Maingonnat, 1989; Alcairo and Zuritz, 1990; Lee and Singh, 1991; Russell et al., 1997). However, there is a paucity of information available on the RTD of food products when crystallization occurs under cooling conditions (Russell et al., 1997; Belhamri et al., 2009). At isothermal conditions, it has been demonstrated that the operating conditions, such as the product flow rate, the rotational speed and the apparent viscosity of the product, have an effect on the RTD of non-Newtonian fluids. Not all authors agree as to their effects, however. An increase in product flow rate has been found to narrow (Alcairo and Zuritz, 1990; Lee and Singh, 1991), or not to affect the RTD (Benezech and Maingonnat, 1989). An increase in rotational speed has been found to broaden (Benezech and Maingonnat, 1989; Russell et al.,

1997), to narrow (Alcairo and Zuritz, 1990) or not to affect the RTD (Lee and Singh, 1991). An increase in the apparent viscosity of the product has been found to broaden (Lee and Singh, 1991) or not to affect the RTD (Benezech and Maingonnat, 1989; Alcairo and Zuritz, 1990). At cooling conditions, during the crystallization of water in ice cream, Belhamri et al. (2009), found that an increase in product flow rate and in rotational speed led to a narrowing of the RTD. Also, in the case of ice cream freezing, Russell et al. (1997) found that ice cream exhibited a broader RTD, as compared to a less shear-thinning fluid, Carbopol. Table 5.2.1. shows a summary of the observed effects by various authors on RTD studies of non-Newtonian shear-thinning fluids in SSHEs under isothermal and cooling conditions.

Table 5.2.1. Summary of RTD studies of Non-Newtonian shear thinning fluids in SSHEs under isothermal and cooling conditions

RTD studies of Non-Newtonian shear thinning fluids in SSHEs under isothermal conditions

Reference	Non - Newtonian shear thinning Fluid	Rotation speed effect	Product flow rate effect	Apparent viscosity effect
Benezech and Maingonnat, 1989	Aqueous Solutions of Guar gum, CMC, and Na Alginate	$\uparrow N_R$ broadened RTD	$\uparrow \dot{V}$ no effect on RTD	$\uparrow \eta_{app}$ no effect on RTD
Alcairo and Zuritz, 1990	A single sphere suspended in aqueous solutions of CMC	$\uparrow N_R$ narrowed RTD	$\uparrow \dot{V}$ narrowed RTD	$\uparrow \eta_{app}$ no effect on RTD
Lee and Singh, 1991	Potato cubes with aqueous solutions of CMC	$\uparrow N_R$ no effect on RTD	$\uparrow \dot{V}$ narrowed RTD	$\uparrow \eta_{app}$ broadened RTD
Russell et al., 1997	Carbopol	$\uparrow N_R$ broadened RTD	-	-

RTD studies of Non-Newtonian shear thinning fluids in SSHEs under cooling conditions

Reference	Non - Newtonian Fluid	Rotation speed effect	Product flow rate effect	Apparent viscosity effect
Russell et al.,1997	Carbopol and Ice cream	-	-	$\uparrow \eta_{app}$ broadened RTD
Belhamri et al., 2009	Ice cream	$\uparrow N_R$ narrowed RTD	$\uparrow \dot{V}$ narrowed RTD	-

Experimental RTD data can be represented by simple hydrodynamic models that can be used to predict the flow pattern and consequently the structural crystallization process.

This information can be very useful to optimize the process and to improve product quality. Several studies in the literature have used non-ideal physical models to describe flow patterns in real systems. The two most widely used RTD models are the plug-flow with axial dispersion model (ADM) and the tanks-in-series model (TSM) (Villermaux, 1993; Levespiel, 1999). Mathematical models such as the gamma distribution model (GDM) can also be used to describe experimental RTD data (Wen and Fan, 1975) and physical interpretations can be attributed to the parameters of this model.

The aims of this work are, firstly, to study the effects of the operating conditions on the experimental RTD and on the axial temperature profile during sorbet freezing in a SSHE, and secondly, to fit the experimental RTD data to a flow model that adequately represents the flow behaviour in the SSHE.

2. Materials and methods

2.1. Working fluid

The working fluid used in these experiments was an ultra high temperature pasteurized lemon sorbet mix (14.6% w/w sucrose, 8% w/w fructose, 0.09% w/w dextrose, 3% w/w lemon juice concentrate 60 Brix, 0.5% w/w locust bean gum / guar gum / hypromellose stabiliser blend). The mix was stored at 5 °C for 24 h prior to use. The rheological properties of sorbet mix and frozen sorbet at different draw (exit) temperatures were measured with a pipe rheometer connected at the outlet pipe of the SSHE. The rheometer was composed of a series of pipes in clear polyvinyl chloride (PVC) of different internal diameters (d_1=0.0272m, d_2=0.0212m, d_3=0.0167m, d_4=0.013m, d_5=0.01m, d_6=0.0058m), making it possible to apply an apparent shear rate range of $4 < \dot{\gamma} < 430$ s^{-1}. The power law model used to characterize the apparent viscosity of the fluid is given in Eq. 1:

$$\eta_{app} = k \cdot \dot{\gamma}^{n-1} \qquad (1)$$

where k is the consistency index, n the flow behaviour index and $\dot{\gamma}$ the shear rate. The physical properties of the working fluid at different temperatures are listed in Table 5.2.2.

Table 5.2.2. Physical properties of the working fluid at different temperatures.

Fluid	Temperature (ºC)	ρ (kg.m^{-3})	Shear rate $\dot{\gamma}$ range 4 – 430 (s^{-1})	
			n	k (Pa.s^n)
Sorbet mix	5.0	1110	0.553	0.455
Sorbet	-3.5	1068	0.414	7.887
Sorbet	-4.0	1055	0.397	13.195
Sorbet	-4.6	1044	0.415	18.452
Sorbet	-5.4	1033	0.405	31.574
Sorbet	-6.1	1026	0.423	31.598

2.2. Crystallization process equipment and operating conditions

The freezing process of sorbet was carried out in a laboratory scale continuous SSHE (WCB® Model MF 50), equipped with a rotor and two rows of scraper blades occupying 46% of the heat exchange cylinder volume (cf. Fig. 5.2.1.).

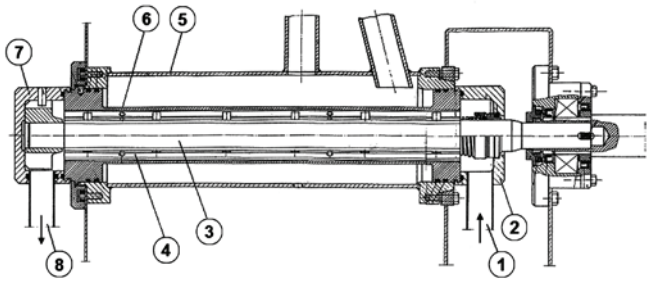


Fig. 5.2.1. Schematic representation of the SSHE WCB® Model MF 50. 1. Inlet connection for sorbet mix. 2. Inlet cover bowl. 3. Rotor. 4. Scraper blades rows. 5. Heat exchange cylinder jacket with vaporizing r22. 6. Heat exchange cylinder. 7. Outlet cover bowl. 8. Outlet pipe for sorbet.

Table 5.2.3. Geometrical characteristics of the SSHE WCB® Model MF 50

Heat exchanger cylinder diameter (d_c)	0.05 m
Heat exchanger cylinder length (L)	0.40 m
Rotor diameter (d_r)	0.046m
Ratio (d_r/d_c)	0.92
Exchange surface	0.0628m^2

The geometrical dimensions of the exchanger are given in Table 5.2.3. The total volume of the SSHE available to the working fluid was 6.66×10^{-4} m^3, which includes the volume available within the heat exchange cylinder, the inlet and outlet bowls, as well as the outlet pipe. This equipment has a nominal capacity of 0.007 to 0.021 kg.s^{-1}. The product flow rate was measured by weighing the product exit stream during a given period of time. The accuracy of this measurement was determined to be $\pm 9.2 \times 10^{-5}$ kg.s^{-1}. The evaporation temperature of chlorodifluoromethane (r22) in the jacket of the exchanger was adjusted within a range of -10 to -20 °C. A calibrated type T (copper - constantan) thermocouple with an accuracy of ±0.2 °C was fixed with conductive aluminium tape on the external surface wall of the cooling jacket, so as to measure the evaporation temperature of the refrigerant fluid. The exterior of the exchanger jacket was isolated with 2 cm thick foam in order to reduce heat loss. The rotational speed was varied within a range of 57 to 105 rad.s^{-1} (545 to 1000 rpm). The rotor speed was measured by means of a photoelectric tachometer (Ahlborn®, type FUA9192) with an accuracy of ±0.105 rad.s^{-1} (±1 rpm). The operating conditions under which the RTD experiments were carried out are given in Table 5.2.4. Each experimental condition was performed twice so as to provide enough experimental data for RTD model fitting. No aeration was employed for any of the RTD experiments.

2.3. Temperature profile measurement

A unique aspect of this work is the use of a wireless temperature sensor data logger to measure the average axial temperature profile inside the SSHE. The thermochron iButton® DS1922L (Maxim®) device is a computer chip enclosed in a stainless steel case (diameter=16.3mm, thickness=6.4mm). The iButton® device includes an internal 3V Lithium battery source, a read/write memory (NV RAM), a real-time clock, and a semiconductor temperature sensor (temperature sensitive p-n silicon diode). The iButton® sensors were calibrated individually to an accuracy of ±0.2 °C within a range of -20 to +20 °C for a sampling rate of 5 seconds. The iButton® sensors were fixed over the rotor surface by means of a thin layer of high-strength neutral silicone adhesive-sealant, at different axial positions through the length of the rotor as shown in Fig. 5.2.2.

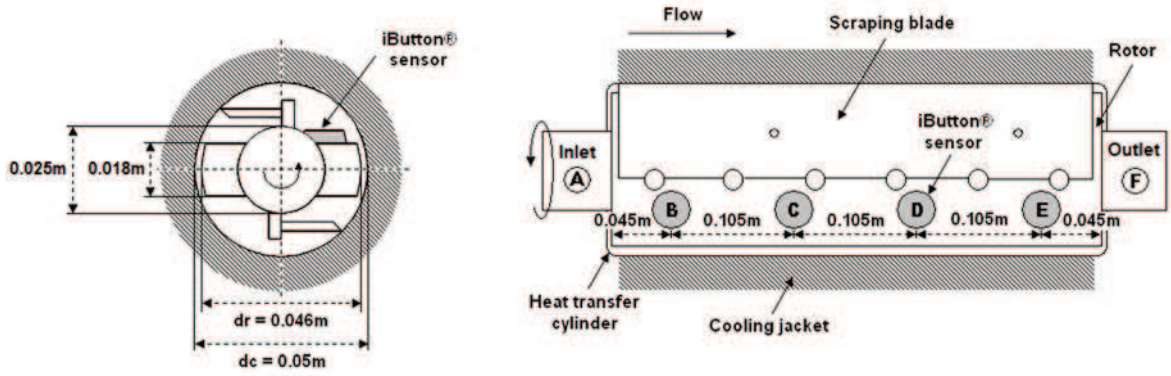


Fig. 5.2.2. Axial position of iButton® sensors in the SSHE.

In addition to the iButton® sensors a calibrated type T thermocouple (accuracy of ±0.2 °C) was introduced at the inlet connexion of the SSHE in order to measure the sorbet mix temperature. The draw temperature of sorbet was measured at the outlet pipe of the exchanger by means of a calibrated Pt100 probe (Baumer®, accuracy of ±0.1 °C). Once the experimental conditions were set and the steady state of the SSHE was established, inlet and draw temperature measurements were recorded every 5 seconds for a period of 10 minutes, by

using a program written in LabVIEW®. The acquisition data of the iButton® sensors were synchronized with inlet and draw temperatures. Data measurements were then transferred to a personal computer by means of a USB port adapter and the read/write software OneWireViewer.

2.4. Residence time distribution measurement

The RTD technique consists of a pulse injection of a small amount of concentrated tracer at the inlet and the continuous measurement of the concentration-time tracer response at the product exit stream of the exchanger. RTD experiments during sorbet freezing were carried out by means of a colorimetric method. A 13 ml pulse of unfrozen sorbet mix coloured with methylene blue (MB) dye at 0.008% (w/w) was used as tracer. MB dye was selected because of its high solubility in sorbet mix and its thermal stability. Preliminary RTD experiments made it possible to validate the chosen MB concentration used in the pulse, so that the exit stream MB concentration was within the range of applicability of the Beer-Lambert law.

The experimental setup for the injection of the tracer is schematically represented in Fig. 5.2.3. The dyed sorbet mix was stored in a syringe connected to a valve and to a stainless steel tube (internal volume of 4 ml). This tube was inserted into the T pipe at the inlet connexion for sorbet mix, making it possible to inject the tracer immediately at the entrance of the SSHE. Before the pulse injection was performed, the volume of the stainless steel tube was filled with tracer, so that the tracer volume of 13 ml was completely injected for each experimental run. During the RTD experiments, the tracer injection was achieved in roughly 0.7 seconds. This represents between 1 to 2% of the theoretical residence time of all the experimental conditions studied, and thus the pulse injection assumption is acceptable for all RTD experiments.

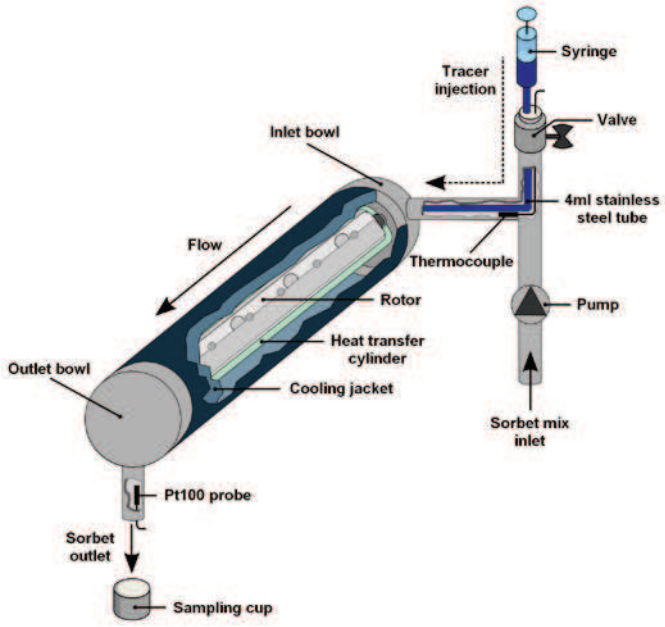


Fig. 5.2.3. Experimental setup for injection of tracer.

Once the experimental conditions had been set and the steady state of the SSHE attained, the pulse injection was performed and simultaneously sampling of the sorbet was carried out at the outlet pipe of the exchanger every 6 to 8 seconds. Subsequently, the samples were thawed at 5 °C and analysed for dye concentration with a spectrophotometer (Beckman Coulter DU® 730) at 662 nm. A previous calibration procedure made it possible to establish the relationship between the light absorbance of collected samples with their corresponding MB concentration.

2.5. Residence time distribution data treatment

The RTD of the process was characterized by the age distribution function $E(t)$, where $E(t)dt$ represents the fraction of fluid that has passed through the exchanger for a length of time between t and $t + dt$ (Danckwerts, 1953). For a pulse injection, the $E(t)$ function is given by Eq. (2).

$$E(t) = \frac{C(t)}{\int_0^\infty C(t)dt} \tag{2}$$

where $C(t)$ is the exit concentration of tracer at a certain time t.

The normalization condition for the probability density $E(t)$ function implies that:

$$\int_0^\infty E(t)dt = 1 \tag{3}$$

The experimental mean residence time t_s is the first moment of the distribution and is defined by Eq. (4).

$$\mu_1 = t_s = \int_0^\infty t \cdot E(t)dt \tag{4}$$

For a fluid flow without dead volume, t_s is equal to the theoretical mean residence time τ given by Eq. (5):

$$\tau = \frac{V}{\dot{V}} \tag{5}$$

where V is the exchanger volume available to the fluid and $\dot{V}$ the volumetric flow rate.

The variance σ^2 is the second moment of the distribution and is an indicator of the spreading around the mean residence time, as shown in Eq. (6).

$$\mu_2 = \sigma^2 = \int_0^\infty (t - t_s)^2 E(t)dt \tag{6}$$

Normalized concentration $E(\theta)$ and time θ were calculated by the following expressions:

$$\theta = \frac{t}{t_s} \tag{8}$$

$$E(\theta) = t_s \cdot E(t) \tag{9}$$

Normalized variance σ'^2 was determined by Eq. (10):

$$\sigma'^2 = \frac{\sigma^2}{t_s^2} \tag{10}$$

Integrals of Eq. (2), (4), and (6) were calculated by using the midpoint rectangle method so as to ensure the mass conservation law.

To verify the measured data, a tracer mass balance was performed between the entrance and the exit of the SSHE. The recovery rate of tracer (RRT) was calculated by Eq. (11):

$$RRT = \frac{\int_0^\infty C(t)dt \times \dot{V}}{C_{pulse}V_{pulse}} \times 100 \qquad (11)$$

where C_{pulse} is the tracer concentration of the pulse injection, and V_{pulse} represents the volume of the pulse injection. The RRT for each of the operating conditions is shown in Table 5.2.4. It can be observed that the total amount of tracer recovered at the exit of the SSHE was on average 102% of the theoretical amount injected, which means that there is an average measurement error of 2%, and we can therefore consider our results as reliable.

Table 5.2.4. Operating conditions and calculated flow regimes during RTD experiments.

Operating conditions						Inlet at 5ºC			Outlet at DT		
Run	MFR [a] ($kg.s^{-1}$)	TR22 [a] (°C)	DRS [a] ($rad.s^{-1}$)	DT [a]* (°C)	RRT [a]* (%)	Re_{ax}	Re_r	Ta_r	Re_{ax}	Re_r	Ta_r
1	0.007	-15.4 ± 0.2	78.5	-5.4 ± 0.2	101 ± 2	0.043	2.33	66.7	0.0006	0.046	2.39
2	0.014	-15.3 ± 0.2	78.5	-4.6 ± 0.1	103 ± 2	0.116	2.33	66.7	0.0029	0.077	3.87
3	0.021	-15.4 ± 0.2	78.5	-4.0 ± 0.1	95 ± 7	0.209	2.33	66.7	0.0079	0.115	6.15
4	0.014	-10.6 ± 0.2	78.5	-3.5 ± 0.1	100 ± 3	0.116	2.33	66.7	0.0069	0.186	9.35
5	0.014	-20.1 ± 0.2	78.5	-6.1 ± 0.1	104 ± 1	0.116	2.33	66.7	0.0017	0.044	2.11
6	0.014	-15.4 ± 0.2	57.1	-4.6 ± 0.1	107 ± 1	0.116	1.47	42.0	0.0029	0.047	2.33
7	0.014	-15.3 ± 0.2	104.7	-4.6 ± 0.1	105 ± 1	0.116	3.54	101.2	0.0029	0.122	6.10

[a] MFR = mix flow rate; TR22 = evaporation temperature of r22; DRS = dasher rotational speed; DT = draw temperature; RRT = recovery rate of tracer. *Values are means of two replicates.

3. Residence time distribution models

As previously mentioned, the experimental RTD data can be represented by a hydrodynamic model that can be used to describe the flow pattern in the SSHE. In this section, three RTD models are presented, which were used to fit the experimental RTD data of this work.

3.1. Plug-flow with axial dispersion model

The plug-flow with axial dispersion model assumes a tracer pulse dispersion process superimposed on a plug flow (Levespiel, 1999). The model parameter is the Peclet number, which is defined as $Pe = uL/D_{ax}$, where u is the mean velocity in the exchanger, L is its length, and D_{ax} *is* the axial dispersion coefficient. The analytical solution of the axial dispersion model with open system boundary conditions is given by Eq. (12):

$$E(\theta) = \frac{1}{2}\left(\frac{Pe}{\pi \cdot \theta}\right)^{1/2} \exp\left(-\frac{Pe(1-\theta)^2}{4\theta}\right) \tag{12}$$

The lower the Peclet number is, the higher the axial dispersion is (Villermaux, 1993).

3.2. Tanks-in-series model

The tanks-in-series model represents the fluid flow within the SSHE by assimilating the exchanger to a number N of completely stirred tanks in series of the same volume. For this model the $E(\theta)$ function was calculated by Eq. (13).

$$E(\theta) = \frac{N \cdot (N \cdot \theta)^{N-1}}{(N-1)!} \exp(-N \cdot \theta) \tag{13}$$

For N = 1, the exchanger corresponds to a single completely stirred tank. When $N \rightarrow \infty$, the system approaches to a plug flow and the RTD curve exhibits less asymmetry (Villermaux, 1993; Levenspiel, 1999).

3.3. The gamma distribution model

The gamma distribution model is not a hydrodynamic model. However, we can interpret the influence of the model parameters on the flow behaviour (Wen and Fan, 1975). The normalized age distribution $E(\theta)$ is approximated by the Γ-distribution and is defined by Eq. (14).

$$E(\theta) = \frac{p^p}{(1-\theta_0)^p \Gamma(p)} (\theta - \theta_0)^{p-1} \exp\left[-p\left(\frac{\theta - \theta_0}{1-\theta_0} \right) \right] \quad (14)$$

where p and θ_0 are the model parameters and Γ denotes the gamma function defined as $\Gamma(p) = \int_0^\infty x^{p-1} e^{-x} dx$.

The parameter p is related to the extent of fluid in the flow direction. As the value of p increases, there is a reduction in axial dispersion and the flow pattern gradually approaches to plug flow behaviour. The parameter θ_0 is considered as a delay dimensionless time, defined as $\theta_0 = D/t_s$, where D represents the delay time of the system, and t_s the mean residence time. An increase of θ_0 also emphasises the effect of plug flow (Wen and Fan, 1975).

3.4. RTD model fitting to experimental RTD data

Normalized experimental RTD curves were fitted to each of the previous models by unknown parameter estimation using the minimization of the sum of squared errors (*SSE*) defined in equation 15:

$$SSE = \frac{1}{M} \sum_1^M \left(E_{\exp}(\theta_i) - E_{th}(\theta_i) \right)^2 \quad (15)$$

where E_{exp} is the normalized experimental RTD, E_{th} the normalized theoretical RTD and M the number of experimental points. The SSE function was minimized using a direct method (simplex) with the *fminsearch* function of MATLAB.

4. Results and discussion

Table 5.2.4. presents the axial Reynolds number, Re_{ax}, the rotational Reynolds number, Re_r, and the Taylor number, Ta_r, respectively, at inlet and outlet temperatures, for each of the operating conditions investigated. According to the average flow regime criteria in SSHEs given by Härröd (1986) (cf. Table 5.2.5.), the dimensionless numbers in Table 5.2.4.

demonstrate that for all experimental conditions, at inlet and outlet temperatures, the SSHE was operated under laminar axial flow, and also under laminar rotational flow. With regard to the presence of Taylor vortices, Dumont et al. (2000) based on visual and electrochemical techniques, showed that the transition between the laminar and vortex flow regime in SSHEs occurs at a critical Taylor number $Ta_{rc} \approx 80$ for $R_r/R_c = 0.6$ ($Ta_{rc} \approx 45$ in the annular space without blades). From the results in Table 5.2.4., we can observe that experiments 1 to 6 were certainly carried out in the absence of Taylor vortices. Concerning experiment 7, it can be seen that at the inlet of the exchanger Taylor vortices may be present. However, when the product begins to freeze during its passage through the SSHE, the apparent viscosity of the product also begins to increase, and the flow regime becomes completely laminar toward the product exit.

Table 5.2.5. Flow regimes criteria according to Härröd (1986).

Rotational flow		Axial flow	
Laminar	$Re_r < 250$	Laminar	$Re_{ax} < 15{,}000$
Taylor vortex	$250 < Re_r < 100{,}000$	Turbulent	$Re_{ax} > 15{,}000$
Turbulent	$Re_r > 100{,}000$		

An example of the gamma distribution (GDM), tank-in-series (TSM) and plug-flow with axial dispersion (ADM) models adjusted to the experimental RTD data is shown in Fig. 5.2.4. The experimental RTD curve in Fig. 5.2.4. was obtained at a mix flow rate of 0.014 $kg.s^{-1}$, dasher rotational speed of 78.5 $rad.s^{-1}$ and refrigerant fluid temperature of -15.3 °C. It can be seen that the experimental data fit the GDM model very satisfactorily; the TSM model shows a reasonably close fit to the experimental RTD curve, whereas the ADM model was the least appropriate model to represent the RTD data. The mean value of the tank-in-series number was $N = 12 \pm 2$, which means that the flow within the SSHE can be represented by roughly 12 continuous completely stirred tank reactors. This information can be highly valuable in further modelling applications of the crystallization process. The mean value of the Peclet number was $Pe = 22 \pm 4$, which indicates a significant axial dispersion within the SSHE.

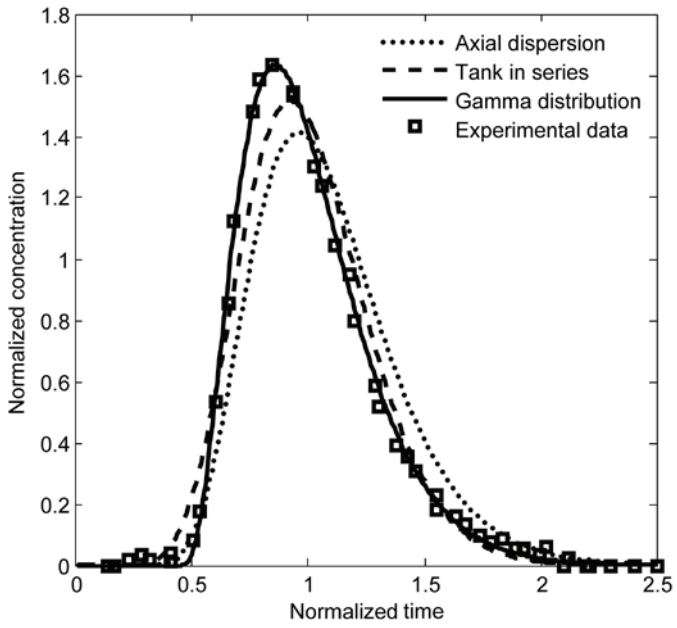


Fig. 5.2.4. RTD experimental curve fitting for the axial dispersion, tank in series and gamma distribution models at mix flow rate of 0.014kg.s^{-1}, rotational speed of 78.5 rad.s^{-1} and refrigerant temperature of -15.3ºC.

From the experimental RTD curve in Fig. 5.2.4., we can observe that a significant portion of the fluid (corresponding to 33% of the total distribution) exits between 0.5 t_s and 0.8 t_s (where t_s is the mean residence time), which are the times when the fluid starts to exit and when the maximum concentration is reached, respectively. It can also be seen that the tail of the distribution (corresponding to 6% of the total distribution) exits after 1.5 t_s. These exit times in the RTD curve indicate significant differences in the axial velocity flow in the exchanger, which are responsible for the significant axial dispersion observed in the SSHE. To understand this effect better, it is useful to refer to the schematic representation (cf. Fig. 5.2.5.A to 5.2.5.D) of the laminar flow of different fluids passing through an annular space with and without rotating blades.

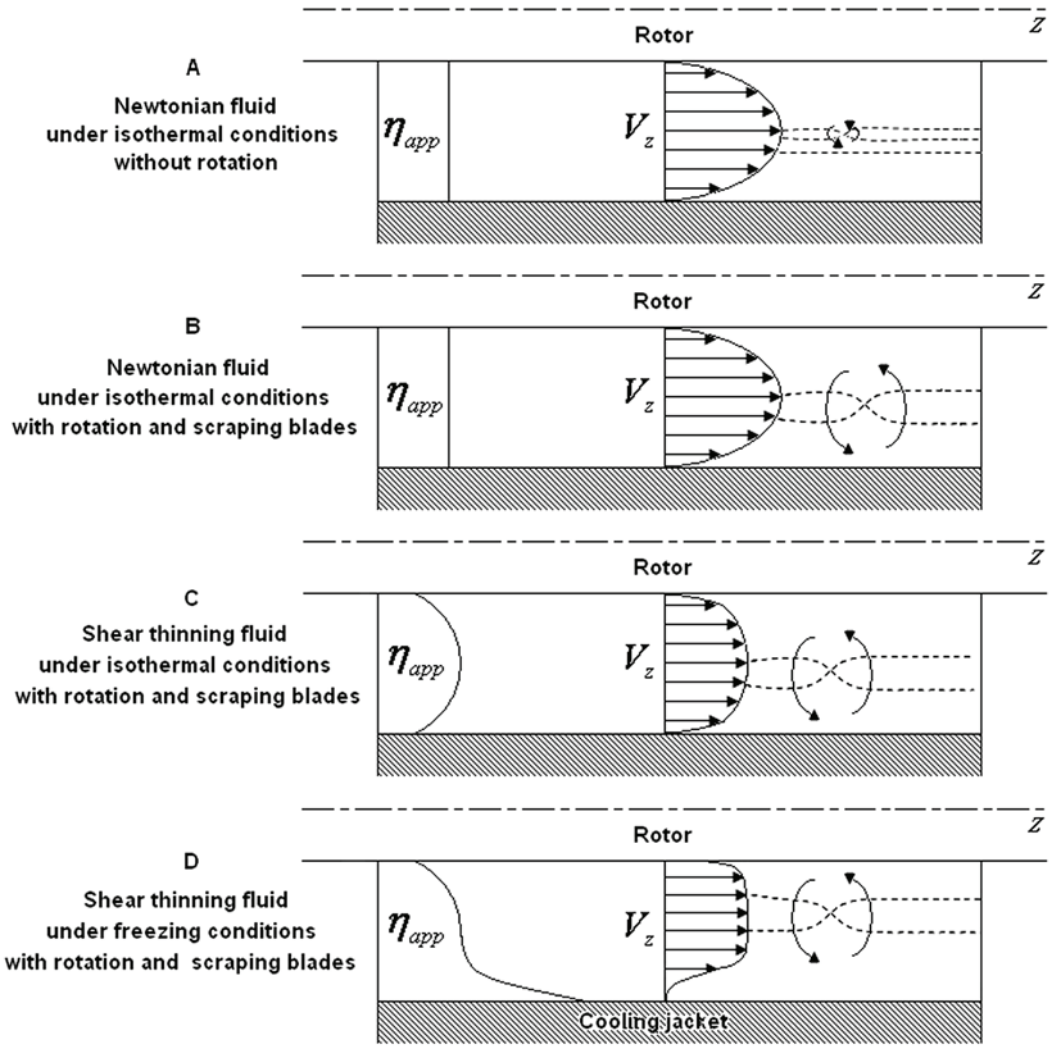


Fig. 5.2.5. Schematic representation of the laminar flow of different fluids passing through an annular space with and without rotating blades.

In the simplest case (Fig. 5.2.5.A), we can observe the roughly parabolic axial velocity profile of a Newtonian fluid at isothermal conditions and in the absence of rotating blades. In this case, there is very limited radial dispersion (only molecular diffusion). For the same Newtonian fluid at isothermal conditions (cf. Fig 5.2.5.B), the presence of rotating blades will significantly increase the radial dispersion, but the parabolic axial velocity profile will remain approximately the same. For a non-Newtonian shear-thinning fluid (as is the case for sorbet) at isothermal conditions and in the presence of rotating blades, the axial velocity profile will become flatter as the flow behaviour of the product becomes more shear-thinning (Edward et

al., 2003) (cf. Fig 5.2.5.C). For a non-Newtonian shear-thinning fluid at cooling conditions, as is the case during the freezing of sorbet flowing through a SSHE (cf. Fig. 5.2.5.D), there is a radial temperature gradient between the wall and the centre of the exchanger. The low temperatures and the ice crystallization at the wall region, will lead to an increase in the ice crystal volume fraction and to an increase in the apparent viscosity of the fluid with respect to its apparent viscosity in the region near the rotor. Consequently, we can consider two coexisting layers of fluid that move across the SSHE at different speeds: one very viscous layer of fluid near the cooling wall, which flows at a low velocity, and another less viscous layer near the rotor, which flows at a higher speed. From the results in Fig. 5.2.4. and Fig. 5.2.5.D, it is likely that the part of the fluid that exits the exchanger typically after 1.5 t_s (tail of RTD), corresponds to the part of the fluid that has the highest viscosity and flows at the slower speed near the cooling wall. The rather flat velocity profile which is expected for the part of the fluid with lower viscosity explains that a large amount of fluid flows out with a residence time near the minimum value (33% of the fluid exits between 0.5 and 0.8 t_s). This is why the RTD curve is very dissymmetric.

4.1. Influence of refrigerant fluid temperature on axial temperature profile and RTD

The average axial temperature profile in the SSHE obtained for different refrigerant fluid temperatures (TR22) at a mix flow rate of 0.014 $kg.s^{-1}$ and dasher rotational speed of 78.5 $rad.s^{-1}$ is shown in Fig. 5.2.6. (cf. Table 5.2.4., runs 2, 4 and 5).

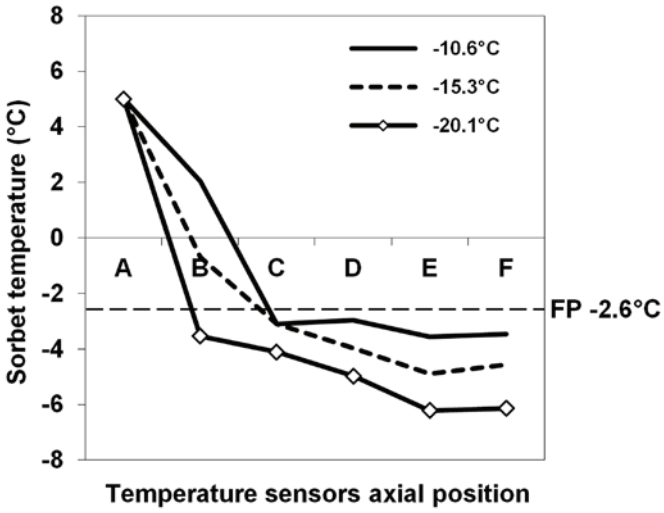


Fig. 5.2.6. Axial temperature profile of sorbet as a function of refrigerant fluid temperature at mix flow rate of 0.014 kg.s^{-1}and rotational speed of 78.5 rad.s^{-1}. FP = Freezing point temperature -2.6 °C.

These results clearly show that a decrease in the refrigerant temperature leads to a reduction in the temperature of the product. We can also distinguish three different transfer stages: a chilling section from point A to B and further in the axial distance until reaching the freezing point temperature of sorbet at -2.6 °C, where ice nucleation is triggered. From this point, ice nucleation and ice crystal growth occur simultaneously up to point E situated at the end of the rotor. Finally, the thermodynamic equilibrium of sorbet takes place at the outlet pipe of the SSHE, characterized by a slight increase in draw temperature between points E to F. It should be noted that these measurements were carried out under steady state conditions and therefore the phenomena of subcooling could not be observed. It can also be seen that at -20.1 °C the chilling section is reduced. This means that at this refrigerant temperature, the freezing of the product starts much nearer to the inlet of the exchanger, with respect to the other refrigerant temperatures.

Normalized RTD curves as a function of refrigerant fluid temperature at a mix flow rate of 0.014 kg.s^{-1} and dasher rotational speed of 78.5 rad.s^{-1} are compared in Fig. 5.2.7. Experimental and modelling parameters of these RTD curves are given in Table 5.2.6.

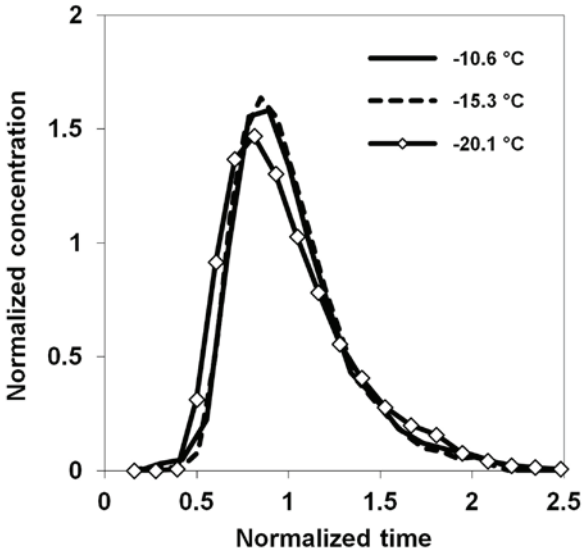


Fig. 5.2.7. Residence time distribution as a function of refrigerant fluid temperature at mix flow rate of 0.014 kg.s^{-1} and rotational speed of 78.5 rad.s^{-1}.

Table 5.2.6. RTD experimental and modelling data at different refrigerant fluid temperatures at 0.014kg.s^{-1}and 78.5 rad.s^{-1}.

RTD experimental data*					RTD modelling data*						
Run	TR22[a] (°C)	t_s (s)	t_s / τ	σ'^2	θ_0	p	SSE[a]	N	SSE[a]	Pe	SSE[a]
4	-10.6	53 ± 1	0.99 ± 0.01	0.089 ± 0.008	0.47	3.5	0.001	13	0.011	23	0.030
2	-15.3	55 ± 2	1.02 ± 0.04	0.082 ± 0.008	0.46	3.8	0.001	13	0.009	25	0.027
5	-20.1	49 ± 0	0.93 ± 0.00	0.108 ± 0.017	0.42	3.1	0.002	9	0.011	17	0.033

[a] TR22 = evaporation temperature of r22; SSE = sum of squared error. *Values are means of two replicates.

It can be seen in Fig. 5.2.7. that the RTD curves obtained at -10.6 ºC and -15.3 ºC exhibit similar fluid flow behaviour. But at -20.1 ºC there is a broadening of the RTD curve, indicating an increase in axial dispersion inside the exchanger (cf. Table 5.2.6., increase in σ'^2 and decrease in parameters *p*, *N* and *Pe* with a decrease in TR22). This effect is explained by the increase in the radial temperature gradient between the wall and the centre of the exchanger with the decrease in TR22, the effect of which leads to a higher variation in the apparent viscosity of the product, increasing the difference of axial flow velocities and leading to an increase in axial dispersion. We can also observe in Fig. 5.2.7. that at -20.1ºC the tail of the RTD curve (the part of the fluid that exits after 1.5 t_s) corresponds to 10% of the

total distribution (6% for the other refrigerant temperatures) and represents the high viscosity layer (δ) that flows at a slower velocity near the cooling wall (cf. Fig 5.2.8.).

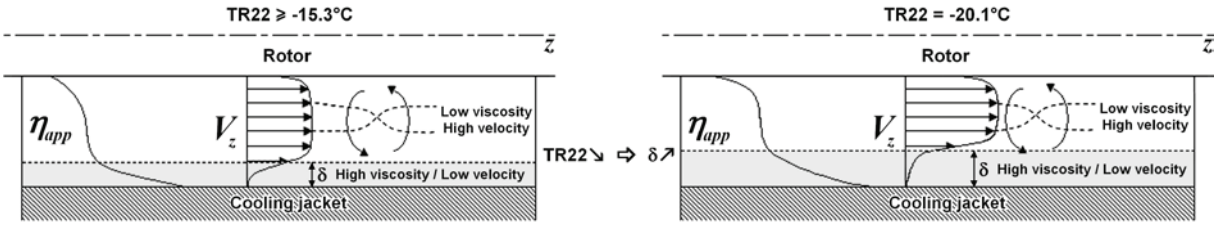


Fig. 5.2.8. Schematic representation of the laminar flow of sorbet passing through an annular space with rotating blades at different refrigerant temperatures.

In addition, this high viscosity layer at the wall region is in our opinion the explanation for the presence of a dead volume of roughly 7% in the SSHE at -20.1 °C (cf. Table 5.2.6., run 5, value of 0.93 for the t_s/τ ratio). It can also be seen that the product starts to exit earlier, at 0.4 t_s (0.5 t_s for the other refrigerant temperatures). This can be explained by the fact that the stagnant and low velocity layer (δ) is thicker at -20.1 °C (cf. Fig 5.2.8.), so that the other part of the fluid has a smaller available section, and therefore flows at a higher velocity (shorter residence time).

4.2. Influence of mix flow rate on axial temperature profile and RTD

Fig. 5.2.9. presents the average axial temperature profile of sorbet in the SSHE as a function of the mix flow rate (MFR) at a refrigerant temperature of -15.3 °C and dasher rotational speed of 78.5 rad.s^{-1} (cf. Table 5.2.4., runs 1, 2 and 3).

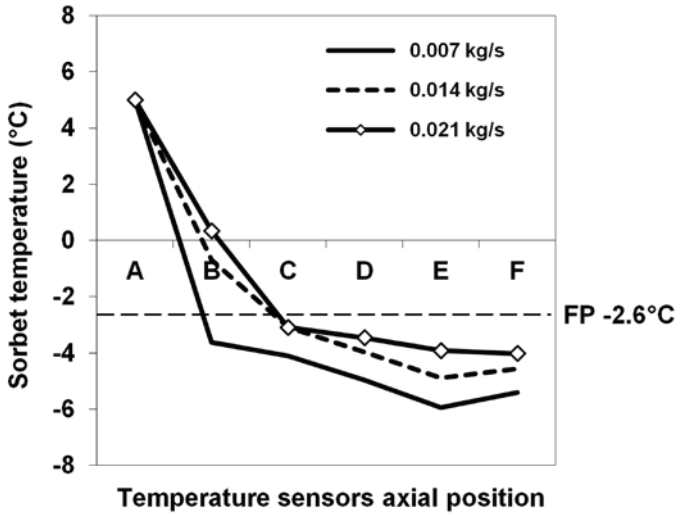


Fig. 5.2.9. Axial temperature profile of sorbet as a function of mix flow rate at rotational speed of 78.5 rad.s^{-1} and refrigerant fluid temperature of -15.3 °C. FP = Freezing point temperature -2.6 °C.

These results show that an increase in product flow rate led to an increase in draw temperature of the product. This effect can be explained by the reduction in the residence time of the product in the SSHE with the increase in product flow rate, which consequently reduces the time available to remove heat from the product and leads to warmer draw temperatures. We can also observe that at 0.007 kg.s^{-1} the chilling section in the exchanger is reduced, which means that for this flow rate the product starts to freeze very near the inlet of the SSHE.

Fig. 5.2.10. shows the normalized RTD curves as a function of the MFR at a refrigerant fluid temperature of -15.3 °C and dasher rotational speed of 78.5 rad.s^{-1}. Experimental and modelling parameters of these curves are given in Table 5.2.7.

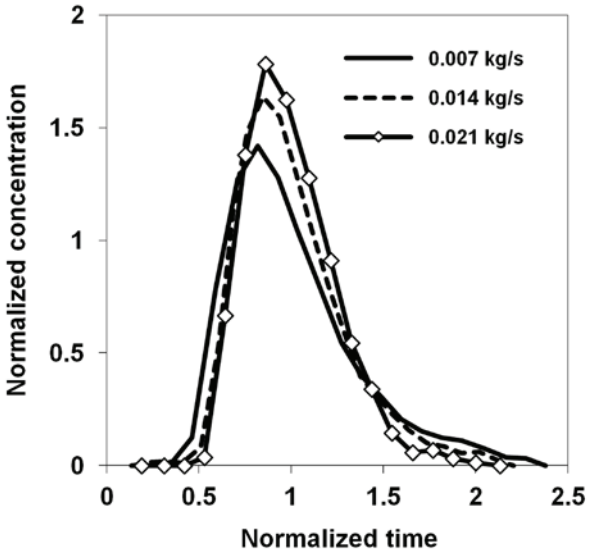


Fig. 5.2.10. Residence time distribution as a function of mix flow rate at rotational speed of 78.5 rad.s^{-1} and refrigerant fluid temperature of -15.3 ºC.

Table 5.2.7. RTD experimental and modelling data at different mix flow rates at -15.3 ºC and 78.5 rad.s^{-1}.

	RTD experimental data*				RTD modelling data*						
Run	MFR[a] (kg.s^{-1})	t_s (s)	t_s / τ	σ'^2	θ_0	p	SSE[a]	N	SSE[a]	Pe	SSE[a]
1	0.007	107 ± 2	1.01 ± 0.01	0.109 ± 0.014	0.39	3.4	0.002	9	0.008	17	0.028
2	0.014	55 ± 2	1.02 ± 0.04	0.082 ± 0.008	0.46	3.8	0.001	13	0.009	25	0.027
3	0.021	35 ± 0	0.97 ± 0.00	0.070 ± 0.013	0.45	4.5	0.002	15	0.009	29	0.028

[a] MFR = mix flow rate; SSE = sum of squared error. *Values are means of two replicates.

The results in Fig. 5.2.10. demonstrate that an increase in product flow rate leads to a narrowing of the RTD curve, indicating a reduction in axial dispersion (cf. Table 5.2.7., decrease of σ'^2 and increase in parameters p, N and Pe with the increase of MFR). These results are consistent with the findings of Alcairo and Zuritz (1990), as well as those of Lee and Singh (1991), who observed that under isothermal conditions an increase in product flow rate resulted in a narrowing of the RTD curves. At cooling conditions Belhamri et al. (2009) also reported a narrowing of the RTD curves with the increase in the product flow rate. The effect observed in Fig. 5.2.10. can be explained by the increase in draw temperature of the product with the increase in product flow rate (cf. Fig. 5.2.9.), the effect of which decreases the apparent viscosity of the product, leading to a more efficient radial mixing, and

consequently to a reduction in axial dispersion in the exchanger (cf. Table 5.2.4., runs 1, 2 and 3, increasing of Re_r and Ta_r with the increase of MFR at outlet temperatures). Lee & Singh (1991) also reported a decrease in the standard deviation of the RTD curves with the decrease in the viscosity of the product, at isothermal conditions. We can also observe in Table 5.2.7. that for these operating conditions the ratio between experimental and theoretical residence time is roughly 1, and therefore we can conclude that there were no dead volumes nor short-circuits within the system at these operating conditions.

4.3. Influence of rotational speed on axial temperature profile and RTD

The effect of dasher rotational speed (DRS) on the average axial temperature profile of the product at a refrigerant temperature of -15.3 °C and mix flow rate of 0.014 $kg.s^{-1}$ is shown in Fig. 5.2.11. (cf. Table 5.2.4., runs 2, 6 and 7). It can be seen that within the first two axial sections of the SSHE (between points A and C) an increase in rotational speed leads to a slight increase in the product temperature. However, this tendency rapidly disappears toward the middle of the exchanger, and throughout the end half of the exchanger the product temperature remains constant (from point C to F). In view of these results, it is our opinion that in the first half of the SSHE the increase in the scraping frequency of the blades leads to a slight warming of the product due to an increase in frictional energy dissipated into the product. However, toward the second half of the exchanger this tendency is counteracted by the improvement of the heat transfer coefficient between the cooling surface and the product, due to the faster removal of the ice crystal build up at the exchanger wall.

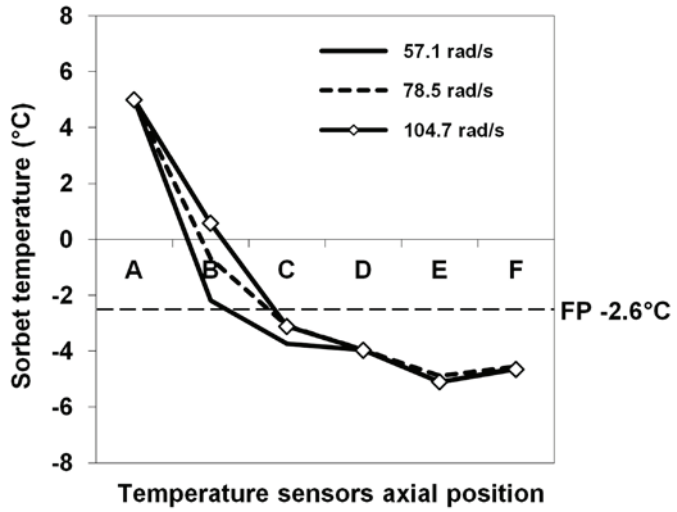


Fig. 5.2.11. Axial temperature profile of sorbet as a function of rotational speed at mix flow rate of 0.014kg.s^{-1} and refrigerant fluid temperature of -15.3°C. FP = Freezing point temperature -2.6 °C.

Normalized RTD curves as a function of dasher rotational speed (DRS) at a refrigerant fluid temperature of -15.3 °C and mix flow rate of 0.014 kg.s^{-1} are compared in Fig. 5.2.12. Experimental and modelling data of these curves are given in Table 5.2.8.

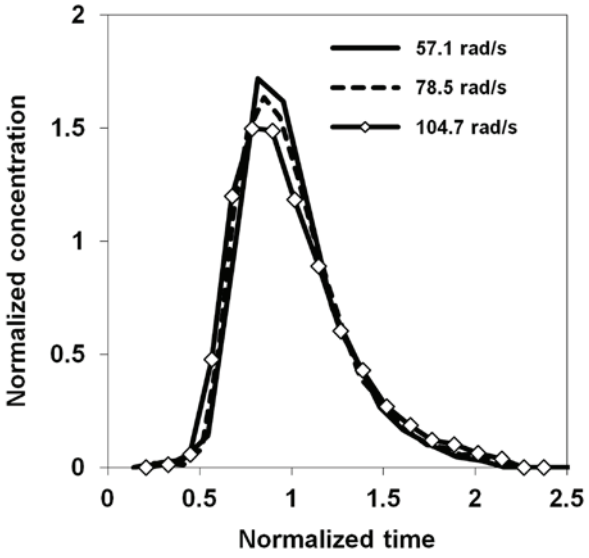


Fig. 5.2.12. Residence time distribution as a function of rotational speed at mix flow rate of 0.014 kg.s^{-1} and refrigerant fluid temperature of -15.3 ºC.

Table 5.2.8. RTD experimental and modelling data at different dasher rotation speeds at 0.014kg.s^{-1} and -15.3 ºC.

	RTD experimental data*				RTD modelling data*						
Run	DRS[a] (rad.s^{-1})	t_s (s)	t_s / τ	σ'^2	θ_0	p	SSE[a]	N	SSE[a]	Pe	SSE[a]
6	57.1	53 ± 1	1.00 ± 0.02	0.085 ± 0.013	0.47	3.6	0.004	13	0.013	24	0.032
2	78.5	55 ± 2	1.02 ± 0.04	0.082 ± 0.008	0.46	3.8	0.001	13	0.009	25	0.027
7	104.7	54 ± 1	1.01 ± 0.00	0.097 ± 0.011	0.47	3.1	0.001	11	0.011	21	0.030

[a] DRS = rotational speed; SSE = sum of squared error. *Values are means of two replicates.

We can observe in Fig. 5.2.12. that an increase in rotational speed results in a broadening of the RTD curve, indicating an increase in axial dispersion (cf. Table 5.2.8., increase of σ'^2 and decrease in parameters p, N and Pe with an increase in DRS). These results are in agreement with those of Benezech and Maingonnat (1989) and Russell et al. (1997), who reported that an increase in the speed of rotation led to a broadening of the RTD curves, for a shear-thinning fluid under isothermal conditions. Based on fluid flow photographs, Russell et al. (1997) concluded that an important contribution to the axial dispersion in the SSHE, was a flow disturbance in the gap between blades that introduced an axial component to the flow, the effect of which was greater at higher rotor speed. The increase in axial dispersion (cf. Fig. 5.2.12.) between DRS at 57.1 and 78.5 rad.s^{-1} could be due to an axial component introduced at the inlet bowl of the SSHE, where there is a substantial change in diameter from the inlet bowl to the exchange cylinder, as well as a change in rotor diameter (cf. Fig 5.2.1.). This effect is probably increased with increasing the rotational speed. The further broadening of the RTD curve at 104.7 rad.s^{-1} could be explained by the presence of Taylor vortices at this DRS (cf. Table 5.2.4., run 7, Ta_r at inlet temperature), which introduces axial disturbances in the flow pattern and further increases the axial dispersion in the exchanger. We can also observe in Table 5.2.8. that there were no dead volumes or short-circuits in the SSHE at these experimental conditions.

5. Conclusions

This work has investigated the influence of the operating conditions of the freezing process of sorbet on the RTD and average axial temperature profile. The GDM model was the most appropriate to describe the experimental RTD data, followed by the TSM model and the ADM model. Experiments showed that a decrease in the refrigerant fluid temperature led to a reduction in the product temperature, and to a reduction in the chilling section of the exchanger, which means that the freezing of the product started very near the entrance of the SSHE at the lower refrigerant temperatures. Low refrigerant temperatures also led to a broadening of the RTD curve, and hence to an increase in axial dispersion in the SSHE. This effect can be explained by the increase in radial temperature gradient between the wall and the centre of the exchanger that leads to a higher viscosity gradient. This effect increased the difference in axial velocities and led to an increase in axial dispersion in the exchanger.

It was also observed that high product flow rates (short mean residence times) led to an increase in the temperature of the product, due to the less time available to remove heat from the product. An increase in product flow rate led to a narrowing of the RTD curve and thus to less axial dispersion. This effect was due to the better radial mixing in the exchanger that was improved by the decrease of the apparent viscosity of the product with warmer draw temperatures.

Our results also demonstrated that an increase in the speed of rotation had no influence on the draw temperature of sorbet. This effect was explained by a compensatory effect between the increase in the frictional energy generated by the scraping action of the blades, and the improvement in the heat transfer rate produced by the faster removal of the ice layer at the exchanger wall. An increase in the rotation speed led to a broadening of the RTD curve and increased the axial dispersion in the SSHE. This effect could be explained in part by the introduction of an axial component at the inlet bowl of the SSHE, where there is a large

change in diameter from the inlet bowl to the exchange cylinder, as well as a change in rotor diameter. This effect was probably increased with increasing the rotational speed. The further broadening of the RTD curve could be explained by the presence of Taylor vortices at the highest rotational speed, which introduced an axial component to the flow and further increased the axial dispersion in the exchanger.

The results obtained in this work can be useful for the optimization and modelling of crystallization processes in SSHEs.

Acknowledgments

The authors gratefully acknowledge the financial support granted by the European Community Seventh Framework through the CAFÉ project (Computer Aided Food processes for control Engineering) Project number 212754.

Abbreviations

ADM – Plug-flow with Axial Dispersion Model

DRS – Dasher Rotational Speed

GDM – Gamma Distribution Model

MB – Methylene blue

MFR – Mix Flow Rate

RTD – Residence Time Distribution

RRT – Recovery Rate of Tracer

SSE – Sum of Squared Errors

SSHE – Scraped Surface Heat Exchanger

TR22 – Evaporation Temperature of r22

TSM – Tank in Series Model

Nomenclature

C dye concentration, %w/w

$C(t)$ concentration of dye in the fluid exit stream at time t, %w/w

D delay time of the system

D_{ax} axial dispersion coefficient, $m^2.s^{-1}$

d_c diameter of heat exchange cylinder, m

d_r diameter of rotor, m

$E(\theta)$ normalized concentration, -

k consistency index for power law fluids, $Pa.s^n$

L heat exchanger cylinder length, m

L_c heat exchanger cylinder length, m

N number of tank in series, -

N_R rotational speed, s^{-1}

n consistency index for power law fluids, -

p extension of fluid mixing on flow direction

Pe Peclet number

Re_{ax} axial Reynolds number $\left[\mathrm{Re}_{ax} = \frac{\rho u^{2-n}(d_c - d_r)^n}{k}\right]$

Re_r rotational Reynolds number $\left[\mathrm{Re}_r = \frac{\rho N_R{}^{2-n}(d_c - d_r)^2}{k}\right]$

Ta_r Taylor number $\left[Ta_r = \left(\frac{r_c - r_r}{r_r}\right)^{0.5} \cdot \frac{\rho(d_c - d_r)^n}{2^n} \cdot \frac{N_R r_r^{2-n}}{k}\right]$

t fluid residence time, s

t_s mean residence time, s

u mean axial velocity, $m.s^{-1}$ $\left[u = \frac{\dot{V}}{\pi\left(d_c^2 - d_r^2\right)/4} \right]$

$\dot{V}$ volumetric flow rate, $m^3.s^{-1}$

V volume available to the working fluid in the SSHE, m^3

Greek symbols

Γ gamma fonction

$\dot{\gamma}$ apparent shear rate, s^{-1}

δ high viscosity and low velocity product layer, -

η_{app} apparent viscosity, Pa.s

θ normalized time, -

θ_0 normalized delay time of the system, -

μ_1 first moment of the residence time distribution, s

μ_2 second moment of the residence time distribution, s

ρ fluid density, $kg.m^{-3}$

σ^2 variance, s^2

σ'^2 normalized variance, -

τ theoretical mean residence time, s

References

Alcairo, E. R. and Zuritz, C. A. (1990). Residence Time Distributions of Spherical-Particles Suspended in Non-Newtonian Flow in a Scraped-Surface Heat-Exchanger. *Transactions of the Asae*, 33, (5), 1621-1628.

Belhamri, R., Fayolle, F., Flick, D. (2009). Simplified flow pattern model in SSHE during crystallisation process. *8th World Congress of Chemical Engineering* Montréal, Quebec, Canada.

Benezech, T. and Maingonnat, J. T. (1989). Etude de la distribution des temps de séjour dans des échangeurs à surface raclée traitant des fluides non-Newtoniens. *Entropie*, 151, 37-46.

Cook, K. L. K. and Hartel, R. W. (2010). Mechanisms of Ice Crystallization in Ice Cream Production. *Comprehensive Reviews in Food Science and Food Safety*, 9, (2), 213-222.

Danckwerts, P. V. (1953). Continuous flow systems. Distribution of residence times. *Chemical Engineering Science*, 2, 1-13.

Dhonsi, D. and Stapley, A. G. F. (2006). The effect of shear rate, temperature, sugar and emulsifier on the tempering of cocoa butter. *Journal of Food Engineering*, 77, (4), 936-942.

Dumont, E., Fayolle, F., Legrand, J. (2000). Flow regimes and wall shear rates determination within a scraped surface heat exchanger. *Journal of Food Engineering*, 45, (4), 195-207.

Edward, L. P., Atiemo-Obeng, V., Kresta, S. M. (2003). Handbook of Industrial Mixing: Science and Practice, Wiley-Interscience. John Wiley & Sons Inc.

Fayolle, F., Mabit, J., Legrand, J. (2005). Determination of heterogeneities in a scraped surface heat exchanger using electrochemical sensors. *Journal of Applied Electrochemistry*, 35, (5), 487-498.

Härröd, M. (1986). Scraped surface heat exchangers - A literature survey of flow patterns, mixing effects, residence time distribution, heat transfer and power requirements. *Journal of Food Process Engineering*, 9, 1-62.

Lee, J. H. and Singh, R. K. (1991). Particle residence time distributions in a model horizontal scraped surface heat exchanger. *Journal of Food Process Engineering*, 14, 125-146.

Levenspiel, O. (1999). Chemical Reaction Engineering, John Wiley & Sons Inc.

Milton, J. L. and Zahradnik, J. W. (1973). Residence time distribution of a votator pilot plant using a non-Newtonian fluid. *Transactions of the Asae*, 16, (6), 1186-1189.

Russell, A. B., Burmester, S. S. H., Winch, P. J. (1997). Characterization of shear thinning flow within a scraped surface heat exchanger. *Food and Bioproducts Processing*, 75, (C3), 191-197.

Sanchez, J., Hernandez, E., Auleda, J. M., Raventos, M. (2011). Review: Freeze Concentration Technology Applied to Dairy Products. *Food Science and Technology International*, 17 (1), 5-13.

Shahidi, F. (2005). Edible oil and fat products: processing technologies, Wiley-Interscience. John Wiley & Sons, Inc.

Trommelen, A. M. and Beek, W. J. (1971). Flow phenomena in a scraped-surface heat exchanger (Votator-type). *Chemical Engineering Science*, 26, (11), 1933-1942

Villermaux, J. (1993). Génie de la réaction chimique, conception et fonctionnement des réacteurs. Paris, Technique et documentation.

Wang, W., Walton, J. H., McCarthy, K. L. (1998). Flow profiles of power law fluids in scraped surface heat exchanger geometry using MRI. *Journal of Food Process Engineering*, 22, 11-27.

Wen, C. Y. and Fan, L. T. (1975). Models for flow systems and chemical reactors. New York, Marcel Decker.

Yataghene, M., Francine, F., Jack, L. (2011). Flow patterns analysis using experimental PIV technique inside scraped surface heat exchanger in continuous flow condition. *Applied Thermal Engineering*, 31, (14-15), 2855-2868.

5.3. Rheological characterization of sorbet using pipe rheometry during the freezing process.

Marcela Arellano[a,b,c,d], Hayat Benkhelifa[b,c,d], Denis Flick[b,c,d], Graciela Alvarez[a,4].

[a]*Irstea. UR Génie des Procédés Frigorifiques. 1 rue Pierre-Gilles de Gennes CS 10030, 92761 Antony Cedex, France*

[b]*AgroParisTech. UMR 1145 Ingénierie Procédés Aliments. 16 rue Claude Bernard, 75231 Paris Cedex 05, France*

[c]*INRA.UMR 1145 Ingénierie Procédés Aliments. 1 avenue des Olympiades, 91744 Massy Cedex, France*

[d]*CNAM. UMR 1145 Ingénierie Procédés Aliments. 292 rue Saint-Martin, 75141 Paris Cedex 03, France*

Abstract

Sorbet produced without aeration is a dispersion of ice crystals distributed randomly in a freeze-concentrated liquid phase. The rheological properties of this suspension will be affected by the viscosity of the continuous liquid phase and the volume fraction of ice crystals. The knowledge of the viscosity of the product is essential for the selection of process equipment, and for the optimal design of piping systems. In this work, the rheology of a commercial sorbet has been studied in situ by means of a pipe rheometer connected at the outlet of a continuous scraped surface heat exchanger (SSHE). This work aimed at studying the influence of the temperature of the product, and thus of the ice volume fraction on the apparent viscosity of the product, at different stages of the freezing process, and secondly, to propose a rheological model to predict the evolution of the apparent viscosity of the product which may help to improve the control of the quality of the product, the design of piping systems and the modelling of the freezing process of sorbet. The pipe rheometer was composed of a series of pipes in PVC of different diameters, making it possible to apply a range of apparent shear rate from 4-430 s^{-1}. Results showed that the flow behaviour index of sorbet decreases as the temperature of the product decreases, the effect of which indicates that the product becomes more shear thinning as the freezing of sorbet occurs. The consistency coefficient and therefore the magnitude of the apparent viscosity of sorbet increase with the decrease in product temperature and with the increase of the ice volume fraction. A rheological model that predicts the apparent viscosity of the product was presented. Comparison between experimental and predicted data showed that the model presents a relative close fit to the experimental data within a 20% error.

Key words: Apparent viscosity; Pipe rheometry; Draw temperature; Ice volume fraction; Freezing; Scraped surface heat exchanger.

4 Corresponding author. Tel.: +33 140 96 60 17; Fax: +33 140 96 60 75.
E-mail address: graciela.alvarez@irstea.fr

1. Introduction

The characterisation of the rheological properties of sorbet has significant applications throughout the manufacturing process of frozen desserts. The understanding of the influence of changes in product microstructure on its rheological properties is necessary for the improvement of the freezing process and the quality of the product. The knowledge of the viscosity of the product is also essential for the selection of process equipment, and for the optimal design of piping systems. The freezing of sorbet is carried out in a continuous scraped surface heat exchanger (SSHE) or freezer. Once the freezing of sorbet starts and ice crystals are being formed, the liquid sorbet mix starts to freeze concentrate and the viscosity of this continuous liquid phase increases (Burns and Russell, 1999; Goff et al., 1995). Simultaneously, the ice crystals are dispersed in the liquid sorbet mix by the rotation of the scraping blades, modifying the fluid flow field and increasing the viscosity of sorbet. Sorbet exiting from the freezer at a draw temperature between -4 to -6 °C, contains roughly 20-40% of the total amount of water in the form of ice crystals, which are suspended in a viscous liquid phase composed of water, sugar, stabilizers (polysaccharides) and salts. At this point, the product must have an adequate viscosity to be pumped for moulding and packaging. Further on, the product is hardened in a blast freezer to attain a core temperature of -18 °C (Cook and Hartel, 2010), where roughly 80% of the amount of water is frozen (Marshall et al., 2003).

The measurement of the viscosity of sorbet and ice cream is highly complex, because the product is temperature sensitive and it behaves as a non-Newtonian shear-thinning fluid (Burns and Russell, 1999; Haddad, 2009). A number of studies in the literature, based on oscillatory rheometry for the analysis of the viscosity of ice cream, have also reported viscoelastic behaviour (Goff et al., 1995; Granger et al., 2004; Wildmoser et al., 2004).

Pipe viscometers have also been used to measure the apparent viscosity of ice cream and sorbet in situ and online during the freezing process (Cerecero, 2003; Martin et al. 2008;

Elhweg et al., 2009). Pipe viscometers are generally composed of a set of pipes of different diameters, through which the product flows under pressure. The relationship between the shear rate and the shear stress is determined from pressure drop and volumetric flow rate measurements. The challenge of pipe rheometry measurements lies on the difficulties of controlling a steady temperature and flow conditions. Furthermore, the effects of wall slip behaviour and viscous dissipation must be evaluated so as to ensure accurate rheological measurements.

Apparent wall slip behaviour occurs in multi-phase systems due to the displacement of the disperse phase away from solid interfaces. This creates a layer of fluid near the wall region that has a lower viscosity and higher velocity than the bulk of the product, forming a layer of high shear rate (Martin and Wilson, 2005). This effect could lead to inaccurate rheological measurements. Mooney (1931) proposed a method to identify the slip wall behaviour. This technique consists on tracing the flow behaviour curves (shear stress versus shear rate) for different pipe diameters and different flow rates. In the absence of wall slip, these curves overlap. However, the separation of these curves reveals the existence of wall slip. Apparent wall slip behaviour has been observed in multi-phase food products such as fruit purees (Balmforth et al. 2007), tomato ketchup (Adhikari and Jindal, 2001) and coarse food suspensions of CMC-green pea solutions. More recently Martin et al. (2008) and Elhweg et al (2009) reported some evidence of apparent wall slip in ice cream, but wall slip effects were neglected due to insufficient data and control of pressure to discern clear trends.

The phenomenon of viscous dissipation refers to the mechanical energy dissipated during the flow of the fluid through the pipe which is converted into internal energy, increasing the temperature of the product along the pipe axis (Winter, 1977). Thus, due to the high shear rates obtained near the pipe wall, the temperature of sorbet will increase near the wall region, leading to the decrease in the viscosity of the product, increasing the fluid flow velocity and

consequently leading to a higher wall shear rate. The impact of viscous dissipation can be assessed by evaluating the Nahme dimensionless number (*Na*), which indicates the degree at which the temperature rise will affect the viscosity of the product (Macosko, 1994). The effect of viscous dissipation becomes significant when Na > 1 (Macosko, 1994). Elhweg et al. (2009) reported that the phenomenon of viscous dissipation in ice cream was significant for a certain range of product temperatures (-6 to -12 °C) and shear rates (0.3 to 360 s^{-1}).

Sorbet produced without aeration is a dispersion of ice crystals distributed randomly in a freeze concentrated liquid phase. The flow of this suspension will be affected by the viscosity of the continuous liquid phase, the volume fraction (ϕ) of ice crystals, crystal-crystal interactions and the ice crystal size. A number of theoretical and empirical equations have been developed to predict the viscosity of concentrated suspensions (Einstein, 1906; Mooney, 1951; Krieger and Dougherty, 1959; Thomas, 1965; Batchelor, 1977). Table 5.3.1. shows a summary of the available models in the literature.

Table 5.3.1. Rheological models to predict the viscosity of a Newtonian suspension as a function of the volume fraction of particles.

Reference	Viscosity Expression	Particle concentration
Einstein, 1906	$\eta = \eta_l(1+2.5\phi)$	$\phi < 0.02$
Mooney, 1951	$\eta = \eta_l \exp\left(\frac{2.5\phi}{1-k\phi}\right)$	For $k = 1.43$ $\phi < 0.35$ For $k = 0.75$ $\phi < 0.58$
Krieger and Dougherty, 1959	$\eta = \eta_l \exp\left(1-\frac{\phi}{\phi_{\max}}\right)^{-2.5\phi_{\max}}$	For high shear rates $\phi_{\max} = 0.71$ For low shear rates $\phi_{\max} = 0.63$
Thomas, 1965	$\eta = \eta_l\left(1+2.5\phi+10.05\phi^2+0.00273\exp(16.6\phi)\right)$	$\phi < 0.625$
Batchelor, 1977	$\eta = \eta_l\left(1+2.5\phi+6.2\phi^2\right)$	$\phi < 0.2$

Most of these models are extended versions of the expression developed by Einstein (1906) to predict the evolution of the viscosity of a Newtonian suspension of rigid spheres

(ϕ < 0.02), as a function of the volume fraction ϕ of the suspended spheres and of the viscosity of the continuous phase η_l, written as:

$$\eta = \eta_l(1 + 2.5\phi) \quad (1)$$

This model takes only into account the Brownian movement of the spheres, neglects particle-particle interactions, and is only valid in the case of dilute solutions.

For higher particle concentrations (ϕ < 0.625) and a range of particle size between 0.099 to 435 μm, Thomas (1965) proposed a semi-empirical expression which predicts the viscosity of Newtonian suspensions as a function of the viscosity of the continuous phase η_l and the volume fraction ϕ of the suspended rigid spheres, expressed as:

$$\eta = \eta_l\left(1 + 2.5\phi + 10.05\phi^2 + 0.00273\exp(16.6\phi)\right) \quad (2)$$

In this model, the first three terms inside the parentheses account for the effect of the hydrodynamic interactions of spheres and particle-particle interactions, whereas the exponential term considers the rearrangement of particles as the suspension is sheared (Thomas, 1965). This model has been widely used to predict the viscosity of ice slurries (Ayel et al., 2003; Hansel, 2000), but has been reported to overestimate the viscosity of ice slurries when the ice concentration exceeds ϕ > 0.15 (Hansel, 2000). Haddad (2009) compared experimental viscosity data obtained in a scraped rheometer, during the batch freezing of a 30% sucrose solution with the predicted values by Thomas equation (Eq. 2). Results showed that the Thomas equation underestimates the viscosity of non-Newtonian shear-thinning suspensions of ice crystals.

The aims of the present work are, firstly, to study the influence of the temperature of the product and thus of the ice volume fraction ($\phi_{v.ice}$), on the apparent viscosity (η_{app}) of sorbet at different stages of the freezing process (i.e. during the flow of the product through the SSHE, through a pipe, and through a product filling machine), and secondly, to propose

an empirical model to predict the evolution of the viscosity, which may help to improve the control of the quality of the product, the design of piping systems and the modelling of the freezing process of sorbet.

2. Materials and methods

2.1. Sorbet freezing and operating conditions

The working fluid used in these experiments was an ultra high temperature pasteurized lemon sorbet mix (14.6% w/w sucrose, 8% w/w fructose, 0.09% w/w dextrose, 3% w/w lemon juice concentrate 60 Brix, 0.5% w/w locust bean gum / guar gum / hypromellose stabiliser blend). The mix was stored at 5 °C for 24 h prior to use. Freezing of the mix was carried out in a laboratory scale continuous pilot SSHE (WCB® Model MF 50). A schematic representation of the experimental platform is shown in Fig. 5.3.1.

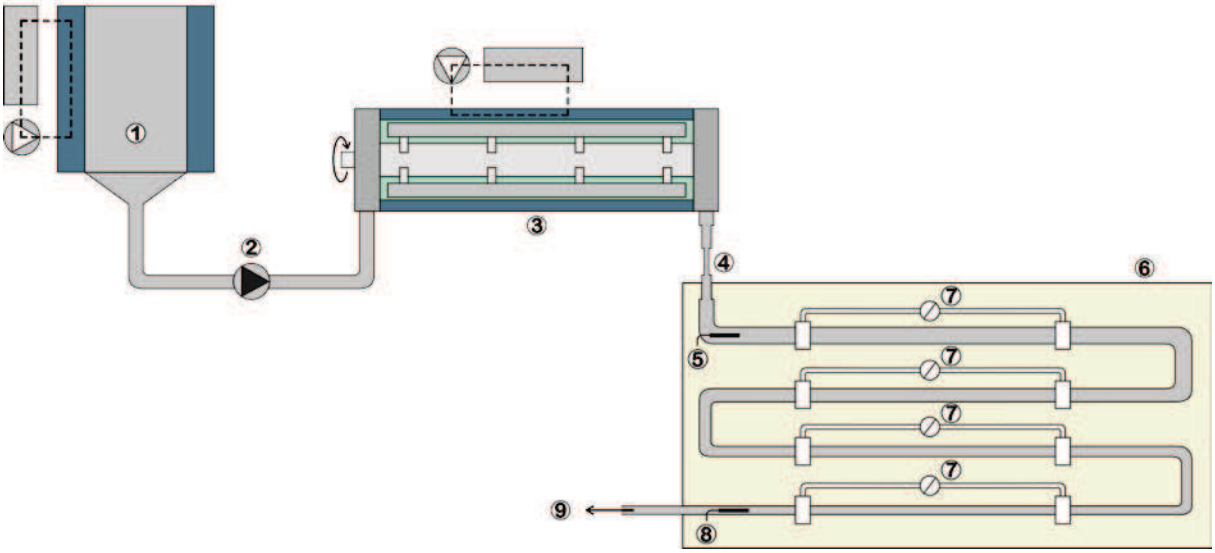


Fig. 5.3.1. Schematic representation of the experimental platform. 1. Refrigerated storage tank (200 l capacity). 2. Volumetric piston pump. 3. Freezer. 4. Contraction/enlargement pipe. 5. Pt100 probe inserted into the inlet of the rheometer. 6. Pipe rheometer. 7. Pressure manometers. 8. Pt100 probe inserted into the outlet of the rheometer. 9. Product exit.

Product flow rate was adjusted within a range of 0.007 to 0.014 $kg.s^{-1}$. The mix flow rate was determined by weighing the product exit stream during a given period of time. The accuracy of this measurement was determined to be $\pm 9.2 \times 10^{-5}$ $kg.s^{-1}$. The dasher speed of the SSHE was fixed at 78.5 $rad.s^{-1}$ (750 rpm). The dasher speed was measured by means of a

photoelectric tachometer (Ahlborn®, type FUA9192) with an accuracy of ±0.105 rad.s^{-1} (1 rpm). The draw (exit) temperature of sorbet was varied by adjusting the refrigerant fluid temperature (r22, chlorodifluoromethane) evaporating in the cooling jacket of the SSHE. A calibrated type T (copper - constantan) thermocouple with an accuracy of ±0.2 °C was fixed with conductive aluminium tape on the external surface wall of the cooling jacket, so as to measure the evaporation temperature of the refrigerant fluid. The exterior of the exchanger jacket was insulated with 2 cm thick polystyrene foam insulation in order to reduce heat loss.

The operating conditions under which the rheological measurements were carried out are given in Table 5.3.3. No aeration was employed for any of the rheological measurements. For the mix flow rate of 0.007 kg.s^{-1}, at least 3 replicates (4 measurements for each run) were performed for each experimental condition, in order to provide enough experimental data for the rheological model fitting. For the mix flow rate of 0.010 kg.s^{-1} and 0.014 kg.s^{-1}, two replicates were performed (4 measurements for each run); these experimental runs were performed to verify the presence of wall slip behaviour and were not taken into account for the fitting of the rheological model.

2.2. Pipe rheometry measurements

Frozen sorbet was pumped from the SSHE, first, into a contraction/enlargement pipe, and then into an instrumented pipe rheometer (cf. Fig. 5.3.1.). The contraction/enlargement pipe was composed of 5 pipes in copper plumbing of 0.10 m length each and of different internal diameters ($d_{1c/e}$=0.025m; $d_{2c/e}$=0.0157m; $d_{3c/e}$=0.0094m; $d_{4c/e}$=0.0157m; $d_{5c/e}$=0.025m). This contraction/enlargement pipe was used to pre-shear the sorbet before it entered into the pipe rheometer, so as to prevent any thixotropic behaviour and to obtain repeatable measurements. The rheometer was composed of sets of 4 pipes in clear polyvinyl chloride (PVC) of different internal diameters (d_1=0.0272m, d_2=0.0212m, d_3=0.0167m, d_4=0.013m,

d_5=0.01m, d_6=0.0058m) connected in series, making it possible to apply an apparent shear rate range of $4 < \dot{\gamma}_w < 430$ s^{-1}. All pipes were insulated with polystyrene foam insulation of 2 cm thickness in order to reduce heat loss. Since the apparent viscosity of sorbet increases with the decrease of the temperature of the product and thus with the increase of the ice volume fraction ($\phi_{v.ice.}$), the use of all the pipes was not possible for all experimental conditions. Therefore, the pipes of diameters d_1 to d_6 were used for measurements of sorbet mix and frozen sorbets with $\phi_{v.ice.}$ of 0.058 and 0.106, diameters d_1 to d_5 for frozen sorbet with $\phi_{v.ice.}$ of 0.166, diameters d_1 to d_4 for $\phi_{v.ice.}$ of 0.234 and 0.305, and d_1 to d_3 for $\phi_{v.ice.}$ of 0.390. Two piezometric rings, located at the measuring points of each pipe, made it possible to measure a pressure drop within each pipe for a length of 0.5 m. Pressure drop measurements were performed by liquid column manometers with an accuracy of ± 2% of the measured value. Pressure drop and flow rate were used to calculate the shear stress and the shear rate by Eq. 5 and 6, respectively, as shown in the following section. The draw temperature of sorbet was measured as it flowed through the pipes of the rheometer by means of calibrated Pt100 probes (accuracy of ±0.1 °C) located in the centre of the inlet and outlet pipes of the rheometer (cf. Fig. 5.3.1.). Thermal steady state in the pipe rheometer was achieved by pumping sorbet into it, until the measured temperatures at the inlet and outlet of the rheometer were brought to the desired experimental draw temperature.

2.2.1. Apparent viscosity calculations

The theory of the pipe rheometer is based on the Rabinowitsch-Mooney equation (Steffe, 1996) which considers the following assumptions: (1) the fluid flow is laminar and steady, (2) there is no slip at the wall of the pipe, (3) the fluid properties are independent of pressure and time, and (4) the temperature is constant throughout the whole system. The general Rabinowitsch-Mooney equation relating shear rate $(\dot{\gamma}_w)$ and shear stress (σ_w) at the wall of the pipe is given by:

$$\dot{\gamma}_w = f(\sigma_w) = \left(\frac{3\dot{V}}{\pi R^3}\right) + \sigma_w \left[\frac{d\left(\dot{V}/\left(\pi R^3\right)\right)}{d\sigma_w}\right] \tag{3}$$

where $\dot{V}$ is the volumetric fluid flow rate, R the inner radius of the pipe and σ_w the shear stress given by:

$$\sigma_w = \frac{(\delta P)R}{2L} \tag{4}$$

where δP is the pressure drop measured over a fixed length L of a horizontal pipe.

Eq. (3) can be solved and simplified in terms of the definition of a power law fluid ($\sigma_w = k(\dot{\gamma}_w)^n$), then the shear rate $\dot{\gamma}_w$ may be determined by:

$$\dot{\gamma}_w = \left(\frac{3n+1}{4n}\right)\left(\frac{4\dot{V}}{\pi R^3}\right) \tag{5}$$

with $n = d\left(ln\left(\delta P\, R/2L\right)\right)/d\left(ln\left(4\dot{V}/\pi R^3\right)\right)$. For each draw temperature obtained at a given product flow rate and rotational speed, n is calculated by taking into account data from all repetitions performed at the same operating condition.

A regression analysis of (σ_w) versus $(\dot{\gamma}_w)$ to fit a power law model was used to characterize the apparent viscosity of non-Newtonians shear-thinning fluids, such as sorbet:

$$\eta_{app} = k \cdot \dot{\gamma}_w^{n-1} \tag{6}$$

where n is the flow behaviour index, $\dot{\gamma}_w$ the shear rate and k is the consistency index. The consistency index k represents the apparent viscosity of the product at a shear rate of $1s^{-1}$.

In order to understand the effect of the apparent viscosity of the product at different stages of the freezing process, we can express the viscosity of the product at the shear rates at which the sorbet is submitted during processing. The average shear rate $\dot{\gamma}$ within SSHEs can be calculated with the model proposed by Leuliet et al., (1986) written as follows:

$$\dot{\gamma} = (3.213\times10^4 \times 1.45^{nL} n^{-0.7115}\dot{V} + 23.44\dot{V}^{-0.03} n^{0.1754} N_R) \tag{7}$$

where nL is the number of scraping blades and N_R the rotational speed of the dasher. The shear rate within the outlet pipe of the SSHE and within a sorbet cup filling machine were determined by Eq. 5 considering a pipe of diameter $d_{outlet.pipe}$ = 0.0225 m and $d_{filling.pipe}$ = 0.03 m, respectively.

2.3. Ice volume fraction calculations

Assuming the thermodynamic equilibrium between ice and the solution of solute (sweeteners content), the ice mass fraction in sorbet $\phi_{m.ice.}$ (kg of ice / kg of sorbet) can be determined from the freezing point curve of sorbet mix, which is a function of the mass fraction of solute w_{ms} in the residual liquid phase. This curve was previously determined by means of differential scanning calorimetric (DSC) measurements as reported by Gonzalez (2012). The expression that characterizes the freezing point curve and links the solute mass fraction at the equilibrium temperature is given by the following equation:

$$w_{ms} = \left(-0.137T - 0.0202T^2 - 0.00167T^3 - 0.0000529T^4\right), \text{ with T in °C} \quad (8)$$

According to a mass balance of solute (sweetener content), the solute is present in sorbet mix at a certain initial mass fraction ($w_{ms.i}$). Then the solute is concentrated as the freezing of sorbet occurs, until it reaches a final mass fraction ($w_{ms.f}$) in the liquid phase. The final liquid phase represents only a fraction $\left(1-\phi_{m.ice.}\right)$ of sorbet, hence the ice mass fraction can be calculated by the following equation:

$$w_{ms.i} = \left(1-\phi_{m.ice.}\right)\cdot w_{ms.f}\left(T\right) \Leftrightarrow \phi_{m.ice.} = 1 - \frac{w_{ms.i}}{w_{ms.f}\left(T\right)} \quad (9)$$

The ice volume fraction (m^3 of ice / m^3 of sorbet) is then determined as follows:

$$\phi_{v.ice} = \frac{\rho_s}{\rho_i}\phi_{m.ice} \quad (10)$$

where ρ_s is the density of sorbet and ρ_i the density of ice.

Once the experimental conditions of the SSHE were set and the thermal steady state of the system was attained, the draw temperature of the product and ice volume fraction data were recorded and calculated every 5 seconds by using a program written in LabVIEW®.

2.4. Viscous dissipation

The effect of viscous dissipation on the apparent viscosity of the product η_{app} at a given apparent shear rate $\dot{\gamma}_w$, can be assessed by the Nahme number, Na, expressed for the pipe flow of a power law fluid as:

$$Na = \frac{\xi k \dot{\gamma}_w^{n+1} R^2}{4\lambda_{sorbet}} \tag{11}$$

where ξ is the temperature sensitivity of viscosity defined as $-(1/\eta_{app})(\partial\eta_{app}/\partial T)$, k and n the consistency and flow behaviour indices, respectively, λ_{sorbet} the thermal conductivity of sorbet, and R the pipe radius (Judy et al., 2002; Elhweg et al., 2009).

The thermal conductivity of sorbet is given by the following expression (Maxwell, 1973):

$$\lambda_{sorbet} = \lambda_w \left[\frac{2\lambda_w + \lambda_{ice} - 2\phi_{v.ice}(\lambda_w - \lambda_{ice})}{2\lambda_w + \lambda_{ice} + \phi_{v.ice}(\lambda_w - \lambda_{ice})} \right] \tag{12}$$

where λ_{ice} is the evolution of the thermal conductivity of ice as a function of the temperature of the product and calculated by the following expression (Levy, 1982):

$$\lambda_{ice} = 2.24 + 5.975 \times 10^{-3}(-T)^{1.156}, \text{ with T in °C} \tag{13}$$

λ_w is the thermal conductivity of the solute solution, determined by the Baloh relation (1967):

$$\begin{aligned} \lambda_w &= (1 - w_{ms}) \cdot (0.563 + 1.976 \times 10^{-3} T - 7.847 \times 10^{-6} T^2) \\ &+ w_{ms} \cdot (0.261 + 0.8 \times 10^{-3} T - 2.3 \times 10^{-6} T^2) \end{aligned}, \text{ with T in °C} \tag{14}$$

with T being the draw temperature of the product and w_{ms} the mass fraction of solute in the residual liquid phase of the sorbet.

3. Results and discussion

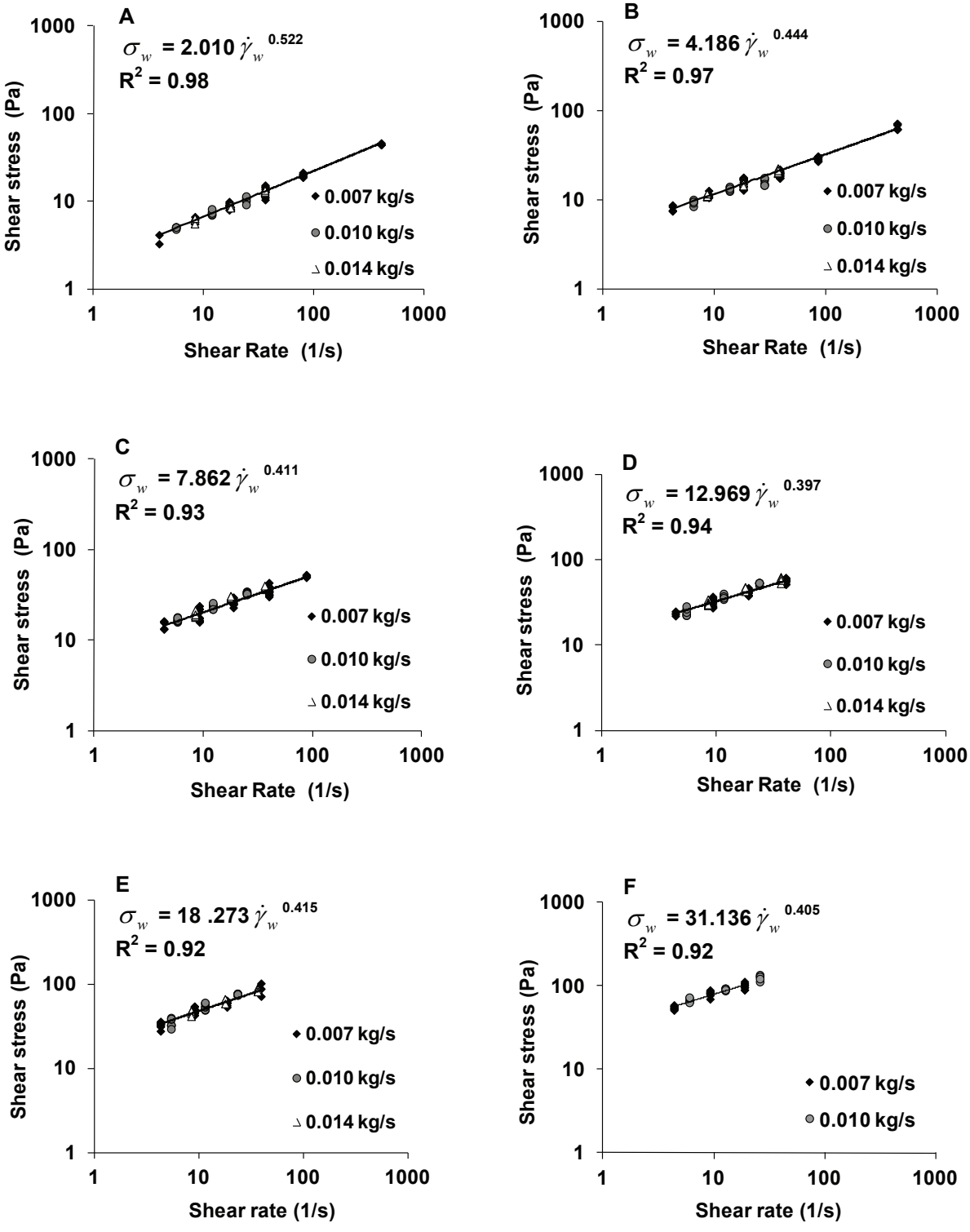


Fig. 5.3.2. Flow behavior curves for sorbet at different temperatures and ice volume fractions. (A) Sorbet at -2.89 °C and $\phi_{v.ice}$ = 0.058. (B) Sorbet at -3.11 °C and $\phi_{v.ice}$ = 0.106. (C) Sorbet at -3.44 °C and $\phi_{v.ice}$ = 0.166. (D) Sorbet at -3.90 °C and $\phi_{v.ice}$ = 0.234. (E) Sorbet at -4.55 °C and $\phi_{v.ice}$ = 0.305. (F) Sorbet at -5.68 °C and $\phi_{v.ice}$ =0.390. Power law model along with the fitted indices correspond only to the rheological measurement of sorbet at a mix flow rate of 0.007 kg.s^{-1} and 78.5 rad.s^{-1}.

3.1. Wall slip and viscous dissipation effects on the apparent viscosity of sorbet

Fig. 5.3.2. shows the flow behaviour curves of sorbet for the three different tested product flow rates, at different product temperatures and therefore at different ice volume fractions. We can observe from these results that the power law model adequately described the shear stress and shear rate data for all experimental conditions ($R^2 > 0.92$). It can also be seen that the different flow curves measured with different pipe diameters overlap, demonstrating thus the absence of wall slip. Therefore we can neglect the wall slip phenomenon.

Table 5.3.2. shows the calculated values of the Nahme number (*Na*) for all the operating conditions performed.

Table 5.3.2. Operating conditions, used rheometer pipes (diameter d_i) and estimated values of Nahme number (*Na*) for sorbet produced at different draw temperatures and different product flow rates at dasher speed = 78.5 rad.s^{-1}.

Mix flow rate = 0.007 kg.s^{-1}							
T inlet* °C	$\phi_{v.ice}$*	d_1 = 0.0272 m	d_2 = 0.0212 m	d_3 = 0.0167 m	d_4 = 0.013 m	d_5 = 0.01 m	d_6 = 0.0058 m
-2.89	0.058	*Na* = 0.0059	*Na* = 0.0100	*Na* = 0.0165	*Na* = 0.0187	*Na* = 0.031	*Na* = 0.09
-3.11	0.106	0.0058	0.0099	0.0164	0.0232	0.039	0.11
-3.44	0.166	0.0056	0.0095	0.0158	0.0246	0.042	
-3.90	0.234	0.0052	0.0090	0.0151	0.0251		
-4.55	0.305	0.0048	0.0084	0.0142	0.0239		
-5.68	0.390	0.0046	0.0081	0.0138			
Mix flow rate = 0.010 kg.s^{-1}							
T inlet* °C	$\phi_{v.ice}$*	d_1 = 0.0272 m	d_2 = 0.0212 m	d_3 = 0.0167 m			
-2.90	0.059	*Na* = 0.0102	*Na* = 0.022	*Na* = 0.044			
-3.12	0.109	0.0104	0.022	0.043			
-3.42	0.164	0.0090	0.018	0.035			
-3.84	0.225	0.0082	0.016	0.028			
-4.48	0.298	0.0075	0.013	0.022			
-5.69	0.390	0.0072	0.011	0.014			
Mix flow rate = 0.014 kg.s^{-1}							
T inlet* °C	$\phi_{v.ice}$*	d_1 = 0.0272 m	d_2 = 0.0212 m	d_3 = 0.0167 m			
-2.90	0.059	*Na* = 0.019	*Na* = 0.033	*Na* = 0.056			
-3.11	0.106	0.018	0.031	0.053			
-3.43	0.164	0.016	0.027	0.047			
-3.89	0.232	0.014	0.024	0.041			
-4.50	0.300	0.012	0.021	0.036			

*T Inlet = product temperature at the inlet of the pipe rheometer; $\phi_{v.ice}$ = Ice volume fraction.

As previously mentioned, the impact of viscous dissipation on the viscosity of the product becomes significant when $Na > 1$. From these results we can observe that the largest estimated Nahme number for all the operating conditions used was 0.11. This small value of *Na* suggests that viscous dissipation effects are negligible for this range of operating conditions.

3.2. Effect of draw temperature and ice volume fraction on the apparent viscosity

Since the apparent viscosity of sorbet exhibited a similar behaviour for the different used flow rates, only the rheological properties of sorbet measured at a mix flow rate of 0.007 $kg.s^{-1}$ will be discussed. Table 5.3.3. presents the operating conditions and the product characteristics under which the rheological measurements were performed. These results show that for the tested mix flow rates, the measured temperature increase between T_{inlet} and T_{outlet} is always very low (T_{inlet} - T_{outlet} < 0.03 °C), which shows that both heat losses and viscous dissipation are quite negligible. The inlet-outlet temperature increase is slightly higher for the lower product temperature, the effect of which is likely due to the higher temperature difference between the environment and the product, leading to an increase of heat loss.

Table 5.3.3. Operating conditions and measured responses during the rheology experiments.

	Operating conditions			Product characteristics		
Run	MFR[a] ($kg.s^{-1}$)	DRS[a] ($rad.s^{-1}$)	TR22[a] (°C)	T_{inlet} (°C)	T_{outlet} (°C)	$\phi_{v.ice}$
1*	0.007	78.5	-	5.03	5.03	-
2**	0.007	78.5	-7.20	-2.89	-2.89	0.058
3**	0.007	78.5	-8.26	-3.11	-3.10	0.106
4**	0.007	78.5	-9.39	-3.44	-3.43	0.166
5**	0.007	78.5	-11.37	-3.90	-3.89	0.234
6**	0.007	78.5	-12.91	-4.55	-4.54	0.305
7**	0.007	78.5	-16.34	-5.68	-5.65	0.390

[a] MFR = mix flow rate; DRS = dasher rotational speed; TR22 = evaporation temperature of r22; T_{inlet} = product temperature at the inlet of the pipe rheometer; T_{outlet} = product temperature at the outlet of the pipe rheometer; $\phi_{v.ice}$ = Ice volume fraction.
*Sorbet mix, mean values of two replicates. **Frozen sorbet, mean values of three replicates.

Table 5.3.4. shows the rheological properties of sorbet mix and frozen sorbet measured at the operating conditions shown in Table 5.3.3. These results confirm the shear-thinning behaviour of sorbet mix and frozen sorbet (flow behaviour index n < 1) since the apparent viscosity of the product decreases with increasing the shear rate.

Table 5.3.4. Measured responses during the rheology experiments.

		Rheological properties			
Run	$\phi_{v.ice}$ [a]	n [a]	k (Pa.s) [a]		
			[a] η_{app} at $\dot{\gamma}_w = 1 s^{-1}$	[a] η_{app} at $\dot{\gamma}_w = 10\ s^{-1}$	[a] η_{app} at $\dot{\gamma}_w = 100\ s^{-1}$
1*	-	0.553	0.455	0.163	0.058
2**	0.058	0.524	1.993	0.666	0.222
3**	0.106	0.444	4.186	1.163	0.323
4**	0.166	0.411	7.862	2.025	0.521
5**	0.234	0.397	12.969	3.235	0.807
6**	0.305	0.415	18.274	4.752	1.236
7**	0.390	0.405	31.136	7.911	2.010

[a] $\phi_{v.ice}$ = Ice volume fraction; n = flow behaviour index; k = consistency index; η_{app} = apparent viscosity; $\dot{\gamma}_w$ = wall shear rate. *Sorbet mix, mean values of two replicates. **Frozen sorbet, mean values of three replicates.

It can also be seen that the flow behaviour index n decreases sharply from n = 0.553 for sorbet mix at 5.03 °C to n = 0.524 for frozen sorbet at -2.89 °C (increase in ice volume fraction of 0.058). Then, there is a further decrease in the flow behaviour index from n = 0.524 to n = 0.411 between the product temperatures of -2.89 to -3.11 °C (ice volume fraction increase from 0.058 to 0.166). Furthermore, from -3.11 °C to -5.68 °C there is an establishment of a plateau at roughly n = 0.405 with the further decrease in the temperature of the product. This effect indicates that sorbet becomes more shear-thinning as the temperature of the product decreases. Cerecero (2003) also reported a decrease in the flow behaviour index and the establishment of a plateau with a decrease in the product temperature during the freezing of sucrose-water solutions (30% w/w). It can also be seen from these results (cf. Table 5.3.4.), that a decrease in the product temperature and increase in the ice volume fraction, leads to an increase in the consistency index of sorbet and therefore to an increase in the magnitude of the apparent viscosity of the product. In view of these results it is

our opinion that this effect is due to two simultaneous phenomena occurring during the freezing of sorbet: firstly, there is a freeze concentration in the content of polysaccharides and sweeteners within the unfrozen phase, increasing the colloidal interparticle forces and leading to the increase in the apparent viscosity of this liquid phase. Secondly, the increase in the volume fraction of the ice crystals suspended in the liquid phase, leads to the increase in hydrodynamic perturbations in the flow field and increases the viscosity of the suspension. Similarly, Cerecero (2003) reported an increase in the viscosity of the product with the increase in the ice volume fraction during the freezing of sucrose-water solutions (30% w/w). Goff et al., (1995) as well as Martin et al. (2008) and Elhweg et al. (2009) reported an increase in the apparent viscosity of ice cream with the decrease in product temperature and the increase in the concentration of ice crystals.

Fig. 5.3.3. presents the apparent viscosity of the product as a function of the shear rate at different draw temperatures and ice volume fractions.

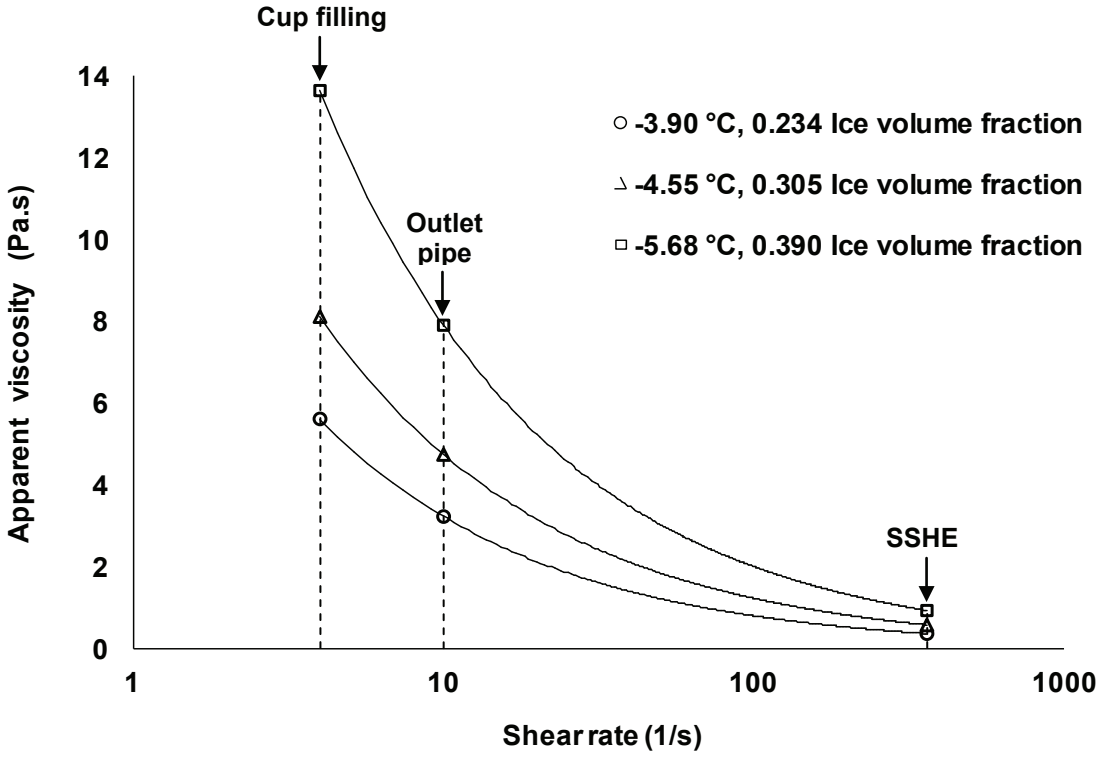


Fig. 5.3.3. Measured apparent viscosity of sorbet at different temperatures, mix flow rate of 0.007 $kg.s^{-1}$ and dasher speed of 78.5 $rad.s^{-1}$ as function of the shear rate.

As previously mentioned, these results can be useful to understand the behaviour of the apparent viscosity of sorbet as it passes through the SSHE, through the outlet pipe of the SSHE and through a cup filling machine. The average shear rate within the SSHE was calculated by Eq. 7 (Leuliet et al., 1986) for a mix flow rate of 0.007 kg.s^{-1} and dasher speed of 78.5 rad.s^{-1}, and determined to be roughly 360 s^{-1}. For this given product flow rate, the shear rate applied within a standard outlet pipe of the SSHE was determined to be roughly 10 s^{-1}, and the shear rate within the cup filling machine was roughly 4s^{-1}. Taking into account this information, it can be seen from Fig. 5.3.3., that the product exhibited the lowest apparent viscosity when it is submitted to higher shear rates, as those applied within the SSHE. Then, when the product flows through the outlet pipe the viscosity of the product is increased. And finally, the highest value of apparent viscosity is reached when the product flows through the cup filling machine, where the product is submitted to the lowest shear rate. This viscosity behaviour throughout the different processing stages is obviously due to the shear-thinning behaviour of sorbet.

3.3. Experimental uncertainty

The estimation of the apparent viscosity is affected by the uncertainties of the parameters R, P and $\dot{V}$ (dR ± 0.02 mm, dP = ± 2% of the measured δP, $d\dot{V}$ ± 8.36x10^{-8} m^3.s^{-1}) which are involved in the relation between the shear stress and the shear rate that determines the apparent viscosity of the product, expressed as:

$$\eta_{app} = \frac{\sigma_w}{\dot{\gamma}_w} = \frac{\frac{(\delta P)D}{4L}}{\left(\frac{3n+1}{4n}\right)\left(\frac{4\dot{V}}{\pi R^3}\right)} \qquad (16)$$

The differential of this equation makes it possible to account the propagation of the uncertainties of the measured variables R, P and $\dot{V}$ into the uncertainty of the estimation of the apparent viscosity η_{app} of the product.

The uncertainty of the estimation of the ice volume fraction $d\phi_{v.ice}$ is principally due to the uncertainty of the temperature of the product T ($dT \pm 0.1$ °C). Therefore, the differential of Eq. 8, makes it possible to account the propagation of the uncertainty of the measured temperature T into the uncertainty of the estimation of the ice volume fraction $d\phi_{v.ice}$.

Fig. 5.3.4. shows apparent viscosity as a function of the ice volume fraction inside the 5 different pipes used in the rheometer for a mix flow rate of 0.007 kg.s^{-1}.

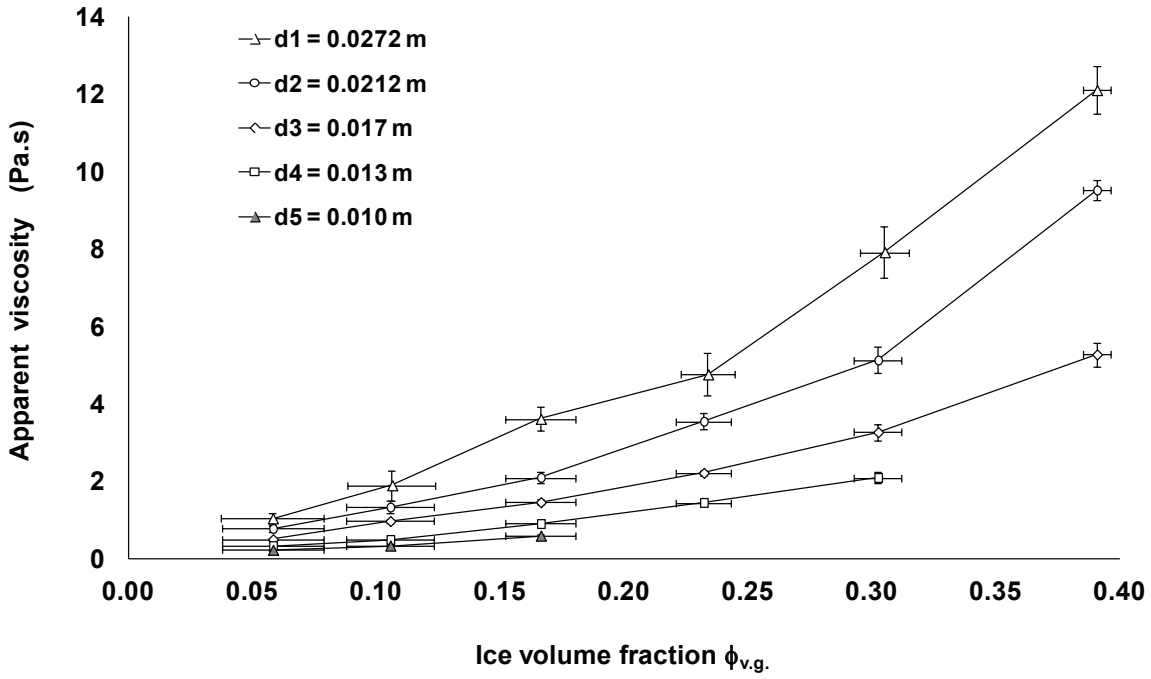


Fig. 5.3.4. Experimental uncertainty of the apparent viscosity of sorbet flowing through pipes of different diameters as a function of the ice volume fraction.

The points represent the mean values for the different replicates. The vertical error bar in Fig. 5.3.4. represents the standard deviation of apparent viscosity due to the variability of pressure drop measurement between the different replicates. This variation of the apparent viscosity measurement is always higher than the calculated uncertainty (not shown); this

result is likely due to the use of a volumetric piston pump which supplies a jerky flow rate and affects the reading of the pressure drop within the liquid column manometers, causing thus a higher measurement error than the accuracy reported by the supplier of the manometers. The horizontal error bar in 5.3.4. represents the calculated uncertainty in the estimation of the ice volume fraction. This uncertainty is higher as the concentration of ice crystals approaches to zero, and thus as the temperature of the product approaches the initial freezing temperature of sorbet at -2.63 °C. This effect is likely due to the accuracy of 0.1 °C of the calibrated Pt100 probe that was used to measured the product temperature, that is to say, when the temperature of the product decreases from -2.63 to -2.73 °C, the concentration of ice crystals increases from 0 to 0.028, thus the propagation of the uncertainty of the product temperature measurement into the calculation of the ice volume fraction is not negligible.

4. Rheological model

As previously mentioned, the rheological properties of sorbet can be adjusted to an empirical expression that can be used to describe the apparent viscosity of the product as a function of the ice volume fraction. In this section, a rheological model is presented which was inspired from Thomas equation (Eq. 2) and predicts the apparent viscosity of sorbet. The parameters of the rheological model were identified by taking only into account the apparent viscosity measurements performed at 0.007 $kg.s^{-1}$.

4.1. Model description

The apparent viscosity of sorbet is affected by the viscosity of the freeze concentrated liquid phase and by the concentration in volume of the ice crystals suspended in the liquid phase. Therefore, the rheological model must take into account the evolution of the viscosity of the liquid phase as the temperature of the mix decreases and as the concentration of solute

increases; and the evolution of the relative viscosity of the sorbet as the ice volume fraction increases. The apparent viscosity of the sorbet mix used in this work was previously studied by Gonzalez (2012). This author expressed the consistency coefficient of the mix as a function of the temperature of the mix T (ranging from -2 to 5 °C, extrapolation to a product temperature of -5.67 °C for this work), and of the concentration of solids w_{ms} (ranging from 0.252 to 0.525), as shown by Eq. 19:

$$k_{mix} = 39.02 \times 10^{-9} \cdot \exp\left(\frac{2242.38}{T + 273.15}\right) \cdot w_{ms}^{2.557} \tag{19}$$

The rheological model must consider as well the evolution of the flow behavior index, from the value of sorbet mix $n_{mix} = 0.553$ at the liquid state, as its decreases sharply at the beginning of the freezing process, and passes through the establishment of a plateau at n= 0.405 with the further decrease in the temperature of the product and the increase in the ice volume fraction $\phi_{v.ice}$. The equation that describes the evolution of the flow behaviour index is written as follows:

$$n = n_{mix}\left[(1-\alpha) + \alpha \exp\left(\frac{-\phi_{v.ice}}{\beta}\right)\right] \tag{20}$$

where the coefficients α and β were identified to be 0.292 and 0.113, respectively, by minimizing the sum of squared errors (SSE) defined in equation 21:

$$SSE = \frac{1}{M}\sum_{1}^{M}\left(n_{measured} - n_{predicted}\right)^2 \tag{21}$$

where *M is* the number of experimental points, $n_{measured}$ is the measured mean value of the flow behaviour index and $n_{predicted}$ the predicted value of the flow behaviour index at a given ice volume fraction.

Fig. 5.3.5. presents the comparison between the experimental and predicted values of the flow behaviour index as a function of the ice volume fraction. It can be seen that the predicted values by Eq. 20 show a reasonably close fit to the experimental means values of the flow behaviour index.

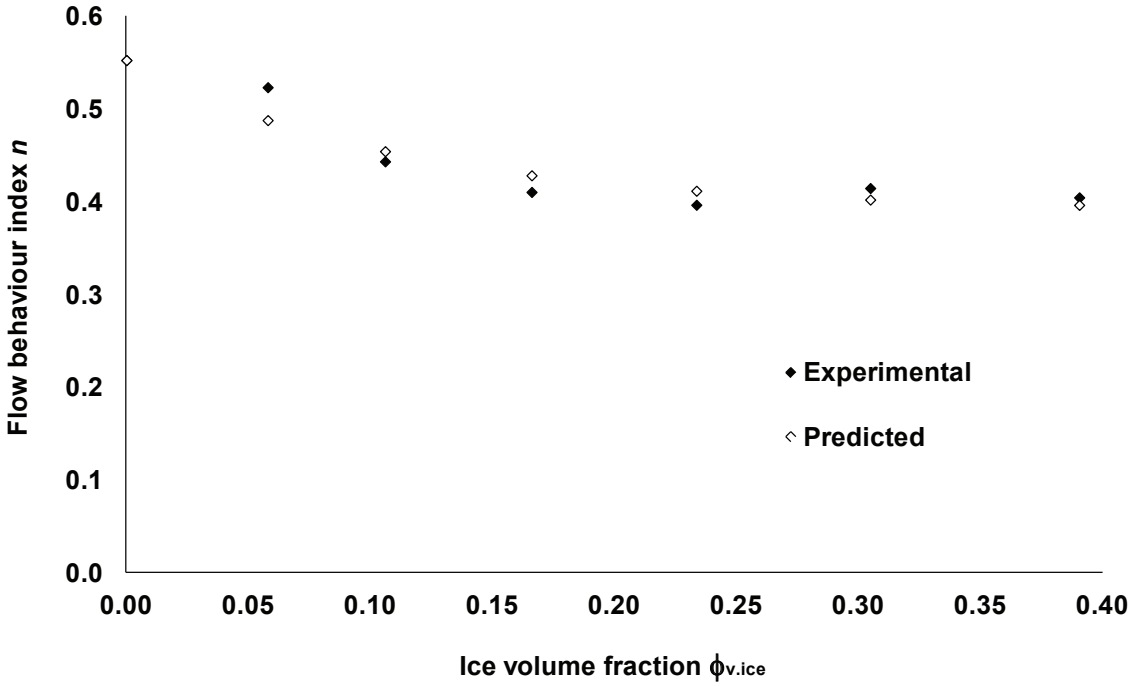


Fig. 5.3.5. Comparison between experimental and predicted values of the flow behaviour index as a function of the ice volume fraction.

Therefore, the rheological model was constructed by taking into account the evolution of the consistency coefficient of the liquid phase k_{mix} (Eq. 19), the evolution of the flow behaviour index n (Eq. 20), and the effect of the increase in the ice volume fraction on the apparent viscosity of sorbet expressed by a modified Thomas equation, as shown in Eq. 22:

$$\eta_{app} = k_{mix} \cdot \left(1 + 2.5\phi_{v.ice} + 10.05\phi_{v.ice}^2 + \chi \exp\{\varsigma \cdot \phi_{v.ice}\}\right) \cdot \dot{\gamma}^{n-1} \quad (22)$$

where the coefficients χ and ς were determined to be 3.319 and 3.421, respectively, by minimizing the sum of squared errors (*SSE*) defined in equation 23:

$$SSE = \frac{1}{M}\sum_{1}^{M}\left(\eta_{app.measured} - \eta_{app.predicted}\right)^2 \quad (23)$$

where M *is* the number of experimental points, $\eta_{app.measured}$ is the experimental apparent viscosity and $\eta_{app.predicted}$ the predicted value of the apparent viscosity for sorbet.

Fig 5.3.6. shows the comparison between the predicted apparent viscosity by the rheological model and the apparent viscosity measured at different product temperatures, different ice volume fractions and different shear rates.

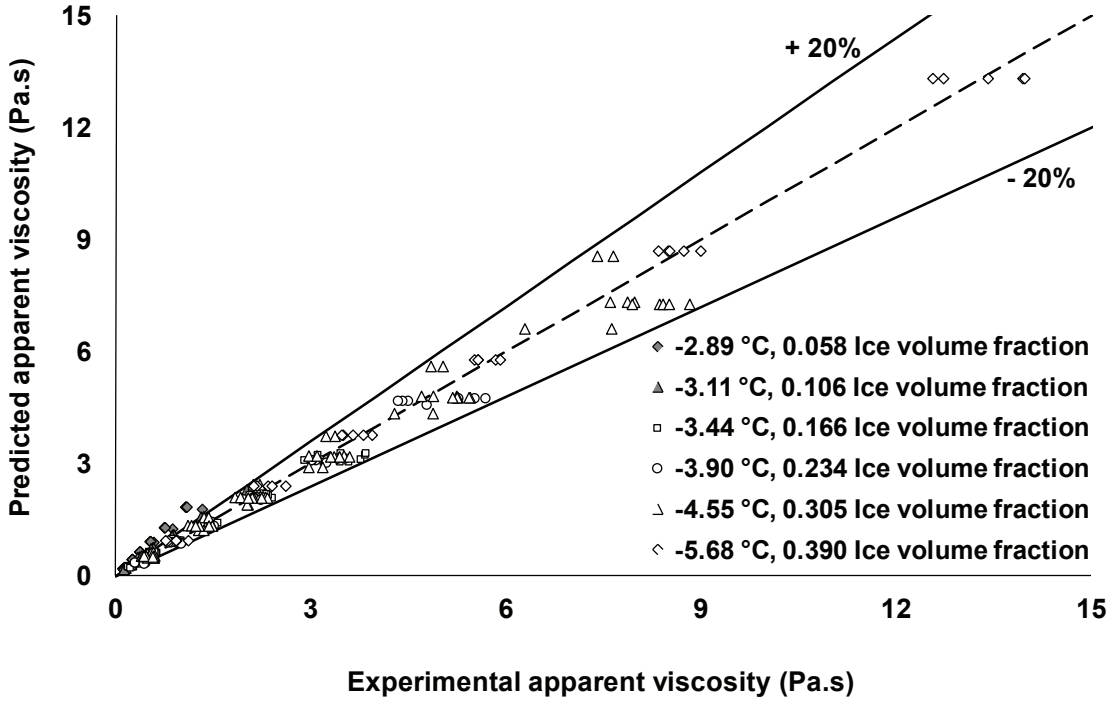


Fig. 5.3.6. Comparison between experimental and predicted values of the apparent viscosity of sorbet at different temperature and different ice volume fractions.

We can observe from these results that rheological model predicts reasonably well the apparent viscosity of the product, although the model prediction of the apparent viscosity at $\phi_{v.ice}$ = 0.058 exceeded the 20% error.

5. Conclusions

This work studied the influence of the temperature of the product and thus of the ice volume fraction on the apparent viscosity of sorbet by pipe rheometry measurements. Experimental data showed that there was no evidence of wall slip behaviour and therefore

wall slip effects were neglected. Results demonstrated that for the set of experimental runs performed, viscous dissipation was negligible.

Experimental results demonstrated that the value of the flow behaviour index decreased sharply from the beginning of the freezing of sorbet until the product reached an ice volume fraction about 17%; subsequently the value of the flow behaviour index remained almost constant forming a plateau with the further decrease of the temperature of the product. The consistency coefficient and therefore the magnitude of the apparent viscosity of sorbet increased with the decrease in the temperature of the product and with the increase in the ice volume fraction. This effect can be explained by two phenomena occurring during the freezing of sorbet: firstly, below the freezing point of sorbet mix, a decrease in the temperature of the product leads to the freeze-concentration of the content of polysaccharides and sweeteners within the liquid phase, the effect of which increased the colloidal forces between particles and increases the apparent viscosity of the unfrozen liquid phase. Secondly, an increase in the ice volume fraction leads to an increase in the hydrodynamic forces between the ice crystals and the surrounding fluid, increasing the apparent viscosity of the suspension of ice crystals.

An empirical rheological model to predict the apparent viscosity of sorbet was presented, the empirical correlation was constructed by taking into the evolution of the apparent viscosity of the unfrozen liquid phase as a function of the product temperature and solute concentration, the evolution of the flow behaviour index as a function of the ice volume fraction, and the effect of the ice volume fraction on the apparent viscosity of the product. The rheological model predicted reasonably well the apparent viscosity of the product.

The results obtained in this work can be useful to improve the control of the quality of frozen desserts and for the improvement of the design of piping systems and the mathematical modelling of the freezing process in SSHEs.

Acknowledgments

The authors gratefully acknowledge the financial support granted by the European Community Seventh Framework through the CAFÉ project (Computer Aided Food processes for control Engineering) Project number 212754.

Abbreviations

DRS – Dasher Rotational Speed

MFR – Mix Flow Rate

SSE – Sum of Squared Errors

SSHE – Scraped Surface Heat Exchanger

TR22 – Evaporation Temperature of r22

Nomenclature

k	consistency coefficient of sorbet, $Pa.s^n$
k_{mix}	consistency coefficient for sorbet mix, $Pa.s^n$
n	flow behaviour index index, -
nL	number of scraping blades, -
L	pipe length, m
R	pipe radius, m
N_R	rotational speed of scraping blades, $rad.s^{-1}$
δP	pressure drop, Pa
$\dot{V}$	volumetric flow rate, $m^{3.}s^{-1}$
T	temperature of the product, °C
w_{ms}	initial mass fraction of solute (sweetener content), -
$w_{ms.i}$	initial mass fraction of solute (sweetener content), -
$w_{ms.f}$	final mass fraction of solute (sweetener content), -

Greek symbols

$\dot{\gamma}$	shear rate, s^{-1}
$\dot{\gamma}_w$	wall shear rate, s^{-1}
σ_w	wall shear stress, Pa
λ_w	thermal conductivity of the solute solution, $W.m^{-1}.K^{-1}$
λ_{ice}	thermal conductivity of ice, $W.m^{-1}.K^{-1}$
λ_{sorbet}	thermal conductivity of sorbet, $W.m^{-1}.K^{-1}$
η_{app}	apparent viscosity, Pa.s

η viscosity of a Newtonian suspension, Pa.s

η_l viscosity of the liquid phase of a suspension, Pa.s

ρ_i ice density, kg.m^{-3}, -

ρ_s sorbet density, kg.m^{-3}, -

ϕ particle concentration, -

$\phi_{m.ice}$ ice mass fraction, -

$\phi_{v.ice}$ ice volume fraction, -

ξ thermal sensibility, K^{-1}

References

Adhikari, B., Jindal V. (2001). Fluid flow characterization with tube viscometer data. *Journal of Food Engineering.* 50. 229-234.

Ayel, V., Lottin, O., Peerhossaini, H. (2003). Rheology, flow behaviour and heat transfer of ice slurries: a review of the state of the art. *International Journal of Refrigeration*. 26: 95–107.

Balmforth, N., Craster, R., Perona, P., Rust, A., Sassi, R. (2007). Viscoplastic dam breaks and the Bostwick consistometer. *Journal of Non-Newtonian Fluid Mechanics.*142:63-78.

Baloh T. (1967). Some diagrams for aqueous sugar solutions. *Zucker.* 20: 668-679.

Batchelor, G. K. (1977). The effect of Brownian motion on the bulk stress in a suspension of spherical particles. *Journal of Fluid Mechanics*. 83: 97-117.

Burns, I. and Russell A. (1999). Process rheology of ice-cream. In ZDS Inter-Ice, Solingen.

Cerecero, R. (2003). *Etude des écoulements et de transferts thermiques lors de la fabrication d'un sorbet à l'échelle du pilote et du laboratoire.* PhD Thesis. INA-PG, Paris, France.

Cook, K. L. K. and Hartel, R. W. (2010). Mechanisms of Ice Crystallization in Ice Cream Production. *Comprehensive Reviews in Food Science and Food Safety,* 9 (2), 213-222.

Einstein, A. (1906). Investigations on the theory of Brownian motion. *Annalen der Physik*. 19: 289-306.

Elhweg, B., Burns, I., Chew, Y., Martin, P., Russell, A., Wilson, D. (2009). Viscous dissipation and apparent wall slip in capillary rheometry of ice cream. *Food and Bioproducts Processing.* 87: 266-272.

Goff, H. D., Freslon, B., Sahagian, M. E., Hauber, T. D., Stone, A. P., Stanley, D. W. (1995). Structural development in ice cream - Dynamic rheological measurements. *Journal of Texture Studies,* 26 (5), 517-536.

Gonzalez, E. (2012). *Contribution au contrôle par la modélisation d'un procédé de cristallisation en continu.* PhD Thesis. AgroParisTech, Paris, France.

Haddad, A. (2009). *Couplage entre écoulements, transferts thermiques et transformation lors du changement de phase d'un produit alimentaire liquide complexe - Application à la maîtrise de la texture.* PhD Thesis. AgroParisTech, Paris, France.

Hansen TM, Kauffeld M. (2000). Viscosity of ice-slurry. 2nd Workshop on ice-slurries, *International Institute of Refrigeration.*

Judy, J., Maynes, D., Webb B.W. (2002). Characterization of frictional pressure drop for liquid flows through microchannels. *International Journal of Heat and Mass Transfer,* 45: 3477–3489.

Krieger, I.M. and Dougherty, T.J. (1959). A mechanism for non-Newtonian flow in suspension of rigid spheres. *Transactions of the Society of Rheology*. 3: 137-152.

Leuillet, J. C., Maingonnait, J. F., Corrieu, G. (1986). Etude de la perte de charge dans un échangeur de chaleur a surface raclée traitant des produits newtoniens et non-newtoniens. *Journal of Food Engineering*. 5: 153-176.

Levy, F. L. (1982). Calculating the thermal conductivity of meat and fish in the freezing range. *Internation Journal of Refrigeration*. 5 (3):149–154.

Macosko, C.W. (1994). Rheology, Principles, Measurements and Applications. New York: VCH Publishers Inc. 550 p.

Marshall, R. T., Goff, H. D., Hartel R. W. (2003). Ice cream. 6th Ed. New York: Klumer Academic/Plenum Publishers. 371 p.

Martin, P., Wilson, D. (2005). A critical assessment of the Jastrzebski interface conditions for the capillary flow of pastes, foams and polymers. *Chemical Engineering Science*. 60: 493-502.

Martin, P., Odic, K., Russell, A., Burns, I., Wilson, D. (2008). Rheology of commercial and model ice creams. Applied Rheology. 18(1), 12913-1:11

Maxwell, J. C. (1954). A Treatise on Electricity and Magnetism. 4th Ed. New York: Dover Publications Inc.

Mooney M. (1931). Explicit formulas for slip and fluidity. *Journal of Rheology*. 2: 210-222.

Mooney M. (1951). The viscosity of a concentrated suspension of spherical particles. *Journal of Colloid Science*. 6: 162-170.

Steffe, J. F. (1996). Tube Viscometry. Rheological methods in Food Process Engineering. East lansing, MI, USA: F. Press. p. 94 -156.

Thomas, D. G. (1965). Transport characteristics of suspension: VIII. A note on the viscosity of newtonian suspensions of uniform spherical particles. *Journal of Colloid Science*. 20: 267-277.

Wildmoser, H., Scheiwiller, J., Windhab, E.J., 2004, Impact of disperse microstructure on rheology and quality aspects of ice cream. *Lebensmittel-Wissenschaft & Technologie*, 37(8): 881–891.

Winter, H. (1977). Viscous dissipation in shear flows of molten polymers. *Advances in Heat Transfer*. 13:205-267

Yarin, L. P., Mosyak, A., Hetsrony, G. (2009). Fluid Flow, Heat Transfer and Boiling in Micro Channels. Berlin: Springer Publishers.

5.4. Influence of ice and air volume fractions on the rheological properties of sorbet.

Marcela Arellano[a,b,c,d], Hayat Benkhelifa[b,c,d], Denis Flick[b,c,d], Graciela Alvarez[a,5].

[a]*Irstea. UR Génie des Procédés Frigorifiques. 1 rue Pierre-Gilles de Gennes CS 10030, 92761 Antony Cedex, France*

[b]*AgroParisTech. UMR 1145 Ingénierie Procédés Aliments. 16 rue Claude Bernard, 75231 Paris Cedex 05, France*

[c]*INRA.UMR 1145 Ingénierie Procédés Aliments. 1 avenue des Olympiades, 91744 Massy Cedex, France*

[d]*CNAM. UMR 1145 Ingénierie Procédés Aliments. 292 rue Saint-Martin, 75141 Paris Cedex 03, France*

Abstract

Sorbet is a complex food consisting of a frozen structure, containing air bubbles, ice crystals and a freeze concentrated liquid phase. The rheology of sorbet is strongly related to microstructure features, such as the dispersion of the air bubbles and ice crystals in the continuous liquid phase. In this work, the rheological properties of sorbet have been studied in situ by means of a pipe rheometer connected at the exit of a scraped surface heat exchanger. This work aimed at studying separately the influence of the ice volume fraction ($\phi_{v.ice}$.) on the increase in the apparent viscosity (η_{app}) of a non aerated frozen sorbet, and the influence of the air volume fraction ($\phi_{v.a.}$.) on the increase in η_{app} of an aerated frozen sorbet. The rheometer was composed of a serie of PVC pipes of different diameters, making it possible to apply a range of apparent shear rate from 4 to 430 s^{-1}. Results showed that in the non aerated frozen sorbet, an increase in $\phi_{v.ice}$. of 23% led to an increase in η_{app} that represents 20 times the viscosity of the non frozen sorbet mix at $\dot{\gamma}$=10s^{-1}. For this given $\phi_{v.ice}$, an increase in $\phi_{v.a.}$ of 50% led to an increase in η_{app} of the aerated frozen sorbet that represents 3 times the viscosity of the non aerated frozen sorbet. This indicates that the influence of $\phi_{v.ice}$ on the increase in η_{app} of the product is predominant, with respect to the effect of $\phi_{v.a.}$. These results can be used as quantitative indicators of sorbet microstructure, which is highly related to the quality attributes of the product.

Key words: Apparent viscosity; Pipe rheometry; Ice volume fraction; Air volume fraction; Freezing; Scraped surface heat exchanger.

5 Corresponding author. Tel.: +33 140 96 60 17; Fax: +33 140 96 60 75.
E-mail address: graciela.alvarez@irstea.fr

1. Introduction

The rheological properties of sorbet are determined by the changes in the microstructure of its components during the manufacturing of the product. During the initial freezing in a scraped surface heat exchanger (SSHE), the formation and dispersion of the ice crystals, together with the freeze-concentration of the continuous liquid phase, lead to the increase of the apparent viscosity of the product. Simultaneously, the injection and dispersion of small air bubbles, which is achieved by the shear stress provided by the rotation of the dasher, leads to the increase in the volume of the aerated sorbet and to another increase in the apparent viscosity of the product. The stability of the air bubbles in the sorbet is achieved thanks to the polysaccharides contained in the liquid phase and to the dispersion of the ice crystals, which separate the air bubbles and prevent their coalescence (Clarke, 2004; Sofjan and Hartel, 2004).

The development of an adequate viscosity of high quality sorbet requires a good control of the incorporation of air and the formation of the ice crystals during the freezing process. A number of studies in the literature, based on oscillatory rheometry for the analysis of the viscosity of hardened ice cream at different temperatures, demonstrated the viscoelastic Non-Newtonian shear-thinning behaviour of the product (Goff et al. 1995; Wildmoser et al., 2004). More recently, Martin et al. (2008) and Elhweg et al., (2009) have reported apparent viscosity measurements carried out by means of a pipe rheometer connected at the exit of the SSHE. These authors reported also the shear-thinning behaviour of ice cream, and an increase in the apparent viscosity with the decrease in the temperature of the product. However, there is little information available on the effects of the air volume fraction on the apparent viscosity of the product as it flows out directly from the SSHE.

In this work, the rheological properties of sorbet have been studied in situ by means of a pipe rheometer connected directly at the exit of a SSHE. This work aimed at studying

separately the influence of the ice volume fraction ($\phi_{v.ice}$) on the increase in the apparent viscosity (η_{app}) of a non aerated frozen sorbet, and the influence of the air volume fraction ($\phi_{v.a.}$) on the increase in η_{app} of an aerated frozen sorbet.

2. Materials and methods

2.1. Sorbet freezing and operating conditions

The working fluid used in these experiments was an ultra high temperature pasteurized lemon sorbet mix (14.6% w/w sucrose, 8% w/w fructose, 0.09% w/w dextrose, 3% w/w lemon juice concentrate 60 Brix, 0.5% w/w locust bean gum / guar gum / hypromellose stabiliser blend). The mix was stored at 5 °C for 24 h prior to use. Freezing of the mix was carried out in a laboratory scale continuous pilot SSHE (WCB® Model MF 50). A schematic representation of the experimental platform is shown in Fig. 5.4.1.

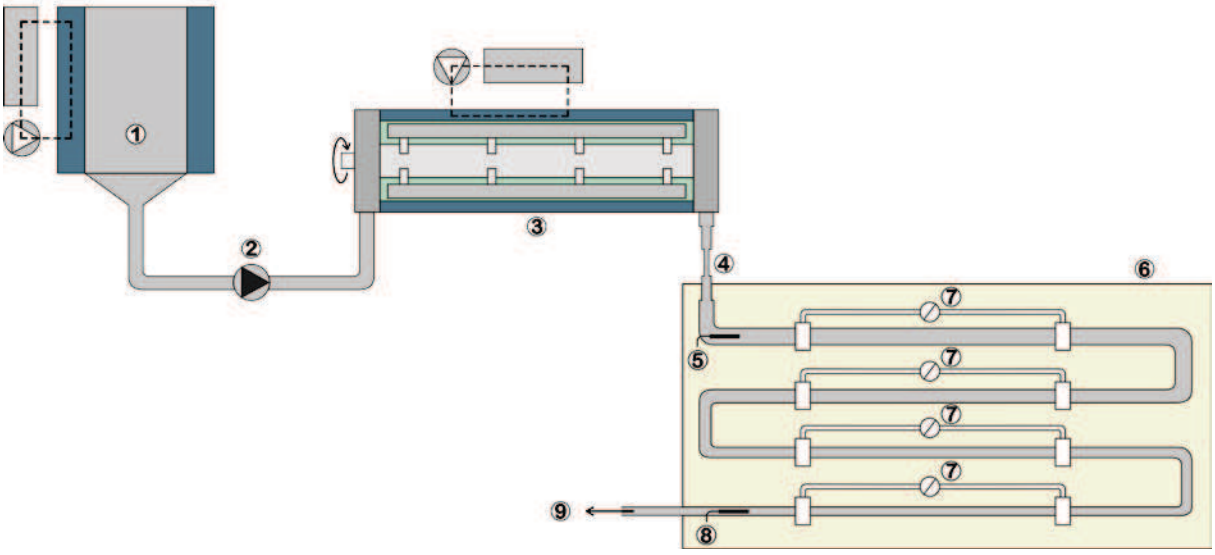


Fig. 5.4.1. Schematic representation of the experimental platform. 1. Refrigerated storage tank (200 l capacity). 2. Volumetric piston pump. 3. Freezer. 4. Contraction/enlargement pipe. 5. Pt100 probe inserted into the inlet of the rheometer. 6. Pipe rheometer. 7. Pressure manometers. 8. Pt100 probe inserted into the outlet of the rheometer. 9. Product exit.

The product flow rate was fixed at 0.007 $kg.s^{-1}$. The mix flow rate was determined by weighing the product exit stream during a given period of time. The accuracy of this measurement was determined to be $\pm 9.2 \times 10^{-5}$ $kg.s^{-1}$. The dasher speed of the freezer was fixed

at 78.5 rad.s^{-1} (750 rpm). The dasher speed was measured by means of a photoelectric tachometer (Ahlborn®, type FUA9192) with an accuracy of ±0.105 rad.s^{-1} (1 rpm). The draw (exit) temperature of sorbet was varied by adjusting the refrigerant fluid temperature (r22, chlorodifluoromethane) evaporating in the cooling jacket of the SSHE. A calibrated type T (copper - constantan) thermocouple with an accuracy of ±0.2 °C was fixed with conductive aluminium tape on the external surface wall of the cooling jacket, so as to measure the evaporation temperature of the refrigerant fluid. The exterior of the exchanger jacket was insulated with 2 cm thick polystyrene foam insulation in order to reduce heat loss.

The rheological measurements of the non-aerated sorbet were carried out without the incorporation of air. For the rheological measurements of the aerated sorbet, air was added at the inlet of the SSHE so as to obtain different overruns (25%, 50%, and 100%). The control of the overrun was carried out by means of weight measurement of unfrozen sorbet mix and frozen sorbet of a constant volume. The percentage of overrun was calculated as the ratio between the increase in volume due to the incorporation of air V_{air} (at atmospheric pressure) to the initial volume of mix V_{mix}, written as follows:

$$Overrun = \frac{V_{air}}{V_{mix}} \times 100 \qquad (1)$$

The volume fraction of air $\phi_{v.a.}$ was calculated as the ratio between the volume occupied by the air V_{air} and the total volume of the aerated product V_{Total}, given by:

$$\phi_{v.a.} = \frac{V_{air}}{V_{mix} + V_{air}} = \frac{V_{air}}{V_{Total}} \qquad (2)$$

The operating conditions under which the rheological measurements were carried out are given in Table 5.4.1.

2.2. Pipe rheometry measurements

Frozen sorbet was pumped from the SSHE, first, into a contraction/enlargement pipe, and then into an instrumented pipe rheometer (cf. Fig. 5.4.1.). The contraction/enlargement pipe was composed of 5 pipes in copper plumbing of 0.10 m length each and of different internal diameters ($d_{1c/e}$=0.025m; $d_{2c/e}$=0.0157m; $d_{3c/e}$=0.0094m; $d_{4c/e}$=0.0157m; $d_{5c/e}$=0.025m). This contraction/enlargement pipe was used to pre-shear the sorbet before it entered into the pipe rheometer, so as to prevent any thixotropic behaviour and to obtain repeatable measurements. The rheometer was composed of sets of 4 pipes in clear polyvinyl chloride (PVC) of different internal diameters (d_1=0.0272m, d_2=0.0212m, d_3=0.0167m, d_4=0.013m, d_5=0.01m, d_6=0.0058m) connected in series, making it possible to apply an apparent shear rate range of $4 < \dot{\gamma}_w < 430$ s^{-1}. All pipes were insulated with polystyrene foam insulation of 2 cm thickness in order to reduce heat loss. Since the apparent viscosity of sorbet increases with the decrease of the temperature of the product and thus with the increase of the ice volume fraction ($\phi_{v.ice.}$), the use of all the pipes was not possible for all experimental conditions. Therefore, the pipes of diameters d_1 to d_6 were used for measurements of sorbets with $\phi_{v.ice.}$ of 0.058 and 0.106, diameters d_1 to d_5 for sorbet with $\phi_{v.ice.}$ of 0.166, diameters d_1 to d_4 for $\phi_{v.ice.}$ of 0.234. The rheological measurements for aerated sorbet with $\phi_{v.ice.}$ of 0.234 were carried out by using the pipes of diameters d_1 to d_3.

Two piezometric rings, located at the measuring points of each pipe, made it possible to measure a pressure drop within each pipe for a length of 0.5 m. Pressure drop measurements were performed by liquid column manometers with an accuracy of ± 2% of the measured value. The draw temperature of sorbet was measured as it flowed through the pipes of the rheometer by means of calibrated Pt100 probes (accuracy of ±0.1 °C) located in the centre of the inlet and outlet pipes of the rheometer (cf. Fig. 5.4.1.). Thermal steady state in the pipe rheometer was

achieved by pumping sorbet into it, until the measured temperatures at the inlet and outlet of the rheometer were brought to the desired experimental draw temperature.

2.2.1. Apparent viscosity calculations

The shear stress was calculated from pressure drop measurements as follows:

$$\sigma_w = \frac{(\delta P)R}{2L} \tag{3}$$

where δP is the pressure drop measured over a fixed length L of a horizontal pipe, and R the inner radius of the pipe.

For a power law fluid, the shear rate $\dot{\gamma}_w$ can be determined by:

$$\dot{\gamma}_w = \left(\frac{3n+1}{4n}\right)\left(\frac{4\dot{V}}{\pi R^3}\right) \tag{4}$$

with $n = d\left(ln\left(\delta P\, R/2L\right)\right)/d\left(ln\left(4\dot{V}/\pi R^3\right)\right)$. For each draw temperature, n is calculated by taking into account data from all repetitions performed at a the same operating condition.

A regression analysis of (σ_w) versus $(\dot{\gamma}_w)$ to fit a power law model was used to characterize the apparent viscosity of non-Newtonians shear-thinning fluids, such as sorbet:

$$\eta_{app} = k \cdot \dot{\gamma}_w^{n-1} \tag{5}$$

where n is the flow behaviour index, $\dot{\gamma}_w$ the shear rate and k is the consistency index.

2.3. Ice volume fraction calculations

Assuming the thermodynamic equilibrium between ice and the solution of solute (sweeteners content), the ice mass fraction in sorbet $\phi_{m.ice.}$ (kg of ice / kg of sorbet) can be determined from the freezing point curve of sorbet mix, which is a function of the mass fraction of solute w_{ms} in the residual liquid phase. This curve was previously determined by means of differential scanning calorimetric (DSC) measurements, as reported by Gonzalez

(2012). The expression that characterizes the freezing point curve and links the solute mass fraction to the equilibrium temperature is given by the following equation:

$$w_{ms} = \left(-0.137T - 0.0202T^2 - 0.00167T^3 - 0.0000529T^4\right), \text{ with T in °C} \quad (6)$$

According to a mass balance of solute (sweetener content), the solute is present in sorbet mix at a certain initial mass fraction ($w_{ms.i}$). Then the solute is concentrated as the freezing of sorbet occurs, until it reaches a final mass fraction ($w_{ms.f}$) in the liquid phase. The final liquid phase represents only a fraction $\left(1-\phi_{m.ice.}\right)$ of sorbet, hence the ice mass fraction can be calculated by the following equation:

$$w_{ms.i} = \left(1-\phi_{m.ice.}\right)\cdot w_{ms.f}\left(T\right) \Leftrightarrow \phi_{m.ice.} = 1 - \frac{w_{ms.i}}{w_{ms.f}\left(T\right)}, \quad (7)$$

The ice volume fraction (m^3 of ice / m^3 of sorbet) is then determined as follows:

$$\phi_{v.ice} = \frac{\rho_s}{\rho_i}\phi_{m.ice}, \quad (8)$$

where ρ_s is the density of sorbet and ρ_i the density of ice.

Once the experimental conditions of the SSHE were set and the thermal steady state of the system was attained, the draw temperature of the product and ice volume fraction data were recorded and calculated every 5 seconds by using a program written in LabVIEW®.

3. Results and discussion

3.1. Influence of ice and air volume fraction on the flow behaviour index

Table 5.4.1. shows the thermal and rheological properties for sorbet mix, non aerated frozen sorbet and aerated frozen sorbet. It can be seen from results in Table 5.4.1. (comparison between points 5 to 8, $\phi_{v.ice} = 0.23$) that when the amount of air incorporated into the product is increased, it is necessary to decrease the temperature of the refrigerant fluid, so

as to obtain the same temperature of the product and therefore the same ice volume fraction. This effect is likely due to the insulating nature of the air bubbles that reduce the heat transfer rate between the wall of the SSHE and the product.

Table 5.4.1. Operating conditions and experimental data obtained during the rheology measurements for non aerated sorbet and for aerated sorbet, produced at a flow rate of 0.007 $kg.s^{-1}$ and dasher rotational speed of 78.5 $rad.s^{-1}$.

Rheological measurement for sorbet mix and frozen sorbet without aeration									
	Operating conditions			Product characteristics			Rheological properties		
Run	TR22[a] (°C)	Overrun %	$\phi_{v.a}$	T Inlet (°C)	T outlet (°C)	$\phi_{v.ice}$	n	k (Pa.s)	η_{app} at $\dot{\gamma}_w = 10\ s^{-1}$
1*	-	-	-	5.03	5.03	-	0.553	0.455	0.163
2**	-7.20	-	-	-2.89	-2.89	0.058	0.524	1.993	0.663
3**	-8.26	-	-	-3.11	-3.10	0.11	0.444	4.186	1.163
4**	-9.40	-	-	-3.44	-3.43	0.17	0.411	7.862	2.025
5**	-10.79	-	-	-3.90	-3.89	0.23	0.397	12.969	3.235
Rheological measurement for aerated frozen sorbet									
	Operating conditions			Product characteristics			Rheological properties		
	TR22[a] (°C)	Overrun %	$\phi_{v.a}$	T Inlet (°C)	T outlet (°C)	$\phi_{v.ice}$	n	k (Pa.s)	η_{app} at $\dot{\gamma}_w = 10\ s^{-1}$
6*	-11.09	25	0.2	-3.89	-3.89	0.23	0.312	21.242	4.355
7*	-11.31	50	0.34	-3.91	-3.91	0.23	0.269	28.854	5.359
8*	-11.53	100	0.5	-3.92	-3.92	0.23	0.257	47.644	8.605

[a] TR22 = evaporation temperature of r22; $\phi_{v.ice}$ = air volume fraction; T Inlet = product temperature at the inlet of the pipe rheometer; T Outlet = product temperature at the outlet of the pipe rheometer; $\phi_{v.ice}$ = Ice volume fraction; n = flow behaviour index; k = consistency index; $\dot{\gamma}_w$ = wall shear rate.
*Values are means of two replicates. **Values are means of three replicates.

Fig. 5.4.2. shows the flow behaviour curves for sorbet mix, non aerated frozen sorbet and aerated frozen sorbet. From results in Table 5.4.1. (runs 1 to 5) and Fig. 5.4.2.(A) we can observe that the flow behaviour index decreases with the decrease in the temperature of the product and therefore with the increase in the ice volume fraction, which indicates that sorbet becomes more shear-thinning with the increase in the ice volume fraction. From results in Table 5.4.1. (run 5 to 8) and Fig. 5.4.2.(B) we can observe that for the given ice volume fraction ($\phi_{v.ice}$ = 0.23), the flow behaviour index of the aerated sorbet decreases further with the increase in the air volume fraction, which indicates that the aerated sorbet becomes more shear-thinning when there is more air incorporated into the product.

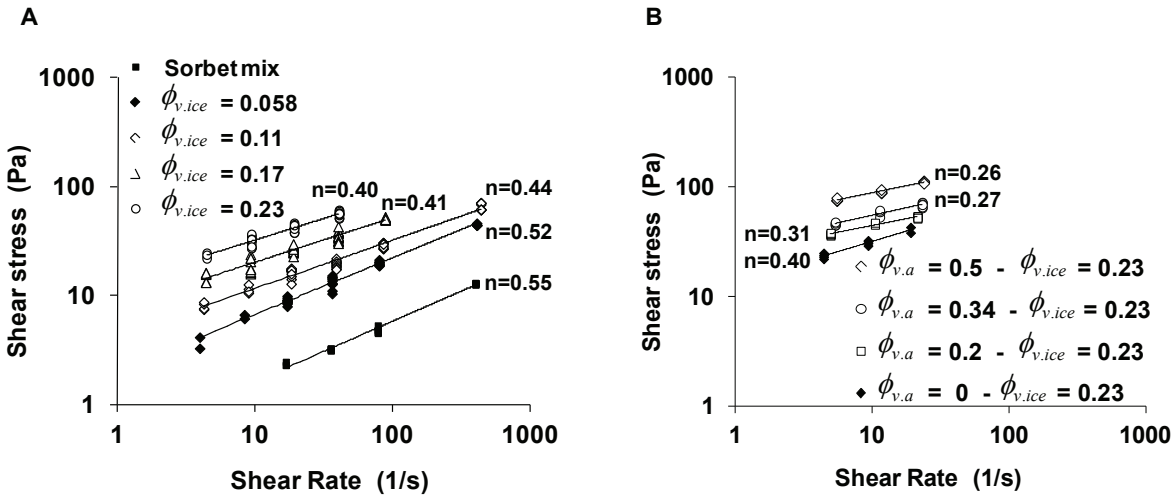


Fig. 5.4.2. (A) Flow behaviour of sorbet mix and frozen sorbet as a function of the ice volume fraction at mix flow rate of 0.007 kg.s^{-1} and rotational speed of 78.5 rad.s^{-1}. (B) Flow behaviour of sorbet at -3.9 °C ($\phi_{v.ice}$ = 0.23) as a function of the air volume fraction ($\phi_{v.a}$) at mix flow rate of 0.007 kg.s^{-1} and rotational speed of 78.5 rad.s^{-1}.

3.2. Influence of ice and air volume fractions on the apparent viscosity

Fig. 5.4.3. shows the evolution of the apparent viscosity for sorbet mix, non-aerated frozen sorbet and aerated frozen sorbet at $\dot{\gamma}$ = 10s^{-1}. We can observe in Fig. 5.4.3. (A), for the non-aerated frozen sorbet, that an increase in ice volume fraction of 23% led to an increase in the apparent viscosity of the frozen sorbet that represents roughly 20 times the viscosity of the sorbet mix. This effect can be explained by two phenomena occurring during the freezing of sorbet: firstly, below the freezing point of sorbet mix, a decrease in the temperature of the product leads to the freeze-concentration in the content of polysaccharides and sweeteners within the liquid phase, the effect of which increases the colloidal forces between particles and increases the apparent viscosity of the unfrozen liquid phase. Secondly, an increase in the ice volume fraction leads to an increase in the hydrodynamic forces between the ice crystals and the surrounding fluid, leading to alterations in the flow field and thus to an increase in the apparent viscosity of the product.

It can also be seen in Fig. 5.3.3. (B), for the aerated frozen sorbet, at this given ice volume fraction ($\phi_{v.ice}$ = 0.23), that an increase in the amount of air incorporated in sorbet of 50% led to an increase in the apparent viscosity of the aerated sorbet that represents roughly

3 times the apparent viscosity of the non-aerated frozen sorbet. The fact that the presence of 50% of air bubbles has less influence on η_{app} than the presence of 23% of ice crystals can be explained by the easier deformation that the air bubbles can undergo when the product flows and is sheared in a pipe, in comparison to the rigid ice crystals which are less deformable. The easy deformation of the air bubble would lead to less strong hydrodynamic alterations in the flow field, and would increase to a minor extent the viscosity of the product, in comparison to the effect that the ice volume fraction has on the apparent viscosity of the product. This effect indicates thus that the influence of the ice volume fraction on the increase in the apparent viscosity of the product is predominant, with respect to the effect of the air volume fraction.

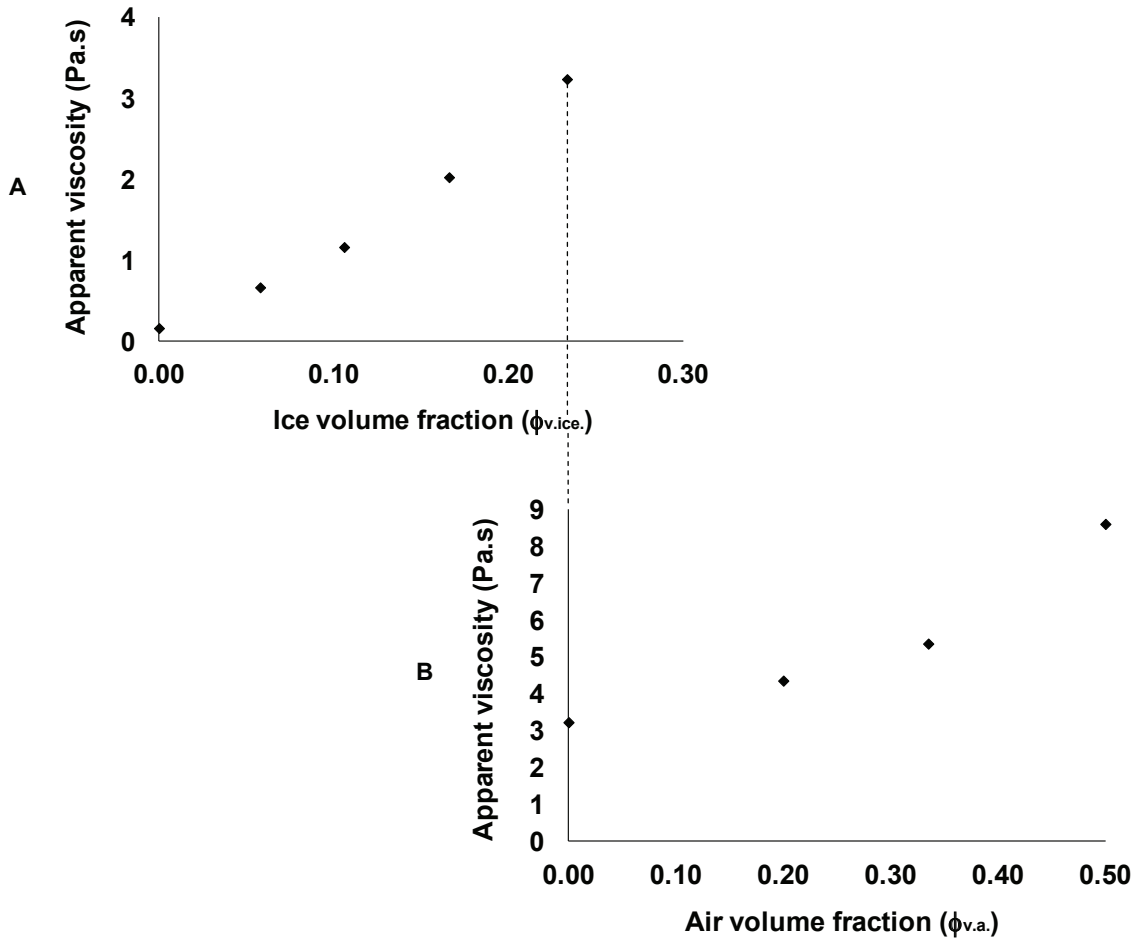


Fig. 5.4. 3. (A) Apparent viscosity of sorbet mix and frozen at $10s^{-1}$
as a function of ice volume fraction at mix flow rate of 0.007 $kg.s^{-1}$ and rotational speed of 78.5 $rad.s^{-1}$.
(B) Apparent viscosity of aerated frozen sorbet at $10s^{-1}$, as a function of air volume fraction $\phi_{v.a}$,
at $\phi_{v.ice}$ of 0.23, mix flow rate of 0.007 $kg.s^{-1}$ and rotational speed of 78.5 $rad.s^{-1}$

4. Conclusions

This work studied separately the influence of the ice volume fraction on the apparent viscosity of a non-aerated frozen sorbet, and the influence of the air volume fraction on the apparent viscosity of an aerated frozen sorbet, by means of a pipe rheometer. Experimental data showed that an increase in the ice volume fraction lead to an increase of the apparent viscosity of the non-aerated frozen sorbet, due in one hand to the freeze concentration in the content of polysaccharides and sweeteners in the liquid phase, and on the other hand to the increase in the volume fraction of the ice crystals.

An increase in air volume fraction resulted in the decrease of the flow behaviour index, which indicated that aerated sorbet becomes more shear-thinning as more air is incorporated into the product. An increase in air volume fraction resulted in a higher product apparent viscosity.

Results also demonstrated that the influence of the ice volume fraction $\phi_{v.ice}$ on the increase in the apparent viscosity of the product is predominant, with respect to the effect of air volume fraction $\phi_{v.a.}$, the effect of which was likely due to the fact that the air bubbles are more easily deformable as compared to the rigid and less deformable ice crystals.

The results obtained in this work can be useful to improve the control of the incorporation of air and the amount of ice crystals formed during the freezing process of sorbet, so as to obtain a better control of the quality of frozen desserts.

Acknowledgments

The authors gratefully acknowledge the financial support granted by the European Community Seventh Framework through the CAFÉ project (Computer Aided Food processes for control Engineering) Project number 212754.

Nomenclature

k consistency coefficient of sorbet, $Pa.s^n$

n flow behaviour index index, -

L pipe length, m

R pipe radius, m

δP pressure drop, Pa

$\dot{V}$ volumetric flow rate, $m^3.s^{-1}$

T temperature of the product, °C

w_{ms} mass fraction of solute (sweetener content) in the liquid phase, -

$w_{ms.i}$ initial mass fraction of solute (sweetener content), -

$w_{ms.f}$ final mass fraction of solute (sweetener content) in the liquid phase, -

Greek symbols

$\dot{\gamma}_w$ wall shear rate, s^{-1}

σ_w wall shear stress, Pa

η_{app} apparent viscosity, Pa.s

ρ_i ice density, $kg.m^{-3}$, -

$\phi_{m.ice}$ ice mass fraction, -

$\phi_{v.ice}$ ice volume fraction, -

References

Clarke, C. (2004). The science of ice cream. 2nd edition. UK. Royal Society of Chemistry.

Elhweg, B., Burns, I., Chew, Y., Martin, P., Russell, A., Wilson, D. (2009). Viscous dissipation and apparent wall slip in capillary rheometry f ice cream. *Food and Bioproducts Processing*. 87: 266-272.

Goff, H. D., Freslon, B., Sahagian, M. E., Hauber, T. D., Stone, A. P., Stanley, D. W. (1995). Structural development in ice cream - Dynamic rheological measurements. *Journal of Texture Studies*, 26 (5), 517-536.

Gonzalez, E. (2012). Contribution au contrôle par la modélisation d'un procédé de cristallisation en continu. *PhD Thesis*. AgroParisTech, Paris, France.

Martin, P., Odic, K., Russell, A., Burns, I., Wilson, D. (2008). Rheology of commercial and model ice creams. *Applied Rheology*. 18(1), 12913-1:11.

Sofjan, R., and Hartel, R. W. (2004). Effects of overrun on structural and physical characteristics of ice cream. *International Dairy Journal*, 14(3), 255-262.

Wildmoser, H., Scheiwiller, J. and Windhab, E.J. (2004). Impact of disperse microstructure on rheology and quality aspects of ice cream. *Lebensmittel-Wissenschaft & Technologie*, 37(8): 881–891.

5.5. Coupling population balance and residence time distribution for the ice crystallization modelling in a scraped surface heat exchanger.

Marcela Arellano[a,b,c,d], Hayat Benkhelifa[b,c,d,6], Graciela Alvarez[a], Denis Flick[b,c,d].

[a]*Irstea. UR Génie des Procédés Frigorifiques. 1 rue Pierre-Gilles de Gennes CS 10030, 92761 Antony Cedex, France*

[b]*AgroParisTech. UMR 1145 Ingénierie Procédés Aliments. 16 rue Claude Bernard, 75231 Paris Cedex 05, France*

[c]*INRA.UMR 1145 Ingénierie Procédés Aliments. 1 avenue des Olympiades, 91744 Massy Cedex, France*

[d]*CNAM. UMR 1145 Ingénierie Procédés Aliments. 292 rue Saint-Martin, 75141 Paris Cedex 03, France.*

Abstract

This paper presents the mathematical modelling of the ice crystallization process occurring during the freezing of sorbet in a continuous scraped surface heat exchanger (SSHE). Two different modelling approaches have been used, both of which include the nucleation, growth and breakage phenomena of the ice crystals. For both models, the rate of ice crystal nucleation and growth were determined by the subcooling degree. The first model combines heat transfer and population balance equations (PBE), assuming plug flow. The evolution of the values of product temperature, mean chord length, ice volume fraction and apparent viscosity were determined as a function of the residence time. The second model is a coupled model of heat transfer and PBE combined with an empirical model of residence time distribution (RTD), which makes it possible to take into account the fact that the fluid fractions flowing throughout the SSHE do not have the same time-temperature history. The values of the variables (product temperature and mean chord length) were determined for each fraction of fluid exiting the SSHE, and the bulk values were then calculated using the RTD. Simulation results were compared to a set of experimental data obtained during the ice crystallization process of sorbet in a continuous SSHE at the laboratory pilot scale. With a first estimated set of model parameters, it has been shown that the experimental tendencies are represented very satisfactorily by the two models within a 10% error limit. These modelling approaches can then be considered as a promising tool for the understanding and the prediction of the ice crystallisation process in SSHEs so as to identify new ways to improve the performance of the process.

Key words: Ice crystallization; Population balance equations; Residence time distribution; Steady state; Scraped surface heat exchanger.

6 Corresponding author. Tel.: +33 144 08 86 11; Fax: +33 144 08 16 66.
E-mail address: hayat.benkhelifa@agroparistech.fr

1. Introduction

Ice crystallization in a scraped surface heat exchanger (SSHE) is a unit operation widely used in the food industry, for the freeze concentration of juice (Sánchez et al., 2009), or milk (Sánchez et al., 2011), and for the freezing of ice cream and sorbet (Cook and Hartel, 2010). In these food applications, product quality is mainly governed by the shape, mean size and ice crystal size distribution (CSD). Furthermore, the CSD should be reproducible in order to assure a constant product quality. It is therefore important to understand the influence of the operating conditions of the freezing process on the kinetics of ice crystallization, so as to improve the control of the process and the quality of the final product. The modelling of the ice crystallization process can help to gain deeper understanding of the freezing process in a SSHE, and also for the identification of new ways to improve the performance of the process. Furthermore, it can reduce the time of scale-up of the process from laboratory scale equipment to industrial scale production.

The mathematical framework used in crystallization processes to describe the evolution of the CSD is the population balance equation (PBE), introduced by Hulburt and Katz (1964) and further developed by Randolph and Larson (1988). The PBE is a hyperbolic partial differential equation, strongly non-linear, which takes into account the ice nucleation and growth kinetics, as well as the agglomeration and breakage phenomena. Well-mixed crystallizers can be modelled by considering the PBE together with the ideal case of the Mixed Suspension Mixed Product Removal (MSMPR), which assumes that temperature and concentration are homogenously distributed and that crystal size distribution is independent of the location in the crystallizer. This approach has been used for the modelling of precipitation reactions (Garside and Shah, 1980) and desalination processes (Mydlarz, 1996).

However, to account the non-ideal mixing crystallizers such as the SSHE, it is necessary to couple the PBE with mass, momentum and energy conservation equations. In

order to solve the PBE, for these more complex cases, it is necessary to adapt existing numerical methods, such as the method of moments and the method of classes.

The method of moments transforms the PBE into a set of ordinary differential equations, in terms of the moments of the crystal size distribution. In most cases, the first four moments of the distribution are taken into account, providing information about the total number of crystals, the mean size, the surface area and the volume of crystals per unit volume of suspension. The main drawback of this approach is that the full reconstruction of the crystal size distribution from its moments is numerically unstable (Rigopoulus and Jones, 2003). The method of classes introduced by Marchal et al. (1988), transforms the PBE into a set of ordinary differential equations, by discretizing the crystal size and thus generating granulometric classes. The main advantage of this method is that the crystal size distribution can be obtained. The method of classes is a robust numerical method, but the choice of the number of classes remains empirical. Nuhw et al. (1996) recommend discretizing the size domain using a number of classes over 50, so that the calculation of the distribution remains independent of the number of classes chosen.

Recently, an approach coupling the computational fluids dynamics (CFD) simulation with the solution of the PBE has been used for the modelling of more complex fluid flow crystallizers. In this approach the CFD simulation is performed to obtain the flow field at steady state, and the solution of the PBE can be solved either by the method of moments or by the method of classes. Woo et al. (2006) reported a full coupled CFD-PBE method to simulate the antisolvent crystallization of paracetamol from an acetone-water mixture in a semi-batch stirred vessel. The flow field and heat transfer were simulated at a steady state in a 2D axisymmetric grid. The PBE was discretized in 40 granulometric classes. The model represented well the trends observed in the crystallizer, but the computational time was high and some model parameters needed to be identified in order to predict more accurately the

experimental data. Lian et al. (2006) used the CFD-PBE approach to simulate the ice crystallization of 25% sucrose/water solution in a batch SSHE. The flow field was solved at steady state for a 2D geometry, in which a constant solution viscosity and negligible ice crystal dispersion were assumed. The PBE was solved by the method of classes by discretizing the size domain in 14 granulometric classes. The authors compared the predicted ice crystal size distribution with experimental data, and found that the CFD-PBE model overestimated the number of small ice crystals and underestimated the number of large ice crystals. The authors discussed that the discrepancies between the model predictions and the experimental data might have been due in part to the lack of accuracy of the measurement technique of the ice crystal size, to the assumptions made to simplify the fluid flow conditions (i.e. constant viscosity throughout the freezing process), and to the simplified models for ice nucleation and growth kinetics. Lian et al. (2006) also suggested that the effect of ice crystallization on the fluid flow properties needs to be taken into account in the modelling of the process, so as to obtain more accurate results.

Benkhelifa et al. (2008) reported a CFD-PBE approach to model the ice crystallization of a 30% sucrose/water solution in a batch SSHE. The authors used a simplified 1D geometry and introduced the mixing diffusivity to represent the radial mixing originated by the scraping blades. The model also considered that ice crystal nucleation and growth kinetics are dependent on the subcooling degree, also referred as the deviation to thermodynamic equilibrium. Heat transfer and PB equations were solved for 3 granulometric size classes by using the finite element method. Authors compared the predicted mean crystal size with experimental data and found that the model overestimates the measured mean ice crystal size. The authors suggested improving the model by increasing the number of classes to solve the PBE and completely reconstruct the ice crystal size distribution, even though the computation time will highly increase.

Dorneanu et al. (2010) proposed a reduced model for the freezing process in a continuous SSHE. The model considers two layers of fluid: a thin frozen ice layer adjacent to the wall of the SSHE, and a bulk layer located between the rotor and the frozen ice layer. It was considered that within the frozen ice layer the ice crystals form and growth into an ice layer of variable thickness, which is periodically removed into the bulk of the fluid by the rotation of the scraper blades. Within the bulk region the ice crystals are dispersed into the bulk fluid and only ice melting was considered. The hydrodynamic complexity within the SSHE was simplified by considering a plug flow at steady state and the product to be well mixed within a cross-sectional area, perpendicular to the axial direction. Heat transfer and PBE were solved for 12 size classes considering two coordinates: time and axial position and internal coordinate of the ice crystals. Simulation results predicted well the expected trends; nevertheless parameter estimation using experimental data was still required so as to assure more accurate results.

More recently, Freireich et al. (2011) reported the incorporation of particle flow information from discrete element simulation in the PB modelling of mixed-coaters. In this approach a discrete element model simulates the trajectory of the particles within each region of the reactor; then it determines the residence time of the particle and generates sub-compartments in order to reproduce the measured residence time of the particle in each region. Subsequently, a system of PBE is written based on the sub-compartments and simulate the population density of particles. This modelling approach made it possible to account for flow heterogeneity in the mixer-coater and provided accurate results for the behavior of the system.

This work presents two different modelling approaches for the modelling of ice crystallization at steady state in a continuous SSHE. The first model combines heat transfer and PBE, assuming plug flow. The second model is a coupled model of heat transfer and PBE combined with an empirical model of residence time distribution (RTD), which makes it possible to take into account the fact that the fluid fractions flowing throughout the SSHE do

not have the same time-temperature history. Simulation results were compared to a set of experimental data obtained during the freezing process of lemon sorbet in a continuous SSHE at the laboratory pilot scale.

2. Experimental

2.1. Ice crystallization process equipment and operating conditions

The experimental data of draw temperature and mean chord length used to compare with the predicted values of the models developed in this work were previously presented in another study (Arellano et al., 2012a). The measurements were carried out during the freezing process of sorbet in a laboratory scale continuous SSHE (WCB® Model MF 50), a schematic representation of which is shown in Fig. 5.5.1.

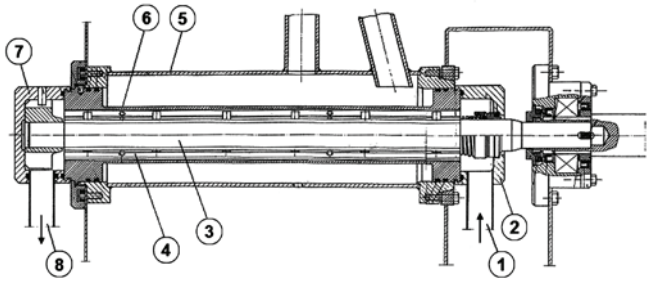


Fig. 5.5.1. Schematic diagram of pilot Freezer WCB MF 50. 1. Inlet connection for sorbet mix. 2. Inlet cover bowl. 3. Rotor. 4. Scraper blades. 5. Freezer jacket with vaporizing r22. 6. Heat exchange cylinder. 7. Outlet cover bowl. 8. Outlet pipe for sorbet.

The inner diameter of the heat exchange cylinder was 0.05 m and the length was 0.40 m. The rotor of the freezer was equipped with two rows of scraper blades and occupied roughly 46% of the freezer barrel volume. The total volume of the SSHE available to the working fluid was 6.66×10^{-4} m^3, which includes the volume available within the heat exchange cylinder, the inlet and outlet bowls, as well as the outlet pipe. The outlet pipe of the SSHE represents 20% of the total available volume to the fluid. The draw temperature of sorbet was measured online at the outlet pipe of the SSHE by means of a calibrated Pt100

probe (Baumer®, accuracy of ±0.1 °C), and the mean chord length of the ice crystals was measured online at the outlet pipe of the SSHE using a Mettler-Toledo Lasentec® FBRM probe (Model S400A-8). The mix used in these experiments was an ultra high temperature pasteurized lemon sorbet mix (14.6% w/w sucrose, 8% w/w fructose, 0.09% w/w dextrose, 3% w/w lemon juice concentrate 60 Brix, 0.5% w/w locust bean gum / guar gum / hypromellose stabiliser blend). The operating conditions and the experimental data used to compare with the results of the model are shown in Table 5.5.1.; these results were extracted from the experimental design reported by Arellano et al. (2012a).

2.2 Residence time distribution measurement and modelling

The empirical model of RTD and the experimental characterization of the RTD were reported in another study (Arellano et al., 2012b). The RTD measurements were carried out in the previously described SSHE, and the operating conditions were that same as those shown in Table 5.5.1. The RTD of the freezing process was measured by means of a colorimetric method. A 13 ml pulse of unfrozen sorbet mix coloured with methylene blue dye at 0.008% (w/w) was used as tracer. In this study the tracer was injected just at the entrance of the SSHE, and the coloured frozen samples were collected at the outlet pipe of the exchanger. Subsequently, samples were thawed at 5 °C and analysed for dye concentration with a spectrophotometer (Beckman Coulter DU® 730) at 662 nm. The RTD of the process was characterized by the age distribution function $E(t)$, where $E(t)dt$ represents the fraction of fluid that has passed through the exchanger for a length of time between t and $t + dt$ (Danckwerts, 1953). Normalized concentration $E(\theta)$ and time θ were calculated from experimental data by the following expressions:

$$E(t) = \frac{C(t)}{\int_0^\infty C(t)dt} \tag{1}$$

$$t_T = \int_0^\infty t \cdot E(t)dt \tag{2}$$

$$\theta = \frac{t}{t_T} \tag{3}$$

$$E(\theta) = t_T \cdot E(t) \tag{4}$$

where $C(t)$ is the exit concentration of tracer at a certain time t (% w/w) and t_T the total experimental mean residence time of the SSHE including the outlet pipe.

As reported by Arellano et al. (2012b), the empirical RTD model that represented the most satisfactorily the experimental RTD data was the gamma distribution model (GDM). In this model, the normalized age distribution $E(\theta)$ is approximated by the Γ-distribution and is defined as follows:

$$E(\theta) = \frac{p^p}{(1-\theta_0)^p \Gamma(p)} (\theta - \theta_0)^{p-1} \exp\left[-p\left(\frac{\theta - \theta_0}{1-\theta_0} \right) \right] \tag{5}$$

where p and θ_0 are the model parameters and Γ denotes the gamma function defined as $\Gamma(p) = \int_0^\infty x^{p-1} e^{-x} dx$.

The parameter p is related to the extension of fluid in the flow direction. As the value of p increases, there is a reduction in axial dispersion and the flow pattern gradually approaches to plug flow behaviour. The parameter θ_0 is considered as a delay dimensionless time, defined as $\theta_0 = D/t_T$, where D represents the delay time of the system. An increase of θ_0 also emphasises the effect of plug flow (Wen and Fan, 1975). Normalized experimental RTD data were fitted to the GDM model by unknown parameter estimation, using the minimization of the sum of squared errors (SSE). The parameters of the GDM model obtained for each experimental condition are shown in Table 5.5.1.; these results were extracted from the experimental design reported by Arellano et al. (2012b).

3. PBE and plug flow modelling approach

This section describes heat transfer, nucleation, growth and fragmentation of ice crystals for a steady state plug flow. The rate of ice crystal nucleation and growth are determined by the subcooling degree. The simulation of the ice crystallization process includes two zones, the heat exchange cylinder of the SSHE which is surrounded by a refrigerating jacket, and the outlet pipe which is assumed as being perfectly insulated. It is important to take into account the outlet pipe because at the SSHE outlet the thermodynamic equilibrium is not yet reached and the ice crystal growth mechanism continues within the outlet pipe. The schematic representation of the considered geometry is shown in Fig. 5.5.2.

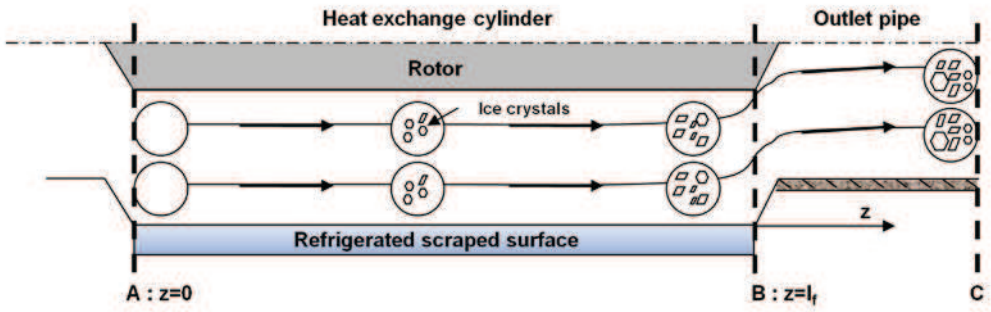


Fig. 5.5.2. Schematic representation of the considered plug flow behaviour of the SSHE.

3.1. Fluid flow

The plug flow approach considers that all the fractions of fluid flowing at time $t = 0$ through the inlet section A (cf. Fig. 5.5.2.) have the same total residence time as expressed by:

$$t_T = \frac{V_T}{\dot{V}} \tag{6}$$

where t_T is the total residence time, $\dot{V}$ is the volumetric flow rate and V_T is the total available volume to the fluid of the SSHE, which includes the volume within the heat exchange cylinder (cf. Fig. 5.5.2., points A to B) and the volume within the outlet pipe (cf. Fig. 5.5.2., points B to C).

The volume within the heat exchange cylinder (gap between the refrigerated scraped surface and the rotor) corresponds to a fraction γ of the total volume of the SSHE. So all the fluid fractions of flow come out of the exchange cylinder through section B (cf. Fig. 5.5.2.) at time $\gamma \cdot t_T$. The freezer is studied at steady state; therefore integrating along the length of the SSHE (z varying from 0 to l_f, cf. Fig. 5.5.2.) is equivalent to integrating versus time (t varying from 0 to $\gamma \cdot t_T$) by following one fraction of fluid. One can imagine that such a fraction of fluid occupies all the section S between the scraped surface wall and the rotor over a small thickness Δz. This fraction of fluid exchanges heat through a surface $2\pi R_c \Delta z$, where R_c is the inner radius of the refrigerated scraped surface of the heat exchange cylinder.

3.2. Energy balance

The energy balance is expressed in terms of the volumetric internal energy U. The heat transfer coefficient h between the refrigerant fluid (temperature T_{rf}) and the solution or sorbet (temperature T) is assumed constant along the freezer. The energy balance equation is written as:

$$S\frac{dU}{dt} = 2\pi R_c h\left(T_{rf} - T\right) + Sv_d \text{, inside the SSHE } (0 < t < \gamma \cdot t_T) \tag{7}$$

$$\frac{dU}{dt} = 0 \text{, inside the outlet pipe, } (\gamma \cdot t_T < t < t_T) \tag{8}$$

where v_d is the viscous dissipation rate by volume unit.

The internal energy is related to the product temperature T and ice volume fraction φ by the following equation:

$$U = \rho_s C_s T + \varphi \rho_{ice} \Delta H_f \tag{9}$$

where ΔH_f is the latent heat of fusion, ρ_{ice} is the density of ice, ρ_s the density of the solution or sorbet and C_s is the specific heat capacity of the solution.

We can therefore obtain an explicit equation for the temperature of the product T as a function of U and ice volume fraction φ, expressed as follows:

$$T = a \cdot U + b \cdot \varphi \tag{10}$$

where a is determined as follows:

$$a = \frac{1}{\rho_s C_s} \tag{11}$$

and b determined by:

$$b = \frac{\Delta H_f}{C_s} \cdot \frac{\rho_{ice}}{\rho_s} \tag{12}$$

The viscous dissipation rate is calculated by the following expression:

$$v_d = \eta_{app} \dot{\gamma}^2 \xi \tag{13}$$

where $\dot{\gamma}$ is the average shear rate in the SSHE, η_{app} the apparent viscosity of sorbet calculated at the average shear rate and for the local ice volume fraction and ξ is an adjustment parameter.

The average shear rate considered inside the freezer was calculated with the model proposed by Leuliet et al., (1986):

$$\dot{\gamma} = (3.213 \times 10^4 \times 1.45^{n_L} n^{-0.7115} \dot{V} + 23.44 \dot{V}^{-0.03} n^{0.1754} N_R) \tag{14}$$

where n_L is the number of scraping blades, n is the flow behaviour index of the sorbet, $\dot{V}$ the volumetric flow rate and N_R the speed of rotation of the scraping blades.

The apparent viscosity of sorbet was modeled by the following empirical correlation obtained from pipe rheometry measurements (Arellano, 2012c):

$$\eta_{app} = k_{mix} \left(1 + 2.5\varphi + 10.05\varphi^2 + 3.319 \exp\{3.421\varphi\}\right) \cdot \dot{\gamma}^{n-1} \tag{15}$$

where φ is the ice volume fraction and k_{mix} is the consistency index of the unfrozen freeze concentrated phase, which is determined by the following empirical equation (Gonzalez, 2012):

$$k_{mix} = 39.02 \times 10^{-9} \cdot \exp\left(\frac{2242.38}{T + 273.15}\right) \cdot w^{2.557} \tag{16}$$

where w is the local mass fraction of solute.-

The evolution of the flow behaviour index n during freezing depends also on the ice volume fraction φ and is determined by the following expression (Arellano, 2012c):

$$n = 0.655\left[\left(1 - 0.292\right) + 0.292\, exp\left(\frac{-\varphi}{0.113}\right)\right] \tag{17}$$

3.3. Population balance

The population of ice crystals is defined by a number density function $\psi(L,t)dL$, representing the number of ice crystals of size between *L* and *L*+*dL* per unit volume at a time *t*. Inside the SSHE ($0 < t < \gamma \cdot t_T$), the population balance considers ice nucleation, growth and breakage by the following equation:

$$\frac{\partial \psi}{\partial t} + \frac{\partial G.\psi}{\partial L} = N\, \delta(L - L_c) + B_b(L) \tag{18}$$

where N represents the ice crystals nucleation rate, B_b the net production of ice crystals due to the breakage phenomena and G the ice crystals growth rate. G can be negative in the case of crystals melting in warm temperature zones. The Dirac function δ denotes that the nucleation mechanism creates ice crystals with a size equal to an initial size L_c.

In the outlet pipe, which is assumed as being perfectly insulated there is no scraping action of the blades, therefore the ice crystal nucleation and the phenomenon of ice breakage were not considered. Only the ice crystal growth phenomenon was taken into account. Inside the outlet pipe ($\gamma \cdot t_T < t < t_T$) the population balance becomes:

$$\frac{\partial \psi}{\partial t} + \frac{\partial G.\psi}{\partial L} = 0 \tag{19}$$

The PBE was discretized in crystal size (L) by the method of classes, using 600 classes.

3.3.1. Ice volume fraction and mean ice crystal size

Considering ice crystals as spherical particles, the ice volumetric fraction φ is given by:

$$\varphi(t) = \int_0^{Lmax} \psi(L,t) \frac{\pi L^3}{6} dL \tag{20}$$

The mean crystal diameter is calculated as expressed by the following expression:

$$d(t) = \int_0^{Lmax} L\psi(L,t)dt \Big/ \int_0^{Lmax} \psi(L,t)dt \tag{21}$$

The surface mean diameter or Sauter can be determined as follows:

$$d_{3.2}(t) = \int_0^{Lmax} L^3\psi(L,t)dt \Big/ \int_0^{Lmax} L^2\psi(L,t)dt \tag{22}$$

The mean diameter is the arithmetic average diameter of the distribution of ice crystals and is equally affected by the lower and upper parts of the distribution. The surface mean diameter makes it possible to compare the volume to surface ratio of the measured particles. Therefore, the surface mean diameter will mainly indicate the evolution of the larger ice crystals.

In order to compare the predicted values of mean crystal diameter with experimental results, it is necessary to transform the mean diameter into a mean chord length which corresponds to the experimental data provided by the focused beam reflectance measurement (FBRM) probe. Wynn (2003) established the relationship between the moments of CLD and PSD, and determined that the mean chord length of a sphere is $\pi/4 \cong 0.785$ times smaller than its mean diameter and the surface mean chord length of a sphere is 2/3 times smaller than its

surface mean diameter. Thus the mean chord length C and mean surface chord length $C_{3.2}$ are given by the following expressions:

$$C = \frac{\pi}{4} \cdot d \tag{23}$$

$$C_{3.2} = \frac{2}{3} \cdot d_{3.2} \tag{24}$$

3.3.2. Subcooling degree

The subcooling degree, also referred as the deviation to thermodynamic equilibrium, determines the rate of the kinetics phenomena of ice crystal nucleation and growth during the freezing process. This thermodynamic driving force for ice crystallization can be characterized by the difference between the solution temperature and the freezing point temperature of the solution. The freezing point depression curve has been determined experimentally for lemon sorbet mix and modelled as proposed by Gonzalez (2012):

$$T_{eq} = -7.68w + 8.64w^2 - 70.10w^3 \text{, in } ^\circ\text{C} \tag{25}$$

where w is the local solute mass fraction of the unfrozen freeze concentrated liquid phase, which can be determined by the following expression:

$$w = \frac{w_0}{1 - \varphi'} \tag{26}$$

where $w_0 = 0.25$ is the initial solute mass fraction of the solution and φ' the ice mass fraction.

3.3.3. Nucleation mechanism

Two types of ice nucleation mechanisms are distinguished: primary or secondary nucleation, with primary nucleation being subdivided into either homogeneous or heterogeneous. Homogeneous primary nucleation occurs in a pure system without the

presence of foreign particles. Heterogeneous nucleation generally takes place more often than homogeneous nucleation, and it occurs by the presence of nuclei inducers, such as foreign particles in the solution or by a rough surface of the wall of SSHE. Collision secondary nucleation occurs due to contact between ice crystals or with the crystallizer walls. However, literature shows that the secondary nucleation mechanism is not predominant in SSHEs (Cook and Hartel, 2010). Therefore, the ice nucleation rate in this model is described by the surface heterogeneous nucleation occurring at the wall of the heat exchanger cylinder. The ice nucleation rate depends on the difference between the freezing point temperature of the solution T_{eq} and the temperature of the refrigerant fluid T_{rf} (which is close to the wall temperature).

$$N = \frac{2\pi R_c}{S} k_n (T_{eq} - T_{rf})^{\alpha} \tag{27}$$

where k_n is the nucleation rate parameter and α the power index.

3.3.4. Growth mechanism

The growth rate is expressed as a function of the difference between the freezing point temperature and the sorbet temperature:

$$G = k_g (T_{eq} - T)^{\beta} \tag{28}$$

where k_g is the growth rate parameter, and β the power index. The growth mechanism is assumed to be independent of the ice crystal size. If $T_{eq} - T < 0$, ice crystals will grow and $G > 0$, or else ice crystals will melt, and $G < 0$.

3.3.5. Breakage mechanism

The breakage mechanism is a function of the rotation speed of the scraping blades N_R, the crystal size L and the crystal population density $\psi(L)$. The net production rate of ice

crystals by breakage $B_b(L)$ takes into account a term $B^-(L)$ for the disappearance of ice crystals and a term $B^+(L)$ for the formation of ice crystals. The breakage considers the division of a crystal of size L' into two crystals of size $L = L'/2^{1/3}$ of same volume, considering that the total crystal volume is preserved.

The number of ice crystals of size between L and $L + dL$ that disappear per time and volume unit is expressed as:

$$B^-(L)dL = \varepsilon N_R L \psi(L) dL \tag{29}$$

with ε the breakage constant.

In this way, the larger the ice crystal size and the higher the rotation speed, the higher the breakage mechanism of ice crystals.

The number of ice crystals being formed of size between L and $L + dL$ per time and volume unit, is equal to twice the number of ice crystals disappearing per unit of time of size between $L' = 2^{1/3} L$ and $L' + dL'$ with $dL' = 2^{1/3} dL$. Thus the rate of formation of ice crystals by breakage is:

$$B^+(L)dL = 2\varepsilon N_R L' \psi(L') dL' \tag{30}$$

Finally, the net production rate becomes:

$$B_b = 2\varepsilon N_R 2^{2/3} L \psi(L') - \varepsilon N_R L \psi(L) \text{ with } L' = 2^{1/3} L \tag{31}$$

4. Modelling approach coupling PBE and RTD

This modelling approach considers that the fractions of fluid do not have the same residence time in the SSHE. It thus would be expected that the fractions of the fluid which remain longer in the SSHE (i.e. which have longer residence time) will exit with a higher ice volume fraction and with larger ice crystals, because they were longer in contact with the

refrigerated scraped surface wall and had more time for ice crystals to growth. Fig. 5.5.3. shows a schematic representation of the fluid flow behavior in the SSHE.

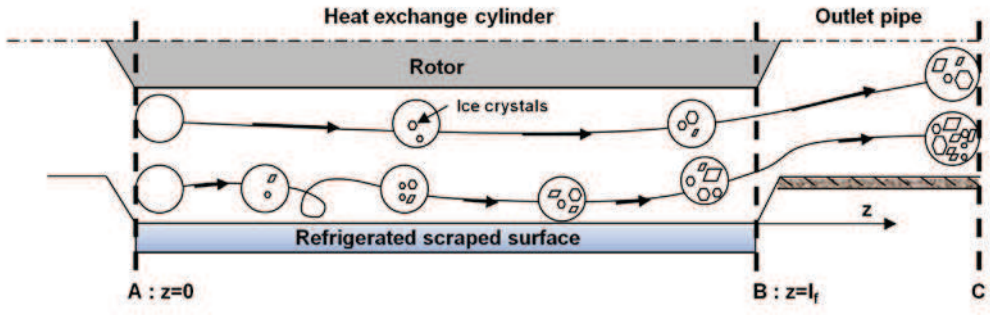


Fig. 5.5.3. Schematic representation of the considered residence time distribution behaviour of the SSHE.

For a fraction of fluid having a residence time t_r the same model as exposed in section 2 is applied to calculate the ice fraction $\varphi_o(t_r)$ and the ice crystal size distribution $\psi_o(L, t_r)$ at the outlet. The fractions of fluid having a residence time comprised between $t_r - dt_r/2$ and $t_r + dt_r/2t_r$ is $E(t_r)dt_r$. Therefore, the bulk outlet ice fraction and size distribution become:

$$\overline{\varphi}_o = \int_0^\infty \varphi_o(t_r)E(t_r)dt_r \tag{32}$$

$$\overline{\psi}_o(L) = \int_0^\infty \psi_o(L,t_r)E(t_r)dt_r \tag{33}$$

As the draw temperature is not a conservative variable, the same procedure is not applicable. Therefore, the bulk value for the internal energy must be calculated first, and afterwards the bulk temperature $\overline{T}_o$ can be obtained from the bulk energy and ice fraction, written as:

$$\overline{U}_o = \int_0^\infty U_o(t_r)E(t_r)dt_r \tag{34}$$

$$\overline{T}_o = a\overline{U}_o + b\overline{\varphi}_o \tag{35}$$

5. Numerical solution of the models.

The algorithm for the numerical solution of the differential equations of both models was developed using Matlab.

The initial conditions for both models are:

- The initial ice volume fraction $\varphi_i = 0$
- $U_i = T_i / a$, where T_i is the initial temperature of the product.
- $\psi(L, t = 0) = 0$, because the initial temperature of the product is superior to the initial freezing point temperature.

Considering a previous work of ice crystallization of a sucrose solution (Lian et al., 2006), the power indices for ice crystal nucleation and growth rates, α and β, were respectively chosen equal to 2 and 1. The heat transfer coefficient h, and the parameters of ice crystal nucleation k_n, growth k_g and breakage ε were identified by comparing the predicted values of the model with the experimental data of draw temperature and mean chord length presented in Table 5.5.1. The estimated values obtained were for wall heat transfer coefficient h = 2500 $Wm^{-2}K^{-1}$, for heterogeneous nucleation coefficient k_n = 9.10^8 $s^{-1}m^{-2}K^{-1}$, for growth coefficient k_g = 6.10^{-7} $ms^{-1}K^{-1}$, for the breakage coefficient ε = 5 m^{-1}. The viscous dissipation adjustment parameter was ξ = 17. The initial crystal size was chosen equal to L_c = 5 µm.

Table 5.5.1. Operating conditions and obtained responses during the ice crystallization modelling.

Operating conditions				RTD modelling parameters		Experimental and modelling results			
Run	$\dot{V}$ [a] (kg.s^{-1})	T_{rf} [a] (°C)	N_R [a] (rad.s^{-1})	θ_0**	p**		T [a](°C)	φ_i [a]	C_i [a] (μm)
1	0.007	-15.3	78.5	0.39	3.4	*E*	-5.98*	0.41	6.31*
						PF	-6.59	0.43	5.79
						RTD	-6.33	0.42	5.83
2	0.014	-15.3	78.5	0.46	3.8	*E*	-4.79*	0.33	6.47*
						PF	-4.91	0.34	6.60
						RTD	-4.83	0.32	6.58
3	0.021	-15.4	78.5	0.45	4.5	*E*	-4.04*	0.25	6.53*
						PF	-3.70	0.22	6.75
						RTD	-3.72	0.22	6.73
4	0.014	-10.6	78.5	0.47	3.5	*E*	-3.41*	0.16	8.1*
						PF	-3.48	0.19	7.46
						RTD	-3.48	0.19	7.44
5	0.014	-19.8	78.5	0.42	3.1	*E*	-6.25*	0.41	6.00*
						PF	-6.13	0.41	6.03
						RTD	-5.87	0.39	6.00
6	0.014	-15.2	57.1	0.47	3.6	*E*	-4.83*	0.33	6.40*
						PF	-5.07	0.35	6.73
						RTD	-5.03	0.33	6.71
7	0.014	-15.3	104.7	0.47	3.1	*E*	-4.76*	0.33	6.32*
						PF	-4.58	0.31	6.43
						RTD	-4.49	0.29	6.39

[a] $\dot{V}$ = mix flow rate; T_{rf} = evaporation temperature of r22; N_R = dasher rotational speed; T = sorbet draw temperature; φ_i = ice volume fraction; C_i = mean chord length; *E* = experimental; *PF* = plug flow model; *RTD* = coupled PBE-RTD model.
*Values were extracted from the experimental design reported by Arellano et al. (2012a) and **Arellano et al. (2012b), respectively.

6. Results and discussion

6.1. PBE and plug flow modelling approach

Fig. 5.5.4. presents the predicted evolution of the mean values of product temperature, mean chord length, surface mean chord length, ice volume fraction and apparent viscosity (at $\dot{\gamma}$ = 10s^{-1}) as a function of the residence time, for sorbet obtained at T_{rf} = -15.3 °C, $\dot{V}$ = 0.014kg.s^{-1} and N_R = 78.5 rad.s^{-1}.

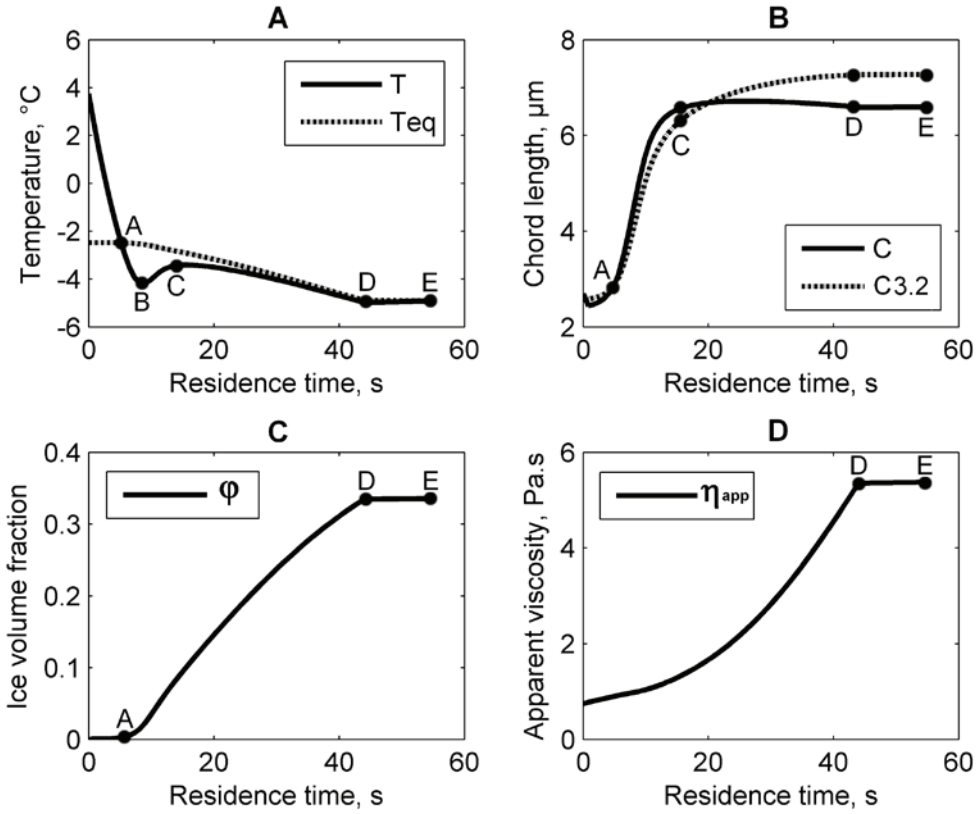


Fig. 5.5.4. Plug flow model predicted mean values of temperature T, ice volume fraction φ, mean crystal chord length C_i, surface mean crystal chord length $C_{i3.2}$ and apparent viscosity η_{app} at $\dot{\gamma}$ = 10 s^{-1} during the freezing of sorbet in the SSHE at $\dot{V}$ = 0.014 $kg.s^{-1}$, N_R = 78.5 $rad.s^{-1}$ and T_{rf} = -15.3 °C. Point D = end of heat exchange cylinder. Point E = outlet of the SSHE (measurement point).

It can be seen in Fig. 5.5.4.A that within the first 5 seconds (before point A), the model predicts a rapid decrease of the temperature of the product from the inlet temperature at 5 °C to the initial freezing point of sorbet mix at -2.6 °C. Then, from point A to B the temperature of the product decreases below its freezing point, and thus there is an increase in the subcooling degree reaching its maximum value at point B. The time period from point A to B indicates thus the beginning of the ice nucleation and ice crystal growth mechanisms. From point B to C, we can observe the gradual decrease in the subcooling degree; within this time period it is likely that the phenomena of ice nucleation and growth occur simultaneously in the SSHE. From point C to D it can be seen that the subcooling degree decreases further but at a slower rate, and also that the product does not reach entirely the equilibrium temperature

at the outlet of the heat exchange cylinder at a time of 44s (point D). Finally, from points D to E we can observe that the temperature of the product no further decreases and that the product reaches the equilibrium temperature within the outlet tube of the SSHE. This effect is obviously due to the fact that there is no heat transfer in the outlet tube.

In Fig. 5.5.4.B we can observe that the mean ice crystal chord length increases within the first 15 s of residence time within the SSHE, corresponding roughly to the time interval between points A to C shown in Fig. 5.5.4.A, where the subcooling degree is higher and when it is likely that the higher rates of ice nucleation and ice crystal growth occur. Further on (from a residence time of 15 s until the outlet of sorbet at 55 s), the mean chord length remains almost unchanged. It can also be seen that there is a slower increase in the surface mean chord length within the first 15 s of the freezing process (between points A to C), as compared with the trend of the mean chord length. However, after 15 s the surface mean chord length continues to increase more slowly until a residence time of 44 s. This effect can be due to the continuous increase in the ice volume fraction from the time interval between 15 to 44 s (cf. Fig. 5.5.4.C) which is reflected in the growth of the larger ice crystals and thus on the surface mean chord length. Finally, after 44 s (in the outlet pipe) the surface mean diameter remains almost unchanged.

We can observe in Fig. 5.5.4.C that the ice volume fraction starts to increase from point A, when the temperature of the product reaches the initial freezing point at -2.6 °C (cf. Fig. 5.5.4.A) and the ice crystals are produced, until sorbet reaches the exit of the heat exchange cylinder at point D (cf. Fig. 5.5.4.A). From point D to E, it can be seen that as the product flows through the outlet pipe of the SSHE, the ice volume fraction increases very slightly as the temperature of the product reaches the thermodynamic equilibrium (cf. Fig. 5.5.4.A).

It can also be seen in Fig. 5.5.4.D that as the product flows through the heat exchange cylinder, the apparent viscosity of sorbet increases with the decrease in the temperature of the product and as the ice volume fraction increases (cf. Fig. 5.5.4.A and 5.5.4.B). Then as the product flows through the outlet pipe, the apparent viscosity of the product remains almost unchanged like the temperature of the product and the ice volume fraction.

6.2 Coupling of PBE and RTD modelling approach

Fig. 5.5.5. shows the predicted cumulative RTD with the GDM parameters for sorbet obtained at T_{rf} = -15.3 °C, $\dot{V}$ = 0.014kg.s^{-1} and N_R = 78.5 rad.s^{-1}.

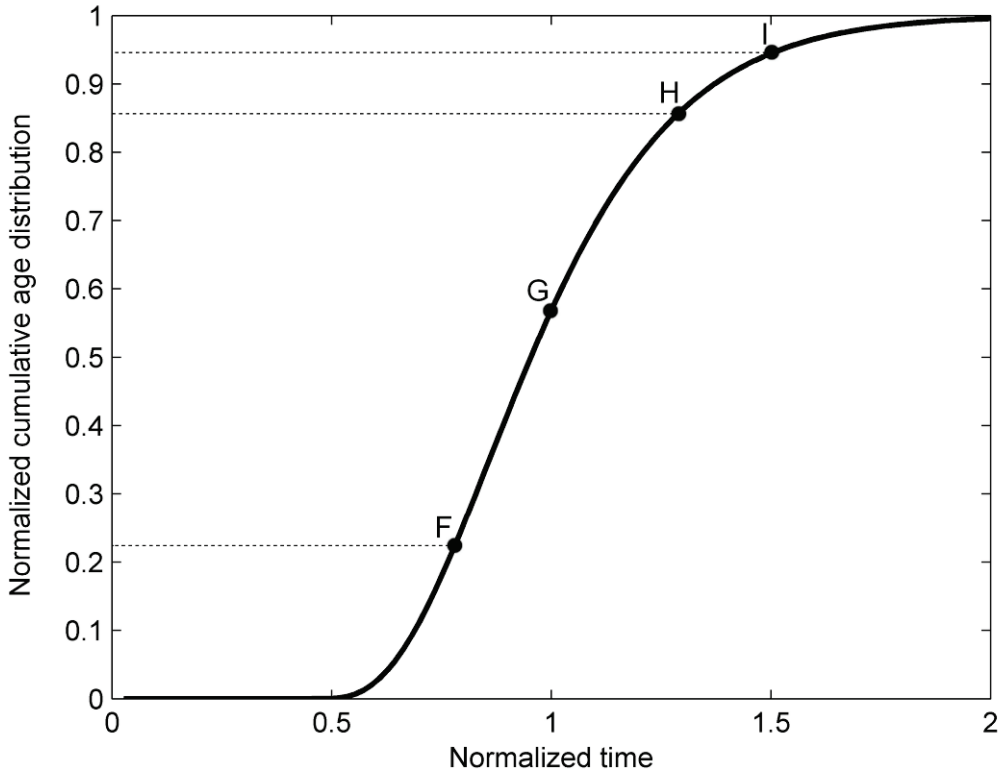


Fig. 5.5.5. RTD curve during the freezing of sorbet in the SSHE at $\dot{V}$ = 0.014 kg.s^{-1}, N_R = 78.5 rad.s^{-1} and T_{rf} = -15.3 °C.

This RTD curve represents the fractions of fluid that exit from the SSHE at different dimensionless residence times. It can be seen from this curve (point F) that roughly 25% of the product exits from the exchanger with a residence time lower than $0.75\,t_T$. Point G

corresponds to the mean residence time t_T. About 15% of the product remains longer than $1.25\,t_T$ in the SSHE (point H) and 5% longer than $1.5\,t_T$ (point I).

Fig. 5.5.6. presents the predicted values of draw temperature, mean and surface mean chord length, ice volume fraction and apparent viscosity (at $\dot{\gamma}$ = 10s^{-1}) for each fraction of fluid exiting from the exchanger at different normalized residence times, for sorbet obtained at T_{rf} = -15.3 °C, $\dot{V}$ = 0.014kg.s^{-1} and N_R = 78.5 rad.s^{-1}. The dashed lines in Fig. 5.5.6. indicate the mean residence time t_T.

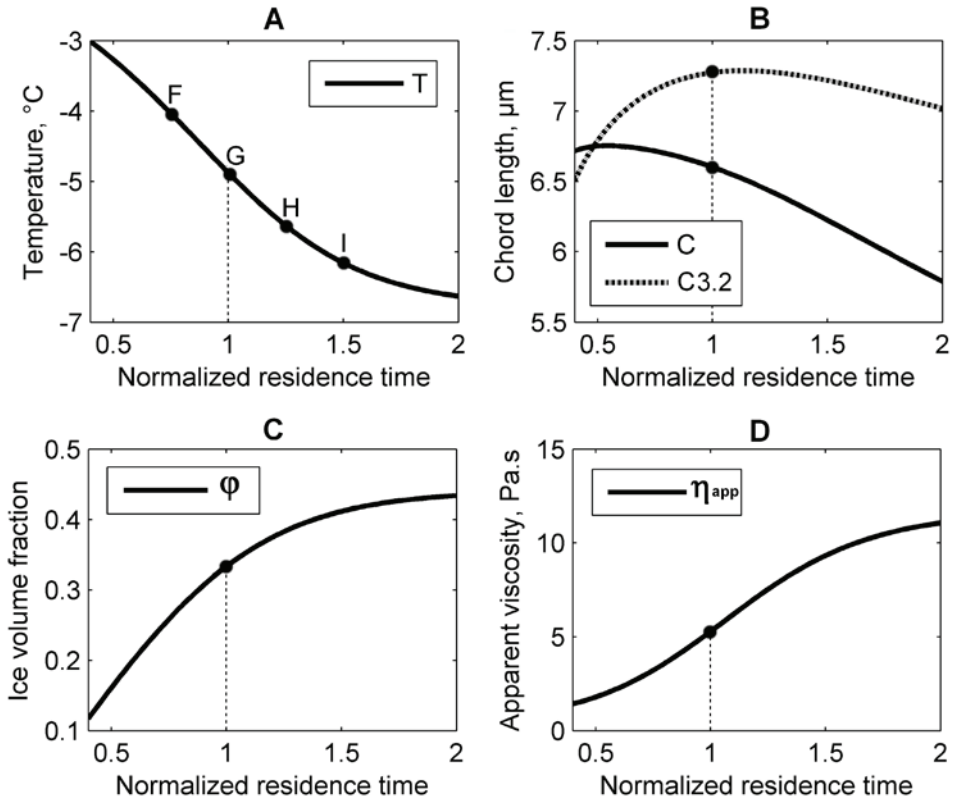


Fig. 5.5.6. RTD model predicted mean values of draw temperature T, ice volume fraction φ, mean crystal chord length C_i, surface mean crystal chord length $C_{i\,2.3}$ and apparent viscosity η_{app} at $\dot{\gamma}$ = 10 s^{-1} during the freezing of sorbet in the SSHE at $\dot{V}$ = 0.014 kg.s^{-1}, N_R = 78.5 rad.s^{-1} and T_{rf} = -15.3 °C.

We can observe in Fig. 5.5.6.A, that the fraction of fluid exiting the SSHE more early at $0.75\,t_T$ (point F) has a higher temperature than the fractions of fluid that come out from the exchanger at t_T, at $1.25\,t_T$ and at $1.5\,t_T$ (point G, H and I, respectively). This effect can be

explained by the fact that the fraction of fluid at $0.75\,t_T$ has a shorter residence time, thus there is less time available to remove heat from the product and the product exits at a warmer temperature.

In Fig. 5.5.6.B we can observe that the ice crystals contained within the fraction of fluid exiting at $0.75\,t_T$ have a slightly larger mean chord length than the fractions of fluid that come out from the exchanger at t_T, at $1.25\,t_T$ and at $1.5\,t_T$. This effect can be explained by the warmer draw temperatures of the product at $0.75\,t_T$ which leads to the melting of the smaller ice crystals and to the survival of the larger ice crystals, resulting thus in slightly larger mean chord length. On the contrary, the fraction of fluid exiting at $1.5\,t_T$ has a lower temperature, and thus a larger quantity of smaller ice crystals survives and the mean chord length is smaller.

The surface mean chord length increases from $0.75\,t_T$ to t_T and then decreases slightly. This effect confirms the survival of the larger ice crystals and the melting of the smaller ice crystals within the time interval between $0.75\,t_T$ and t_T. After $1.25\,t_T$ the surface mean chord length decreases, the effect of which is likely due to the larger quantity of smaller ice crystals that survive and the breakage of the larger ones.

We can observe in Fig. 5.5.6.C that the fraction of fluid exiting the SSHE at $0.75\,t_T$ has a lower ice volume fraction than the fractions of fluid exiting at t_T, at $1.25\,t_T$ and at $1.5\,t_T$. This effect is likely due to the warmer temperature of the product at $0.75\,t_T$, due to the shorter residence time and to the less time available to reduce the temperature of the product (cf. Fig. 5.5.6.A, point F).

It can be seen in Fig. 5.5.6.D that the fractions of fluid exiting earlier from the SSHE at $0.75\,t_T$ exhibit a lower apparent viscosity than the fractions of fluid exiting after t_T. This effect is likely due to the higher product temperature and thus to the lower ice volume fraction

contained within sorbet at this residence time. Thus, we can also observe that the fraction of fluid which remains longer in the SSHE and exits at $1.5\,t_T$ has a lower draw temperature, a higher ice volume fraction and a higher apparent viscosity.

Fig. 5.5.7. presents the predicted ice crystal size distributions of the fraction of fluid exiting the SSHE at $0.75\,t_T$, t_T, $1.25\,t_T$ and $1.5\,t_T$, for sorbet obtained at T_{rf} = -15.3 °C, $\dot{V}$ = 0.014kg.s^{-1} and N_R = 78.5 rad.s^{-1}.

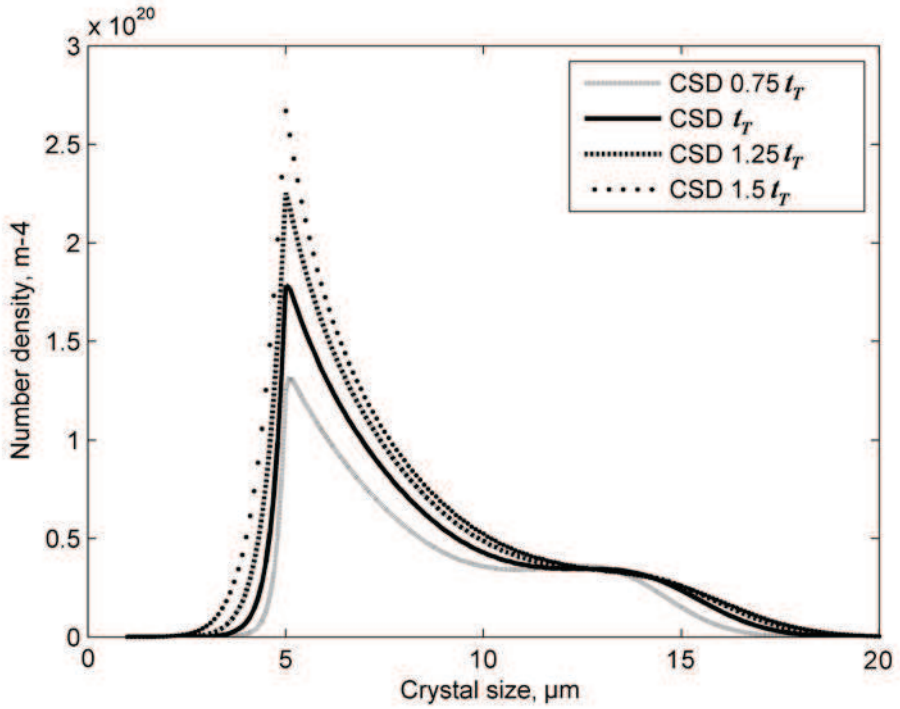


Fig. 5.5.7. Ice crystals number density CSD at different residence times t_T, during ice crystallization of sorbet in the SSHE at $\dot{V}$ = 0.014 kg.s^{-1}, N_R = 78.5 rad.s^{-1} and T_{rf} = -15.3 °C.

We can see from these results that the increase in the residence time leads to the increase in the population of smaller ice crystals (ice crystals of size between 5 to 10 µm). The effect of which is likely due to the lower product temperatures reported in Fig. 5.5.6.A (decrease in the product temperature with the increases in the residence time, from point F to I) which make it possible the survival of a larger quantity of small ice crystals. It can also be seen that the population of ice crystals within the size interval between 10 to 15 µm

remains almost unchanged. Finally, we observe that the increase in the residence time leads to a slight increase in the population of larger ice crystals (ice crystals of size between 15 to 20 µm). The effect of which is likely due to the continuous growth of the ice crystals with the decrease in the temperature of the product. The increase in the population of both the smaller and larger ice crystals with the increase in the residence time can explain that the mean ice crystal chord length remained almost unchanged after a residence time of 15 s in Fig. 5.5.5.B.

6.2 Comparison between the two models

Fig. 5.5.8. shows the comparison between the ice CSD at the outlet of the SSHE obtained by the plug flow (PF) modelling approach and by the residence time distribution (RTD) modelling approach, for sorbet produced at T_{rf} = -15.3 °C, $\dot{V}$ = 0.014kg.s^{-1} and N_R = 78.5 rad.s^{-1}.

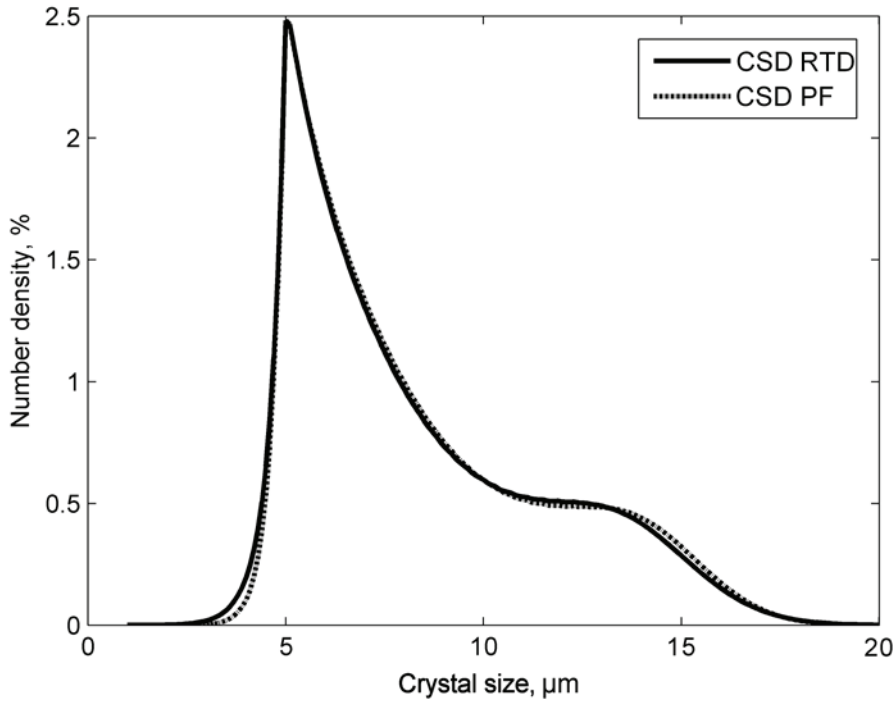


Fig. 5.5.8. Comparison between the CSDs predicted by the plug flow (PF) and the residence time distribution (RTD) models at mean residence times t_T during the ice crystallization of sorbet in a SSHE at 0.014 kg.s^{-1}, 78.5 rad.s^{-1} and -15.3 °C.

It can be seen that the crystal size distributions for both modelling approaches are very similar. This effect can be explained by the fact that when all fractions of fluid are mixed to constitute the bulk ice CSD, the different ice crystal sizes from the different fractions of fluids compensate each other. That is to say, the ice crystals contained in the fractions of fluid that exit earlier from the SSHE and have a larger mean chord length (due to the survival of the larger ice crystals and to the melting of the small ice crystals), compensate the ice crystals contained in the fractions of fluid that exit later from the SSHE and have a smaller chord length (due to the survival of a larger quantity of small ice crystals and the breakage of the larger ones). This result shows that even if the RTD is broadened from 0.5 to 2 times the mean residence time t_T, the use of a plug flow approach can be used to represent very satisfactorily the fluid flow and the ice CSD during the ice crystallization process in SSHEs.

Fig. 5.5.9. presents the comparison of the predicted values of draw temperature (cf. Fig. 5.5.9.A) and mean chord length (cf. Fig. 5.5.9.B) by the PBE-PF model and by the PBE-RTD model with the experimental measurements at the operating conditions shown in Table 5.5.1. We can observe from these results that both models predict very satisfactorily the temperature of the product and the mean ice crystal chord length within a 10% error limit.

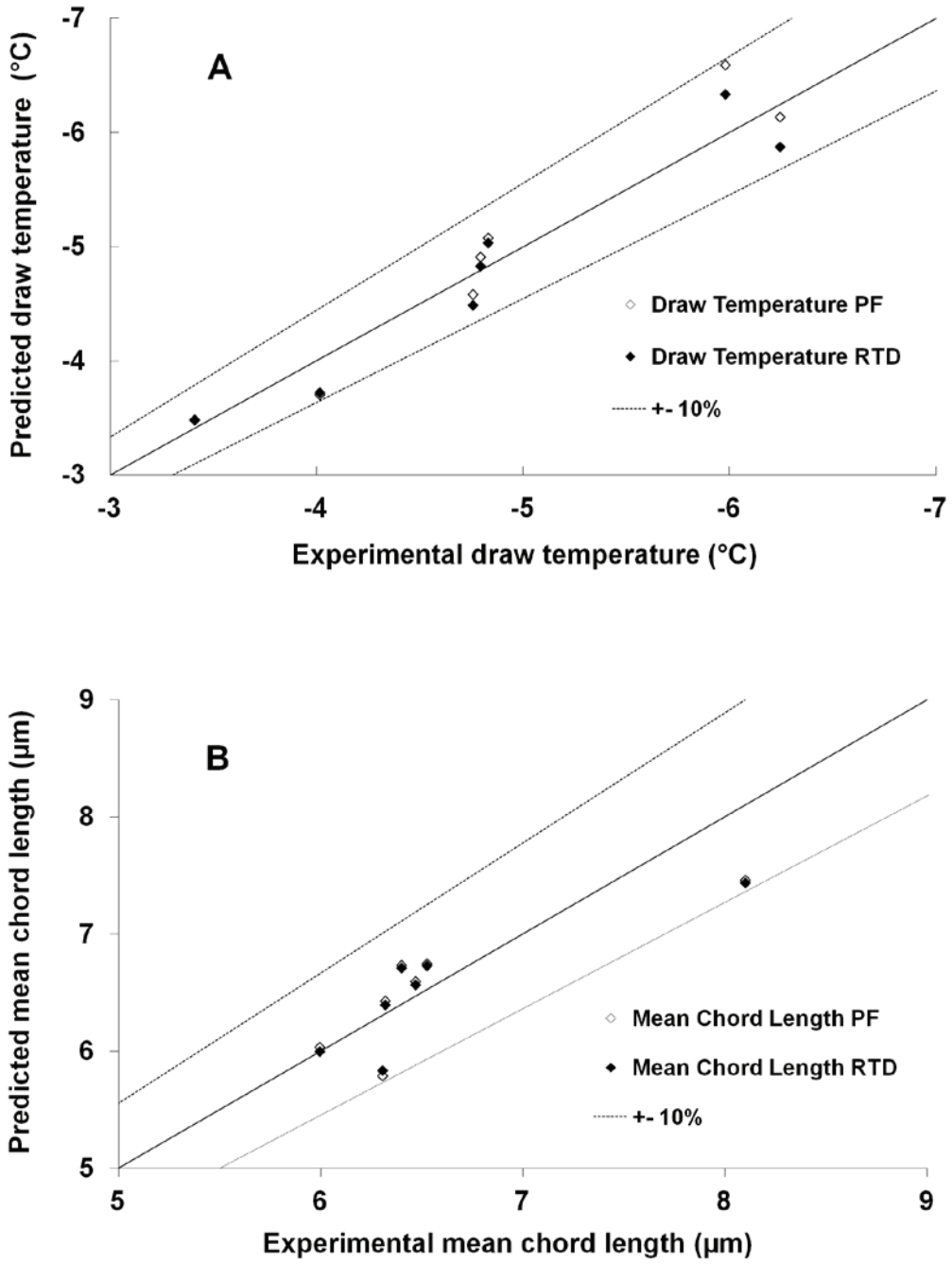


Fig. 5.5.9. Comparison of the predicted values of draw temperature (A) and mean chord length (B) by the PBE-PF and the PBE-RTD models with the experimental measurements during the ice crystallization of sorbet in a SSHE for the operating conditions tested.

7. Conclusions

The mathematical modelling of the ice crystallization process of sorbet in a continuous SSHE has been presented in this work. Two different modelling approaches have been used,

both of which include the nucleation, growth and breakage phenomena of the ice crystals. For both models, the rate of ice crystal nucleation and growth were determined by the subcooling degree. The first model combines heat transfer and PBE, assuming plug flow. This model made it possible to predict the evolution of the temperature of the product, the mean and surface mean chord length, the ice volume fraction and the apparent viscosity of the product as a function of the residence time. The second model is a coupled model of heat transfer and PBE combined with an empirical model of RTD, which makes it possible to take into account the fact that the fluid fractions flowing throughout the SSHE do not have the same time-temperature history. This modelling approach gave insight into the values of the variables (product temperature and mean chord length), for each fraction of fluid that flows through the SSHE, and made it possible to calculate the bulk values.

A comparison between the ice CSD at the outlet of the SSHE obtained by the PBE-PF model and by the PBE-RTD model showed that the ice CSD of both modelling approaches were very similar. The effect of which is explained by the blending of the fractions of fluid that constitute the ice CSD at the outlet, some of which exit earlier from the SSHE and have a larger ice crystal size (due to the survival of the larger ice crystals and to the melting of the small ice crystals), and others that exit later from the SSHE and have a smaller crystal size (due to the survival of a larger quantity of small ice crystals and the breakage of the larger ones), resulting thus in a compensation effect between the ice crystal sizes of all the fractions of fluid.

A comparison of the predicted data of draw temperature and mean chord length by the PF model and by the RTD model with the experimental data obtained for different operating conditions demonstrated that both models predicted very satisfactorily the experimental tendencies within a 10% error limit.

These modelling approaches can be useful to gain deeper understanding of the ice crystallization process in SSHEs so as to identify new ways to improve the performance of the process. These models can also be applied to help for the scale-up of the process from laboratory pilot scale equipment to industrial scale SSHEs.

Acknowledgments

The authors gratefully acknowledge the financial support granted by the European Community Seventh Framework through the CAFÉ project (Computer Aided Food processes for control Engineering) Project number 212754.

Nomenclature

B_b net production rate of ice crystals by breakage, m^{-1}

$C(t)$ concentration of dye in the fluid exit stream at time t, %w/w

C_s specific heat capacity of the solution or sorbet, $J.kg^{-1}K^{-1}$

C mean chord length, m

$C_{3,2}$ surface mean chord length, m

D delay time of the system, s

d mean diameter, m

$d_{3,2}$ surface mean diameter or Sauter diameter, m

$E(t)$ age distribution function, s

$E(\theta)$ normalized age distribution function, -

G ice crystal growth rate, $m.s^{-1}K^{-1}$

h heat transfer coefficient, $W.m^{-2}K^{-1}$

k_g ice crystal growth coefficient, $m.s^{-1}K^{-1}$

k_n heterogeneous ice nucleation coefficient, $m^{-2}s^{-1}K^{-1}$

k_{mix} consistency coefficient for sorbet mix, $Pa.s^n$

L crystal size, m

L_c initial crystal size, m

n flow behaviour index index, -

nL number of scraping blades, -

N ice crystal nucleation rate, $m^{-2}s^{-1}K^{-1}$

N_R rotational speed of scraping blades, $rad.s^{-1}$

p parameter related to the extent of fluid in the flow direction, -

R_c radius of the heat exchange cylinder, m

S area of the section of fluid between the heat exchange cylinder and the rotor, m^2

t fluid residence time, s

t_r residence time, s

t_T total mean residence time, s

T temperature of the product, °C

T_{eq} freezing point of the solution at equilibrium, °C

T_{rf} temperature of the refrigerant fluid, °C

U volumetric internal energy,

v_d viscous dissipation, Wm^{-3}

V_T available volume to the fluid, m^3

$\dot{V}$ volumetric flow rate, m^3s^{-1}

w mass fraction of solute (sweetener content), -

Greek symbols

Γ gamma function

ψ number density function of ice crystals, m^{-4}

ε breakage coefficient

η_{app} apparent viscosity, Pa.s

ρ_{ice} ice density, $kg.m^{-3}$

ρ_s sorbet density, $kg.m^{-3}$

φ ice volume fraction, -

φ' ice mass fraction, -

ξ viscous dissipation coefficient, -

θ normalized time, -

θ_0 normalized delay time of the system, -

Subscript

i inlet – initial

o outlet

References

Arellano, M., Benkhelifa, H., Flick, D., Alvarez, G. (2012a). Online ice crystal size measurements during sorbet freezing by means of the focused beam reflectance measurement (FBRM) technology. Influence of operating conditions. *Journal of Food Engineering*, 113, 351-359.

Arellano, M., Benkhelifa, H., Alvarez, G., Flick, D. (2012b). Experimental study and modelling of the residence time distribution in a scraped surface heat exchanger during sorbet freezing. *Journal of Food Engineering* (submitted).

Arellano, M., Benkhelifa, H., Flick, D., Alvarez, G. (2012c). Rheological characterization of sorbet using pipe rheometry during the freezing process. *Journal of Food Engineering* (submitted).

Benkhelifa H., Haddad Amamou A., Alvarez G., Flick D. (2008). Modelling fluid flow, heat transfer and crystallization in a scraped surface heat exchanger. *4th International Symposium Model-It: Applications of Modelling as an Innovative Technology in the Agri-Food Chain*, Madrid, Spain. 11/06/08.

Cook, K. L. K. and Hartel, R. W. (2010). Mechanisms of Ice Crystallization in Ice Cream Production. *Comprehensive Reviews in Food Science and Food Safety,* 9 (2), 213-222.

Danckwerts, P. V. (1953). Continuous flow systems. Distribution of residence times. *Chemical Engineering Science*, 2, 1-13.

Dorneanu, B., Bildea, C., Grievink, J., Bongers, P. M. (2010). A reduced model for the freezing step in ice cream manufacture. *20th European Symposium on Computer Aided Process Engineering – ESCAPE*

Freireich, B., Li, J., Litster, J., Wassgrena, C. (2011). Incorporating particle flow information from discrete element simulations in population balance models of mixer-coaters. *Chemical Engineering Science.* 66, 3592-3604.

Garside, J. and Shah, M. B. (1980). Crystallization kinetics from MSMPR crystallizers. *Industrial Engineering and Chemical Process Design and Development*, (19), 509-514.

Gonzalez, E. (2012). *Contribution au contrôle par la modélisation d'un procédé de cristallisation en continu.* PhD Thesis. AgroParisTech, Paris, France.

Hulburt, H. and Katz, S. (1964). Some problems in particle technology: A statistical mechanical formulation. *Chemical Engineering Science,* 19, 555–574.

Leuillet, J. C., Maingonnait, J. F., Corrieu, G. (1986). Etude de la perte de charge dans un échangeur de chaleur a surface raclée traitant des produits newtoniens et non-newtoniens. *Journal of Food Engineering*. 5: 153-176.

Lian, G., Moore, S., Heeney, L. (2006). Population balance and computational fluid dynamics modelling of ice crystallisation in a scraped surface freezer. *Chemical Engineering Science,* 61(23), 7819-7826.

Marchal, P., David, R., Klein, J. P., Villermaux, J. (1988). Crystallization and precipitation engineering—I. An efficient method for solving population balance in crystallization with agglomeration. *Chemical Engineering Science*, 43, 59–67.

Muhw, H., David R., Villermaux, J. (1996). Cyrstallization and precipitation engineering - VI. Solving population balance in the case of the precipitation of silver bromide crystals with high primary nucleation rates by using the first order upwind differentiation. *Chemical Engineering Science*, 51(2), 309-319.

Mydlarz, J. (1996). Modelling of growth rate for MSMPR crystallizer data. *Crystal Research and Technology,* (31), 541-565.

Randolph, A. and Larson, M. (1988). Theory of particulate processes: analysis and techniques of continuous crystallization. New York, NY: Academic Press.

Rigopoulos, S. and Jones A. G. (2001). Dynamic modelling of a bubble column for particle formation via a gas–liquid reaction. *Chemical Engineering Science*, 56, 6177–6184

Sánchez, J., Ruiz, Y., Auleda, J. M., Hernández, E., Raventós, M. (2009). Review: Freeze Concentration in the Fruit Juices Industry. *Food Science and Technology International*, 15, (4), 303-315.

Sánchez, J., Hernández, E., Auleda, J. M., Raventós, M. (2011). Review: Freeze Concentration Technology Applied to Dairy Products. *Food Science and Technology International*, 17, (1), 5-13.

Wen, C. Y. and Fan, L. T. (1975). Models for flow systems and chemical reactors. New York, Marcel Decker.

Woo, X. Y., Tan, R. B. H., Chow, P.S., Braatz, R. D. (2006). Simulation of mixing effects in antisolvent crystallization using a coupled CFD-PDF-PBE approach. *Crystal Growth and Design*, 6(6), 1291-1303.

Wynn, E. J. W. (2003). Relationship between particle-size and chord-length distributions in focused beam reflectance measurement: stability of direct inversion and weighting. *Powder Technology, 133* (1-3), 125-133.

Chapter 6 - Conclusions and perspectives

Chapter 6 - Conclusions and perspectives

The formation of the smallest possible ice crystals is the main objective of the freezing process of sorbet, in order to improve product quality. The optimization of the freezing process requires a good control of the operating conditions and the understanding of the development of the ice crystals inside the scraped surface heat exchanger (SSHE). The main objective of this work was to study the influence of the operating conditions of the freezing process on the ice crystals size distribution, draw temperature and the apparent viscosity of sorbet. The axial product temperature profile and the residence time distribution (RTD) were also investigated as a function of the freezing operating conditions. This work was focused on providing a better understanding of the coupled interactions of heat transfer, fluid flow, shear and ice crystallization kinetics on the development of the ice crystals in the SSHE.

The experimental part of this study was organized as follows: an ultra high temperature pasteurized lemon sorbet mix was used for the experiments carried out in this work. The freezing of sorbet was performed in a continuous SSHE at the pilot scale. The operating conditions of the freezing process that were investigated were the mix flow rate, the dasher rotational speed and the evaporation temperature of the refrigerant fluid. In order to follow the ice crystallization kinetics, the chord length distribution (CLD) of ice crystals in sorbet was measured at the outlet of the SSHE by means of the focused beam reflectance measurement (FBRM). This technique made it possible to follow directly online the evolution of the ice crystal CLD, in sorbets containing up to 40% of ice. In parallel, the draw temperature of the product was measured at the outlet of the SSHE with a Pt100 probe. This measure allows the determination of the ice volume fraction. Furthermore, the axial product temperature profile in the SSHE was investigated, by means of wireless temperature sensors (iButtons®) positioned through the axial length of the rotor. The fluid flow in the SSHE was

characterized by measuring the residence time distribution (RTD) of the product obtained with a colorimetric technique. Finally the rheological properties of the sorbet at the freezer exit were investigated by using a pipe rheometer.

This experimental study gave the main following results:

Concerning the effect of the refrigerant fluid temperature, a decrease in this temperature led to the reduction in the ice crystal size and to lower draw temperatures (higher ice volume fractions). This effect can be explained by the enhanced cooling rate that led to formation of more ice crystals that grow with a thinner structure from the ice debris of previous scrapings. Furthermore, a decrease in the refrigerant fluid temperature caused a broadening of the RTD. This effect can be explained by the increase in radial temperature difference between the wall and the centre of the exchanger, increasing the radial differences in apparent viscosity and increasing the difference in axial velocities, resulting thus in higher axial dispersion.

The study of the influence of the mix flow rate showed that the draw temperature of the product decreased with decreasing this flow rate. This effect is explained by the increased residence time of the product in the SSHE with decreasing the mix flow rate, which makes it possible to remove more heat from the product. Moreover, the mix flow rate had no significant effect on the ice crystal CLD. This can be explained by a compensatory effect between two phenomena occurring during the freezing process: on the one hand, at lower mix flow rates, there is more time available for crystal growth. On the other hand, decreasing mix flow rate leads to lower draw temperatures (higher ice volume fractions) and to a higher product viscosity. This effect increases shear stress and leads to the breakage of the larger ice crystals. Finally, an increase in the product flow rate led to a narrowing of the RTD and to less

axial dispersion. This can be explained by the better radial mixing which is improved by the reduction of the apparent viscosity of the product with warmer product temperatures.

Concerning the influence of the dasher speed, the experimental measurements showed that a slight reduction in the ice crystal CLD was obtained with increasing dasher speed. This effect could be explained by the formation of new ice crystals by secondary nucleation, induced either by the smaller ice clumps detached from the cooling wall or by the remaining ice debris produced during the breakage of the larger ice crystals. Furthermore, experimental data demonstrated that an increase in dasher speed led to warmer product temperatures in the first half of the SSHE. This effect can be explained by the increase in the frictional energy dissipated into the product. However, on the last half of the SSHE, an increase in dasher speed had a negligible effect on the temperature of the product; this can be explained by the enhancement in the heat transfer rate produced by the faster removal of the ice layer at the exchanger wall.

The effects of product temperature and ice volume fraction on the apparent viscosity of non aerated sorbet were also investigated. The experimental data showed that sorbet mix and frozen sorbet exhibited a shear-thinning behaviour. The flow behaviour index showed a decreasing trend with the decrease in product temperature, from the beginning of the freezing until the product reached an ice volume fraction about 17%. Then, the flow behaviour index remained almost constant, with the further decrease of the temperature of the product until an ice volume fraction about 40%. Concerning the apparent viscosity of sorbet, it increased with decreasing the product temperature (higher ice volume fraction). This effect can be explained by two simultaneous effects occurring during the freezing of sorbet: first, the freeze-concentration of the liquid phase with the decrease in product temperature results in the increase

in the colloidal forces between particles and increases the apparent viscosity of this continuous phase. Secondly, the increase in the ice volume fraction leads to an increase in the hydrodynamic forces between the ice crystals and the surrounding liquid phase, increasing the apparent viscosity of sorbet.

Then, an empirical rheological model for the non aerated sorbet was proposed by taking into account the evolution of the viscosity of the unfrozen liquid phase, the evolution of the flow behaviour index and the effect of the ice volume fraction on the apparent viscosity of the product. This rheological model predicted reasonably well the evolution of apparent viscosity of the product. This empirical model was used for the ice crystallization modelling to account for the viscous dissipation in the SSHE during the freezing process.

In the case of the aerated sorbet, the effect of the air volume fraction on the apparent viscosity of sorbet was investigated. Experimental rheological data showed that an increase in the air volume fraction led to an increase of the apparent viscosity of aerated sorbet. However, the influence of the ice volume fraction $\phi_{v.ice}$ on the increase in the apparent viscosity of the product is predominant, with respect to the effect of air volume fraction $\phi_{v.a.}$. This effect is likely due to the fact that the air bubbles are more easily deformable than ice crystals.

In parallel to the experimental study, two modelling approaches have been developed. The first one concerned the modelling of the global fluid flow by comparing the experimental data of the RTD study to different common RTD models (plug flow with axial dispersion, tank-in-series…). The gamma distribution model was the most appropriate model to describe the experimental RTD.

The second approach was the development of two mathematical models coupling heat transfer, fluid flow and ice crystallization kinetics. The first model combines heat transfer and population balance equations (PBE) assuming plug flow (PF). The PBE included ice nucleation, growth and breakage of ice crystals. The first two phenomena were determined by the subcooling degree. This PF modelling approach made it possible to predict the evolution of product temperature, mean chord length, ice volume fraction and apparent viscosity of sorbet as a function of the residence time. The second model considers the coupling of heat transfer and PBE, and combines it with the empirical gamma distribution RTD model obtained in article 2. This model made it possible to account for flow and viscosity heterogeneities in the SSHE for the modelling of the ice crystallization process. Furthermore, this RTD modelling approach gave insight into the values of product temperature and mean chord length for each fraction of fluid that flows through the SSHE, and made it possible to calculate the bulk values.

Experimental data of ice crystal CLD and draw temperature were used for the estimation of the parameters of the ice crystallization model developed in this work. With a first set of estimated parameters, the comparison of the predicted data of draw temperature and mean chord length obtained by the PF model and by the RTD model with the experimental data obtained for different operating conditions, demonstrated that both models predicted very satisfactorily the experimental tendencies within a 10% error limit. A comparison between the ice crystal size distribution at the outlet of the SSHE obtained by the PF and the RTD modelling approaches showed that the ice crystal size distribution of both models were very similar. This effect is explained by the blending of the fractions of fluid that constitute the ice crystal size distribution at the outlet: some fractions of fluid exit earlier from the SSHE and have a larger ice crystal size (due to the survival of the larger ice crystals and to the melting of the small ice crystals), and others that exit later from the SSHE and have a smaller crystal size (due to the survival of a

larger quantity of small ice crystals and the breakage of the larger ones), resulting thus in a compensation effect between the ice crystal sizes of all the fractions of fluid. It seems that there is almost a perfect compensation on the ice crystal sizes among all the fractions of fluid.

These modelling approaches made it possible to have a deeper understanding of the coupled phenomena of heat transfer, fluid flow, shear and ice crystallization kinetics occurring during the freezing process in SSHEs. These models can also be used to identify new ways to optimize the freezing process, or to help for the scale-up of the process from laboratory pilot scale equipment to industrial scale SSHEs.

As a global conclusion to this work, the methodology developed during this study was used for the CAFÉ project to improve the understanding of the impact of the freezing operating conditions on the main quality aspects of sorbet. The experimental data obtained in this work was useful for the selection of the most suitable dynamic models for the online control of the freezing process, and for the identification of the parameters of the developed dynamic models. This experimental databasis along with online experimental trials at the SSHE allow the sensor development partners of the CAFÉ project to validate the measured trends by the new developed sensors. The freezing process was selected as a demonstration process of the optimal control strategies developed within the framework of the CAFÉ project in March 2013, when the project will be finalised.

Concerning the perspectives of this study, the influence of the amount of air incorporated into the product on the ice crystal size and the RTD were not studied in this work. Yet this information is still needed to improve the knowledge of the development of ice crystals in SSHE with aeration. Information of the effect of the amount of air incorporated into the product and the

pressure in the heat exchanger cylinder on the RTD can be very valuable to account for other changes in fluid flow behaviour and viscosity on the ice crystallization modelling. The rheological measurements of sorbet with aeration in this case can be used as a basis for the construction of a rheological model, which takes into account the influence of the air volume fraction on the apparent viscosity of sorbet. This model can then be used to account for the apparent viscosity effects on the ice crystallization modelling. The development of a mathematical model that takes into account the incorporation of air bubbles during the freezing process would be very useful so as to represent more accurately the ice crystallization during the freezing process of ice cream and sorbet. The development of a mathematical model that takes into account the incorporation of air bubbles during freezing would be very useful so as to represent more accurately the ice crystallization mechanism occurring during the freezing process of ice cream and sorbets. The breakage and the coalescence of the air bubbles could be represented by another population balance; however, this approach will certainly increase the computation time significantly.

Furthermore, in the case of ice cream, the presence of fat globules and fat crystals in the product must be taken into account. During the freezing process, the fat globules are submitted to high shear forces which remove the surfactants that constitute the fat membrane surface and expose then a free membrane fat globule. The fat globules are consequently susceptible to partial coalescence, resulting in fat agglomerates that cover parts of the surface of the air bubbles and contribute to the stabilization of the foam structure. The degree of fat partial coalescence or fat destabilization affects the creaminess and the resistance to meltdown of ice creams. In the case of a scientific collaboration with the department of food science of the University of Wisconsin-Madison, a PhD student has used the online measurement techniques developed in this work, such as the FBRM sensor, the Pt100 probe and the pipe rheometer, so as to study the effect of the freezing operating conditions on the degree of fat destabilization in ice creams.

This general methodology that combines the experimental characterization of the crystallization process by using online sensors to assess the product quality, with the modelling of the interactions between heat transfer, fluid flow and crystallization kinetics could be applied for the study of other crystallized foods such as butter or chocolate.

Chapitre 6 - Conclusions et perspectives

Chapitre 6 - Conclusions et perspectives

La formation des cristaux de glace les plus petits possibles est l'objectif principal du procédé de congélation d'un sorbet. L'optimisation du procédé de congélation demande un bon contrôle des conditions opératoires et une bonne compréhension du développement des cristaux de glace dans l'échangeur de chaleur à surface raclée (ECSR). L'objectif principal de ce travail était l'étude de l'influence des conditions opératoires du procédé de congélation sur la distribution de taille des cristaux de glace, sur la température de sortie du produit et sur la viscosité apparente du sorbet. Le profil axial de température de produit et la distribution de temps de séjour du produit (DTS) ont été aussi étudiés en fonction de conditions opératoires de congélation. Cette étude a cherché à fournir une meilleure compréhension du couplage entre les phénomènes de transfert de chaleur, d'écoulement du fluide, de cisaillement et les cinétiques de cristallisation sur le développement des cristaux de glace dans l'ECSR.

La partie expérimentale de cette étude a été organisée de la façon suivante:

Un mix commercial de sorbet stérilisé a été utilisé pour les expériences réalisées dans ce travail. La congélation du mix de sorbet a été effectuée dans un ECSR continu à l'échelle pilote. Les conditions opératoires du procédé de congélation qui ont été étudiées sont le débit de mix de sorbet, la vitesse de raclage et la température du fluide réfrigérant. Afin de suivre les cinétiques de cristallisation de la glace, la distribution de taille de cordes des cristaux dans le sorbet a été mesurée à la sortie de l'ECSR à l'aide de la technique FBRM (focused beam reflectance measurement). Cette technique de mesure a permis le suivi de l'évolution de la taille des cristaux de glace dans des sorbets ayant une teneur en glace jusqu'à 40%. En parallèle, la température du produit a été mesurée en ligne à la sortie de l'ECSR avec une sonde Pt100. De plus, le profil axial de température du produit dans l'ECSR a été étudié à l'aide de capteurs de température sans fil (iButtons®) positionnés le long de l'axe du rotor.

L'écoulement dans l'ECSR a été caractérisé en mesurant la distribution des temps de séjour (DTS) à l'aide d'une technique colorimétrique. Finalement, les propriétés rhéologiques du sorbet à la sortie de l'ECSR ont été étudiées à l'aide d'un viscosimètre tubulaire.

Cette étude expérimentale a donné les résultats principaux suivants:

En ce qui concerne l'effet de la température du fluide réfrigérant, la diminution de cette température a conduit à une réduction de la taille des cristaux de glace et à des températures de produit plus basses (fraction volumique de glace plus élevée). Cet effet peut être expliqué par l'augmentation du refroidissement qui induit un plus grand sous-refroidissement et donc à davantage de croissance de cristaux de glace plus nombreux, avec une structure plus fine, formés à partir des débris de glace qui restent sur la paroi après le raclage par la lame. De plus, la diminution de la température du fluide frigorigène induit un élargissement de la DTS. Cet effet peut s'expliquer par l'augmentation de la différence de température radiale entre la paroi et le centre de l'échangeur, qui augmente les différences radiales de viscosité apparente et accroit la différence des vitesses axiales, résultant ainsi en une augmentation de la dispersion axiale.

L'étude de l'influence du débit de mix a démontré que la température du produit en sortie est plus basse lorsqu'on diminue le débit de produit. Cet effet est expliqué par l'augmentation du temps de séjour avec la réduction du débit, ce qui permet d'éliminer plus de chaleur du produit. De plus, le débit de mix n'a eu aucun effet sur la distribution de taille des cristaux. Cela peut être expliqué par un effet compensatoire entre deux phénomènes qui ont lieu pendant le procédé de congélation: d'une part, à faibles débits de produit il y a plus de temps pour la croissance des cristaux de glace. D'autre part, la diminution du débit de produit entraîne une diminution de la température de sortie du produit (fraction de glace plus élevée),

une augmentation du taux de cisaillement et par conséquent davantage d'attrition des cristaux. Finalement, une augmentation du débit de mix conduit à un rétrécissement de la DTS et à une diminution de la dispersion axiale. Cela peut être expliqué par un meilleur mélange radial dans l'ECSR qui est amélioré par la diminution de la viscosité apparente du produit avec des températures du produit plus chaudes.

Concernant l'influence de la vitesse de raclage, les mesures expérimentales ont montré qu'une légère réduction de la taille des cristaux de glace a été obtenue avec l'augmentation de la vitesse de rotation des lames racleuses. Cet effet pourrait être expliqué par la formation de cristaux de glace par nucléation secondaire à partir des amas de glace plus petits qui sont détachés de la paroi de refroidissement, ou à partir des fragments de cristaux produits lors de l'attrition des grands cristaux de glace. De plus, les données expérimentales ont démontré qu'une augmentation de la vitesse de raclage conduit à des températures de produit plus élevées dans la première moitié axiale de l'ECSR. Cet effet peut être expliqué par l'augmentation de la dissipation de l'énergie de frottement des lames dans le produit. Toutefois, sur la dernière moitié axiale de l'ECSR, une augmentation de la vitesse de raclage n'a pas d'effet sur la température du produit. Cela peut s'expliquer par l'amélioration du taux de transfert de chaleur produite par l'élimination plus rapide de la couche de glace à la paroi de l'échangeur.

Les effets de la température du produit et de la fraction volumique de glace sur la viscosité apparente du sorbet non foisonné on été étudiés. Les données expérimentales ont montré que le mix de sorbet et le sorbet congelé présentent un comportement rhéofluidifiant. Une diminution de la température du produit conduit à la diminution de l'indice d'écoulement, depuis le début de la congélation jusqu'à ce que le produit atteigne une fraction volumique d'environ 17% de glace. Ensuite, l'indice d'écoulement reste à peu près constant lorsque la

température diminue davantage et ce jusqu'à une fraction volumique d'environ 40% de glace. De plus, la viscosité apparente du sorbet augmente avec la diminution de la température du produit (et l'augmentation de la fraction volumique de glace). Cet effet peut s'expliquer par deux phénomènes simultanés qui ont lieu lors du procédé de congélation: premièrement, la concentration par congélation de la phase liquide avec la diminution de la température du produit, conduit à l'augmentation des forces colloïdales entre les particules et augmente la viscosité apparente de cette phase continue. Deuxièmement, l'augmentation de la fraction volumique de glace conduit à l'augmentation des forces hydrodynamiques entre les cristaux de glace et la phase liquide, en augmentant la viscosité apparente du produit.

Suit à ces essais expérimentaux, un modèle rhéologique empirique pour le prédire la viscosité du sorbet non foisonné a été développé. Ce modèle prend en compte l'évolution de la viscosité de la phase liquide non congelée, l'évolution de l'indice de l'écoulement et l'effet de la fraction volumique de glace sur la viscosité apparente du produit. Ce modèle rhéologique prédit assez bien l'évolution de la viscosité apparente du produit. Il a été utilisé pour la modélisation de la cristallisation de la glace afin de tenir compte de la dissipation visqueuse au cours du processus de congélation.

Dans le cas du sorbet foisonné, l'effet de la fraction volumique d'air sur la viscosité apparente du produit a été étudié. Les données expérimentales rhéologiques ont démontré qu'une augmentation de la fraction volumique d'air conduit à une augmentation de la viscosité apparente du sorbet aéré. Cependant, l'influence de la fraction volumique de glace $\phi_{v.ice}$ sur l'augmentation de la viscosité apparente du produit est prédominante par rapport à l'effet de la fraction volumique d'air $\phi_{v.a.}$. Cet effet est probablement dû au fait que les bulles d'air sont plus facilement déformables que les cristaux de glace.

En parallèle à l'étude expérimentale, deux approches de modélisation ont été développées. La première concerne la modélisation globale de l'écoulement du fluide en confrontant les données expérimentales de l'étude DTS à différents modèles usuels (piston à dispersion axiale, réacteurs en série…). Le modèle de distribution gamma (GDM) a été le modèle le plus approprié pour décrire la DTS expérimentale.

La deuxième approche a concerné le développement de deux modèles mathématiques, qui prennent en compte le couplage entre le transfert de chaleur, l'écoulement du fluide et les cinétiques de cristallisation de la glace. Les équations de bilan de population (EBP) incluent les phénomènes de nucléation de la glace, la croissance et la fragmentation des cristaux de glace. Les deux premiers phénomènes ont été déterminés par le degré de sous-refroidissement. Le premier modèle combine transfert de chaleur et EBP, en supposant un écoulement piston (EP). Cette approche de modélisation avec écoulement piston a permis de prédire l'évolution de la température du produit, de la corde moyenne de cristaux, de la fraction volumique de glace et de la viscosité apparente du sorbet en fonction du temps de séjour. Le deuxième modèle considère le couplage de transfert de chaleur et de bilan de population combiné avec le modèle empirique DTS obtenu dans l'article 2. Ce modèle a permis la prise en compte des hétérogénéités d'écoulement de produit et de viscosité apparente du produit dans l'ECSR pour la modélisation du procédé de cristallisation de la glace. En outre, ce modèle a permis d'obtenir un bon aperçu des valeurs de la température du produit et de la longueur de corde moyenne pour chaque fraction de liquide qui traverse l'échangeur, et a permis de calculer les moyennes de mélange.

Plusieurs données expérimentales de distribution de taille de cristaux de glace et de température de sortie du produit ont été utilisées pour l'estimation des paramètres du modèle de

cristallisation de la glace développé dans ce travail. À partir d'une première estimation des paramètres du modèle, la comparaison des données prédites avec les deux modèles de la température de sortie et de la longueur de corde des cristaux de glace avec les données expérimentales obtenues pour différentes conditions opératoires, a démontré que les deux modèles prédisent de façon satisfaisante les tendances expérimentales (dans une limite de +/- 10%). Une comparaison entre les distributions de taille de cristaux de glace à la sortie de l'ECSR obtenues par le modèle EP et par le modèle DTS a montré que les distributions de taille obtenues par ces deux approches de modélisation sont très similaires. Cet effet peut s'expliquer par le mélange des fractions de fluide qui contribuent à la distribution de taille des cristaux de glace à la sortie: certaines fractions de fluide sortent plus tôt de l'ECSR avec une plus grande taille de cristaux de glace (en raison de la survie des grands cristaux de glace et de la fonte des petits cristaux de glace), et d'autres sortent plus tard de l'ECSR avec une taille de cristaux plus petite (en raison de la survie d'une plus grande quantité de petits cristaux de glace et de la rupture des cristaux plus grands). Il semblerait qu'il y ait une compensation presque parfaite sur les tailles de cristaux de glace entre toutes les fractions de fluide.

Ces approches de modélisation ont permis d'avoir une meilleure compréhension des effets couplés des phénomènes de transfert de chaleur, de l'écoulement du fluide, du cisaillement et des cinétiques de cristallisation de la glace qui ont lieu au cours du processus de congélation dans l'ECSR. Ces modèles peuvent être utilisés pour identifier de nouvelles façons d'optimiser le procédé de congélation, ou pour aider à l'extrapolation du procédé depuis l'équipement à l'échelle pilote vers l'échelle industrielle.

En conclusion globale de ce travail, la méthodologie développée dans cette étude a été utilisée dans le cadre du projet CAFÉ pour améliorer la compréhension de l'impact des

conditions opératoires du procédé de congélation sur les principaux aspects de la qualité du produit. Les données expérimentales obtenues dans ce travail ont été utiles pour la sélection des modèles dynamiques les plus appropriés pour le contrôle en ligne du procédé de congélation et pour l'identification des paramètres des modèles dynamiques développés. La base de données expérimentale, ainsi que des essais expérimentaux en ligne, ont rendu possible la validation des mesures obtenues par les capteurs développés par des partenaires du projet. La congélation de sorbet a été sélectionnée comme procédé de démonstration des stratégies de contrôle optimales développées dans le cadre du projet CAFÉ en mars 2013, lorsque le projet sera finalisé.

Concernant les perspectives de ce travail, l'influence de la quantité d'air incorporée dans le produit sur la taille des cristaux de glace et sur la DTS n'a pas été étudiée dans ce travail. Cependant, ces informations seront nécessaires pour améliorer les connaissances sur le développement des cristaux de glace dans l'ECSR avec de l'air. Des informations sur l'effet du taux de foisonnement et la pression dans le cylindre d'échange sur la DTS, peuvent être très utiles pour prendre en compte d'autres changements du comportement de l'écoulement du fluide et de la viscosité du produit dans la modélisation de la cristallisation de la glace. Les mesures rhéologiques de sorbet avec aération réalisées dans ce travail peuvent être utilisées comme base pour la construction d'un modèle rhéologique, qui prendrait en compte l'influence de la fraction volumique d'air sur la viscosité apparente du sorbet. Ce modèle pourrait ensuite être utilisé pour tenir compte des effets de la viscosité apparente dans la modélisation de la cristallisation de la glace. Le développement d'un modèle mathématique tenant compte de l'incorporation de bulles d'air dans le produit au cours de la congélation serait très utile afin de représenter plus fidèlement le mécanisme de cristallisation de la glace lors du procédé de congélation de la glace des crèmes glacées et des sorbets. Le fractionnement et la coalescence des bulles d'air pendant le procédé de congélation pourrait

être représenté par un autre bilan de population, cependant, cette approche augmentera sans doute de façon significative le temps de calcul du modèle.

En outre, dans le cas de la crème glacée, la présence de globules gras et de cristaux de matière grasse doivent être prise en compte. Lors du procédé de congélation, les globules gras sont soumis à des forces de cisaillement importantes qui détachent les agents tensio-actifs qui constituent la membrane de surface des globules gras. Les globules gras sont ensuite susceptibles de coalescer partiellement, donnant lieu à des agglomérats de matière grasse qui recouvrent certaines parties de la surface des bulles d'air et contribuent à la stabilisation de la structure de la mousse. Le degré de coalescence partielle des globules gras ou la déstabilisation de la matière grasse affectent l'onctuosité et la résistance à la fonte des crèmes glacées. Dans le cas d'une collaboration scientifique avec le département des Sciences des Aliments de l'Université de Wisconsin-Madison, une doctorante a utilisé les techniques de mesure en ligne développées dans ce travail, telles que le capteur FBRM, la sonde Pt100 et le rhéomètre tubulaire, afin d'étudier l'effet des conditions opératoires du procédé de congélation sur le degré de déstabilisation de la matière grasse dans les crèmes glacées.

Cette méthodologie générale qui combine la caractérisation expérimentale du procédé de cristallisation, en utilisant des capteurs en ligne pour évaluer la qualité du produit, avec la modélisation des interactions entre le transfert de chaleur, l'écoulement de fluide et les cinétiques de cristallisation, pourrait être appliquée par la suite pour l'étude d'autres aliments cristallisés comme le beurre et le chocolat.

Publications and communications

Publications and communications

Publications

1. ARELLANO M., BENKHELIFA H., FLICK D., ALVAREZ G. 2012. Online ice crystal size measurements during sorbet freezing by means of the focused beam reflectance measurement (FBRM) technology. Influence of operating conditions. *Journal of Food Engineering*. (113) 351-359.

2. ARELLANO M., BENKHELIFA H., FLICK D., ALVAREZ G. 2012. Experimental study and modelling of the residence time distribution in a scraped surface heat exchanger during sorbet freezing. *Journal of Food Engineering* (submitted paper).

3. ARELLANO M., BENKHELIFA H., FLICK D., ALVAREZ G. 2012. Rheological characterization of sorbet using pipe rheometry during the freezing process. *Journal of Food Engineering* (submitted paper).

4. ARELLANO M., BENKHELIFA H., FLICK D., ALVAREZ G. 2012. Influence of ice volume fraction and air volume fraction on the rheological properties of sorbet.

5. ARELLANO M., BENKHELIFA H., ALVAREZ G., FLICK D. 2012. Coupling population balance and residence time distribution for the ice crystallization modelling in a scraped surface heat exchanger. *Chemical Engineering Science* (submitted paper).

Communications

1. ARELLANO M., BENKHELIFA H., ALVAREZ G. Sept. 2010. Online measurements by image analysis of ice crystal size in frozen sucrose solutions. Application to frozen desserts. Berlin FOOD. PhD Conference. Berlin, Germany. (Poster presentation)

2. ARELLANO M., GONZALEZ J. E., ALVAREZ G., BENKHELIFA H., FLICK D., LEDUCQ D. May, 2011. Online ice crystal size measurements by the focused beam reflectance method (FBRM) during sorbet freezing. 11th International Congress on Engineering and Food (ICEF11) Athens, Greece. Procedia Food Science. 1, 1256-1264. (Oral presentation)

3. BENKHELIFA H., ARELLANO M., ALVAREZ G., FLICK D. May, 2011. Ice crystals nucleation, growth and breakage modelling in a scraped surface heat exchanger. 11th International Congress on Engineering and Food (ICEF11) Athens, Greece. Congress Proceedings. Paper: FMS30. (Oral presentation)

4. VILAS C., BALSA-CANTO E., ARELLANO M., BENKHELIFA H., ALVAREZ G. May, 2011. Model identification of the ice cream crystallization process. 11th International Congress on Engineering and Food (ICEF11) Athens, Greece. Congress Proceedings. Paper: MCF163. (Poster presentation)

5. ARELLANO M., GONZALEZ J. E., LEDUCQ D., BENKHELIFA H., FLICK D., ALVAREZ G. August, 2011. Effect of sorbet freezing process on draw temperature and ice crystal size using focused beam reflectance method (FBRM) online measurements. 23rd International Congress of Refrigeration (ICR2011) Prague, Czech Republic. Congress Proceedings. ID: 949. (Oral presentation)

6. GONZALEZ-RAMIREZ J. E., ARELLANO M., LEDUCQ D., ALVAREZ G., BENKHELIFA H., FLICK D. August, 2011. Moments model for a continuous sorbet crystallization process. 23rd International Congress of Refrigeration (ICR2011) Prague, Czech Republic. Congress Proceedings. ID: 950. (Oral presentation)

7. ARELLANO M., BENKHELIFA H., FLICK D., ALVAREZ G. August, 2012. Characterization of the residence time distribution in a scraped surface heat exchanger during the freezing of sorbet. 16th World Congress of Food Science and Technology (IUFoST2012) Foz do Iguaçu, Parana State, Brazil. (Poster presentation)

8. ARELLANO M., BENKHELIFA H., FLICK D., ALVAREZ G. August, 2012. Online capillary rheometry of commercial sorbet. 16th World Congress of Food Science and Technology (IUFoST2012) Foz do Iguaçu, Parana State, Brazil. (Poster presentation)

Appendix

Appendix

Modelling PSD to CLD

The relationship between PSD and CLD has been the subject of many articles and several methods for converting PSD to CLD have been developed. This section describes the mathematical approach develop in this work for the modelling of PSD to CLD. The modelling of PSD to CLD model is based on the following assumptions:

1. The analyzed particles are spherical and of the same size L.
2. There is no overlapping of particles when a particle is been scanned across.
3. The probability of detection in the measured volume is the same for large and small particles.
4. The laser beam reflection is always the same regardless of the angle of incidence.

The starting point for converting PSD to CLD is to define the probability density function of how intercepted particles give rise to chord lengths. Consider a laser beam intercepting an spherical particle, the laser beam crossing at a random distance of the centre of the particle as depicted in Fig. 1, where L is the diameter of the particle, C the chord length of the particle, C_m the measured chord length of the particle at any given time, r the distance between the centre of the particle, and r_m the distance between the centre of the particle centre and C_m.

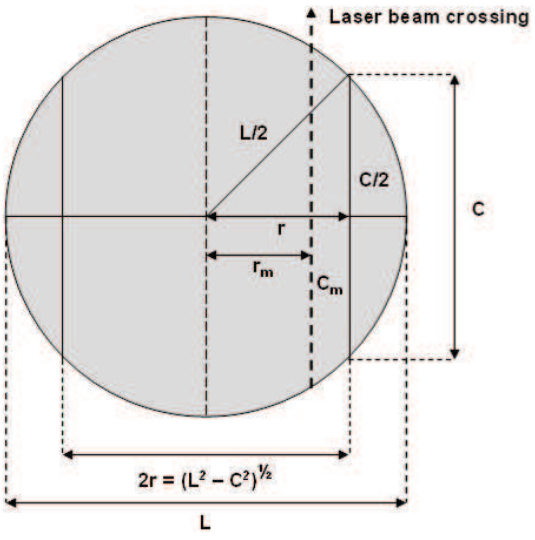


Fig. 1. Laser beam intercepting a spherical particle, crossing at a random distance of the centre of the particle.

Therefore, in order to measure a chord length C_m, greater than C, the r_m distance between the particle's centre and the laser beam must be smaller than r.

Being $P(r_m < r)$ the probability that $C_m > C$:

$$P(r_m < r) = \frac{2r}{L} = \frac{\sqrt{L^2 - C^2}}{L} \rightarrow \sqrt{1 - \left(\frac{C}{L}\right)^2}$$

And $P(r_m > r)$ the probability that $C_m < C$:

$$P(r_m > r) = 1 - P(r_m < r) \rightarrow 1 - \sqrt{1 - \left(\frac{C}{L}\right)^2}$$

Expressing a ratio $x = \frac{C}{L}$ allows us to define the cumulative distribution function of chord lengths for a given diameter as:

$$f(x) = f\left(\frac{C}{L}\right) = \begin{cases} x \rightarrow 1 - \sqrt{1 - x^2} & : \quad 0 < x < 1 \\ x \rightarrow 1 & : \quad x > 1 \end{cases}$$

The probability density function of chord length for a given diameter is thus the derivative of the function $f(x) = f\left(\frac{C}{L}\right)$ and can be defined as:

$$f'(x) = f'\left(\frac{C}{L}\right) = \begin{cases} x \rightarrow \dfrac{x}{\sqrt{1 - x^2}} & : \quad 0 < x < 1 \\ x \rightarrow 0 & : \quad x > 1 \end{cases}$$

Now, consider a class i of a particle's diameter D_i; comprehended in this class there are several classes of chord length that must be distributed in the lower or equal classes to i according to the FBRM CLD.

Each CLD class follows a geometric sequence of initial value D_1 and final value D_{100} with a progression ratio α, which makes it possible to determine the proportion of chord length to be distributed in each of the CLD classes.

Thus, we define three classes of chord lengths comprehended in the class i of a particle's diameter D_i as: 1, $i-j$ and i. Being β_i the proportion of chord length distributed in the same class than D_i and expressed by:

$$\beta_i = \int_{\frac{D_{i-1}^*}{D_i}}^{\frac{D_i}{D_i}} f'(x)dx = \int_{\frac{D_{i-1}^*}{D_i}}^{1} \frac{x}{\sqrt{1-x^2}}dx = \int_{\alpha^{-1/2}}^{1} \frac{x}{\sqrt{1-x^2}}dx = \left[1-\sqrt{1-x^2}\right]_{\alpha^{-1/2}}^{1} = \sqrt{1-\alpha^{-1}}$$

The proportion β_{i-j} is distributed between the classes 1 and i, given by:

$$\beta_{i-j} = \int_{\frac{D_{i-j-1}^*}{D_i}}^{\frac{D_{i-j+1}^*}{D_i}} f'(x)dx = \left[1-\sqrt{1-x^2}\right]_{\alpha^{-\left(j+\frac{1}{2}\right)}}^{\alpha^{-\left(j-\frac{1}{2}\right)}} = \sqrt{1-\alpha^{-(2j-1)}} - \sqrt{1-\alpha^{-(2j+1)}}$$

The chord length proportion β_1 distributed in the class 1 is expressed as:

$$\beta_1 = \int_{\frac{D_0}{D_i}}^{\frac{D_2}{D_i}} f'(x)dx = \left[1-\sqrt{1-x^2}\right]_{\alpha^{-\left(i-\frac{1}{2}\right)}}^{\alpha^{-\left(i-\frac{3}{2}\right)}}$$



Online Measurements by Image Analysis of Ice Crystal Size in Frozen Sucrose Solutions. Application to Frozen Desserts.

M. Arellano [1], H. Benkhelifa [2], G. Alvarez [1]

(1) CEMAGREF. Refrigeration Process Engineering. BP 44, 92163 Antony, France.
(2) AGROPARISTECH. 16 rue Claude Bernard, 75231 Paris Cedex 05, France.

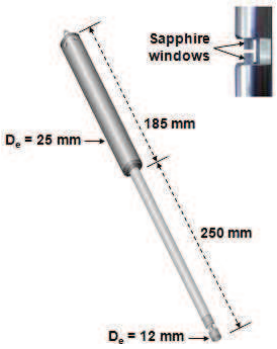


Ice crystal size in frozen desserts determines to a large extent the product's final texture [1]. The monitoring of the product's ice crystal size is then useful to understand the mechanisms of ice crystal formation during freezing processes and therefore to improve the product's final quality.

This work presents a new online microscopy system and an image treatment methodology capable of following the ice crystal size distribution during batch freezing of sucrose solutions.

1 Online Imaging System – EZ Probe D12

- 2 sapphire visualization windows. Space between windows: 1mm. Visualization field depth: 1000 µm.
- Lower window → Optical fiber. Cold light source at 3400K.
- Upper window → CCD Sensor. Acquisition of 25 images/sec.
- 2D images in 256 gray values. Size: 1.15 x 0.86 mm. Resolution: 720 x 576 pixels.



EZ Imaging Probe D12 [2]

2 Experimental Setup – Batch Freezing

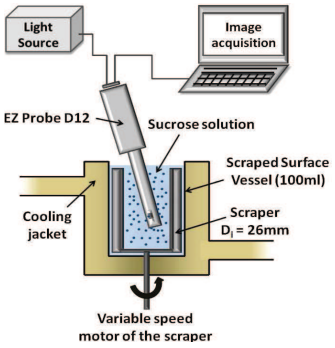


Image acquisition during batch freezing

- Solution: sucrose/water (30/70%).
- Batch freezing in a scraped surface heat exchanger.

  Rotation speed: 300 rpm.
  Wall temperature: -10℃.
  Freezing point: -2.4℃.
- Real time acquisition of 2D images of ice crystals. Up to 10% of ice content.

3 Image Analysis – Multi-scale Segmentation Approach

- Image Analysis Algorithm implemented with Matlab®.
- 2 main steps: edge detection and particle segmentation [3].

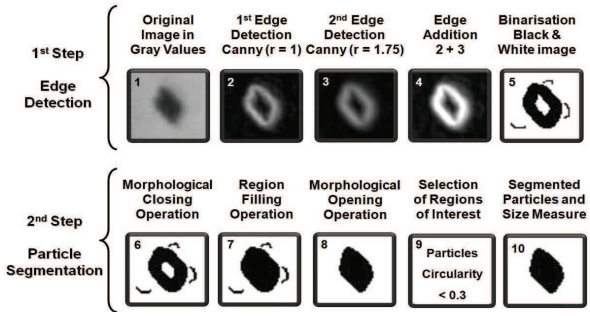
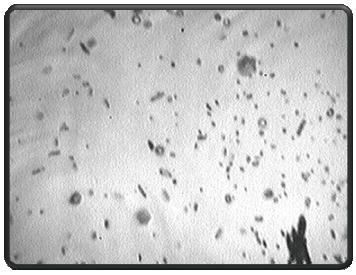
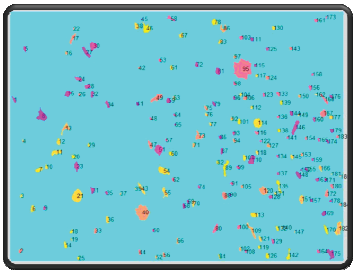


Image Analysis Algorithm

- Good performance of the image analysis method.
- Processing time: 15 sec to analyze one image.

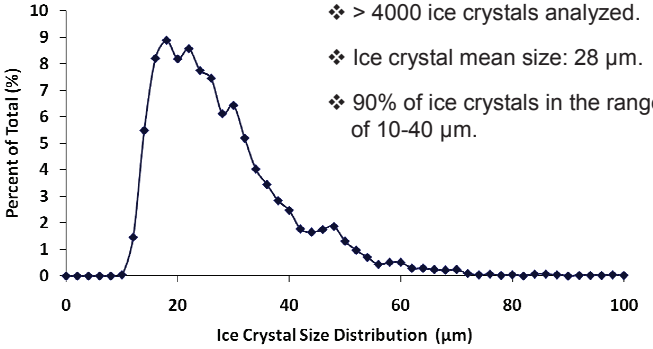


Original Image in gray values



Final segmentation of particles

4 Results – Ice Crystal Size Distribution



- > 4000 ice crystals analyzed.
- Ice crystal mean size: 28 µm.
- 90% of ice crystals in the range of 10-40 µm.

5 Conclusion and Future Work

- This microscopy technique is a promising tool to follow the ice crystal size distribution during freezing process.
- Ice crystal size distribution and mean crystal size obtained.
- Short processing time; feasibility to analyze image sequences.
- To use this microscopy technique in a pilot scale freezer to visualize the ice crystal size distribution during the freezing of lemon sorbet.

References:
[1] R. W. Hartel. Ice crystallization during the manufacture of ice cream. Trends in food science & technology. October 1996. Vol. 7.
[2] Presles B., Debayle J., Rivoire A., Pinoli JC. Fevotte G. In situ particles size measurements during crystallization processes using image analysis. Récents progrès en génie des procédés. 2009. No. 98
[3] Calderon De Anda J., Wang X. Z., Roberts K.J. Multi-scale segmentation image analysis for the in-process monitoring of particle shape with batch crystallizers.

Acknowledgments: This work is supported by the European Commission through the European Project CAFE (Computer Aided Food processes for control Engineering).

Berlin FOOD. PhD Conference. 8-10 Sep. 2010
Cemagref. GPAN. Refrigeration Process Engineering Unity.
AgroParisTech. UMR n°1145 GENIAL Food Process Engineering Unity.

Abstract

The partial freezing of the mix inside the scraped surface heat exchanger (SSHE) is the most critical step in sorbet manufacturing, since it is the only stage where new ice crystals are produced; further in the process these ice crystals will only grow. The main objective of the freezing process is to form the smallest possible ice crystals, so as to assure a smooth texture in the final product. During the freezing process the product is subjected to coupled interactions of fluid flow, heat transfer, ice phase change and shear. These interactions are determined by the freezing operating conditions and affect the evolution of the ice crystals size distribution (CSD) and the final texture of the product. This work presents the experimental characterization and the modelling of the initial freezing process of a sorbet. The freezing of sorbet was carried out in a SSHE at the pilot scale. The main objective of this work was the study of the influence of the freezing operating conditions on the final product characteristics: ice CSD, product temperature, ice volume fraction, apparent viscosity. The product flow behaviour in the SSHE was characterized by an experimental and modelling study of the residence time distribution (RTD) of the product. An ice crystallization modelling approach, taking into account the coupling of an empirical RTD model with heat transfer equations and a population balance of the different ice crystal size classes was developed. With a first set of estimated parameters, the ice crystallization model predicts satisfactorily the experimental trends, and made it possible to have an insight on the evolution of ice CSD during the freezing process in the SSHE.

Key words: Ice crystallization; Scraped surface heat exchanger; Residence time distribution; Apparent viscosity; Population balance equations.

Résumé

La congélation partielle du mix dans un échangeur de chaleur à surface raclée (ECSR) est l'étape la plus critique dans la fabrication d'un sorbet, car c'est la seule étape où de nouveaux cristaux de glace se forment; par la suite ces cristaux ne font que grossir. L'objectif principal est de produire un grand nombre de cristaux les plus petits possibles afin d'obtenir une texture onctueuse. Pendant le procédé de congélation, le produit est soumis à des interactions couplées d'écoulement du fluide, de transfert de chaleur, de changement de phase et de cisaillement. Ces interactions sont déterminées par les conditions opératoires du procédé de congélation et affectent l'évolution de la distribution de taille des cristaux de glace, ainsi que la texture finale du produit. Ce travail présente la caractérisation expérimentale et la modélisation du procédé de congélation d'un sorbet. La congélation du sorbet à été effectuée dans un ECSR à l'échelle pilote. L'objectif principal de ce travail est l'étude de l'influence des conditions opératoires du procédé de congélation sur les caractéristiques finales du produit: distribution de taille de cristaux de glace, température du produit, fraction volumique de glace et viscosité apparente. Le comportement de l'écoulement du produit dans l'ECSR a été caractérisé par une étude expérimentale et une modélisation de la distribution du temps de séjour (DTS). Une approche de modélisation de la cristallisation de la glace couplant le modèle de DTS avec des équations de transfert de chaleur et de bilan de population des différentes classes de taille de cristaux a été développée. À partir d'une première estimation des paramètres, le modèle de cristallisation prédit de façon satisfaisante les tendances expérimentales et donne un bon aperçu de l'évolution de la distribution de taille des cristaux de glace au cours du procédé de congélation dans l'ECSR.

Mots clés: Cristallisation de la glace; Échangeur de chaleur à surface raclée; Distribution des temps de séjour; Viscosité apparente; Équations de bilan de population.